DOCTORAL THESIS

Exploring Pole-Skipping in Holographic Systems

by:

Banashree Baishya

196121006

Supervisor:

Prof. Debaprasad Maity

A thesis submitted in fulfilment of the requirements

for the degree of Doctor of Philosophy

to the

Department of Physics,

Indian Institute of Technology, Guwahati

North Guwahati-781039, Assam

Declaration

I, Banashree Baishya, hereby declare that this thesis, titled "Exploring Pole-Skipping in Holographic Systems", and the work presented within, are my own. I confirm that:

- This work has not been previously accepted in any form for a degree and is not currently under consideration for any degree.
- This thesis is the result of my own investigations, except where otherwise stated. Other sources are acknowledged by giving explicit references. A bibliography is appended.

Signed: Banashree Baishya

Date: 31/01/25

Certificate

This is to certify that the thesis titled "Exploring Pole-Skipping in Holographic Systems", submitted by Banashree Baishya, a student of the Department of Physics at the Indian Institute of Technology, Guwahati, for the award of the degree of Doctor of Philosophy, is a record of original research conducted under my supervision. The results presented in this thesis have not been submitted elsewhere for the award of any degree.

Debaprasad Maity

Prof. Debaprasad Maity

Department of Physics, IIT Guwahati

Guwahati-781039, Assam, India

DATE 31/01/25

Dedicated to

Maju pehi

Acknowledgments

This thesis would not have been possible without the proper guidance and the help of several individuals who, in one way or another, contributed and extended their valuable assistance in the preparation and completion of this study. I am deeply grateful to all those who made this work possible.

First and foremost, I express my deepest gratitude to my supervisor, Prof. Debaprasad Maity (Debu sir), for his invaluable guidance, support, and encouragement throughout my PhD journey. His expertise and insightful feedback have greatly shaped my research and have been instrumental in the successful completion of this thesis within the time frame given to an Indian student.

I am also immensely thankful to all the faculty members of IIT Guwahati, whose assistance and resources made this research possible. A special thanks to my doctoral committee members, Prof. Bibhas Ranjan Majhi, Prof. Santabrata Das, and Prof. Sovan Chakrabarty for their constructive critiques and suggestions, which enriched the quality of my work. A special thanks goes to Prof. Sourabh Basu, whose course on Condensed Matter Physics proved immensely beneficial for my understanding. I am equally appreciative of the speakers from the Gravity/High Energy Journal Club and the in-house talks, from which I have gained valuable insights throughout this journey. I thank my research group members Sovan Sau, Rajesh Karmakar, Sourav Pal, Gargi Sen, Rajesh Mondal, Ayan Chakraborty, Suvasish Maiti, Jitumani Kalita and Sitesh for all the weekly discussions.

I am grateful to our current HOD Prof. Bosanta Ranjan Boruah, ex HOD Prof. Perumal Alagarsamy and Prof. Subhradip Ghosh for their help at specific times. I thank Basab Bijoy Purkayastha for helping me with various technical details and providing a good chair to sit in for 4 long years.

I am obliged to all my school, college and university teachers who ignited my curiosity to learn physics. A special thanks to Prof. Madhurjya P Bora (Master's advisor) and Prof. Sanjeev Kalita for guiding me in the General Relativity course in my Master's.

I thank my colleagues and collaborators with whom I have had the opportunity to learn and investigate several interesting problems in physics. It was a pleasure to work with Prof. Sayan Chakrabarti, Dr. Kuntal Nayek, Dr. Adrita Chakraborty and Nibedita Padhi. I further thank Prof. Arnab Kundu and Dr. Suman Das for all the physics discussions.

To my dear friends Krishna, Rittu, Swapan, Upasana, Sanjukta, Nilakshi and Partha, thank you for your endless support and inspiration throughout this journey. My life has changed a lot in a good way after meeting Gariyoshi and Malaya who influenced me drastically in my PhD life. I thank (Lipika, Dipankar, Seshadri, Samik, Chinmoy and Shantanu)- the Heptagon group, for all the feasts and mental support during my PhD. Dipankar- who has always been a good friend to me and Lipika - without whom life here would have been less spicy.

I thank Joydeep da for discussing various useful stuffs in our gang, which motivated me a lot in my PhD. I extend my gratitude to Diksha and Manisha for all the fun we had together at various places. I thank Shivam and Kaustubh for all the physics discussions and Kajal for our weekly calls. I am obliged to Partha da for all the advice and support at various times. Finally, I thank Aditya, Akhil and Rohit for the weekly Polchinski discussions.

I am grateful to Akhil for all the affection, trust and support. From discussing physics to playing Sudoku, irritating me to cheering my little successes, he has been the closest. Thank you for listening to me on my worst days and nights!

I extend my gratitude to my Dewta, Maa, Dada, Dwisha bou, Babu, Uncle, Aunty, Dhun, Usha pehi and Majoni pehi. Especially, my dada (Jyoti) has been a constant supporter and cheerleader of all my achievements. Thank you for being my family!

Thank you all!

Abstract

The thesis constitutes five main chapters. Discussion of our works starts from the second chapter. The second chapter is comprised of two of our research works. In the first work, the holographic phenomena of pole-skipping were studied in the presence of scalar-Gauss-Bonnet interaction in a four-dimensional Anti-de Sitter-Schwarzchild black hole background. We have initiated a novel study to understand the response of those pole-skipping points under the application of external sources. The source is identified with the holographic dual operator of the bulk scalar field with its non-normalizable solutions. We have analysed in detail the dynamics of pole-skipping points in both sound and shear channels, considering linear perturbation in bulk. In the perturbative regime, characteristic parameters for chaos, namely Lyapunov exponent and butterfly velocity, remain unchanged. However, the momentum values of the pole-skipping points in various modes are found to be affected by the scalar source. Further, the diffusion coefficient has been observed to evolve non-trivially under the application of external sources. In the second work, we have investigated the holographic fermionic pole-skipping phenomena for a class of interacting theory in a charged AdS black hole background. We have studied two types of fermion-scalar interactions in the bulk: Dipole and Yukawa type interaction. Depending upon the interaction we have introduced both real and charged scalar fields. We have particularly analyzed the effect of scalar condensation on the fermionic pole-skipping points and discussed their behaviour near critical temperatures. In the third chapter, we have analysed the pole-skipping phenomena of finite temperature Yang-Mills theory with quark flavors which is dual to D3-D7 brane systems in bulk. We also have considered the external electric field in the boundary field theory which is dual to the world volume electric field on the D7 brane. We have worked in the probe limit where the D7 branes do not back-react to the D3 brane background. In this scenario,

we have computed the characteristic parameters of the chaos namely, Lyapunov exponent λ_L and butterfly velocity v_b from the pole-skipping points by performing the near effective horizon analysis of the linearised Einstein equations. Unlike pure Yang-Mills, once charged quarks with a background electric field are added into the system, the characteristic parameters of the chaos show non-trivial dependence on the quark mass and external electric field. We have observed that λ_L and v_b decrease with increasing electric field. We have further performed the pole-skipping analysis for the gauge invariant sound, shear, and tensor modes of the perturbation in the bulk and discuss their physical importance in the holographic context. In the fourth chapter, we have investigated two salient chaotic features, namely Lyapunov exponent and butterfly velocity, in the context of an asymptotically Lifshitz black hole background with an arbitrary critical exponent. These features are computed using three methods: entanglement wedge method, out-of-time-ordered correlator computation and pole-skipping. We have presented a comparative study of the aforementioned features where all of these methods yield exactly similar results for the butterfly velocity and Lyapunov exponent. This establishes an equivalence between all three methods for probing chaos in the chosen gravity background. Furthermore, we have evaluated the chaos at the classical level by computing the eikonal phase and Lyapunov exponent from the bulk gravity. These quantities emerge as nontrivial functions of the anisotropy index. By examining the classical eikonal phase, we uncover different scattering scenarios in the near-horizon and near-boundary regimes. We have also discussed potential limitations regarding the choice of the turning point of the null geodesic in our approach.

List of publications

In particular, the thesis is based on the following publications:

1. B. Baishya and K. Nayek, *"Probing pole-skipping through scalar Gauss-Bonnet coupling"*, *Nucl. Phys. B* 1001 (2024) 116521 [arXiv: 2301.03984] .

2. B. Baishya, S. Chakrabarti, D. Maity *"Effect of scalar condensation on fermionic Pole-Skipping"*, *Eur. Phys. J. C 84 (2024) 12, 1247* [arXiv: 2311.05314] .

3. B. Baishya, S. Chakrabarti, D. Maity, K. Nayek *"Pole-skipping and chaos in D3-D7 brane systems"*, *Phys. Rev. D 110 (2024) 086003* [arXiv: 2312.01829] .

4. B. Baishya, A. Chakraborty, N. Padhi *" Entanglement wedge method, OTOC and pole skipping"*, *Phys.Rev.D 111 (2025) 106013* [arXiv: 2406.18319] .

Conferences attended

1. Student Talks in Trending Topics in Theory (July 4- 15, 2022), IIT Indore, India

2. Nonperturbative and Numerical Approaches to Quantum Gravity, String Theory and Holography (22 August - 02 September 2022), ICTS, Bengaluru, India

3. 17th Kavli Asian Winter School on Strings, Particles and Cosmology (January 9 - 18, 2023), Institute of Basic Science, Daejeon, South Korea

4. Student Talks in Trending Topics in Theory (July 4-15, 2023), IIT Mandi, India

5. International Conference on Gravitation and Cosmology (December 6-9, 2023), IIT Guwahati, India
6. International Strings Meeting (December 10-16, 2023), IIT Bombay
7. Student Talks in Trending Topics in Theory (July 1-13, 2024), IIT Bombay, India
8. Quantum information, Quantum Field Theory and Gravity (August 19-24, 2024), ICTS, Bengaluru, India
9. National Strings Meeting, (December 9-14, 2024), IIT Ropar, India
10. Strings 2025, (January 6-10, 2025), New York University, Abu Dhabi, UAE
11. 19th Asian Winter School on strings, particle physics and cosmology (January 13-22, 2025), TSIMF, Sanya, China

List of Figures

List of Tables

Contents

Chapter 1

Introduction

No problem is too small or too trivial if we can really do something about it.

Richard P. Feynman

In theoretical physics, the quantum theory of fields implements ideas from classical theory of fields, quantum mechanics, and the special theory of relativity. Quantum Field Theory (QFT) is necessary in both particle physics and condensed matter physics, helping us understand how elementary excitations behave both in perturbative and non-perturbative regimes. However, in this framework, it has been proved to be very difficult to incorporate gravity due to its nature as a background, on which the very quantization is being performed. Gravity is addressed through the principle of the General theory of Relativity (GR), introduced by Albert Einstein. It is a theory of spacetime that can assume a non-trivial geometric form in response to any form of energy-momentum tensor. One of the most elegant ways to visualize the geometric nature of spacetime is to place a football on a stretched rubber sheet and observe how the geometric shape of the sheet surrounding the football changes its nature. The heavier the football is, higher the deformation of the sheet becomes. Keeping in mind its non-triviality, this simple observation can be translated into the fact that the more massive an object is, the more it distorts the spacetime. This theory explains how matter bends spacetime, and how that curved spacetime guides the movement of matter.

Treating gravity as a geometrical phenomenon, Einstein wrote down the famous equation,

$$E_{\mu\nu} = R_{\mu\nu} - \frac{1}{2}g_{\mu\nu}R + \Lambda g_{\mu\nu} = 8\pi G_N T_{\mu\nu}\,, \tag{1.1}$$

where $E_{\mu\nu}$ represents the Einstein tensor, $R_{\mu\nu}$ stands for Ricci tensor, $g_{\mu\nu}$ denotes the metric tensor and R represents the Ricci scalar. Additionally, G_N stands for Newton's constant, $T_{\mu\nu}$ represents the stress-tensor and Λ represents the cosmological constant. As gravity is universal in nature, it is proved to be applicable for a wide range of scales starting from near the Planckian to cosmological size. This very equation tells us how our earth moves around the Sun, and the background spacetime can be described precisely by the well-known Kerr geometry [1]. On the cosmological scale, our current universe is observed to be expanding at an accelerating rate. Surprisingly, such expansion can be described by the same equation (1.1) with an energy-momentum tensor which describes the famous cosmological constant $\Lambda > 0$ of our universe. The spacetime with positive cosmological constant is famously known as the de Sitter spacetime [2]. This automatically generalizes two more possible geometries of spacetime with homogeneous energy-momentum tensor. $\Lambda = 0$ corresponds to the Minkowski spacetime or flat spacetime, and $\Lambda < 0$ corresponds to the well-known Anti-de Sitter (AdS) spacetime [3]. More importantly, such spacetime possesses a negative curvature. In terms of its practical application, particularly in describing the evolution of our universe, AdS spacetime may seem to be unmotivated. However, from the theoretical perspective, it has been found to play a key role in understanding a fundamental question related to the quantization of gravity [4, 5]. In spite of classical gravity being extremely successful in explaining physics at a wide range of scales, the question of quantum aspects of gravity is far from being understood. Tracing back the Big Bang expansion of our universe to a very early enough time, one can not avoid quantum effects from gravity [6, 7]. Therefore, it is a very well-motivated problem to put QFT and GR together in the study of our universe.

A correspondence that brought a revolution in the string theory community in the late '90s [8], has indeed found an intriguing connection between GR and QFT. This correspon-

dence has connected QFT and GR in a way that is beyond the conventional approaches known at that time. It is believed that these two theories are just the two sides of the same coin. Soon after this great discovery, Gubser, Klebanov, Polyakov [9] and Witten[10] independently constructed a general mathematical framework that quantitatively connects the two apparently independent theories. Rather than treating Quantum Field Theory (QFT) and General Relativity (GR) as separate frameworks, this approach suggests they provide the same descriptions of the same underlying physics. This idea is formalized in the AdS/CFT correspondence, which is the duality between a theory of gravity in an asymptotically AdS spacetime and a field theory residing on its boundary. In this context, gravity is associated with the bulk, while the conformal field theory (CFT) is localized on the boundary. This dimensional reduction from bulk to boundary gives this duality a holographic nature. Particularly, the gravity theory in classical or semi-classical regimes has been shown to correspond to a large N gauge theory on the boundary, where N effectively describes the number of degrees of freedom. One of the fascinating properties of this correspondence is the strong/weak duality which states that strongly coupled field theory on the boundary is dual to the weakly coupled gravity theory in the bulk. This very strong-weak duality opens up a wider possibility of its applicability in the realm of a wide range of theoretical problems. In particular, strongly coupled many-body physics arises in many condensed matter systems where the phenomenological application of such duality found its natural place to be studied [11–14]. In the following sections, we will give a brief description of AdS/CFT correspondence and how we have used it as a mathematical tool in our work.

1.1 AdS/CFT correspondence

As we have already described, the AdS/CFT correspondence allows us to study strongly coupled gauge field theory on the boundary of AdS in terms of a weakly coupled gravity theory in bulk. In string theory, whereas open string excitations are known to be connected to gauge field theory, closed strings relate to the well-known theory of gravity [8, 15]. In describing

open strings, the concept of D-brane emerges [16], and these are shown to play a key role in deriving this correspondence. In superstring theory, strings live in ten-dimensional target spacetime [15, 17]. Unlike strings, D-branes are objects that exist in the ten-dimensional target space, where open strings are attached to them through Dirichlet boundary conditions. Again, by worldsheet duality, the same D-branes are shown to be the source of closed strings. This precise connection between open and closed strings via D-branes presents itself in terms of AdS/CFT correspondence. However, such correspondence becomes apparent in specific limits of the effective coupling parameter g_sN. Where g_s represents the coupling of strings and N denotes the number of coincident D-branes. In superstring theory, D-branes are extended in any number of $p \leq 9$ spatial dimensions and the world volume of Dp brane is $(p+1)$, which lives in $p+1$ dimensional bulk spacetime. Most studied correspondence is a system involves a large N number of coincident D3-branes in low energy limit of type IIB string theory [1], which lives in ten-dimensional flat Minkowski spacetime.

When $g_sN << 1$, string theory in flat Minkowski space with N coincident D3 branes contains excitations of open strings living on the brane world volume and closed string excitations in the bulk. Therefore, one can express the system in terms of action that constitutes a contribution from closed strings action (brane), open strings action (bulk) and interactions between brane and bulk modes. The intriguing observation made by Maldacena is the decoupling limit of the aforementioned theory for low-energy excitations. In low energy limit, it turned out that all the brane and bulk modes become massless and their coupling vanishes. In this limit, massless excitations of N coincident D3branes give rise to $N = 4$ super Yang-Mills (SYM) theory living in $(3 + 1)$ D brane world volume and the massless bulk modes give rise to type-II B supergravity in flat space.

However, when $g_sN >> 1$, the charged D3 branes become extremely heavy and curve the surrounding spacetime giving rise to extremal black D3 brane supergravity solution [18]

[1] A type of string theory where open strings are attached to D-branes with an odd value of p.

as

$$ds^2 = f(r)^{-\frac{1}{2}}(-dt^2 + dx^2 + dy^2 + dz^2) + f(r)^{\frac{1}{2}}(dr^2 + r^2 d\Omega_5^2) \tag{1.2}$$

$$f(r) = 1 + \frac{4\pi g_s N l_s^2}{r^4} \;\; ; \;\; F_5 = (1+*)dtdxdydzdf^{-1}\,. \tag{1.3}$$

Where, l_s represents the string length, and F_5 denotes the five-form field strength which is coupled to the D3-brane. $r = 0$ implies the location of the horizon. Such a supergravity solution can be realized as the condensation of closed-string modes [19, 20]. In this case, closed strings propagate in the curved background which has been sourced by the D3-branes. For this case also, there exists a decoupling limit for the low-energy excitations. From the asymptotic observer's perspective, there exist two types of low energy limits of perturbation. One is obvious long wavelength perturbation modes moving in the bulk. The second one is the brane fluctuation mode with energy say E_b localized near the horizon of the black D3 branes. Those brane excitations modes when approaching the boundary, their energy becomes exponentially redshifted $E = E_0 e^{-\frac{2\pi}{\beta}t}$, with β being the inverse black D3-brane temperature. These two types of low energy perturbation with respect to boundary observer are again shown to be decoupled. Interestingly, for this case, we have two decoupled type-II B supergravity theories, one in asymptotic flat spacetime and another one in near the horizon region $r = 0$ of the geometry. It is the near horizon geometry of the black D3 brane equation (1.2) which ends up being the well known $\mathrm{AdS}_5 \times \mathrm{S}_5$ described as

$$ds^2 = \left[\frac{r^2}{l^2}(-dt^2 + dx^2 + dy^2 + dz^2) + \frac{l^2}{r^2}dr^2\right] + l^2 d\Omega_5^2\,, \tag{1.4}$$

Where part of the metric within the squared bracket is AdS_5 with radius of curvature defined as $l = (4\pi g_s N l_s^2)^{1/4}$.

Different descriptions of the same systems of N parallel D3 branes from the perspective of field theory of open strings, and supergravity, therefore, have common sector of supergravity in flat space $\mathbb{R}^{9,1}$ background, in their low energy limit. This very fact leads to the famous equivalence of Type IIB supergravity theory on $AdS_5 \times S_5$ and $N = 4, U(N)$ super-Yang-Mills theory in $\mathbb{R}^{3,1}$ by Maldacena [8], and more generally,

Type IIB superstring theory on $AdS_5 \times S_5 \simeq N = 4, U(N)$ *super-Yang-Mills theory in* $\mathbb{R}^{3,1}$

The sign $\simeq$ implies a duality between these two theories. This duality immediately suggests that the parameters on the two sides of the theories are related to each other. On the left-hand side of the duality, we have string coupling g_s and the curvature scale of AdS l. On the field theory side, we have the Yang-Mills coupling g_{YM} and the rank of the gauge group N, which is related through the 't Hooft coupling $\lambda = g_{YM}^2 N$ [21]. The relationship between the aforesaid parameters between these two theories is,

$$g_{YM}^2 = 4\pi g_s \sim \frac{\lambda}{N}, \qquad \frac{l}{l_s} = (4\pi g_s N)^{1/4} \sim \lambda^{1/4}. \tag{1.5}$$

If we avoid string loop corrections, l is considered to be very large in string units and that automatically gives the condition $\lambda >> 1$. This is the strong coupling limit of the gauge theory. Again, to suppress quantum corrections, we can consider g_s to be very small and turn into $\lambda << 1$ of the gauge theory. Hence, classical gravity in the bulk is valid in $N >> \lambda >> 1$ in the parameter space. This specific characteristic gives the correspondence another name: strong/weak duality.

The immediate and the most important check of this duality is that the symmetries of the two sides match with each other [8, 22, 23]. The isometry group of AdS_5 is $SO(4,2)$ and for S_5, it is $SO(6)$. Therefore, full isometry of $AdS_5 \times S_5$ is $SO(4,2) \times SO(6)$. On the CFT side, the conformal group in 4-dimension is $SO(4,2)$. The six scalar fields and four fermions in the gauge theory are related via an R-symmetry as $SU(4) \simeq SO(6)$. The symmetry group of Yang-Mills theory $SO(4,2) \times SO(6)$ is therefore, identical to that of the isometry group of $AdS_5 \times S_5$.

Right after this conjecture was proposed by Maldacena, the detailed dictionary between these two theories has explicitly been formulated by [9, 10]. The most fundamental aspect of this duality is that every classical field living in $AdS_5 \times S_5$ spacetime which is identified as bulk corresponds to a quantum operator of a dual gauge field theory living in the boundary of the same spacetime. It is considered holographic because it links a d dimensional field theory defined by a set of operators $\mathcal{O}_i$ to a gravitational field theory in $d+1$ dimensional

spacetime. This is the dictionary of AdS/CFT which says how to calculate the observables in the boundary theory from bulk computations (see [24–26] for review). The dictionary provides us one to one correspondence between the bulk fields ϕ_i living in $d+1$ dimensional bulk to associated operators $\mathcal{O}_i$ of conformal field theory (CFT) on d dimensional boundary. This theory can be viewed as a sum of operators [26–29],

$$\mathcal{L}_{\text{CFT}} = \sum_i c_i \mathcal{O}_i \,. \tag{1.6}$$

Here, $\mathcal{O}_i$ are the operator residing on the CFT side and c_i are the dimensionless coefficients. Every field in the bulk is dual to an operator in the boundary. More precisely, the question is how to connect a field living in the bulk (gravity) to an operator residing in the boundary (CFT) side. To calculate the observables, we begin by deforming the Lagrangian on the CFT side by adding a source term ϕ_0 that couples to the corresponding operator $\mathcal{O}$ on the boundary side. We can write the deformed Lagrangian as,

$$\mathcal{L} = \mathcal{L}_{\text{CFT}} + \int \mathrm{d}^d x \, \phi_0 \mathcal{O} \,. \tag{1.7}$$

The exponential of the deformed part will give the generating function for the correlation functions of the operator $\mathcal{O}$.

$$e^{W(\phi_0)} = \langle e^{\int \mathrm{d}^d x \, \phi_0 \mathcal{O}} \rangle_{\text{CFT}} \,. \tag{1.8}$$

Where $W(\phi_0)$ is generating functional for the correlation functions of the operator $\mathcal{O}$. The n-point function can be computed by taking the nth functional derivative of $W(\phi_0)$ with respect to the source ϕ_0 and then setting $\phi_0 = 0$. More specifically,

$$\langle \mathcal{O}(x_1) .... \mathcal{O}(x_n) \rangle = \frac{\delta^n W}{\delta \phi_0^n} |_{\phi_0 = 0} \,. \tag{1.9}$$

This is the GPKW dictionary (Gubser, Polyakov, Klebanov, Witten) [9, 10] which says that (d+1)-dimensional on-shell gravitational action is identified with generating function of field theory correlators as

$$e^{W(\phi_0)} = \langle e^{\int \mathrm{d}^d x \, \phi_0 \mathcal{O}} \rangle_{\text{CFT}} = e^{S_{\text{bulk}} \phi(x,r)} = \mathcal{Z}_{\text{gravity}} [\phi_0(x) = \phi(x,r)_{\text{boundary}}] \,. \tag{1.10}$$

Field theory operator	Bulk field
Stress tensor $T_{\mu\nu}$	Bulk graviton $g_{\mu\nu}$
U(1) current J_μ	Bulk gauge field A_μ
Scalar operator $\mathcal{O}$	Bulk scalar ϕ
.....	.....

Table 1.1: Dictionary of AdS/CFT

$\mathcal{Z}_{\text{gravity}}$ is the partition function in the gravity side. The boundary value of the bulk field is recognized as the source of the operator. The correlation functions of operators inserted at different boundary points can be thought of as bulk fields propagating between these points. This map holds true for various fields in the bulk side to the boundary operator which we have shown in Table 1.1. In the next sub-section, we explicitly compute two - point correlation function for a scalar field which we extensively apply in our thesis work.

1.1.1 Scalar two-point function

Let us consider a complex scalar field Φ of mass m propagating in a curved background. We can write the action as,

$$\mathcal{S} = -\int \mathrm{d}^{d+2}x\sqrt{-g}\left(g^{\mu\nu}\partial_\mu\bar{\Phi}\,\partial_\nu\Phi + m^2\bar{\Phi}\Phi\right) . \tag{1.11}$$

We can easily find out the equation of motion for the scalar field,

$$\partial_\mu\left(\sqrt{-g}\,g^{\mu\nu}\partial_\nu\Phi\right) - m^2\sqrt{-g}\,\Phi = 0\,. \tag{1.12}$$

The background we have considered is a Schwarzschild-AdS$_{d+2}$ black holes in planar coordinate as

$$\begin{aligned} \mathrm{d}s^2 &= -\frac{f(r)r^2}{l^2}\mathrm{d}t^2 + \frac{l^2}{f(r)r^2}\mathrm{d}r^2 + + \frac{r^2}{l^2}\mathrm{d}x^i\mathrm{d}x_i, \quad i = 1, ..., d, \\ &= -\frac{f(r)r^2}{l^2}\mathrm{d}\bar{v}^2 + 2\,\mathrm{d}\bar{v}\mathrm{d}r + \frac{r^2}{l^2}\mathrm{d}x^i\mathrm{d}x_i, \end{aligned} \tag{1.13}$$

where $f(r) = 1 - \left(\frac{r_0}{r}\right)^{d+1}$. We set $l = 1$. $r = r_0$ defines the position of the horizon. The Hawking temperature T is related to the emblackeing factor $f(r)$ as $r_0^2 f'(r_0) = 4\pi T$ and r_0 is the horizon radius. For our later purpose, let us symbolize the inverse temperature as $\beta = 1/T = 4\pi/r_0^2 f'(r_0)$. We are interested in calculating the retarded Green's function, and for which we take the following scalar field ansatz $\Phi(r, \bar{v}, x) = \phi(r)e^{-i\omega\bar{v}+ikx}$, with $\bar{v} = t + r_*$ being the null co-ordinate. $\mathrm{d}r^* = \mathrm{d}r/r^2 f(r)$ is the Tortoise coordinate [30]. The radial component of the scalar field $\phi(r)$ satisfies the following equation of motion [31, 32],

$$\frac{\mathrm{d}}{\mathrm{d}r}\left[r^d\left(r^2 f(r)\partial_r\phi(r)\right) - i\omega\phi(r)\right] - i\omega r^d\partial_r\phi(r) - r^{d-2}(k^2 + m^2r^2)\phi(r) = 0\,. \tag{1.14}$$

Near the AdS boundary, the solution behaves as,

$$\phi(r) = r^{\Delta-d-1}\phi_A(\omega, k) + r^{-\Delta}\phi_B(\omega, k)\,. \tag{1.15}$$

Here, ω is the frequency and k is the momentum of the field. The exponent Δ and scalar field mass m are related as,

$$\Delta = \frac{d+1}{2} + \sqrt{\frac{(d+1)^2}{4} + m^2}\,. \tag{1.16}$$

On the CFT side, the exponent Δ can be identified as scaling dimension of the operator $\mathcal{O}$ such that under $x \to \lambda x$ transformation the said operator transforms as $\mathcal{O}'(\lambda x) \to \lambda^{-\Delta}\mathcal{O}(x)$. Now, from the ϕ solution (1.15), we can see that, one part is leading and the other part is sub-leading near the UV boundary ($r \to \infty$). As $\Delta - d - 1 > -\Delta$, so $r^{\Delta-d-1}$ is the leading part (non-normalizable near boundary) and $r^{-\Delta}$ is the sub-leading part (normalizable near boundary). Here, by normalizable, we meant that the action evaluated on the boundary with

this solution is finite. Let us calculate the on–shell variation of the scalar field action as:

$$\begin{aligned}\delta\mathcal{S} &\sim \lim_{r\to\infty}\int \mathrm{d}^{d+1}x\sqrt{-g}(g^{rr}\,\partial_r\Phi\delta\bar{\Phi}) \\ &\sim \lim_{r\to\infty}\int \mathrm{d}^{d+1}x((\Delta-d-1)\phi_A\delta\phi_B+(-\Delta)\phi_B\delta\phi_A+(\Delta-d-1)\phi_A\delta\phi_A r^{2\Delta-d-1}).\end{aligned} \tag{1.17}$$

For typical non-normalizable mode, the third term in the above expression for the linear variation diverges. Hence, one uses the appropriate boundary term of the scalar field action

$$\begin{aligned}\delta\mathcal{S}_{boundary} &\sim (\Delta-d-1)\int d^{d+1}\sqrt{-\gamma}\delta\bar{\Phi}(x,r=\infty)\Phi(x,r=\infty) \\ &\sim (\Delta-d-1)\int d^{d+1}(r^{2\Delta-d-1}\phi_A\delta\phi_A+\phi_B\delta\phi_A+\phi_A\delta\phi_B)\end{aligned} \tag{1.18}$$

By subtracting the boundary term from equation (1.17), we can arrive at the on-shell variation of the action as

$$\delta\mathcal{S}_{On-shell}=\delta\mathcal{S}-\delta\mathcal{S}_{boundary} \sim \int d^{d+1}(d+1)\phi_B\delta\phi_A\,. \tag{1.19}$$

Note the equivalence between the above equation (1.19) and Eq. (1.7) discussed in the previous section. We can straightforwardly identify non-normalizable mode $\phi_A=\lim_{r\to\infty} r^{1+d-\Delta}\phi(r)$ acting as a source. The normalizable part ϕ_B, on the other hand, is recognized as the vacuum expectation value of the dual operator $\mathcal{O}$,

$$\langle\mathcal{O}\rangle=\phi_B=\frac{1}{(d+1)}\frac{\delta\mathcal{S}_{On-shell}}{\delta\phi_A}\,. \tag{1.20}$$

From the linear response theory, we know that $\langle\mathcal{O}\rangle=\phi_B=G^R_{\mathcal{O}\mathcal{O}}\phi_A$. Now, one can immediately identify the Retarded Green's function from the boundary behaviour of the field as the ratio of the coefficients of the subleading part to the leading part,

$$G^R_{\mathcal{O}\mathcal{O}}\approx\frac{\phi_B(\omega,k)}{\phi_A(\omega,k)}=\frac{1}{(d+1)\phi_A}\frac{\delta\mathcal{S}_{On-shell}}{\delta\phi_A}\,. \tag{1.21}$$

This thesis will focus on a phenomenon that deals with this two-point function. For the gravitational perturbations, we will see how this two-point function captures the chaotic properties of a thermal system.

1.2 Chaos

Chaos is related to the sensitivity of the system under the initial condition (see [33–36] for review). In the classical system, the state of a system can be fully described by the locus of coordinate $X = (q, p)$, where q and p represent vectors implying position and associated conjugate momenta respectively. Let us consider a reference trajectory $X(t)$ in phase space with the initial condition $X(0) = X_0$. In the initial condition, making an infinitesimal change $X_0 \to X_0 + \delta X_0$ yields a corresponding change in trajectory as $X(t) \to X(t) + \delta X(t)$. If the system under study is chaotic in nature, the deviation of this new trajectory from the reference one will increase exponentially as time progresses. For such a system, the infinitesimal change can be expressed as

$$|\delta X(t)| = |\delta X_0| \exp(\lambda_L t) \Rightarrow \frac{|\delta X(t)|}{|\delta X_0|} \sim \exp(\lambda_L t). \tag{1.22}$$

This exponent λ_L is s referred to as the Lyapunov exponent. It is always greater than zero. Using the Hamilton's equation, we can write,

$$\begin{aligned} \frac{\delta X(t)}{\delta X(0)} &= \frac{\delta q(t)}{\delta q(0)} \\ \{q(t), p(0)\}_{p.b} &= \frac{\delta q(t)}{\delta q(0)}\frac{\delta p(0)}{\delta p(0)} - \frac{\delta q(t)}{\delta p(0)}\frac{\delta p(0)}{\delta q(0)} = \frac{\delta q(t)}{\delta q(0)} \\ \text{So,} \quad \{q(t), p(0)\}_{p.b} &= \exp(\lambda_L t) \end{aligned} \tag{1.23}$$

The suffix "p.b" refers to the Poisson bracket between the position at time t and the initial momentum. This is the quantity of our interest that quantifies the measure of chaos of a classical system. By inverting the above equation one can compute the Lyapunov exponent in this way,

$$\lambda_L = \lim_{t\to\infty} \lim_{\delta X_0 \to 0} \frac{1}{t} \log\left(\frac{\delta X(t)}{\delta X_0}\right). \tag{1.24}$$

When $\lambda_L > 0$, the trajectory is sensitive to the initial conditions. Then, the system is said to be chaotic which has been studied quite extensively in the literature (for instance see [34–36]). By looking into the last equation (1.23), one can naturally extend such definition for

the quantum system by converting all the phase space variables into operators and Poisson bracket into commutator as,

$$\{q(t), p(0)\}_{p.b} \rightarrow \frac{1}{i\hbar}[\hat{q(t)}, \hat{p(0)}]\,, \tag{1.25}$$

where $\hat{q(t)}$ and $\hat{p(0)}$ are Heisenberg operators. Chaotic behaviour in a system can emerge from a complicated Hamiltonian or its interaction with a thermal heat bath.

Consider a classical thermal system with inverse temperature β. If $G(X)$ is a function of the phase space coordinates, its expectation value over all microstates can be calculated as:

$$\langle G\rangle_\beta = \frac{\int \mathrm{d}X e^{-\beta H(X)} G(X)}{\int \mathrm{d}X e^{-\beta H(X)}}\,. \tag{1.26}$$

Here, $H(X)$ is the Hamiltonian of the system. The above definition can be straightforwardly generalized for a quantum many-body system at finite temperatures. If our physical quantity of interest is taken to be $C(t) = -\left(\frac{\delta X(t)}{\delta X_0}\right)^2$, one can quantify the quantum analogue of the classical Lyapunov exponent using the following measurable quantity,

$$< G(t) >= -\langle\left(\frac{\delta X(t)}{\delta X_0}\right)^2\rangle_\beta = -\langle[\hat{q(t)}, \hat{p(0)}]^2\rangle_\beta\,. \tag{1.27}$$

Since the commutation relation is antisymmetric in nature, it is the expectation value of square of the commutator, which is physically measurable. The minus sign is assumed so that the norm come out to be positive. Indeed, this definition can further be generalized for any two physical operators (W, V) as [37],

$$C(t) = -\langle[\hat{W(t)}, \hat{V(0)}]^2\rangle_\beta\,. \tag{1.28}$$

The quantity $C(t)$ is called the double commutator as two commutators are multiplied in the expression. This quantity is very important in the understanding of chaos in quantum regime. One can further write the double commutator by doing the multiplication of the two commutators in (1.28) as,

$$\begin{aligned} C(t) = \langle & V^\dagger(0)W^\dagger(t)W(t)V(0) + V^\dagger(0)W^\dagger(t)W(t)V(0) \\ & - \underbrace{W^\dagger(t)V^\dagger(0)W(t)V(0) - V^\dagger(0)W^\dagger(t)V(0)W(t)}_{\text{out-of time-ordered}}\rangle_\beta\,. \end{aligned} \tag{1.29}$$

First two terms in the above equation are time-ordered. But, the second two terms are out-of-time-ordered. Considering V and W as unitary ($V^\dagger = V^{-1}, W^\dagger = W^{-1}$) and hermitian operators ($V^\dagger = V, W^\dagger = W$), we can reduce the above double commutator to [38–40],

$$C(t) \approx 2 - 2\langle \text{OTOC} \rangle_\beta \,. \tag{1.30}$$

It is therefore important to realize that the out of time-ordered component of the above expression indeed captures how an early perturbation V affects the later measurements on W. This has been shown to represent one of the well-known diagnostics to measure the chaotic nature of a system.

For the physical behaviour of chaos, it is important to realize two important time scales of a thermal quantum system. The dissipation time scale (t_d) and scrambling time scale (t_*). Dissipation time is defined as after perturbing a thermal state, how much time it takes to dissolve the perturbation and return back to the initial unperturbed state. Scrambling time is defined as the time it takes for information to become distributed across all the degrees of freedom of the system [41, 42]. Basically, at t_*, the commutator becomes of $\mathcal{O}(1)$.

For a class of chaotic systems [43–47] including holographic ones [38, 39, 41], it has been shown that $C(t)$ has different behaviour at different regime of those time scales as follows,

$$C(t) = \begin{cases} N^{-1} \,, & t < t_d \\ N^{-1} e^{\lambda_L t} \,, & t_d << t << t_* \\ \mathcal{O}(1) \,, & t > t_* \end{cases} . \tag{1.31}$$

Where N is the degree of freedom (d.o.f) of the system under consideration. Below the dissipation time, the commutator is involved only with some local operators and so the growth will be slow. The growth is polynomial in time (t) and very weakly dependent on the number of d.o.f (N). After crossing dissipation time, more and more operators are involved in the commutator under expansion, and once the time $t = t_*$ reaches, the system becomes fully scrambled. Then the double commutator becomes of order one and the system saturates. The commutator value has to grow to explain chaos or the OTOC has to decrease.

To understand better, let us express the OTOC in terms of following inner product of two states,

$$\text{OTOC} = \langle\psi_2|\psi_1\rangle\,, \tag{1.32}$$

where,

$$|\psi_1\rangle = W(-t)V(0)|\beta\rangle = e^{-iHt}W(0)e^{iHt}V(0)|\beta\rangle\,, \tag{1.33}$$

$$|\psi_2\rangle = V(0)W(-t)|\beta\rangle = V(0)e^{-iHt}W(0)e^{iHt}|\beta\rangle\,. \tag{1.34}$$

Here, $|\beta\rangle$ is a thermal state. For the $|\psi_1\rangle$ construction, we first operate with V on the thermal state $|\beta\rangle$ at time $t = 0$. It will create a perturbed state. Now, if we evolve the state backwards in time with e^{iHt} below the dissipation time scale, the perturbation will be dissolved. Then after acting with operator W we evolve the state forward in time by operating with e^{-iHt}. Under this time evolution, the previously perturbed state will not appear again. Now for the state $|\psi_2\rangle$, starting from the thermal state $|\beta\rangle$, we first evolve the state backwards in time with e^{iHt} and then operate with W at $t = 0$. Then after we evolve the state forward in time with e^{-iHt}. In this evolved state, operating with an operator V will create a perturbation at $t = 0$. Therefore, we have created two states by repetitive operator insertion at different times and different evolutions. As a result, two states have been created: $|\psi_1\rangle$ with no perturbation and $|\psi_2\rangle$ with a perturbation. The two states are assumed to have less superposition and hence $\langle\psi_2|\psi_1\rangle \approx 0$ suggesting the very large value of the double commutator $C(t)$ (see (1.29)) or the system is said to be chaotic. However, if for some reason $|\psi_1\rangle$ and $|\psi_2\rangle$ has a large superposition, $\langle\psi_2|\psi_1\rangle_\beta \approx 1$, then the double commutator will vanish. In this case, the system is not chaotic.

In the holographic perspective, we can compute OTOC in the bulk gravity side. In the language of holography, boundary thermal state corresponds to a black hole in the bulk. In thermal field theory, the concept of thermofield double state is introduced that can mimic the system to be entangled with an environment due to which thermality is realized. Interestingly the thermofield double (TFD) is a special class of entangled state defined on two copies of the system Hamiltonian which are non-interacting. The TFD state at inverse temperature β

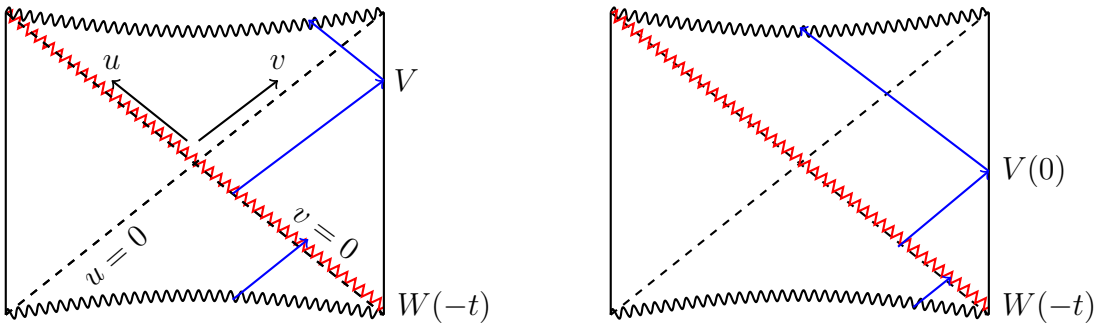

Figure 1.1: *Left:* in state *Right:* out state. In both the diagram, the red zigzag line represents the shock wave. u and v are the null coordinates as described by expression (1.37) and $uv = 0$ is the horizon.

is defined as,

$$|\text{TFD}\rangle = \frac{1}{\sqrt{Z(\beta)}} \sum_n e^{-\frac{\beta E_n}{2}} |E_n\rangle_L |E_n\rangle_R, \tag{1.35}$$

where, Left L, and Right R, correspond to two copies of the Hamiltonian with energy eigenvalue E_n. $Z(\beta)$ is the canonical partition function Then, for any operator $\hat{A}$, associated to the actual quantum system, $\langle \hat{A} \rangle_\beta = Z(\beta)^{-1} \,\text{Tr}\, (e^{-\beta \hat{H}} \hat{A})$.

The most intriguing fact about this formalism is that the TFD state has a nice interpretation in terms of dual two entangled black holes known as eternal black holes [48]. It has two black hole boundaries which are entangled geometrically by a wormhole (see Figure 1.1) that connects their interiors. On the two boundaries, two copies of finite temperature field theories identified as L and R live which are entangled to each other. In this black hole background, the state $|\psi_1\rangle$ stated earlier can be thought of as the "in" state and state $|\psi_2\rangle$ can be thought of as the "out" state. In the bulk, OTOC can be thought of as scattering amplitude between the out-state and the in-state.

We have pictorially represented in-state and out-state in Figure 1.1 with the help of a Penrose diagram of a two-sided black hole. In the diagram, the two thick lines are the two boundaries of the black hole and the two dashed lines are the horizons of the black hole. Basically, it is an extended Penrose diagram that has two asymptotically AdS spacetimes

and hence two theories live on the boundaries of the two spacetimes. The construction of eternal black holes and thermal description is based on Israel's description of a two-sided black hole [49]. The basic elementary state in this holographic set-up is that any boundary perturbation and its evolution in time corresponds to a bulk excitation or particle coming from the past horizon. It hits the boundary followed by entering into the future horizon (see blue lines in Fig.1.1). This immediately suggests that if one introduces a boundary perturbation in the asymptotic past, the bulk particle's energy becomes highly blue-shifted producing a localized shock wave along (v, x) direction represented by red zigzag lines in Fig.1.1, and the amount of perturbation it generates is

$$T_{vv} \sim \frac{1}{\beta} e^{\frac{2\pi t}{\beta}} \delta(v)\delta^{d-1}(x). \tag{1.36}$$

where, (u, v) are the Kruskal-Szekeres coordinates defined as

$$u = e^{\frac{\pi}{\beta}(r_* - t)}, \quad v = e^{\frac{\pi}{\beta}(r_* + t)}. \tag{1.37}$$

Where, $\beta = 1/T = 4\pi/r_0^2 f'(r_0)$ which is also identified as field theory temperature. Such shock wave once absorbed makes the black hole a little bigger with modified geometry,

$$ds^2 = 2G(u, v)dudv + H_{ij}(u, v)dx^i dx^j - 2G(u, v)h(x, t)\delta(v)dv^2 \tag{1.38}$$

Where, $G(u, v) = (\beta^2 G_{tt}/8\pi^2 uv)$, where $G_{tt}(r) = f(r)r^2/l^2$.

In this geometric background particle crossing the shock wave experiences a time shift of an incoming particle represented by blue lines. The amount of shift has been calculated to be directly proportional to the profile of shock wave as $u \to u + h(x, t)$ [38, 39, 50, 51]. Details of this shift will be discussed in the fourth chapter of the thesis. It is this shift function that precisely controls the OTOC correlation functions.

Keeping the aforesaid elementary bulk excitations in mind, we can now represent the bulk states associated with the boundary OTOC states introduced earlier. In the left panel of the figure Figure 1.1, we have represented the in-state $W(-t)V(0)|\beta\rangle$. Acting with operator V on $|\beta\rangle$ is dual to a particle propagating in the black hole background. Now, acting

with operator W at time $-t$ at the boundary means a particle has been released from the asymptotic past ($t < 0$). For the observer at $t = 0$ on the boundary this particle energy will be highly blue shifted as approaching towards the horizon [51]. As mentioned earlier this highly energetic particle can be approximated as a shock wave localized along the horizon in this gravity background [52, 53]. So, the in-state is comprised of two particles, one corresponds V with finite energy and the other one corresponds W with very high energy. In the back reacted shock-wave geometry, the V particle trajectory hits the boundary with a time delay and then falls into the black hole (see the left panel of the figure Figure 1.1). In the right panel of the figure, we have represented the out-state $V(0)W(-t)|\beta\rangle$. The bulk is again comprised of two particles. However, due to operator ordering for this case, particle V does not observe any time shift from the boundary perspective boundary observer. The OTOC is the scattering amplitude of these two states. From both the pictures, it is clear that when there is no shift in the particle trajectory, the OTOC inner product becomes $\langle\psi_2|\psi_1\rangle = 1$ and hence the double commutator $C(t)$ vanishes with no signature of chaos. On the other hand, if the shift is too large, the particle due to V perturbation will fall into the black hole [54], leading to the maximal chaos with $\langle\psi_2|\psi_1\rangle \sim 0$. Interestingly, the shock wave profile, chaos and the time shift tuned out to connected thought following relation

$$C(t,x) \sim h(t,x) \simeq G_N e^{\frac{2\pi}{\beta}(t-\frac{|x|}{v_B})} \quad ; \quad v_B = \sqrt{\frac{G'_{tt}(r_0)}{(d-1)G'_{ii}}}, \tag{1.39}$$

Where the Lyapunov exponent is $\lambda_L = 2\pi/\beta$. Further, if the perturbation is localized in space, the spatial spreading of the perturbation is quantified by another well-known parameter called butterfly velocity v_B.

For a thermal quantum field theoretic system, if one generalizes the double commutator for two operators separated by both spatial and temporal distance (x, t) respectively [38, 55],

$$C(t,x) \approx \langle -[V(0,0), W(t,x)]^2 \rangle_\beta \,, \tag{1.40}$$

for a class of CFT proposed in [56–61] and SYK models [62–65], the above commutator

assumes precisely the same form as Eq.(1.39) signifying chaotic growth,

$$C(t,x) \approx \exp\left\{\lambda_L \left(t - t_* - \frac{|x|}{v_B}\right)\right\}, \tag{1.41}$$

The butterfly velocity, v_B, is essentially the low-energy Lieb-Robinson velocity, which limits the speed at which quantum information can propagate [45]. This velocity controls how information spreads out in space after the scrambling time. In thermal quantum systems with many degrees of freedom, it has been shown that this Lyapunov exponent is bounded [40],

$$\lambda_L \leq \frac{2\pi}{\beta} \tag{1.42}$$

This bound is famously known as MSS bound (Maldacena-Shenker-Stanford bound).

OTOC has been extensively studied in the context of black holes and quantum chaos [38–40, 50, 66]. From the field theory perspective, it has been computed in 2D CFT [59, 67], the Ising chain [68], rational CFT [69], driven CFT [60], and numerically in the quantum Lifshitz model [70]. In the gravitational bulk, OTOC has been calculated in an eternal black-hole geometry [48] when shock waves collide near the black hole horizon [38, 39, 50, 66]. Notably, the chaotic behaviour of a many-body system is also captured in the two-point energy density correlation function at the *pole-skipping* point [71–74], which is holographically related to the near-horizon properties of the bulk metric perturbation. This phenomenon is very useful while studying many-body chaos. For a one-sided black hole background, pole-skipping is enough to comment on the chaotic behaviour of the boundary system. For the shock wave computation, we need to construct a two-sided black hole and calculate the scattering amplitude of particles colliding near the horizon. So, this is a four-point computation in the boundary theory. But, to compute pole-skipping, a two-point function computation is enough. So, it is a convenient method to study chaos. Below, we will briefly review pole-skipping and discuss it with examples.

1.3 Pole-skipping: a brief review

Pole-skipping is a universal phenomenon observed in holographic systems, described by Einstein's gravity coupled with matter fields. One can perceive this phenomenon from the two-point retarded Green's function $G^R_{\mathcal{OO}}$ discussed earlier from the holographic perspective. In the previous section, we discussed about OTOC, which is a four-point correlation function to study the chaotic behaviour of a thermal system. However, with the help of AdS/CFT, one can decode important information about the chaotic nature of a system from a two-point correlation function through the phenomena called pole-skipping [71–73]. Pole-skipping points are a special class of points in momentum space where the two-point correlation function becomes undetermined signifying the existence of non-unique solutions (1.21). In the momentum space, there exists some frequency (ω) and momentum (k) where $G^R_{\mathcal{OO}} = \phi_B/\phi_A$ assumes $0/0$ form. Where ϕ_A and ϕ_B are the source and expectation values of a boundary scalar operator which we discussed in the AdS/CFT section. The same can be generalized for the other fundamental fields in the bulk as well. The point in momentum space (ω_*, k_*) where $\phi_B(\omega_*, k_*) = \phi_A(\omega_*, k_*) = 0$ is called pole-skipping points. Basically, the lines of poles and lines of zeros cross each other at the pole-skipping point. In the holographic set-up, these points depend on the nature of the gravitational background, and near-horizon physics plays a vital role.

In the holographic context, our goal would be to compute the condition for which the source and expectation of the dual boundary operator vanish. A simple example for studying pole-skipping is a minimally coupled scalar field in an asymptotically AdS spacetime. We have already written the equation of motion (EOM) in the Schwarzschild AdS$_{d+2}$ black hole background in equation (1.14). Assuming the regularity condition near the horizon, we expand the solution as $\phi(r) = \phi(r) = (r - r_0)^\alpha(\phi_0 + \phi_1(r - r_0) + ...)$ near the black hole horizon r_0. Inserting this into the above equation of motion, to leading order we get a quadratic equation of α as

$$\alpha(4\pi T\alpha - 2i\omega) = 0\,. \tag{1.43}$$

Solving this, we get two roots for α as,

$$\alpha_1 = 0\,, \qquad \alpha_2 = \frac{i\omega}{2\pi T}\,. \tag{1.44}$$

- At $\alpha_1 = 0$, the solution satisfies ingoing boundary conditions at the horizon and the solution is regular.

- At $\alpha_2 = \frac{i\omega}{2\pi T}$, the field solution near the horizon takes this form,

$$\Phi = e^{-i\omega t + ik^i x_i} e^{\frac{i\omega}{2\pi T}\ln(r-r_0)}(\phi_0 + \phi_1(r-r_0) + ...). \tag{1.45}$$

  This is indeed outgoing near the horizon. Therefore, one can have a unique scalar field solution in the bulk if one chooses only the physical ingoing one. However, non-uniqueness arises if we consider imaginary $\omega = -2\pi i n T$ such that α_2 becomes positive integer n. This choice frequencies turn the solution Φ ingoing at the horizon. The frequency ω_n is known as bosonic Matsubara frequency in the literature [75]. [2]

Therefore, at those special Matsubara frequencies, the scalar field has two regular and ingoing solutions at the horizon. Then the dilemma appears: which solution to choose to calculate the boundary retarded Green's function. This makes the Green's function non-unique at the boundary or leads to multi-valued Green's function [76, 77].

Finally, inserting the scalar field expansion up to the first order in the EOM,

$$\begin{aligned} -\left(k^2 + m^2 r_0^2 + i\omega d r_0\right)\phi_0 + (4\pi T - 2i\omega)\, r_0^2 \phi_1 = 0 \\ \implies \frac{\phi_1}{\phi_0} = \frac{(k^2 + m^2 r_0^2 + i\omega d r_0)}{(4\pi T - 2i\omega)}. \end{aligned} \tag{1.46}$$

With this constraint relation between the field coefficients, one can write down all the higher order coefficients ϕ_n in terms of ϕ_0. For a given ingoing solution, the boundary Green's

[2] These frequencies appear in the Fourier series of expansion of bosonic fields in imaginary time formalism.

$$\phi(i\omega_n) = \frac{1}{\sqrt{\beta}} \int_0^\tau \mathrm{d}\tau e^{i\omega_n \tau} \phi(\tau)$$

. Bosonic field $\phi(\tau)$ is periodic in imaginary time τ and ω_n's are Matsubara frequencies.

function can be shown to follow $G^R_{\mathcal{O}\mathcal{O}} \propto \frac{\phi_1}{\phi_0}$. However, at bosonic Matsubara frequency it turns out that $\omega = \omega_1 = -2\pi i T$ and equation (1.46) boils down to

$$\left(k^2 + m^2 r_0^2 + 2\pi d T r_0\right) \phi_0 = 0\,. \tag{1.47}$$

This immediately implies,

$$\omega_1 = -2\pi i T\,, \qquad k_1^2 = -m^2 r_0^2 - 2\pi d T r_0\,. \tag{1.48}$$

and at this special point, the boundary Green's function becomes undetermined. These are the pole-skipping points. Basically, at this point, the lines of poles and zeroes intersect. We can further generalize those and construct any general order pole-skipping point from the scalar field equation of motion. For example, following the same procedure, the second-order bosonic Matsubara frequency becomes,

$$\omega = \omega_2 = -4\pi i T \;\;;\;\; k_2^2 = -m^2 r_0^2 + 16\pi r_0 T - 2d(1+d) r_0^2 \tag{1.49}$$

At higher Matsubara frequencies also, one can find these pole-skipping points. Doing order-by-order expansion of the field, generally, we compute these points. So, at various orders, one can write the equation of motion in terms of the expansion coefficients. Setting these coefficients to be zero, one can write,

$$M(\omega, k^2).\phi = \begin{pmatrix} M_{11} & 2\pi T - i\omega & 0 & 0 & \dots \\ M_{21} & M_{22} & 4\pi T - i\omega & 0 & \dots \\ M_{31} & M_{32} & M_{33} & 6\pi T - i\omega & \dots \\ \dots & \dots & \dots & \dots & \dots \end{pmatrix} \begin{pmatrix} \phi_0 \\ \phi_1 \\ \phi_2 \\ \vdots \end{pmatrix} = 0 \tag{1.50}$$

It is very easy to write ϕ_n in terms of ϕ_0 from these equations in an iterative manner. But, at higher Matsubara frequency $\omega = -2in\pi T$, the co-efficient of ϕ_n vanishes. So, this is not possible to express the ϕ_n in terms of ϕ_0. However, one can write a submatrix $\tilde{M}$ from the bigger matrix M consisting only of the first n rows and n columns.

$$\tilde{M}(\omega_n, k^2).\tilde{\phi} = 0 \tag{1.51}$$

where, $\tilde{\phi} = (\phi_0, \phi_1, ..., \phi_{n-1})$. For any value of k, if $\tilde{M}$ is invertible, then ϕ_n becomes a free parameter. Then, one can use the other equations of (1.50) to construct a unique ingoing solution with normalization ϕ_n. But, if for a value of k, the $\tilde{M}$ is not invertible, then we get an extra solution which is ongoing. One can compute the pole-skipping points at higher Matsubara frequencies as,

$$\omega_n = -2\pi i n T \, , k^2 = k_n^2 \, , \det \tilde{M}(\omega_n, k_n^2) = 0 \tag{1.52}$$

Similarly phenomena for fermions [78–80], vector [81, 82] and tensor fields [83] have also been extensively studied. However, most of the pole-skipping studies have been performed for non-interacting theories. In this thesis, we consider interacting theories and discuss their behaviour in terms of Gauss-Bonnet-scalar interaction, and fermion-scalar interaction.

Connection to chaos: As discussed in the earlier section, the holographic gravitational shock wave is a useful tool to understand chaos for holographic field theory. Interestingly, this has been further shown to be related to the behaviour of hydrodynamic sound modes corresponding to linearized gravitational waves at those pole-skipping points [84].

$$\omega_* = i\lambda_L, \qquad k_* = \frac{i\lambda_L}{v_B} \, . \tag{1.53}$$

The special points in the sound modes are directly connected to parameters of many-body chaos, namely Lyapunov exponent λ_L and butterfly velocity v_B. The simplest model from which we can realise this phenomenon is SYK chain [62], where the energy-density two-point function takes the form

$$G^R_{T_{00}T_{00}}(\omega, k) = C \frac{i\omega(\frac{\omega^2}{\lambda^2} + 1)}{-i\omega + D_E k^2} \, . \tag{1.54}$$

Where C is a constant and D_E is the energy diffusion constant. The authors have computed the Lyapunov exponent (λ_L) and butterfly velocity (v_B) in this system and found that $\lambda_L = \frac{2\pi}{\beta}$ and $v_B = \sqrt{D_E \lambda_L}$. Again, from the denominator of the above expression, we can see that

it has a line of poles at $\omega = -iD_E k^2$. Now, one can see that this pole line exactly passes through (1.53). But, the interesting point is, at this point, the numerator also becomes zero. Pole-skipping is a general phenomenon observed in systems that exhibit maximal chaos [71].

It suggests that the four-point OTOC computation in strongly coupled theories is holographically dual to probing the system through hydrodynamic sound modes. This connection can be better understood from [72], where the authors have demonstrated that the OTOC and pole-skipping behaviour have the same gravitational source. Near this special point (1.53), they have studied the retarded energy-density correlation function $G^R_{T^{00}T^{00}}$. Considering the background (1.13), if one wishes to calculate the energy-density correlation, then they have to perturb all the longitudinal modes as $g_{\mu\nu} \to g_{\mu\nu} + \delta g_{\mu\nu}(r)e^{-i\omega v+ikx}$. The longitudinal modes in this channel are: $\delta g_{vv}, \delta g_{rr}, \delta g_{rr}, \delta g_{vx}, \delta g_{vr}, \delta g_{xx}, \delta g_{rx}$. We know that the solutions which govern the retarded two-point function are regular and ingoing at the horizon. So, we can expand the perturbations near the horizon r_0 as

$$\delta g_{\mu\nu}(r) = \delta g^{(0)}_{\mu\nu} + \delta g^{(1)}_{\mu\nu}(r - r_0) + \dots . \tag{1.55}$$

Inserting the expansion into the linearised Einstein's equations, we can divide these whole set of equations into two parts: the temporal (vv) component of the equation ($\delta E_{vv} = 0$) and the other component equations ($\delta E_{ab} = 0$, $a, b \neq v$). Here, $E_{\mu\nu}$ is the Einstein tensor as defined in equation (1.1) and $\delta E_{\mu\nu}$ implies the perturbed Einstein equation. At the pole-skipping point, the other component equations are well-defined except the vv component. The vv component of the equation can be written as,

$$\delta E_{vv} = \left(-id\omega r_0 + k^2\right) \delta g^{(0)}_{vv} - i(2\pi T + i\omega)\left[\omega \delta g^{(0)}_{xx} + 2k\delta g^{(0)}_{vx}\right] = 0 . \tag{1.56}$$

We can see that the location of the pole-skipping point is very important in this regard. At $\omega = 2\pi i T$, the above equation reduces to

$$\left(2d\pi T r_0 + k^2\right) \delta g^{(0)}_{vv} = 0 . \tag{1.57}$$

For any generic value of k, we notice that $\delta g^{(0)}_{vv} = 0$. At a specific value of momentum k, the linearised vv component of the equation is zero. That precisely means that there will

not be any constraint relation between the perturbed coefficients. So, there arises an extra ingoing solution at the pole-skipping point which leads to an ill-defined Green's function at boundary. Comparing with expression (1.53), one can easily write,

$$\lambda_L = 2\pi T\,, \qquad\qquad v_B = \sqrt{\frac{d+1}{2d}} \tag{1.58}$$

This is the result for the Schwarzchild-AdS$_{d+2}$ black hole. This is a special case where the butterfly velocity is dimensional dependent only. From expressions (1.58), we can realise that only by studying the linearised vv component of Einstein's equation, one can extract the Lyapunov exponent and butterfly velocity of a strongly coupled field theory. This method is very convenient as we don't need a two-sided black hole to compute the parameters of chaos. So, a two-point function computation is enough to comment on many-body chaos.

A number of research works have investigated the chaotic nature of holographic systems using the pole-skipping (P-S) method in various contexts such as black hole backgrounds [74, 85, 86], plasma physics [87–89], conformal field theories [90–92], topologically massive gravity [93], holographic systems with chiral anomalies [94], little string theory [95], stringy corrections [73], brane systems [96], and higher derivative corrections [86, 97, 98]. This phenomenon has been extensively explored in different directions, including [79, 81, 99–110]. Pole-skipping has also been studied in the context of hydrodynamic transport phenomena [73, 88, 102, 111, 112].

We have organized this thesis as follows: Chapter 1 provides a brief review of AdS/CFT (holographic) correspondence, detailing how to calculate a scalar two-point function in asymptotically AdS spacetime. The chapter also covers the physics of OTOC and chaos from both bulk and boundary perspectives, concluding with a discussion on pole-skipping and a literature review.

Chapter 2 is based on two works [109, 113], where we explore two types of theories. We examine a gravitational theory with a scalar Gauss-Bonnet interaction term, neglecting the back-reaction of higher derivative terms on the background geometry. The dispersion relations for shear and sound modes are modified by these higher derivative terms, and we calcu-

late the Lyapunov exponent and butterfly velocity from the sound channel after performing singularity analysis. We also study fermionic pole-skipping with dipole and Yukawa couplings, where a scalar couples to fermions, leading to a condensate at a critical background temperature. The focus is on how fermionic pole-skipping points change as the temperature approaches the critical value.

In Chapter 3, based on our work [96], we investigate the chaotic behaviour of a holographic QCD model in the presence of an external electric field. We assume that the number of flavor branes is much smaller than the number of color branes, so that back-reaction effects can be ignored. Our findings show that the external electric field reduces the Lyapunov exponent and butterfly velocity up to a certain critical value. We examine shear, sound, and tensor channels in this context.

Chapter 4, based on [114], proves the equivalence of three methods for studying chaos —entanglement wedge, OTOC, and pole-skipping in a non-relativistic background. We demonstrate that all three methods yield the same Lyapunov exponent and butterfly velocity, which depend on the anisotropic index and background temperature. Additionally, we compute the Lyapunov exponent using geodesic instability analysis in the classical regime.

Finally, Chapter 5 summarizes the work and suggests potential future directions.

Chapter 2

Pole-skipping in interacting theories

In high-energy and condensed matter physics, the study of interacting theories is essential to understand many-body physics. In strongly correlated systems, interactions enable the exchange of energy and momentum between particles, leading to transport phenomena that differ significantly from free theories. This makes the study of pole-skipping in interacting theories particularly insightful for examining how chaos and transport emerge from these complex interplays. So far, the pole-skipping studies have been performed with higher curvature corrections [86], finite coupling corrections [97], with various matter fields [80, 105] and in different black hole backgrounds [104, 107, 115, 116]. In this chapter we discuss on our work [98], considering a particular class of higher derivative interacting theory coupled to the scalar field and study its effect on the pole-skipping phenomena. The low energy effective action of string theory particularly brings a special class of higher derivative term called Gauss-Bonnet (GB), and the effect of such term in the pole-skipping context has already been explicitly studied [86, 97], particularly in more than four dimensions. Due to the effect of these corrections, the Lyapunov exponent and butterfly velocity have been analyzed. We aim to understand the effect of the GB term in four-dimensional bulk. In four dimensions, one notes that pure GB term is a topological invariant, and hence does not lead to any modifications at the level of the field equations. One of the non-trivial modifications to theories with GB term is to introduce scalar fields ϕ coupled to the GB term [117]. Our approach in this work was bottom-up and purely phenomenological. With the scalar field coupled to GB theory, we investigated the simultaneous effect of both higher derivative term

and scalar field interaction on the pole-skipping phenomena. The scalar field in the (3+1)-dimensional bulk is associated with a dual scalar operator in the three-dimensional boundary field theory. From the boundary field theory side, we further investigate how the influence of a dual scalar source at the boundary may affect the pole-skipping phenomena which may be interpreted as a stringy effect at low energy. We consider a phenomenological form of the coupling $\zeta(\phi) \sim \phi^p$, where p is an integer. In the top-down string theory construction, a higher derivative Gauss-Bonnet term usually appears with a dilaton scalar where dilaton is coupled exponentially. We further consider the background as a Schwarzchild Anti-de Sitter black hole, whose dual field theory is at a finite temperature. In this background, we study the pole-skipping phenomena. Particularly in the sound channel, the flow and decay of energy density are shown to be affected by the aforementioned interaction. Unlike the free theory, we find decay in momentum density in the shear channel at a higher value of p. The diffusion coefficient has been observed to have a significant effect due to scalar-GB coupling.

We briefly mention the result and methodology of this work as follows: The classical scalar field in the bulk can be understood as dual to a composite scalar operator (say $\mathcal{O}$) in the boundary thermal field theory. Therefore, the classical solution of the scalar field in the bulk with regularity condition at the horizon is interpreted in terms of linear response theory as $\mathcal{O}_c \propto \mathcal{O}_s$. The condensate of the dual operator $\mathcal{O}_c$ is mapped with the normalizable mode of ϕ, and source $\mathcal{O}_s$ associated with the operator is identified with the non-normalizable mode of ϕ. We consider those masses of the scalar field for which the above mapping is unique for simplicity. The relation between $(\mathcal{O}_s, \mathcal{O}_c)$ does depend on how the bulk filed is coupled with the background metric. In all previous studies of pole-skipping, the interaction was taken to be minimal. In this work, we assume the existence of non-minimal GB coupling, and that will naturally modify the relation between $(\mathcal{O}_s, \mathcal{O}_c)$, which we observe to have a non-trivial effect on the pole-skipping phenomena. Particularly, such interaction will be shown to affect the liner momentum k appearing in the dispersion relation. However, as we are not considering the backreaction of the interaction, we do not expect any modification in

the ω value of the pole-skipping points. In the shear channel, we find a similar effect on k. For $p > 3$, we find imaginary k which implies the exponential decay or growth of the corresponding density function. Here we calculate the diffusion coefficient from the lowest point. It shows that the rate of diffusion decreases with the increase of scalar source and it is always below $1/4\pi T$ for $p > 3$. On the other hand, in the sound channel, we find the effect of interaction for all $p > 1$ are similar. In this channel, without interaction, k^4 has pure real (< 0) values. Due to interaction, it encounters an imaginary part which increases with the effect of the scalar source. As the real $k^4 < 0$ gives k with equal real and imaginary parts indicating the energy transport and decay/growth of energy density respectively. With the effect of interaction, the real and imaginary parts of k become unequal. Thus one can conclude this is a result of the variation of thermal transport due to interaction.

2.1 Holographic Gravity Background:

In the holographic model, as we want to study pole-skipping at finite temperatures, we need to use a black hole solution in bulk. We consider a four-dimensional Anti-de Sitter Schwarzchild black hole with scalar propagating in the background. Then, the associated Einstein's action in the bulk theory as,

$$\mathcal{S}_{EH} = \int d^4x\sqrt{-g}\left(\kappa\mathcal{R} + \Lambda - \frac{1}{2}\left((\partial\Phi)^2 + m^2\Phi^2\right)\right), \tag{2.1}$$

where $\kappa = (16\pi G_N)^{-1}$ is a constant related to the four-dimensional Newton's constant with mass dimensions 2 (here we set it to unity.). The associated Einstein's equation and stress-tensor are given by,

$$\mathcal{G}_{\mu\nu} \equiv \mathcal{R}_{\mu\nu} - \frac{1}{2}\mathcal{R}g_{\mu\nu} = \frac{1}{2\kappa}\Lambda g_{\mu\nu} + T^{\Phi}_{\mu\nu}\,, T^{\Phi}_{\mu\nu} \quad = \nabla_\mu\Phi\nabla_\nu\Phi - \frac{1}{2}g_{\mu\nu}\left(\nabla_a\Phi\nabla^a\Phi + m^2\Phi^2\right). \tag{2.2}$$

This gives the $3+1$ dimensional AdS-Schwarzchild black hole solution and scalar solution as

$$ds^2 = L^2\left[-r^2 f(r)dt^2 + \frac{dr^2}{r^2 f(r)} + r^2\left(dx^2 + dy^2\right)\right], \qquad \Phi = 0, \tag{2.3}$$

where $f(r) = 1 - \left(\frac{r_0}{r}\right)^3$ and L is the AdS radius. In the Einstein action, R is the Ricci scalar of the background (2.3) and Λ is related to the cosmological constant in four dimensions. In our case, $\Lambda = 6\kappa/L^2$ and r is the radial coordinate of the black hole with the horizon radius r_0. The horizon radius is related to the temperature T of the black hole as $4\pi T = r_0^2 f'(r_0) = 3r_0$, where prime denotes derivative with respect to r. In the action (2.1), we have considered two-fold perturbation to achieve desired model. First we take perturbation in the background scalar as $\Phi = 0 + \beta \times \phi(r)$ and then we consider the perturbation in the background Lagrangian with a perturbative interaction $\frac{1}{2}\lambda\zeta(\phi)\mathcal{R}_{GB}$, where β and λ are arbitrary coupling constants which are very small ($\ll 1$) real numbers. $\phi(r)$ is the minimally coupled scalar field of mass m. $\zeta(\phi)$ is a dimensionless real scalar functional. We have considered $\zeta(\phi) = L^p\phi^p$, $p \in \mathbb{Z}^+$ setting $L = 1$. The term $\mathcal{R}_{GB}$ is the higher-ordered Gauss-Bonnet curvature term (in $4d$), which is coupled to the scalar $\phi(r)$ through ζ. The Gauss-Bonnet term can be written as,

$$\mathcal{R}_{GB} = \mathcal{R}_{\mu\nu\rho\sigma}\mathcal{R}^{\mu\nu\rho\sigma} - 4\mathcal{R}_{\mu\nu}\mathcal{R}^{\mu\nu} + \mathcal{R}^2.$$

With the scalar-Gauss-Bonnet interaction term, the background action takes the following form as

$$\mathcal{S} = \int d^4x\sqrt{-g}\left[\kappa\mathcal{R} + \Lambda - \beta^2\frac{1}{2}\left(\partial_\mu\phi\partial^\mu\phi + m^2\phi^2\right) - \lambda\zeta(\phi)\mathcal{R}_{GB}\right]. \tag{2.4}$$

Note that in dimension more than four, the GB term can give rise to non-trivial effects. Pole-skipping has been exclusively studied previously in the five dimensions without any scalar source [86] and the back-reaction of the higher curvature has been considered on the background. In our study, we are interested in $p \neq 0$ cases and treating λ as a perturbative parameter, our background will remain unaffected by the back-reaction of the scalar field as the background value of the scalar field is $\Phi = 0$. Taking the variation of the metric tensor

in (2.4), we get the Einstein equation as follows

$$
\begin{aligned}
&(\kappa - 2\lambda\nabla_\rho\nabla^\rho\zeta(\phi))\mathcal{G}_{\mu\nu} - \frac{1}{2}g_{\mu\nu}(\Lambda + \frac{1}{2}\lambda\zeta(\phi)\mathcal{R}_{GB}) \\
&+ \lambda\zeta(\phi)\left(\mathcal{R}_\mu{}^{\rho\sigma\tau}\mathcal{R}_{\nu\rho\sigma\tau} - 4\mathcal{R}_{\rho\mu}\mathcal{R}^\rho_\nu + \mathcal{R}\mathcal{R}_{\mu\nu}\right) - \lambda\left(\mathcal{R}\nabla_{(\mu}\nabla_{\nu)}\zeta(\phi)\right. \\
&\left.-4\mathcal{R}_{\rho(\mu}\nabla_{\nu)}\nabla^\rho\zeta(\phi) + 2\left(g_{\mu\nu}\mathcal{R}_{\rho\sigma} + \mathcal{R}_{\mu(\rho\sigma)\nu}\right)\nabla^\rho\nabla^\sigma\zeta(\phi)\right) - \beta^2 T^\phi_{\mu\nu} = 0,
\end{aligned}
\tag{2.5}
$$

where $\mathcal{G}_{\mu\nu}$ is the Einstein tensor. The aforementioned scalar field ϕ is a minimally coupled scalar in the black hole background (2.1). Due to vanishing background scalar, the stress tensor of the scalar does not appear in the Einstein equation. We can use the standard Klein-Gordon equation with the interaction term for the scalar ϕ equation. In the interaction term, the scalar couples with the second-order curvature terms. Taking this curvature coupling into account the Klein-Gordon equation of ϕ becomes modified as,

$$
\frac{1}{\sqrt{-g}}\partial_\mu\left(\sqrt{-g}g^{\mu\nu}\partial_\nu\phi\right) - m^2\phi + \frac{\tilde{\lambda}}{2}\mathcal{R}_{GB}\frac{\partial}{\partial\phi}\zeta(\phi) = 0. \tag{2.6}
$$

This correction of the KG equation will give $\tilde{\lambda} = \lambda/\beta^2$ order additional contribution in the scalar field solution. We are interested in the linear λ interaction terms in the bulk action. So, the correction in the scalar field solution will not affect our results. We can discard this correction in the KG equation in most of the cases where the full bulk solution ϕ is considered.

We aim to compute the pole-skipping points by doing near-horizon analysis. Therefore, it is fruitful to perform our calculations in the ingoing Eddington-Finkelstein co-ordinate. Because, in this coordinate, we can treat horizon at a regular point. So, it is very convenient for our analysis. We consider $v = t + r_*$, where v is the null coordinate and r_* is the tortoise coordinate. The metric (2.3) transforms into,

$$
ds^2 = -r^2 f(r)dv^2 + 2dvdr + r^2\left(dx^2 + dy^2\right). \tag{2.7}
$$

The metric (2.3) is singular at $r = r_0$. In this new coordinate, the apparent singularity is removed. The metric has rotational symmetry in the (x, y) plane.

In this background, solving the Klein-Gordon equation near the boundary ($r \to \infty$) gives,

$$\lim_{r\to\infty} \phi(r) = \mathcal{O}_s r^{\Delta-3} + \mathcal{O}_c r^{-\Delta}. \tag{2.8}$$

Where, at infinity (where is our boundary), the leading coefficient $\mathcal{O}_s$ is the source, and the subleading coefficient $\mathcal{O}_c$ is the condensation of the dual boundary dual operator. Since we choose the standard quantization, the scaling dimension of the dual operator is $\Delta = 3/2 + \sqrt{9/4 + m^2}$. There is a lower bound on the scalar mass called the bound of BF (Breitenlohner and Freedman) [118] which states that $m^2 \geq -d^2/4$ for $(d+1)$ gravitational background. For the scalar mass $m^2 \geq -\frac{d^2}{4}$, $\mathcal{O}_c$ is always a normalizable mode, which is the standard quantization of the scalar. In this range $\mathcal{O}_s$ acts as source and $\mathcal{O}_c$ as response. But, for $-\frac{d^2}{4} \leq m^2 \leq -\frac{d^2-4}{4}$, both $\mathcal{O}_s$ and $\mathcal{O}_c$ are normalizable. So they source two different theories. Besides the standard one, $\mathcal{O}_c$ sources an alternative quantization in this mass range.

We can easily get the source and condensation from equation (2.8) by performing some algebra, as shown in [119] and get,

$$\mathcal{O}_s = \lim_{r\to\infty} \frac{r^{3-\Delta}\left(\Delta\phi(r) + r\phi'(r)\right)}{2\Delta - 3}, \tag{2.9}$$

$$\mathcal{O}_c = \lim_{r\to\infty} \frac{r^{\Delta}\left((\Delta-3)\phi(r) - r\phi'(r)\right)}{2\Delta - 3}. \tag{2.10}$$

Important to remember that due to regularity conditions at the horizon, we have only one free parameter, and from the boundary field theory point of view the appropriate free parameter $\mathcal{O}_s$ is identified as the source in the boundary which is applied on the system under consideration. Our goal is to investigate the response of such perturbation parameterized by $\mathcal{O}_s$ on the dual field theory particularly on pole-skipping phenomena. To this end let us further point out that in some parameter space, the real scalar field can undergo source-free condensation if the underlying black hole is charged (see [119]). We consider an uncharged black hole, therefore, this does not arise. We leave it for our future study.

2.1.1 Stability analysis of background

Now we would like to comment on the stability of the Schwarzchild-AdS under the given perturbation. In terms of free energy, one expects the perturbative contribution to be sufficiently smaller than the original background contribution. Under a given perturbative interaction, the stability of the system is broadly indicated by the thermodynamic stability. Due to perturbation, the change of free energy of the system should be negligible so that it does not disturb the thermodynamic stability. From the thermal partition function, one can show that the thermodynamic free energy F is related to the on-shell bulk action $\mathcal{S}^E$ in Euclidean signature as $F = T\mathcal{S}^E$ [120]. So comparing the bulk on-shell one can conclude about the stability of the gravity background. So we will perform the holographic renormalization which one needs to regulate the divergence due to the asymptotic AdS. We first consider that the asymptotic boundary is located at $r = r_b$ and add the appropriate counter term S_{ct} [121–124].

$$S_{ct} = \begin{cases} \int d^3x \times r_b^3(2\kappa - \frac{3-\Delta}{2}\phi^2(r_b) - \frac{12\lambda}{(\Delta-3)p+3}\phi^p(r_b)) & \text{for } \Delta \neq 3 - \frac{3}{p} \\ \int d^3x \times r_b^3(2\kappa - \frac{3-\Delta}{2}\phi^2(r_b) - 12\lambda\phi^p(r_b)\ln r_b) & \text{for } \Delta = 3 - \frac{3}{p}. \end{cases}$$

Now, we perform integration on the radial coordinate and finally, we take $r_b \to \infty$ limit in it. Thus we get total on-shell action free from all divergences. Since our background is asymptotically AdS_4, the Gibbons-Hawking-York surface contribution is negligible ($\sim \frac{\Phi(r_b)^p}{r_b^3}$) with asymptotic correction. We will just calculate the change of on-shell action with respect to the unperturbed on-shell action to show the stability of the background. Given the background metric and solving scalar field ϕ from K-G equation (as we are interested in the linear perturbation in action, we exclude λ term correction of K-G equation, we numerically

find the quantity $N_p(m^2) = \text{Log}_{10}\left|\frac{1}{\lambda}\frac{S_\lambda}{S_0}\right|$, where

$$S_0 = \int_{r_0}^{r_b} dr\sqrt{-g}\left[\kappa\mathcal{R} + \Lambda - \frac{1}{2}\left(g^{rr}(\partial_r\phi(r))^2 + m^2\phi(r)^2\right)\right] + r_b^3\left[2\kappa - \frac{3-\Delta}{2}\phi^2(r_b)\right].$$

$$S_\lambda = \int_{r_0}^{r_b} dr\sqrt{-g}\left[\frac{\lambda}{2}\phi(r)^p\mathcal{R}_{GB}\right] - \frac{12\lambda}{(\Delta-3)p+3}r_b^3\phi^p(r_b) \qquad \text{for } \Delta \neq 3 - \frac{3}{p}$$

$$= \int_{r_0}^{r_b} dr\sqrt{-g}\left[\frac{\lambda}{2}\phi(r)^p\mathcal{R}_{GB}\right] - 12\lambda r_b^3\phi^p(r_b)\ln r_b \qquad \text{for } \Delta = 3 - \frac{3}{p}.$$

Now we numerically plot the quantity N_p with m^2 in Figure 1. So to be in perturbative regime we need $\left|\frac{S_\lambda}{S_0}\right| = 10^{N_p}\lambda \ll 1$, i.e., $0 < \lambda \ll 10^{-N_p}$. From the numerical plot, we see that as the absolute value of scalar mass decreases the range of λ value becomes narrow to maintain a stable perturbative regime. Thus we get an upper-bound on λ, i.e. $0 \leq \lambda \ll 10^{-N_p}$. This is shown in Figure 2.1 for various values of p. For example, if $m^2 = -2$ and $p = 2$, we have $N_p = 1.44$, therefore $0 < \lambda \ll 0.035$. Similarly for $m^2 = -2$ and $p = 3$ we have $0 < \lambda \ll 0.001$.

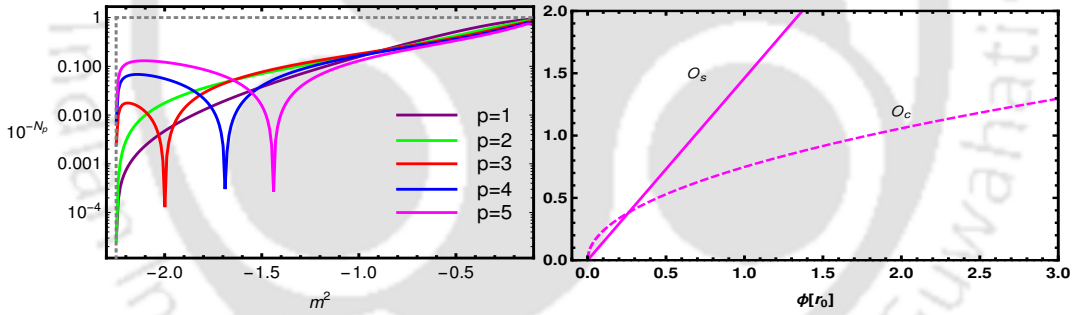

Figure 2.1: Left: 10^{-N_p} vs m^2 for $p = 1,\ 2,\ 3,\ 4\ \&\ 5$. Right: The plot of $\mathcal{O}_s$ (solid line) and $\mathcal{O}_c$ (dashed line) with $\phi(r_0)$ for $r_0 = 1$. Here we take scalar mass $m^2 = -2$.

2.1.2 Scalar field perturbation

In this section, we study the effect of the perturbation on the dispersion relation associated with the scalar field ϕ which is a minimally coupled scalar with mass m. This scalar field ϕ is regular at the horizon and decays in the asymptotic limit. With these conditions, the solution of the scalar can be found from the equation (2.6). Now assuming the scalar field

is a function of the radial coordinate r only, i.e., $\zeta(\phi) = \phi(r)^p$. We take the near-horizon expansion of the field as $\phi(r) = \sum_{n=0}^{\infty} \phi^{(n)}(r_0)(r-r_0)^n$ where, $\phi^{(n)} \equiv \frac{d^n\phi(r)}{dr^n}|_{r=r_0}$. From this series, the first derivative of ϕ at $r = r_0$ can be found as,

$$3r_0\phi'(r_0) = m^2\phi(r_0) - 18\lambda\, p\, \phi(r_0)^{p-1}. \tag{2.11}$$

Similarly, we can also find the higher order derivatives in terms of $\phi(r_0)$. We can solve the scalar field from the K-G equation numerically by providing some horizon value to the scalar field. From this solution, we can evaluate $\mathcal{O}_s$ and $\mathcal{O}_c$ as shown in (2.9). For the near horizon study, the regularity condition of the scalar field on the horizon is very important. So, for numerical evaluation of the source $\mathcal{O}_s$ or to get a consistent solution of $\phi(r)$; $\phi(r_0)$ should be finite and small enough so that the near-horizon expansion remains convergent. From the Figure 2.1 we see that source $\mathcal{O}_s$ and its near horizon value $\phi(r_0)$ is exactly linear. On the other hand, $\mathcal{O}_c$ is linear with only a small value of $\phi(r_0)$ and so with $\mathcal{O}_s$. Both of these quantities are monotonically increasing with the near horizon value of the scalar. Because of this behaviour, we will see later that the pole-skipping points show similar behaviour with sources of both of the allowed quantizations. Now to study the dispersion relation of the scalar field, we take the perturbation $\phi(r) \to \phi(r) + e^{-i\omega v+ikx}\varphi(r)$. The linearized equation from (2.6) is

$$\begin{aligned} &r^2 f(r)\varphi''(r) + \left(r^2 f'(r) + 4rf(r) - 2i\omega\right)\varphi'(r) + (6\lambda(p-1)p(f(r)^2 \\ &- 2f(r) + 3)\phi(r)^{p-2} - \frac{k^2 + m^2r^2 + 2ir\omega}{r^2})\varphi(r) = 0. \end{aligned} \tag{2.12}$$

Expanding the solution near the horizon $r = r_0$ and using the matrix method as given in [78], we get the pole-skipping points (ω, k). We find the lowest order point is $\omega_1 = -\frac{3}{2}ir_0 = -2i\pi T$ and

$$k_1^2 + r_0^2\left(m^2 - 18\lambda p(p-1)\phi(r_0)^{p-2} + 3\right) = 0.$$

Without any perturbation ($\lambda = 0$), we get the results for pure Schwarzchild black hole $k_1^2 = -(3+m^2)r_0^2$, i.e., k_1 is completely imaginary. But, due to the effect of the interaction, k_1

can be real after a particular value of $\mathcal{O}_s$. Similar behaviour is also found for the higher-order pole-skipping points. Though we keep λ small enough in the perturbative regime, k_1^2 becomes positive as the scalar source increases. So k_1 becomes real. From the equation of the perturbed scalar (2.12), it is clear to predict that for $p = 0$ and 1, there is no effect on (ω, k), i.e., we get the values of the black hole background without any perturbation. For $p \geq 2$, p effects k_1 in similar way as λ does. For the small enough $\mathcal{O}_s$, we have found k_1 in the imaginary plane which has been plotted in the left panel of Figure 2.7. Here we have

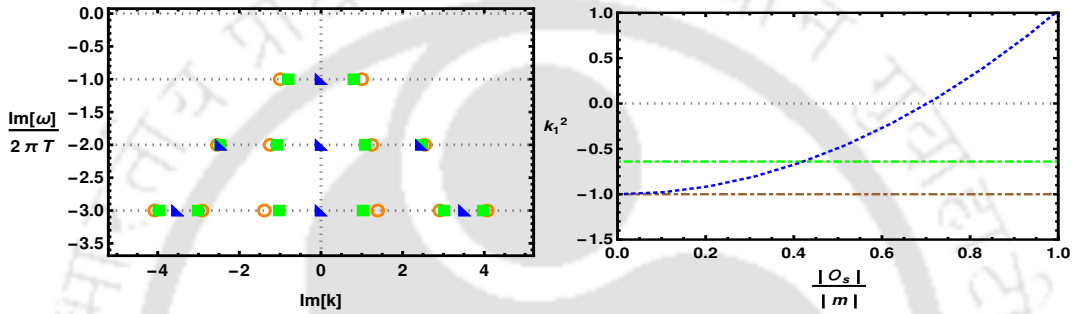

Figure 2.2: Left: The plot of $\frac{\text{Im}[\omega]}{2\pi T}$ vs Im $[k]$ at $|\mathcal{O}_s| = 5.167|m|$ for $p = 1$ (orange circle), $p = 2$ (green rectangle) and $p = 4$ (blue triangle). Right: The plot of k_1^2 vs $\frac{|\mathcal{O}_s|}{|m|}$ for $p = 1$ (brown dot-dashed line), $p = 2$ (green dot-dashed line) and $p = 4$ (blue dotted line). Here we have taken scalar mass $m^2 = -2$, $\lambda = 10^{-2}$ and $r_0 = 1$.

plotted first three PS points (ω, k) in the complex plane for $p = 1,\ 2\,\&\,4$[1]. For $p = 1\,\&\,2$, we have found $2n$-number of points for k_n, i.e., n number of complex roots for k_n. However, for $p = 4$, we have found one real and $n - 1$ complex root of each k_n. Because of these real roots, we have three points on the Im(k) axis. For $p = 2$, the interaction imposes a constant shift in k. But for $p \geq 3$ the shift due to the interaction is proportional to the source. So, as the source goes to zero, k_n becomes the same as the pure AdS black hole. These have been

[1]In the Figure 2.2, $p = 3$ case has been skipped to plot. The reason is the following. From Figure 2.1, we have $\lambda \lesssim 10^{-4}$ for $m^2 = -2.0$ and $p = 3$. At this narrow range of λ, the shift of momentum value is visually negligible. But in this figure, our goal is to neatly represent the variation of the momentum values for various p. So we choose a higher λ to get enough shift in momentum. We have taken $\lambda = 10^{-2}$ which is no more stable region for $p = 3$ but shows clear variation for $p = 1,\ 2\,\&\,4$ at that mass value.

shown in the right panel of the same figure. Here, we have presented the variation of k_1^2 with the scalar source $\mathcal{O}_s$ for $\phi\mathcal{R}_{GB}$, $\phi^2\mathcal{R}_{GB}$ & $\phi^4\mathcal{R}_{GB}$. It is found that k_1 becomes real-valued above a certain value of $\mathcal{O}_s$. Now, if we allow only the imaginary values of k_1, we need to put a cutoff on $\mathcal{O}_s$. The same behaviour can be found for the higher order k. For $\phi^3\mathcal{R}_{GB}$ interaction, we find similar behaviour of pole-skipping points as they do for $p > 2$. But for this interaction, the allowed value of λ is so small that placing it in the same graph is not convenient.

2.2 Metric perturbations

In the pole-skipping phenomena, we study the properties of the stress-energy tensor of the boundary field theory.The AdS/CFT duality says, the bulk fields are mapped to boundary operators. Therefore, the boundary stress-energy tensors are associated with the metric perturbation of the bulk. In bulk, we consider the metric perturbation $g_{\mu\nu} \to g_{\mu\nu} + e^{-i\omega v+ikx}\delta g_{\mu\nu}(r)$, where ω and k are the energy and momentum parameters of the fluctuation, which propagates radially. So, in the boundary field theory, we have two point correlators which are $< T_{vv}, T_{vv} >$, $< T_{vv}, T_{vx} >$, $< T_{vv}, T_{xx} >$, $< T_{vv}, T_{yy} >$ in longitudinal mode and $< T_{vy}, T_{vy} >$, $< T_{vy}, T_{xy} >$, $< T_{xy}, T_{xy} >$ in a transverse mode where $T_{\mu\nu}$ is the stress-energy tensor on the boundary. The metric perturbation: δg_{vv}, δg_{vx}, δg_{xx}, δg_{yy} and δg_{vy}, δg_{xy} are associated to the above two modes respectively. We impose the radial gauge condition $\delta g_{r\mu} = 0$ for all μ. We also use the traceless perturbation for simplicity, i.e., $g^{\mu\nu}\delta g_{\mu\nu} = 0$ which gives $\delta g_{yy} = -\delta g_{xx}$. The longitudinal modes are the scalar modes, it does not couple with a minimally coupled scalar. Therefore we can perturb only $g_{\mu\nu}$ without effecting ϕ. Finally, we have three independent perturbations in longitudinal mode and two in transverse mode.

2.2.1 Shear Channel

As the momentum vector (ω, k) of the metric fluctuation is taken along (v, x)-plane, for shear mode, we consider the components coupled to y-direction. Here we take g_{xy} and g_{vy} as the only non-vanishing perturbations and these are completely decoupled from the longitudinal perturbations. These are associated with T_{vy}, T_{xy} on the boundary. The linearised Einstein equations will give the dynamics of these fluctuations. At some special values of $(\omega,\ k)$, the solution of those equations near the horizon becomes non-unique and gives more than one independent solution. Those special points $(\omega,\ k)$ in this holographic gravity background are connected to the intersection of poles and zeros of the boundary Greens function, $G_{\mu y,\nu y}$ where $\mu,\ \nu = v,\ x$. Now we put these perturbations in the metric (2.7) and find the linearised form of the field equation with only non-vanishing perturbations g_{xy} and g_{vy}. We find that vy, ry and xy components of the linearised equations are only non-trivial, whereas other equations are self-satisfied. Out of these three equations, we find two coupled second-order differential equations as $\delta g''_{vy}(r) = f_1\left(\delta g'_{vy},\ \delta g_{vy},\ \delta g_{xy}\right)$ and $\delta g''_{xy}(r) = f_2\left(\delta g'_{vy},\ \delta g_{vy},\ \delta g_{xy}\right)$. Again, under diffeomorphism transformation with the vector field $e^{-i\omega v+ikx}\xi^{\mu}$, one can show that δg_{vy} and δg_{xy} will form a gauge invariant combination $\mathcal{Z}_{sh}$ as, $\mathcal{Z}_{sh} = \left(\omega\delta g_{xy} + k\delta g_{vy}\right)/r^2$. So, two second-order differential equations (DE) of δg_{vy} and δg_{xy} combine into a single second-order DE of $\mathcal{Z}_{sh}$. The final master equation is

$$\mathcal{M}_{sh}\mathcal{Z}''_{sh}(r) + \mathcal{P}_{sh}\mathcal{Z}'_{sh}(r) + \mathcal{Q}_{sh}\mathcal{Z}_{sh}(r) = 0. \tag{2.13}$$

Where, the coefficients $\mathcal{M}_{sh}$, $\mathcal{P}_{sh}$ and $\mathcal{Q}_{sh}$ are functions of ω, k and $\phi(r)$. The details expressions are given in the appendix. There we have considered the coefficients up to λ order. As $\lambda = 0$ the master equation reduces to the same as the pure AdS black hole. The near horizon structure of the master variable is taken as follows. $\mathcal{Z}_{sh} = \sum_{n=0} Z_n \times (r - r_0)^n$. Now we expand the master equation (2.13) around $r = r_0$. At zeroth order $\mathcal{O}((r - r_0)^0)$, it gives the linear algebraic equation of Z_0 and Z_1. The coefficients of Z_0 and Z_1 are functions of two primary variables ω and k. So, at a particular point, $\omega = \omega_1$ the vanishing of the

coefficient of Z_1 indicates that Z_1 is arbitrary. Again at the same ω value, we find a special value of $k = k_1$ where the coefficient of Z_0 vanishes. Therefore at the point $(\omega_1,\, k_1)$ the near horizon solution of $\mathcal{Z}_{sh}$ is defined with two arbitrary parameter $Z_0,\, Z_1$ and the solution is combination of two arbitrary solutions $C_1(r-r_0)Z_0 + C_2(r-r_0)Z_1$. So we find a non-unique solution at the point $(\omega_1,\, k_1)$ – which is the first order pole-skipping point. Here we find $\omega_1 = -\frac{3}{2}ir_0$ and

$$k_1^2 = 3r_0^2\left[1 - 3\lambda\phi(r_0)^p\frac{\xi(2\xi^2-\xi-17)}{2\xi+1}\right] \tag{2.14}$$

where, $\xi = m^2p/3$. We find ω_1 same as the previous result [76] for AdS_4 black hole. But k_1 contains a non-trivial shift due to the interaction. At $\lambda = 0$, it gives the same k_1^2 as given in [76]. With nonzero λ, the shift in momentum depends on the details properties of the scalar field and its interaction namely, power p of the interacting field ϕ, the value of the field at horizon $\phi(r_0)$ and mass of it m. Now the scalar mass m can not be zero to get the nonzero shift. Also, we need to maintain the value of λ in such a way that the shift remains small enough, i.e., the absolute value of the correction term inside the square bracket in (2.14) is always less than unity[2]. Next few higher-order pole-skipping points are $\omega_n = -\frac{3}{2}inr_0$ for $n = 2,\, 3, \ldots$ and k_n's are higher orders in ξ.

$$\begin{aligned}
k_2^2 &= 3\sqrt{2}r_0^2\left[1 - \frac{3\lambda\xi\phi(r_0)^p}{4(2\xi+1-\sqrt{2})^2}\Big(12\xi^4 + 4(21-\sqrt{2})\xi^3 + (209-74\sqrt{2})\xi^2\right.\\
&\quad \left.+(134-238\sqrt{2})\xi + 136 + 20\sqrt{2})\Big)\right]\\
k_3^2 &= 3\sqrt{3}r_0^2\left[1 + \frac{(5-\sqrt{3})\lambda\xi\phi(r_0)^p}{66(6\xi-3+2\sqrt{3})^3}\Big(-3888\xi^6 + 54432\xi^5 - (32400-21528\sqrt{3})\xi^4\right.\\
&\quad +(976140-224964\sqrt{3})\xi^3 - (1108017-786374\sqrt{3})\xi^2 + (1134059-427507\sqrt{3})\xi\\
&\quad \left.+295381\sqrt{3} - 222201\Big)\right]
\end{aligned}$$

[2]In four-dimensional AdS-Schwarzchild blackhole, the momentum of quasinormal mode in the shear channel is a real number. Here we have considered the perturbative correction, i.e., without backreacted background. So its effect should not change the momentum so much that it turns into a complex or imaginary. To constrain this we should not count the correction under square bracket in (2.14) more than unity.

Here we have consciously ignored the background scalar stress-tensor contribution for the numerical analysis to present the effect of interaction clearly. To do this we have assumed $\beta^2 \ll \lambda \ll 1$. Anyway, we can consider the background profile and carry out the analysis. We have shown it in the appendix. These same assumptions also continue into the sound mode analysis. In all of these k values, the absolute value of the perturbative correction increases with $\phi(r_0)$ i.e. with $\mathcal{O}_{s,c}$ but the sign of the term is solely decided by the factor $m^2 p$. We find that k_n^2 can be both greater or less than $3\sqrt{n}r_0^2$ depending on the value of $m^2 p$. For example $k_1^2 > 3r_0^2$ for $\frac{3}{4}\left(1-\sqrt{137}\right) \leq m^2 p < -\frac{3}{2}$ and $-\frac{9}{4} \leq m^2 \leq -\frac{5}{4}$. However, for other higher mode points, k_n^2 is always less than $3\sqrt{n}r_0^2$. It puts no further restriction on scalar mass. In Figure 2.3, we have plotted $\frac{k_1^2}{3r_0^2}$. The ratio has been varied with the scalar source

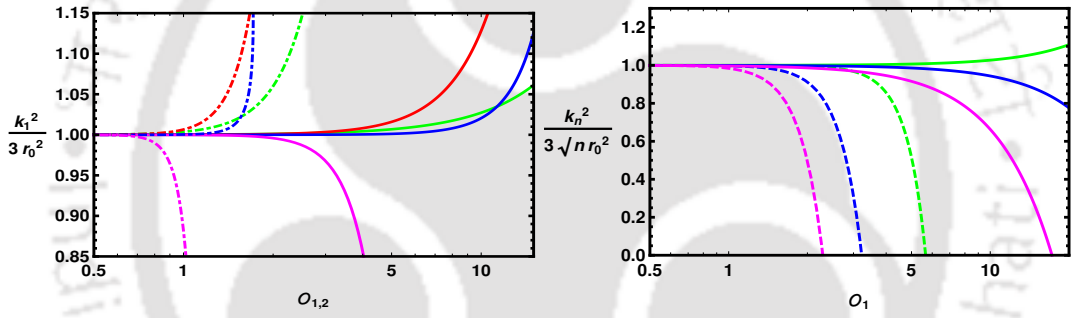

Figure 2.3: *Left*: The plot of $\frac{k_1^2}{3r_0^2}$ vs $\mathcal{O}_2 = \frac{\sqrt{|\mathcal{O}_c|}}{|m|}$ (dashed line) and $\mathcal{O}_1 = \frac{|\mathcal{O}_s|}{|m|}$ (solid line) where $p = 2$ (green color), $p = 3$ (red color), $p = 4$ (blue color), and $p = 5$ (magenta color). *Right*: The plot of $\frac{k_n^2}{3\sqrt{n}r_0^2}$ vs $\mathcal{O}_1$ for $n = 1$ (green color), $n = 2$ (blue color), $n = 3$ (magenta color) and for two different powers $p = 2$ (solid line) and $p = 5$ (dashed line). Here we have taken $\lambda = 10^{-5}$ and $m^2 = -2.0$

.

$\mathcal{O}_s$ and response $\mathcal{O}_c$ for four different order of interaction $p = 2,\ 3,\ 4\,\&\,5$ with perturbation parameter $\lambda = 10^{-5}$ and scalar mass $m^2 = -2$. Figure [2.3] depicts that while the source is off, the ratio is equal to unity. As the source increases from zero, the ratio deviates from unity and increases or decreases according to the power of the Scalar-Gauss-Bonnet interaction term p. At the given mass value, for $0 < p \leq 4$, the ratio increases with the source, and for

$p \geq 5$ the ratio decreases. It has been depicted in the left panel of the figure. In the left plot, we have plotted $k_1^2/(3r_0^2)$ with both $\mathcal{O}_c$ and $\mathcal{O}_s$. This is a very special case from the point of view of the mass of the scalar field ϕ. When $m^2 = -2$, both the asymptotic co-efficients ($\mathcal{O}_c$ and $\mathcal{O}_s$) are normalizable modes in standard and alternate quantizations. So, we can take any one of them as the source and examine the effect on the PS points. To visualise this point, we have shown the effect of sources in both quantizations on the momentum values of the shear mode. We have observed that momentum values are very large at smaller source $\mathcal{O}_c$(in alternate quantization) as compared to source $\mathcal{O}_s$ (in standard quantization). Whereas on the right panel of the same figure, $k_1^2/(3r_0^2)$, $k_2^2/(3\sqrt{2}r_0^2)$ and $k_3^2/(3\sqrt{3}r_0^2)$ have been varied with the scalar source for $p = 2$ and $p = 5$. $k_1^2/(3r_0^2)$ increases with source $\mathcal{O}_1$ for $p = 2$ and decreases for $p = 5$ which is consistent with analytical observations as discussed above. On the other hand, $k_2^2/(3\sqrt{2}r_0^2)$ and $k_3^2/(3\sqrt{3}r_0^2)$ decrease with source for both $p = 2\,\&\,5$. It is expected to find similar behaviour with $\mathcal{O}_2$.

The boundary Green's functions of these quasi-normal modes have been studied earlier for the boundary theory corresponding to the AdS-Schwarzchild bulk [125]. At the hydrodynamic limit, one finds the standard dispersion relation $\omega = \frac{-ik^2}{4\pi T}$ [76]. On the other hand, in our model, we have found that the ω value of the pole-skipping point has matched with the first non-hydrodynamic mode of the quasi-normal mode of pure AdS-Schwarzchild case [125–127]. Now plotting these two modes – standard hydrodynamic mode and our pole-skipping points – we find that the first order pole-skipping point is almost the collision point $(k_{eq},\, \omega_{eq})$ of the hydrodynamic and non-hydrodynamic modes. Therefore, using the first order pole-skipping point, we find the approximate value of the upper bound of diffusion constant [128] and that bound can be written as $\omega_{eq}/(-ik_{eq}^2)$. Here, in our case, we find the diffusion constant $\mathcal{D}_s$ from pole-skipping as

$$\mathcal{D}_s = \frac{i\omega_1}{k_1^2} = \frac{1}{2r_0}\left[1 + 3\lambda\phi(r_0)^p \frac{\xi(2\xi^2 - \xi - 17)}{2\xi + 1}\right] \tag{2.15}$$

Its upper bound is $\mathcal{D}_s(\lambda \neq 0) < \mathcal{D}_s(\lambda = 0)$, i.e., the interaction decreases the upper bound for the negative mass regime. The interaction effect gives a higher upper bound for a positive

mass regime than the pure AdS-Schwarzchild. For $d+2$ dimensional pure AdS-Schwarzchild black hole, the diffusion constant is bounded[3] as $1 \leq 4\pi\mathcal{D}_s T \leq \frac{d+1}{d}$. If the scalar field follows the BF bound and unitarity condition, the scalar mass follows the bound $-2.25 < m^2 < -1.25$. The term $\mathcal{D}_s T$ in (2.15) can be found in $1 \leq 4\pi\mathcal{D}_s T \leq \frac{3}{2}$ for all $p \leq 6$ for the mass ranges given in Table 2.1. In the allowed mass range, the diffusion constant violates the bounds for $p \geq 7$. In Figure [2.4], the left panel shows the plot of the pole-skipping points

Table 2.1: The mass range associated to p to follow the allowed bound of the diffusion coefficient

Interaction order p (ϕ^p)	mass range
$p = 1$	$-2.25 < m^2 < -1.5$
$p = 2$	$-2.25 < m^2 < -1.25$
$p = 3$	$-2.25 < m^2 < -1.25$
$p = 4$	$-2.007 < m^2 < -1.25$
$p = 5$	$-1.605 < m^2 < -1.25$
$p = 6$	$-1.338 < m^2 < -1.25$

in the $\omega - k$ plane. Here we have plotted the standard dispersion relation of the boundary theory in a low-frequency regime, $\omega(k) = -i\mathcal{D}_s k^2$ where $\mathcal{D}_s = \frac{1}{4\pi T}$ given in [76]. When $\lambda = 0$ or the perturbative correction is very small, the first pole-skipping point falls on the dispersion curve. As the effect of interaction increases the first pole-skipping point skips the dispersion curve. But, the other pole-skipping points always stay away from the dispersion curve. At the right panel of Figure [2.4], we have plotted the diffusion constant obtained in (2.15). Here the $4\pi\mathcal{D}_s T$ have been varied with the scalar source in standard quantization and in alternate quantization for three different p values. As the source is zero the diffusion constants for all $2 \leq p \leq 6$ become equal to the upper bound $\frac{3}{8\pi T}$. In the plot, as the source increases from zero, the diffusion constants start falling from the highest bound. For the

[3]For pure Schwarzchild-AdS$_{d+2}$, the shear mode diffusion rate is $\frac{1}{4\pi T}$, where $T = \frac{d+1}{4\pi} r_0$ and r_0 is the horizon [129]. So $\mathcal{D}_s T$ is independent of the dimensions of the black hole. The first order pole-skipping point of the shear mode is dimension dependent, $\omega = -\frac{d+1}{2} i r_0$ and $k_1^2 = \frac{d(d+1)}{2} r_0^2$. Therefore $\frac{i\omega_1}{k_1^2} = \frac{1}{d\, r_0} = \frac{d+1}{d} \frac{1}{4\pi T}$

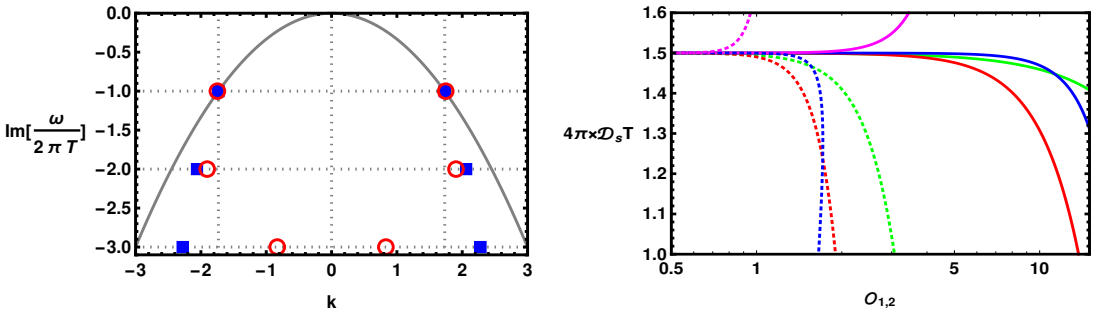

Figure 2.4: *Left*: The plot of P-S points in $\omega - k$ plane for $\lambda = 0$ (blue box) and $\lambda = 10^{-5}$ (red circle), $\mathcal{O}_1 = 5.167$, $p = 3$ and $m^2 = -2$. Three different shapes have been used for three different modes. The solid curve (grey colour) is $\omega = \frac{-ik^2}{4\pi T}$. *Right*: Plot of $4\pi\mathcal{D}_s T$ vs $\mathcal{O}_2$ (dashed line) and $\mathcal{O}_1$ (solid line) for $p = 2$ (green line), $p = 3$ (red line), $p = 4$ (blue line) and $p = 5$ (magenta line). In all these plots, $m^2 = -2.0$ and $\lambda = 10^{-5}$

.

coupling function $\zeta(\phi) \sim \phi^2$ and ϕ^3, the diffusion constant decreases monotonically. At a particular value of the sources, $4\pi\mathcal{D}_s T$ has become equal to unity, and for further increase of source value, it has fallen below its lower bound. For $p = 4$, the diffusion constant is found to remain very close to its upper bound for a comparatively long range of $\mathcal{O}_{1,2}$. After that, it started decreasing very rapidly and reached below 1. At these higher values of the source, the $p = 4$ curve seems to give two different values of $\mathcal{D}_s T$ at a single value of scalar source $\mathcal{O}_{1,2}$. Again, after a certain value of the source, the diffusion constant violates the lower bound. This issue is important to study in future using full backreacted metric [130]. Since our whole calculation is assumed to be in a perturbative regime, we are free to choose any tiny value of λ and any small range of the scalar source for the numerical evaluation. Thus the better estimation in our case always makes $1 \ll 4\pi\mathcal{D}_s T \leq \frac{3}{2}$ for $1 < p \leq 6$.

2.2.2 Sound Channel

The longitudinal components of the metric perturbation are called the scalar or sound modes of the perturbation. These are associated with the energy density correlation on the boundary.

The corresponding stress-energy tensors in this mode are T_{vv}, T_{vx}, T_{xx} and T_{yy} on the boundary field theory. These make the two points correlation functions $G_{vv,vv}$, $G_{vv,vx}$, $G_{vv,xx}$ and $G_{vv,yy}$ which are induced by the metric perturbations. In holographic gravity theory the required perturbations are δg_{vv}, δg_{vx} and δg_{xx} with the trace-less perturbation, i.e., $\delta g_{yy} = -\delta g_{xx}$. Like the shear mode, the metric perturbations also combine into a diffeomorphism invariant master variable $\mathcal{Z}_{so}$.

$$\mathcal{Z}_{so} = \frac{1}{r^2}[k^2\delta g_{vv} + 2\omega\, k\delta g_{vx} - \frac{k^2}{2}(2f'(r) + rf(r) - \frac{4\omega^2}{k^2})\delta g_{xx}] \tag{2.16}$$

The second-order differential equations of $\delta g_{vv}(r)$, $\delta g_{vx}(r)$ and $\delta g_{xx}(r)$ are combined into the master equation.

$$\mathcal{M}_{so}\mathcal{Z}''_{so}(r) + \mathcal{P}_{so}\mathcal{Z}'_{so}(r) + \mathcal{Q}_{so}\mathcal{Z}_{so}(r) = 0 \tag{2.17}$$

The coefficients of (2.17) are linear in λ which are given in the appendix. At $\lambda = 0$, the master equation reduces to the same for the pure Schwarzchild-AdS$_4$ background. Considering the near horizon structure of $\mathcal{Z}_{so}$ similar to $\mathcal{Z}_{sh}$, we find the pole-skipping points for various orders.

Here we find two types of pole-skipping points from this master equation (2.17). The denominator of $\mathcal{P}_{so}$ and $\mathcal{Q}_{so}$ of the above-written master equation contains a common term $3k^2 - 4\omega^2 + k^2 f(r)$. At the near horizon regime, it introduces a pole at $3k^2 - 4\omega^2 = 0$. Now if we consider $3k^2 \neq 4\omega^2$ we get only $\omega_n = -\frac{3}{2}inr_0$ for $n = 1,\, 2\cdots$ at the lower-half plane of complex ω. But when we impose the condition $3k^2 = 4\omega^2$, we can also find ω in the upper-half plane of ω, $\omega_n = \frac{3}{2}inr_0$. It will be discussed later. Now we focus on the unequal condition.

For $3k^2 \neq 4\omega^2$, the first order pole-skipping point is found at $\omega_n = -\frac{3}{2}nir_0 = -2\pi inT$

and first two k_n^4 are given as

$$k_1^4 + 9r_0^4 - 27\xi\lambda(1+i)r_0^4(\xi + 2(1+i))\phi(r_0)^p = 0 \tag{2.18a}$$

$$k_2^4 + 18r_0^4 + \frac{9\lambda\xi p r_0^4}{5\sqrt{2}-2i}(3\xi((5\sqrt{2}-2i)3\xi + 40i - 64\sqrt{2}) + 126(3\sqrt{2}-4i))\phi(r_0)^p = 0 \tag{2.18b}$$

$$k_3^4 + 27r_0^4 - \frac{6\lambda\xi p r_0^4\phi(r_0)^p}{91\sqrt{3}+63i}[27(37\sqrt{3}+3i)\xi^3 - 189(61\sqrt{3}+11i)\xi^2 + 189(306\sqrt{3}+31i)\xi - 27(5369\sqrt{3}+69i)] = 0 \tag{2.18c}$$

Higher order k can also be found in the same way. At $\lambda = 0$, we get the Schwarzchild-AdS$_4$ values $k_1^4 = -9r_0^4$, $k_2^4 = -18r_0^4$ and so on. In (2.18a), the imaginary part $3\lambda\left(12 + pm^2\right) m^2 p r_0^4 \phi(r_0)^p$ is zero for $m^2 = -\frac{12}{p}$ which is beyond the BF bound $-\frac{9}{4} < m^2$ for $p \leq 5$. But for $p \geq 6$ we can make k_1^4 real at that specific value of m^2. A similar behaviour is also expected from the higher order k. Here we have compared the position of pole-skipping points of ϕ^2 inter-

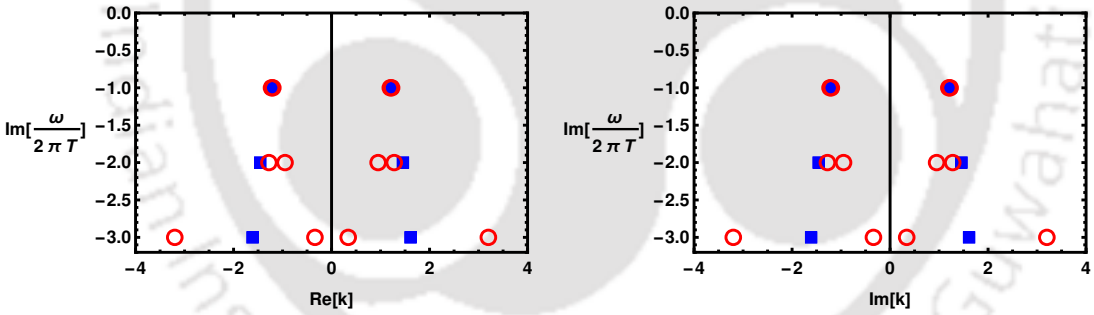

Figure 2.5: The plot of real part (right panel) and imaginary part (left panel) of k vs Im$[\frac{\omega}{2\pi T}]$ for $p = 3$, $m^2 = -2$, $\mathcal{O}_1 = 7.234$, $\lambda = 0$ (blue rectangle) and $\lambda = 10^{-5}$ (red circle).

action with the absence of interaction ($\lambda = 0$) in Figure 2.5. The real and imaginary parts of k have been separately plotted against Im$[\omega/2\pi T]$. In both cases, the real and imaginary parts are almost equal to each other in each mode. For each part, the values have mirror symmetry with respect to the Re$[k]$ = Im$[k]$ = 0 axes. The shift due to interaction is very hard to identify in k_1. For k_2 and k_3 on the other hand, one observes a measurable amount of shift. It has been depicted in above Figure 2.5. Without interaction, in each of these three

modes, only four real numbers make four different complex k (having equal absolute values of real and imaginary parts). With interaction, the same happened for k_1. But for k_2 and k_3 eight real numbers make four complex values of k. Again we have numerically shown the

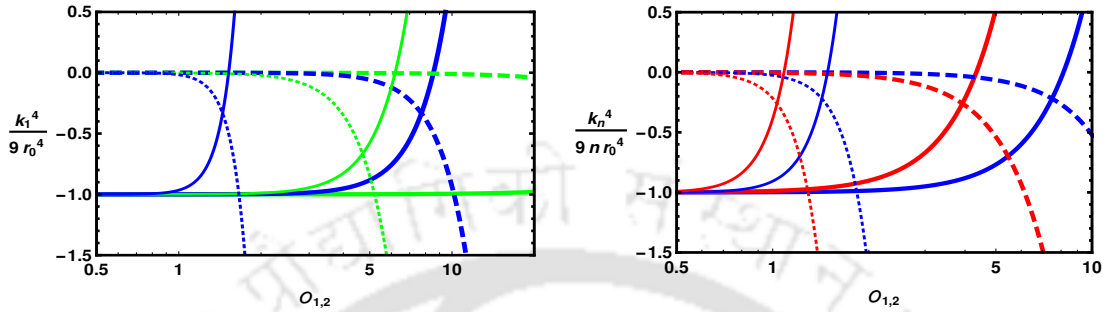

Figure 2.6: *Left*: The plot of real (solid line) and imaginary (dashed line) parts of $\frac{k_1^4}{9r_0^4}$ against $\mathcal{O}_1$ (thick lines) and $\mathcal{O}_2$ (thin lines) for interaction order of scalar $p = 2$ (green colour) and $p = 4$ (blue colour) with $\lambda = 10^{-5}$. *Right*: The plot of real (solid line) and imaginary (dashed line) parts of $\frac{k_n^4}{9r_0^4}$ vs $\mathcal{O}_1$ (thick lines) and $\mathcal{O}_2$ (thin lines) for next two orders of pole-skipping $n = 2$ (blue colour) and $n = 3$ (red colour); with $\lambda = 10^{-5}$ and $p = 3$, $m^2 = -2$.

variation of k with the source $\mathcal{O}_s$ in standard quantization and $\mathcal{O}_c$ in alternate quantization of the scalar in Figure 2.6. At the left plot of this figure, we have plotted the real and imaginary parts of $k_1^4/(9r_0^4)$ against the source in standard and alternate quantization separately. Here we have evaluated the ratio of our result with the result of pure AdS-Schwarzchild. This ratio has no explicit r_0 dependent. It depends on the scalar mass (m), interaction order (p), and scalar value on the horizon. For $\lambda = 10^{-5}$, $m^2 = -2$, and for different p the ratio has been evaluated. When the source is off, the imaginary part of the mentioned ratio is zero, whereas the real part is -1. Which is consistent with the case without interaction. The imaginary part in k^4 is contributed only from the interaction. As we have seen the source is linearly proportional to $\phi(r_0)$, so, $\phi(r_0)$ also goes to zero as the source becomes zero and thus vanishes the correction term in (2.18a). For $p = 2\,\&\,4$ we have found the same behaviour as $\mathcal{O}_{1,2}$ go to zero (eventually $\mathcal{O}_s \to 0$). Now if the source is turned on and increased gradually, as long as the source is small enough, both the imaginary and real parts change slowly with $\mathcal{O}_1$. A

similar behaviour is found for the variation with $\mathcal{O}_2$, but their variation of k^4 is faster. As p increases, the rate of change also increases. The reason is clear from the presence of $\phi(r_0)^p$ factor in the correction terms. During this change the imaginary part of the ratio $k_1^4/9r_0^4$ shifts from 0 towards -1 and the real part changes in the exact opposite direction. Therefore the absolute value of the real (imaginary) part decreases (increases). Thus at some point on $\mathcal{O}_{1,2}$, real and imaginary lines cross each other where their value is exactly equal and lie in between 0 and 1. Again after a certain amount of increase in the source, the real part crosses the horizontal axis. At that value $\mathcal{O}_{1,2}$, k_1^4 becomes a completely imaginary number. These two cross-over points highly depend on p, in the given plot, the $p = 4$ plot has made the first cross-over than the $p = 2$ plot. As the source value increases further the real (imaginary) values become more and more positive (negative). Since we are interested in the perturbative effect, we will not consider those high values of k_1^4. At the right panel of the same figure, we have plotted the ratio $k_n^4/(9nr_0^4)$ for the second ($n = 2$) and third ($n = 3$) order pole-skipping. Here interaction order is fixed at ϕ^3. We have noticed that the behaviour of the real and imaginary parts of the ratio is almost identical to the left panel. We have found that the two cross-overs for each of these two modes of k. At these cross-over points, the behaviour of k_n^2 is completely identical to before. For the higher order of pole-skipping, k_n, the cross-over points come closer to $\mathcal{O}_{1,2} = 0$. Therefore the order of interaction and the order of the pole-skipping affect k in the same way. Mainly the location of the cross-over points is almost identically affected by these two parameters. The cross-over points can be found analytically from (2.18a)-(2.18b). For example, the real and imaginary parts of k_1^4 are $\text{Re}[k_1^4] = -9r_0^4\left(1 - \frac{1}{3}\lambda p^2 m^4 \phi(r_0)^p\right)$ and $\text{Im}[k_1^4] = 3\lambda m^2 p r_0^4 \left(12 + m^2 p\right)\phi(r_0)^p$. The first cross-over happens at the values of $\mathcal{O}_{1,2}$ corresponding to $\phi(r_0) = (-4\lambda m^2 p)^{-1/p}$ where the real and imaginary part of k_1^4 are equal to each other. The (second) cross-over on the $\mathcal{O}_{1,2}$ axis occurs for $\phi(r_0) = \left(\frac{3}{\lambda p^2 m^4}\right)^{1/p}$. Here k_1^4 is completely imaginary $9ir_0^4\left(\frac{12}{m^2 p} + 1\right)$. The first cross-over occurs only if $m^2 < 0$. For a moment if we assume that $m^2 > 0$, then there is only the second cross-over where the k_1^4 becomes completely imaginary.

2.3 Analysis of chaos

2.3.1 From vv component of linearised Einstein equation

From the shock wave analysis [39], it is found that the exponential factor of OTOC can be directly observed from the δE_{00} component of the linearized Einstein equation in the ingoing Eddington-Finkelstein co-ordinate. In the discussed background (2.7), the information about OTOC can be obtained from the vv component of the equation (2.5). Considering the metric perturbation coupled with the vv component of the metric (which are actually the perturbations associated with the sound mode) one can write the δE_{vv} at $r = r_0$ as follows.

$$\delta g_{vv}(r_0)\left(k^2 - 2ir_0\omega\right) + k\delta g_{vx}(r_0)\left(2\omega - 3ir_0\right) = 0 \tag{2.19}$$

Since it is well-known that at the special points $(\omega_*,\, k_*)$, we have no constraint on the perturbed metric components at $r = r_0$ [72]. Therefore in the above equation the coefficients of $\delta g_{vv}(r_0)$ and $\delta g_{vx}(r_0)$ have to zero. Thus we have $\omega_* = \frac{3ir_0}{2} = 2\pi iT$, and $k_*^2 = -3r_0^2$. This (ω_*, k_*) is the zeroth order pole-skipping point which is connected to the Lyapunov exponent and butterfly velocity as shown in (1.53). In our model, we get, $\lambda_L = 2\pi T$ and $v_B = \frac{\sqrt{3}}{2}$, which is the exact result[76] as in the case of background where the coupling term is not present in the action.

2.3.2 From the master equation

In the last section, where we have discussed the pole-skipping of the sound mode perturbation, we took the condition that $3k^2 \neq 4\omega^2$. Because we have seen at the horizon the differential equation (2.17) encounters a singularity. Here we will discuss that issue. From past works [76, 86], we have seen that $3k^2 = 4\omega^2$ had come with a new set of points $(\omega,\, k)$ in $\mathrm{Im}[\omega] > 0$ plane which was actually related to the chaos parameters. In our case, we can re-arrange the master equation (2.17) as

$$\mathcal{Z}''_{so}(r) + P(r)\mathcal{Z}'_{so}(r) + Q(r)\mathcal{Z}_{so}(r) = 0 \tag{2.20}$$

In this equation, the denominators of both $P(r)$ and $Q(r)$ has a multiplicative factor of $(3+f(r))\,k^2-4\omega^2$ which reduces to $3k^2-4\omega^2$ at $r=r_0$. So to get the regular solution of (2.20) at $r=r_0$, we must impose an extra condition on ω or k. Here we will find it.

First we put $k=\frac{2}{\sqrt{3}}\omega$ in (2.20) and expand it around $r=r_0$. We find that $P(r)$ and $Q(r)$ possess the first and second order pole at $r=r_0$.

$$\begin{aligned}
P(r) &= \frac{P_{-1}}{(r-r_0)}+\mathcal{O}((r-r_0)^0)\\
P_{-1} &= -1-\frac{2i\omega}{3r_0}-\frac{144\lambda i r_0\omega\zeta'(r_0)}{3r_0-2i\omega}\\
Q(r) &= \frac{Q_{-2}}{(r-r_0)^2}+\mathcal{O}\left((r-r_0)^{-1}\right)\\
Q_{-2} &= 1+\frac{2i\omega}{3r_0}+\frac{4i\lambda\omega(27r_0^2+12ir_0\omega+4\omega^2)\zeta'(r_0)}{r_0(3r_0-2i\omega)}
\end{aligned}$$

Therefore $r=r_0$ is a regular singular point for the differential equation (2.20). Now, suppose $\mathcal{Z}_{so}$ has a series solution near the singular point given as $\mathcal{Z}_{so}=(r-r_0)^l\sum_{n\in[0,\mathbb{Z}^+)}\mathcal{Z}_n(r-r_0)^n$. The only condition which makes this solution regular at the horizon is $l=0,1,2,\cdots$. Therefore the first recursion relation coming from (2.20) is

$$l^2+l\,(P_{-1}-1)+Q_{-2}=0. \tag{2.21}$$

This gives two roots (say, l_1 and l_2) in the following form.

$$\begin{aligned}
l_1 &= 1-6\lambda(3r_0-2i\omega)\zeta'(r_0)\\
l_2 &= 1+\frac{2i\omega}{3r_0}+6\lambda\frac{(3r_0+2i\omega)^2}{3r_0-2i\omega}\zeta'(r_0)
\end{aligned}$$

So for arbitrary interaction, the only possible integer roots are $l_1=1$ and $l_2=0$. This gives only two values of ω as $\pm\frac{3}{2}ir_0$. Therefore we get the same values of the chaos parameters as we have already found in the last subsection. Generally, near-horizon analysis of the vv component of Einstein's equation is adequate to extract the chaotic parameters of the system. In this work, we have investigated the chaotic property of the system with another approach also: from the singularity analysis of the master equation. We found an exact match between the Lyapunov exponent from both analyses.

In this work, we have mainly studied the effect of higher derivative terms on pole-skipping points. We have analysed the scalar and metric perturbations and the dispersion relations from these modes. In the next section, we will study the fermionic channel and investigate the effect of scalar condensate on fermionic pole-skipping points.

2.4 Scalar condensation in fermionic sector

Despite various studies[78–80], the fermionic pole-skipping still lacks physical motivation. In this work, we have given a novel interpretation of fermionic pole-skipping in the presence of a condensate term. Perturbing the fermion in a black hole background, one can study the fermionic pole-skipping. It has been observed that the pole-skipping points recovered from the fermionic Green's function match with the pole-skipping points extracted from the near-horizon analyses. Similar to the pole-skipping phenomenon, this intersection of lines of poles and zeroes occurs in some overdoped metals. Experimental studies on doped cuprates revealed this anomalous behaviour. Generally, the Fermi surface is defined by the poles of Green's function $G(k,\omega)$ at frequency $\omega = 0$ (near T_c). In the Mott insulator, the Fermi surface disappears while the zero surface appears. So, the point of transition from metals to insulators can be thought of as a pole-skipping point, where both poles and zeroes surfaces overlap. However, it's still a point of discussion how these metals transit into the Mott insulator[131]. Studying pole-skipping in holographic systems may give an insight into the transition. The dipole coupling model can be a very good candidate for studying this overlapping phenomenon[132].

In this work, we investigated the holographic fermionic pole-skipping phenomena for a class of interacting theory in a charged AdS black hole background. We have studied two types of fermion-scalar interactions in the bulk: Dipole and Yukawa type interaction. Depending upon the interaction, we introduced both real and charged scalar fields. We have particularly analyzed the effect of scalar condensation on the fermionic pole-skipping points and discussed their behaviour near critical temperatures. We consider an asymptotically AdS

background with a charged black hole in the bulk. In our present study, we particularly focus on investigating the influence of different interactions in the phenomena of pole-skipping. We consider charged fermions propagate in the Reissner-Nordström-AdS$_4$ black hole background with different coupling terms such as dipole coupling and Yukawa coupling. We further assume that those couplings are facilitated by a bulk scalar, for which we consider both neutral and charged scalar fields. We investigate the non-trivial effect of different scalar field configurations on fermionic pole-skipping phenomena. We will solve the scalar field in RN-AdS$_4$ background and this geometry has a metric as (setting AdS radius $L = 1$),

$$dS^2 = r^2\left[-f(r)dt^2 + dx^2 + dy^2\right] + \frac{1}{r^2 f(r)}dr^2 \tag{2.22}$$

The emblackening factor $f(r)$ and gauge field at the horizon $r_0 = 1$ is,

$$f(r) = 1 + \frac{3\eta}{r^4} - \frac{1+3\eta}{r^3}, \quad A_t = \mu\left(1 - \frac{1}{r}\right)dt \tag{2.23}$$

We have treated $\frac{Q^2}{3}$ as η, where Q is the charge of the black hole and μ is the chemical potential. The temperature of the Black hole is $T = \frac{3}{4\pi}(1-\eta)$ and we will work in the range $0 < \eta < 1$.

2.4.1 Real scalar field

We consider the action that coupled to gravity in AdS$_4$ with real massive scalar field Φ is,

$$\mathcal{S} = \frac{1}{2\mathcal{K}^2}\int d^4x\sqrt{-g}\left[\mathcal{R} + \frac{6}{L^2} - \frac{1}{4}F^2 + \frac{1}{\lambda}\left(-\frac{1}{2}g^{\mu\nu}\nabla_\mu\Phi\nabla_\nu\Phi - V(\Phi)\right)\right], \tag{2.24}$$

where L is the AdS radius and λ is the coupling constant. Later on, we will set $L = 1$ for our convenience and λ to be very large. We choose the potential as,

$$V(\Phi) = \frac{1}{4}\left(\Phi^2 + m_\Phi^2\right)^2 - \frac{m_\Phi^4}{4}. \tag{2.25}$$

We derive the scalar field equation and get

$$\frac{1}{\sqrt{-g}}\nabla_\mu\left(\sqrt{-g}g^{\mu\nu}\nabla_\nu\Phi\right) - \left(\Phi^2 + m_\Phi^2\right)\Phi = 0\,. \tag{2.26}$$

Now, we will shift our co-ordinates to ingoing Eddington-Finkelstein co-ordinates by making the following transformation,

$$v = t + r_*, \qquad \frac{dr_*}{dr} = \frac{1}{r^2 f(r)}, \qquad r_0^2 f'(r_0) = 4\pi T, \tag{2.27}$$

where T is the Hawking temperature. In the new coordinate, the metric and gauge connection are expressed as,

$$dS^2 = -r^2 f(r) dv^2 + 2dvdr + r^2(dx^2 + dy^2), \tag{2.28}$$

$$A = \mu \left[1 - \left(\frac{r_0}{r}\right)\right] dv. \tag{2.29}$$

Considering $\Phi(r, v, x, y) = \phi(r)$, the Klein-Gordon (K-G) equation becomes,

$$\phi''(r) + \left(\frac{f'(r)}{f(r)} + \frac{4}{r}\right)\phi'(r) - \frac{(\Phi^2(r) + m_\phi^2)}{r^2 f(r)}\phi(r) = 0\,. \tag{2.30}$$

The above equation is the radial part of the whole K-G equation, where $\phi(r)$ is the radial part. As we want to solve the radial equation, we have not considered the time and spatial part. Expanding the equation (2.30) upto first order at the horizon yields the following equation,

$$\phi'(r_0) = \frac{(\phi(r_0)^2 + m_\Phi^2)\,\phi(r_0)}{r_0^2 f'(r_0)}\,. \tag{2.31}$$

The asymptotic (at $r \to \infty$) behaviour of equation (2.30) gives,

$$\lim_{r\to\infty} \phi(r) = \mathcal{O}_1 r^{\Delta-3} + \mathcal{O}_2 r^{-\Delta}\,, \tag{2.32}$$

where, at infinity (where is our boundary), normalizable co-efficient $\mathcal{O}_1$ is generically identified as a source and non-normalizable co-efficient $\mathcal{O}_2$ is the condensation and scaling dimension of operator, $\Delta = \frac{3}{2} + \sqrt{\frac{9}{4} + m_\Phi^2}$ is related to mass of scalar. We have previously discussed this from the equation (2.8). If we consider the mass within the specific range $-\frac{9}{4} < m_\Phi^2 < -\frac{5}{4}$, there exist two different AdS-invariant quantization schemes [133]. One Lagrangian can give rise to two theories in AdS space depending upon the scheme. Both $\mathcal{O}_1$ and $\mathcal{O}_2$ are normalizable solutions[134] with this given m_Φ^2. So, we can treat any of them as

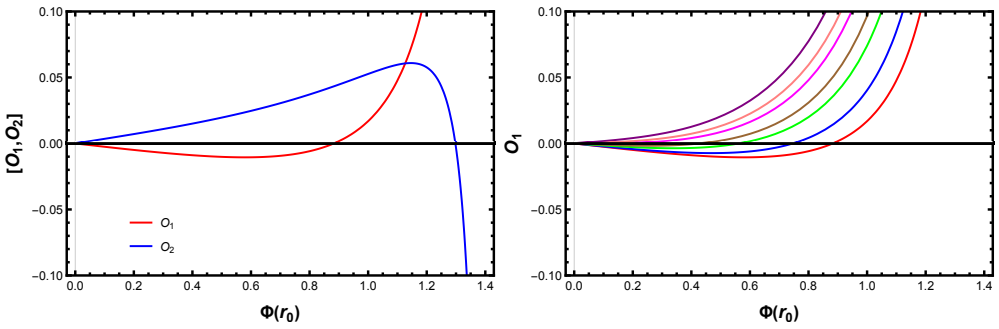

Figure 2.7: *Left:* Behaviour of $\mathcal{O}_1$ and $\mathcal{O}_2$ with increasing horizon value of real scalar field at T=0.0002. *Right:* Behaviour of $\mathcal{O}_1$ with horizon value of real scalar field by varying temperature. The temperature values from the purple curve to the red curve are (0.0016, 0.0012, 0.001, 0.0007, 0.0005, 0.0003, 0.0002) respectively. We have fixed $m_\Phi^2 = -2.1$ in both the plots. The critical temperature T_c has been calculated from the curve beyond which it does not touch the horizontal axis.

a condensate of the field theory operator depending upon the scheme. From equation (2.32), we can write,

$$\lim_{r\to\infty} r\phi'(r) = (\Delta-3)\mathcal{O}_1\, r^{\Delta-3} - \Delta\mathcal{O}_2\, r^{-\Delta}\,. \tag{2.33}$$

Solving the K-G equation near the boundary, we can easily write $\mathcal{O}_1$ and $\mathcal{O}_2$ as,

$$\mathcal{O}_1 = \lim_{r\to\infty} \frac{r^{3-\Delta}\left(\Delta\phi(r) + r\phi'(r)\right)}{2\Delta-3}, \tag{2.34a}$$

$$\mathcal{O}_2 = \lim_{r\to\infty} \frac{r^{\Delta}\left((\Delta-3)\phi(r) - r\phi'(r)\right)}{2\Delta-3}. \tag{2.34b}$$

Now, choosing the standard scheme of quantization, we can treat $\mathcal{O}_1$ as the source and $\mathcal{O}_2$ as condensate. We derive the equation of motion for the scalar field and impose regularity at the horizon to establish the boundary conditions. Using the shooting method, we then solve for the scalar field from the near-horizon region to the boundary by appropriately choosing the mass of the scalar field (m_Φ), the temperature, and the scalar field value at the horizon ($\phi(r_0)$). Once the numerical solution is obtained we compute $\mathcal{O}_1$ and $\mathcal{O}_2$ from eq. (2.34) as depicted in the left panel of Figure 2.7 at T=0.0002. The right panel of Figure 2.7 is generated by varying the temperature to study the source behaviour. We can see from the

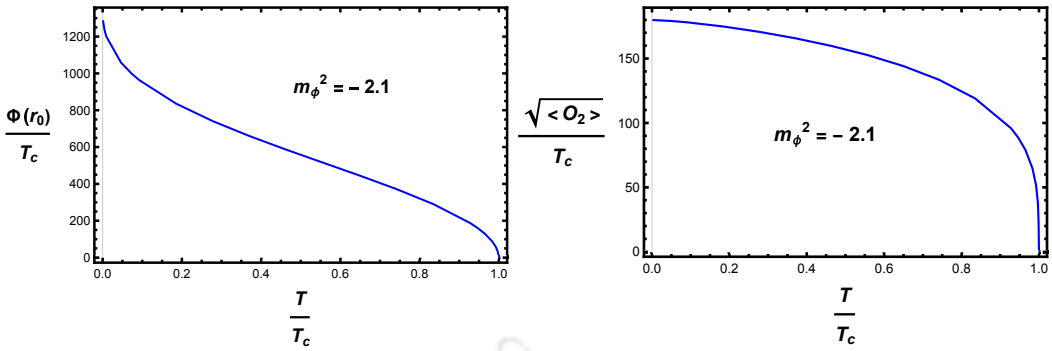

Figure 2.8: *Left:*Behaviour of $\phi(r_0)$ with increasing temperature. *Right:* Behaviour of $\sqrt{\mathcal{O}_2}$ by varying temperature. Both the plots are for real scalar fields. We see that at a certain value of temperature, the horizon value of the field vanishes and the condensate also vanishes at the same temperature. $< . >$ means the vacuum expectation value of the operator.

right plot of the Figure 2.8 that as we increase the temperature, after a critical temperature the horizon value turns to zero. With the given parameters $m_\phi^2 = -2.1$, the critical temperature is obtained as $T_c = 0.0011$. Near this critical temperature T_c, we have fitted $\phi(r_0)$ with $\gamma(T_c - T)^\delta$, which gives the exponent value $\delta \approx 0.56 \pm 0.009$ and $\gamma \approx 40.91$. The exponent is close to the mean field value $1/2$. Near $T = T_c$, to the leading order we can assume $\phi = \epsilon^\delta(\psi(r) + \mathcal{O}(\epsilon))$ with $\epsilon = T_c - T$, and $\delta > 0$. For the phase transition to occur, it is the ϕ^2 term that plays an important role in equation (2.30). Since near $T = T_c$, the coefficients of ϕ'' and ϕ' are polynomials in ϵ. The coefficient ϕ^2 should also be polynomial in ϵ for consistency and hence 2δ should be integer with its lowest value being $\delta = 1/2$.

2.4.2 Charged scalar field

Now, we consider a minimally coupled charged scalar field $\tilde{\Phi}$ in Reissner-Nordström-AdS$_4$ (RN-AdS$_4$) black hole space-time ,

$$\mathcal{S} = \frac{1}{2\mathcal{K}^2}\int d^4x\sqrt{-g}\left[\mathcal{R} + \frac{6}{L^2} - \frac{1}{4}F^2 + \frac{1}{\lambda}\left(|\partial\tilde{\Phi} - iq_sA\tilde{\Phi}|^2 - V(\tilde{\Phi})\right)\right] .$$

Again we will consider λ to be very large so that the charged scalar does not back-react on the background geometry. Here, q_s is the charge of the scalar field and A is the gauge field.

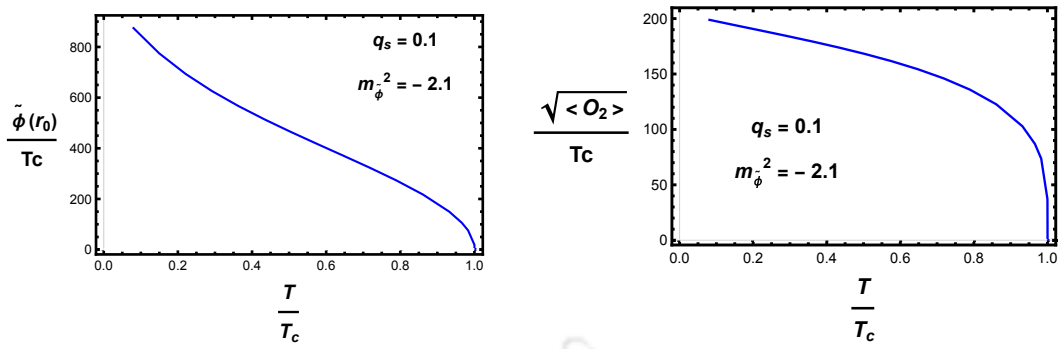

Figure 2.9: *Left:* Behaviour of horizon value of the scalar field with temperature. *Right:* Behaviour of $\sqrt{\mathcal{O}_2}$ with temperature. Both the plots are for charged scalar fields. At a certain value of temperature T_c, we see that the horizon value of the charged scalar field and charged scalar condensate vanishes.

We will work with the same potential as in the case of the real scalar field, but ϕ is replaced by $|\tilde{\Phi}|$. Assuming the ansatz $\tilde{\Phi} = \tilde{\phi}(r)$, we get the K-G equation as

$$\tilde{\phi}''(r) + \left(\frac{f'(r)}{f(r)}\right)\tilde{\phi}'(r) - \frac{1}{r^2 f(r)}\Big((m^2 + \tilde{\phi}^2(r)) - q_s^2 A^2(r) f(r)\Big)\tilde{\phi}(r) = 0\,. \tag{2.35}$$

Solving the equation of motion (EOM) near the AdS boundary, we can calculate the source and condensate value which gives the same form as (2.34). The asymptotic behaviour of this EOM gives the same form as equation (2.32). So, with the same approach as in the case of the real scalar field, we can calculate $\mathcal{O}_1$ and $\mathcal{O}_2$ numerically for the charged case also.

In Figure 2.9, we choose to work in standard quantization. For the given mass $m_{\tilde{\phi}}^2 = -2.1$ and charge $q_s = 0.1$ the associated critical temperature comes out to be $T_c = 0.0014$. We can see that at critical temperature T_c, both the horizon value of the scalar field and condensate become zero. Near this critical temperature T_c, we have fitted $\tilde{\phi}(r_0)$ with $\alpha(T_c - T)^\beta$, which gives the exponent value $\beta \approx 0.58 \pm 0.01$ and $\alpha \approx 45.38$. Here the exponent is close to the mean field value which is expected.

2.5 Pole-skipping analysis

For the pole-skipping phenomenon, we will be working in ingoing Eddington-Finkelstein co-ordinates (2.28). Since our metric is not diagonal, we choose a frame given by,

$$E^{\underline{v}} = \frac{1+f(r)}{2} r dv - \frac{dr}{r}; \quad E^{\underline{r}} = \frac{1-f(r)}{2} r dv + \frac{dr}{r},$$
$$E^{\underline{x}} = r dx; \quad E^{\underline{y}} = r dy, \tag{2.36}$$

for which

$$ds^2 = \eta_{\underline{ab}} E^{\underline{a}} E^{\underline{b}} \qquad \eta_{\underline{ab}} = diag(-1,1,1,1).$$

The underlined co-ordinates are assumed to be flat tangent space co-ordinates and the non-underlined are the spacetime co-ordinates. The Gamma matrices in appropriate basis are assumed as,

$$\Gamma^{\underline{r}} = \begin{pmatrix} \mathbb{I} & 0 \\ 0 & -\mathbb{I} \end{pmatrix}, \qquad \Gamma^{\underline{v}} = \begin{pmatrix} 0 & i\sigma^2 \\ i\sigma^2 & 0 \end{pmatrix} \tag{2.37}$$

$$\Gamma^{\underline{x}} = \begin{pmatrix} 0 & \sigma^1 \\ \sigma^1 & 0 \end{pmatrix}, \qquad \Gamma^{\underline{y}} = \begin{pmatrix} 0 & \sigma^3 \\ \sigma^3 & 0 \end{pmatrix}. \tag{2.38}$$

In the above-written Gamma matrices, σ's are the Pauli matrices. We consider the interacting charged Fermion Lagrangian as

$$\mathcal{L} = \sqrt{-g} i \bar{\Psi} (\not{D} - m + \zeta(\phi)) \Psi \tag{2.39}$$

Where,

$$\not{D} = e^M_{\underline{c}} \Gamma^{\underline{c}} (\partial_M + \frac{1}{4} \omega_{\underline{ab}M} \Gamma^{\underline{ab}} - iqA_M), \tag{2.40}$$

here, M is space coordinate, a, b, c are flat coordinates, $e^M_{\underline{c}}$ are vielbein and $\omega_{\underline{ab}M}$ are spin connection terms. $\Gamma^{\underline{ab}}$ is a Gamma matrix that will follow Clifford algebra. Now, in this section, we will calculate the P-S points for the following fermionic coupling prescription, $\zeta(\phi)$ as

- When $\zeta(\phi) = -ip\phi\not{F}$: The interaction term $-ip\bar{\psi}\phi\not{F}\psi$ is known as dipole coupling where the gauge field A_μ is coupled with a real scalar field $\phi(r)$ with a coupling parameter p. Here, $\not{F} = \frac{1}{2}\Gamma^{\underline{ab}} e^M_{\underline{a}} e^N_{\underline{b}} F_{MN}$ and F_{MN} is the electromagnetic field strength.

- When $\zeta(\phi) = g\phi$: The interaction term $g\bar{\psi}\phi\psi$ is the Yukawa coupling term and g is the coupling parameter.

The equation of motion for Ψ is,

$$(\not{D} - m + \zeta(\phi))\Psi = 0. \tag{2.41}$$

In the momentum space, we decompose $\Psi = \psi(r)e^{-i\omega v + ik_x x}$ setting $k_y = 0$ using the rotational symmetry in the x-y plane. So, we will write $k_x = k$ in our calculations. With this equation (2.41) becomes,

$$\begin{aligned}\Bigg[\Gamma^{\underline{v}}\left[-\frac{r}{2}(1-f(r))\partial_r - \frac{i\omega}{r} - \frac{iqA_v}{r} - \frac{3}{4}(1-f(r)) + \frac{rf'(r)}{4}\right] \\ +\Gamma^{\underline{r}}\left[\frac{r}{2}(1+f(r))\partial_r - \frac{i\omega}{r} - \frac{iqA_v}{r} + \frac{3}{4}(1+f(r)) + \frac{rf'(r)}{4}\right] \\ +\frac{ik}{r}\Gamma^{\underline{x}} - m + \zeta(\phi)\Bigg]\psi = 0\,.\end{aligned} \tag{2.42}$$

As the matrix $\Gamma^{\underline{r}}$ has two eigen values 1 and -1, we can decompose ψ into two spinor components as ψ_+ and ψ_-. Further, we can introduce another decomposition for $\psi_\pm$ as the two matrices $\Gamma^{\underline{r}}$ and $k_x\Gamma^{\underline{vx}}$ are independent and commuting. Below we have written the decompositions as

$$\psi = \psi_+ + \psi_-, \qquad \Gamma^{\underline{r}}\psi_\pm = \pm\psi_\pm, \qquad \Gamma^{\underline{r}}\Gamma^{\underline{a}}\psi_\pm = \pm\Gamma^{\underline{a}}\psi_\pm \tag{2.43}$$

$$\psi_+ = \psi^+_+ + \psi^-_+, \qquad \psi_- = \psi^+_- + \psi^-_- \qquad k_x\Gamma^{\underline{vx}}\psi^\pm_\pm = \pm k\psi^\pm_\pm \tag{2.44}$$

Now, we can decompose the spinor ψ into 4 spinor components $(\psi^+_+, \psi^-_+, \psi^+_-, \psi^-_-)$ and get 4 coupled Dirac component equations; where, $a = v, x, y$. Then, expanding the Dirac component equations near the horizon order by order, we can calculate the P-S points in each order as shown in detail in the appendix.

2.5.1 P-S with real scalar coupling

As we have discussed in the previous section, the coupled scalar can be real or charged. In this section, we will discuss the effect of condensate on P-S points taking the scalar to be real in equation (2.41). Zeroth order P-S points are found to be,

$$\omega_0 = -\pi i T, \;\; k_0 = \begin{cases} \pm(imr_0 + p\mu\phi(r_0)), & \text{Dipole coupling} \\ \pm(imr_0 + igr_0\phi(r_0)), & \text{Yukawa coupling.} \end{cases} \tag{2.45}$$

Point to notice that for both the couplings, the pole-skipping points receive the modification only in the linear momentum sector not in the frequency sector. If we don't consider the coupling terms in the action, we have purely imaginary momentum in the pole-skipping points. However, it seems that by adding interaction to the theory, the momentum values achieve a correction term leaving the frequency unchanged! Similar studies have been done in anisotropic plasma ([87]), where they have studied quantum chaos by pole-skipping by perturbing the metric. They got a complex momentum and justified that while the imaginary value of the momentum follows the dispersion curve for momentum diffusion, the real part puts a constraint. This means that the imaginary part of the momentum is the diffusive mode and the real part is the propagating mode. However, it is interesting to observe that due to dipole interaction, the fermionic perturbation acquires a real momentum $\propto \mu\phi(r_0)$ at the pole-skipping point which is temperature-dependent. On the other hand, the Yukawa interaction induces a temperature-dependent spatially growing/decaying mode which is $\propto g\phi(r_0)$. We will observe the same effect in the charged scalar-fermion interaction as well.

Here, (ω_0, k_0) is the zeroth order frequency and momentum. The 1st-order P-S points are $\omega_1 = -3\pi i T$ and 3 associated values of momentum as shown in the appendix. For every order n, we get $2n+1$ values of momentum. Particularly, the noteworthy finding of the present analysis is the scaling behaviour of the pole-skipping momentum near the phase

transition point as

$$k_0 = \begin{cases} \pm(imr_0 + 40.9p\mu(T_c - T)^{\frac{1}{2}}), & \text{Dipole coupling} \\ \pm(imr_0 + 40.9igr_0(T_c - T)^{\frac{1}{2}}), & \text{Yukawa coupling.} \end{cases} \tag{2.46}$$

The scaling exponent turns out to be again $1/2$ as expected from the background condensation. The last equality corresponds to the P-S point near the critical temperature. At higher order too, this equality holds, which we can see from the momentum values written in the appendix. We can see that near T_c, the P-S points vanish which is the same scenario as arises in [132]. In [132], they have discussed how with addition of the coupling term resists the coincidence of lines of poles and zeroes. But, this case is true for $T \to 0$ temperature. In this work, we have shown that for massless fermions, this is indeed true near T_c.

Effect of real scalar Condensate:

From (2.32), we can recognize the co-efficient of slow fall off as the source term $\mathcal{O}_1$ and co-efficient of fast fall off as the condensate term (response) $\mathcal{O}_2$ of the system. Critical temperature T_c is that temperature below which $\mathcal{O}_1 = 0$, sourceless condition. In the right of the Figure 2.7 we have plotted the dependence of $\mathcal{O}_1$ in terms of the horizon value of the scalar field. Upon increasing the temperature, the curves are approaching towards the origin signifying the existence of critical temperature T_c at which condensate vanishes. Once we obtained the critical temperature we plotted the condensate as well as the horizon value of condensed scalar field $\phi(r_0)$ with increasing temperature as shown in Figure 2.8.

Our goal for this work is to understand the effects of this scalar condensation on the pole-skipping points. From equation (2.45), we can see the horizon value of the scalar field is affecting the pole-skipping point. We have plotted the dynamics of pole-skipping points with varying temperatures in Figure 2.10. And, we observed that as the temperature increases movement of the pole-skipping point follows the same behaviour as the horizon value of the scalar field. Finally, as the critical temperature is reached, associated momentum saturates with the value which is obtained without interaction. It was expected that beyond the criti-

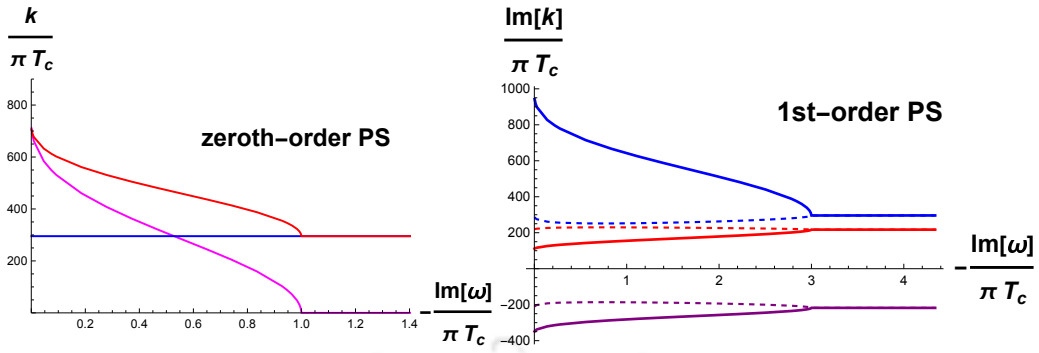

Figure 2.10: *Left:* Movement of zeroth order PS with temperature. The magenta and blue coloured lines are for real and imaginary values of momentum with dipole coupling, while the red colour line is for the imaginary value of momentum with Yukawa coupling. *Right:* Movement of first order pole-skipping point with temperature. Here, we have considered $p = 1, g = 1, m = 1, m_\phi^2 = -2.1$ and $q = 1$. The thick lines are for momentum values with Yukawa coupling and the dashed lines are for momentum values with dipole coupling. In both the plots, μ is also varying as $\sqrt{3\eta}$.

cal temperature, condensate vanishes without any source term. For completeness, we have plotted both zeroth and first-order pole-skipping points.

2.5.2 P-S with charged scalar coupling

As we have discussed in the previous section, we can carry the same discussion with charged scalar field and study pole-skipping phenomena.

$$\mathcal{L} = \sqrt{-g} i \bar{\Psi} (\not{D} - m + \zeta(|\tilde{\phi}|^2)) \Psi \,, \tag{2.47}$$

where, $\tilde{\phi}$ is the charged scalar field. We have already analysed the behaviour of this charged scalar field in detail in section (2.4.2). Here also, we can talk about dipole and Yukawa coupling as discussed in the previous section, but with the charged scalar coupling.

- when $\zeta(|\tilde{\phi}|^2) = -ip|\tilde{\phi}|^2 \not{\Gamma}$: This is charged dipole coupling and will see the effect of this interaction term in P-S points.

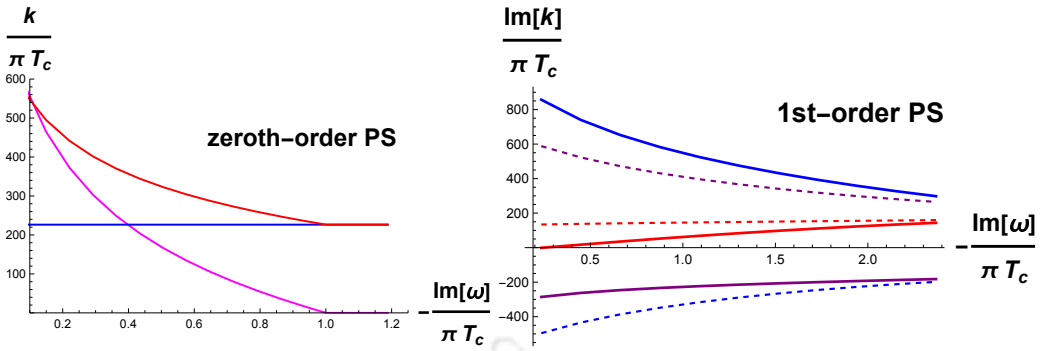

Figure 2.11: *Left:* Movement of zeroth order PS with temperature. The magenta and blue coloured lines are for real and imaginary values of momentum with charged dipole coupling, while the red colour line is for the imaginary value of momentum with charged Yukawa coupling.*Right:* Movement of first order pole-skipping point with temperature. Here, we have considered $p = 1, g = 1, m = 1, m_\phi^2 = -2.1, q = 1$ and $q_s = 0.1$. The thick lines are for momentum values with charged Yukawa coupling and the dashed lines are for momentum values with charged dipole coupling. In both the plots, μ is also varying as $\sqrt{3\eta}$.

- when $\zeta(|\tilde{\phi}|^2) = g|\tilde{\phi}|^2$: This is charged Yukawa coupling and will see the effect of this interaction term in P-S points.

We will follow the same procedure as discussed in the appendix to calculate the P-S points. Zeroth order P-S points are,

$$\omega_0 = -\pi i T,\ k_0 = \begin{cases} \pm(imr_0 + p\mu|\tilde{\phi}(r_0)|^2), \text{ch. Dipole} \\ \pm(imr_0 + igr_0|\tilde{\phi}(r_0)|^2), \text{ch. Yukawa.} \end{cases} \tag{2.48}$$

Here, again (ω_0, k_0) is the zeroth order frequency and momentum. We have explicitly written down the first-order momentum value in the appendix. Particularly, the noteworthy finding of the charged scalar analysis is the scaling behaviour of the pole-skipping momentum near the phase transition point as

$$k_0 = \begin{cases} \pm(imr_0 + (45.38)^2\, p\mu(T_c - T)), \text{ch. Dipole coup.} \\ \pm(imr_0 + (45.38)^2\, igr_0(T_c - T)), \text{ch. Yukawa coup.,} \end{cases} \tag{2.49}$$

The scaling exponent turns out to be unity instead of $1/2$ of the real scalar field. For the first order too, we have verified this behaviour. It is very clear from the Figure 2.11 too. After reaching the critical frequency (where $T = T_c$), momentum values saturate at the mass value of fermion.

Effect of complex scalar Condensate:

Solving the complex scalar EOM (2.35) near the boundary of AdS, we have evaluated the source and condensate term for the complex scalar field in section 2.4.2. For this case, we also find the critical temperature T_c, beyond which the charge scale becomes trivially zero in source-less conditions. Once we obtain the scalar condensate at different temperatures below $T < T_c$, Figure 2.11 depicts the effect of condensation on the zeroth and first order P-S points movement with increasing temperature. After crossing the critical temperature, the P-S points saturate at every order. For massless fermions, P-S points vanish after critical temperature, which seems very interesting. In the Figure 2.11, we have plotted both zeroth and first-order P-S points for both couplings. For Yukawa coupling, the zeroth order momentum is purely imaginary, so the effect of the coupling terms is additive to the mass of the fermions. But, for dipole coupling, the momentum value is complex. So, we have plotted both real and imaginary values of momentum of dipole coupling in the left of Figure 2.11. For the first-order P-S points movement, we have only shown the movement of the imaginary values of momentum for both couplings.

We have studied the P-S phenomenon with 2 types of couplings: dipole and Yukawa, where we have probed a scalar field, which can be real or charged. From the dictionary of AdS/CFT, we know that the scalar field near the AdS boundary admits both source and condensate with some specific range of mass values (obeying BF bound). There exists a temperature when this source is zero, still, condensate is finite, which is called the critical temperature. Calculating the P-S points with various couplings as we have mentioned, we have studied the behaviour of these P-S points with increasing temperature up to the critical temperature (T_c). We have seen that after crossing T_c, the P-S points saturate at the

mass value of fermion. For massless fermions, P-S points vanish after crossing T_c, which seems very interesting. For real scalar coupling, the momentum values are $\propto (T_c - T)^{1/2}$, while for charged scalar coupling, the momentum values are $\propto (T_c - T)$. We have checked this dependence on temperature upto third order and shown the results in appendix. In the next chapter, we aim to study the chaotic behaviour of a holographic QCD system by pole-skipping analysis. We introduce an effective horizon and perform pole-skipping near this effective horizon.

Chapter 3

Pole-skipping and chaos in D3-D7 brane systems

The QCD theory is very interesting to study quantum chaos [135–137]. In the quenched approximation of QCD where external fermion states have been ignored (or treat fermions as non-dynamical fields), the chaotic nature of the theory has been extensively studied [138, 139]. In the unquenched QCD, i.e., in the presence of light quarks, the chaotic nature of the system is expected to be different from the quenched case. Initially, the light quarks will be bounded in the form of neutral meson. But once these mesons melt into the charged quarks and anti-quarks, the Coulomb's interaction among these charged candidates is supposed to decrease the chaotic nature. This kind of effect in quantum chaos is very much new and interesting to study. On the other hand, if we apply an external electric field, the quark/anti-quark separation in meson increases and finally dissociates. This leads to a phase transition between the neutral meson-dominated insulating phase and the charged quark/anti-quark-dominated conducting phase. The chaotic parameters of the theory are also expected to show non-trivial change through this transition. In our present work, we represent this novel feature of quantum chaos.

In this work, we study pole-skipping and the associated behaviour of the characteristic parameters of quantum chaos in 3+1-dimensional Yang-Mills theory in the presence of quark flavors at a finite temperature. The chaotic nature of the YM theory with quenched flavor is well explored. But, it is still very exciting to see the effect of flavor on the chaotic properties

of the unquenched theory. In holography, the dual gravity theory of such a system can be achieved by probing D7 branes in the black-D3 brane background [140].

3.1 Gravitational background

The type II superstring theory, at a low energy limit, reduces to the ten-dimensional supergravity action. The Dp branes are the solution to this action, where p is the spatial dimension along the brane. Branes having the Arnowitt-Deser-Misner (ADM) mass equal to its charge are called extremal or Bogomol'nyi-Prasad-Sommerfield (BPS) branes. We consider non-extremal D3 brane in the bulk. Then, we construct a decoupled geometry where N_c number of D3 branes are closely located. The decoupled geometry is the Schwarzschild-AdS$_5$ black-hole geometry. The corresponding boundary theory is $\mathcal{N} = 4$ Yang-Mills theory at finite temperature with N_c color charge. We further consider N_f number of BPS D7 probe branes embedded in the bulk in the presence of Maxwell's field. According to the AdS/CFT dictionary, on the boundary we have the finite temperature $SU(N_c)$ $\mathcal{N} = 4$ Yang-Mills theory with probe hypermultiplet quark flavors [140]. We will be working in the probe limit $N_f << N_c$ so that the probe brane does not back-react on the background geometry.

3.1.1 Review of black D3 brane solution

In this sub-section, we will briefly review the black-D3 brane solution. It starts with solving the ten-dimensional supergravity action in the low energy limit [18]. The bulk action is given as,

$$\mathcal{S}_{10} = \frac{1}{2\kappa^2}\int d^{10}x\sqrt{-g}\left(\mathcal{R} - \frac{1}{2}\partial\Phi\cdot\partial\Phi - \frac{2}{5!}F^2\right). \tag{3.1}$$

Here, $2\kappa^2 \sim g_s^2\ell_s^8$; g_s is string theory coupling constant which is related to the $3+1$ dimensional YM theory coupling as $4\pi g_s = g_{YM}^2$ and ℓ_s is fundamental string length. g and R are the determinants of the metric and Ricci scalar defined on the $9+1$ dimensional background spacetime, Φ is the dilaton field and F is the RR 5-form field. The black D3 brane solution

[18] has been found as,

$$dS^2 = -\left(1-\frac{r_+^4}{r^4}\right)\left(1-\frac{r_-^4}{r^4}\right)^{-\frac{1}{2}}dt^2 + \left(1-\frac{r_-^4}{r^4}\right)^{\frac{1}{2}}dx_i dx^i + \frac{dr^2}{\left(1-\frac{r_+^4}{r^4}\right)\left(1-\frac{r_-^4}{r^4}\right)} + r^2 d\Omega_5^2, \tag{3.2}$$

where $(t,\, x_i)$ coordinates define the four dimensional worldvolume of the D3 brane and Ω_5 is transverse five-sphere. r defines the radial coordinate. r_+ and r_- are respectively the positions of horizon and singularity. Now, making a coordinate transformation $r = \rho\left(1+\frac{r_-^4}{\rho^4}\right)^{1/4}$, in (3.2), the black D3 brane solution can be written as

$$ds_{10}^2 = \left(1+\frac{r_-^4}{\rho^4}\right)^{-\frac{1}{2}}\left(-f(\rho)\mathrm{d}t^2 + \mathrm{d}\vec{x}^2\right) + \left(1+\frac{r_-^4}{\rho^4}\right)^{\frac{1}{2}}\left(\frac{\mathrm{d}\rho^2}{f(\rho)} + \rho^2\mathrm{d}\Omega_5^2\right), \tag{3.3}$$

$$\text{where, } f(\rho) = 1-\frac{\rho_h^4}{\rho^4} \qquad \rho_h^4 = r_+^4 - r_-^4, \tag{3.4}$$

$$\text{and,} \quad \Phi = \Phi_0\,(\text{constant}), \quad F_{[5]} = Q\,(1+{}^*)\,\text{Vol}\,(\Omega_5)\,. \tag{3.5}$$

In this new coordinate, the metric horizon is located at $\rho = \rho_h$. The ADM mass and charge of the brane are,

$$M \sim (5r_+^4 - r_-^4), \qquad Q^2 = 4r_+^2 {r_-}^2. \tag{3.6}$$

In the extremal or BPS limit, the solution reduces to BPS D3 brane. At this limit, $r_-^4 = r_+^4 = R_4^4\ell_s^4$, where $R_4^4 = 4\pi g_s N_c$. For non-extremal cases, we have $\rho_h^4 = r_+^4 - r_-^4$. We can see at the BPS limit, $\rho_h \to 0$ gives an extremal solution. We will be working in non-extremal limits.

Now we take following scaling, $r_-^4 \equiv R_4^4\ell_s^4$, $\rho_h \equiv r_h\ell_s^2$ and $\rho \equiv \ell_s^2 r$, where r_h is a fixed point on r. Then we take the decoupling limit ($\ell_s \to 0$) in the metric, which gives decoupled geometry near the brane

$$\frac{ds_{10}^2}{\ell_s^2} = \frac{r^2}{R_4^2}\left(-f(r)\mathrm{d}t^2 + \mathrm{d}\vec{x}^2\right) + \frac{R_4^2}{r^2}\left(\frac{\mathrm{d}r^2}{f(r)} + r^2\mathrm{d}\Omega_5^2\right), \tag{3.7}$$

where,

$$f(r) = 1-\frac{r_h^4}{r^4}. \tag{3.8}$$

This near-horizon geometry is AdS_5-Schwarzschild $\times$ S_5 which provides a finite temperature to the boundary gauge theory. The temperature is

$$T = \frac{r_h}{\pi R_4^2} = \frac{r_h}{\pi\sqrt{g_{YM}^2 N_c}}. \tag{3.9}$$

Here the bulk theory has two independent parameters – temperature T and string constant g_s. The holographic boundary theory is pure YM theory which also has two free parameters – temperature T and YM coupling $g_{YM}^2 = 4\pi g_s$. Since the transverse five-sphere has a constant radius, the background action is reducible to the five-dimensional integration as given below.

$$\mathcal{S}_{bulk} = \frac{1}{g_s^2}\int R_4^5 \mathrm{d}\Omega_5 \int \mathrm{d}^5x\sqrt{-g_{(5)}}\left(\mathcal{R}_{(5)} + \frac{12}{R_4^2}\right), \tag{3.10}$$

and further, the Einstein equation can be written for the five-dimensional AdS background as,

$$\mathcal{R}_{(5)\mu\nu} - \frac{1}{2}\left(\mathcal{R}_{(5)} + \frac{12}{R_4^2}\right) g_{(5)\mu\nu} = 0, \tag{3.11}$$

where $\mathcal{R}_{(5)\mu\nu}$ and $\mathcal{R}_{(5)}$ are the Ricci tensor and Ricci scalar respectively for the five-dimensional AdS background metric $g_{(5)\mu\nu}$ with the AdS radius R_4.

For the upcoming pole-skipping calculations, we need to frame the background solutions in the Eddington-Finkelstein (EF) coordinate. Our present background (3.7) can be transformed into ingoing EF coordinate with the transformation $v = t + \int \frac{R_4^2 \mathrm{d}r}{r^2 f(r)}$. In EF coordinate, the metric takes the form,

$$\begin{aligned}\frac{ds_{10}^2}{\ell_s^2} &= \frac{r^2}{R_4^2}\left(-f(r)\mathrm{d}v^2 + \mathrm{d}\vec{x}^2\right) + 2\mathrm{d}v\mathrm{d}r + R_4^2\mathrm{d}\Omega_5^2 \\ &= g_{(5)\mu\nu}\mathrm{d}x^\mu \mathrm{d}x^\nu + R_4^2\mathrm{d}\Omega_5^2.\end{aligned} \tag{3.12}$$

Here, v is the null coordinate, r is the radial coordinate, and $\vec{x}$ corresponds to the spatial coordinate x, y, z. Now, using the standard polar coordinates on the S_5, we can be written as,

$$\mathrm{d}\Omega_5^2 = \mathrm{d}\theta^2 + \sin^2\theta \mathrm{d}\Omega_3^2 + \cos^2\theta \mathrm{d}\varphi^2. \tag{3.13}$$

Table 3.1: AdS_5 is covered by co-ordinate $t, \vec{x}, r$ and the S^5 is covered by $\vartheta_1, \vartheta_2, \vartheta_3, \theta$ and φ

	t	x	y	z	r	ϑ_1	ϑ_2	ϑ_3	θ	φ
D3	✓	✓	✓	✓	×	×	×	×	×	×
D7	✓	✓	✓	✓	✓	✓	✓	✓	×	×

3.1.2 Embedding D7 brane

Without disturbing the background geometry, the transverse hypersphere can be unfolded as

$$\frac{ds_{10}^2}{\ell_s^2} = \frac{r^2}{R_4^2}\left(-f(r)\mathrm{d}v^2 + \mathrm{d}\vec{x}^2\right) + 2\mathrm{d}v\mathrm{d}r + R_4^2\left[\mathrm{d}\theta^2 + \sin^2\theta\mathrm{d}\Omega_3^2 + \cos^2\theta\mathrm{d}\varphi^2\right], \tag{3.14}$$

where the three sphere Ω_3 is spanned by the angular coordinates $\{\vartheta^1,\ \vartheta^2,\ \vartheta^3\}$. The D3 brane is delocalised along $\{v,\ x,\ y,\ z\}$ while localised in r and Ω_5. We consider D7 brane as a probe brane in this background. This D7 brane is placed in such a way that it fills the D3 brane's world volume and further extends along $\{r,\ \Omega_3\}$. Again, this D7 brane is wrapped on Ω_3, hence it is localised in $\{\theta,\ \varphi\}$.

In Poincare coordinate it can be easily shown that the six-dimensional transverse space $\mathbb{R}^1 \times \mathbb{S}^5$ (given by $\{r,\ \Omega_5\}$) of D3 brane has been separated here into two part as $\mathbb{R}^1 \times \mathbb{S}^3$ (given by $\{r\sin\theta,\ \Omega_3\}$) and $\mathbb{R}^1 \times \mathbb{S}^1$ (given by $\{r\cos\theta,\ \varphi\}$). So the angle between $\mathbb{S}^3$ and $\mathbb{S}^1$ can be found to be θ. We parameterize the localization of D7 in terms of embedding function $\theta \equiv \theta(r)$ and $\varphi =$ constant on $\mathbb{R}^1 \times \mathbb{S}^1$ surface. Due to the rotational symmetry on $\mathbb{S}^1$ of $\mathbb{R}^1 \times \mathbb{S}^1$, the distance of the D7 brane from the D3 brane is the radius of $\mathbb{S}^1$, $r\cos\theta(r)$.

The parameterization of the eight-dimensional world volume of D7 brane in EF coordinates is as follows.

$$\xi^0 \equiv v; \quad \xi^i \equiv x^i; \text{ for } i = 1,\ 2\,\&\,3; \quad \xi^4 \equiv r; \tag{3.15}$$

$$\xi^i_{\Omega_3} \equiv \vartheta^i, \text{ for } i = 5,\ 6\,\&\,7\,; \theta \equiv \theta(r)\,, \varphi = \text{constant}. \tag{3.16}$$

The induced metric on the D7 brane is expressed as,

$$\begin{aligned}\frac{ds^2_{D7}}{\ell_s^2} =& g_{(5)vv}\mathrm{d}v^2 + 2g_{(5)vr}\mathrm{d}v\mathrm{d}r + R_4^2\theta'(r)^2\mathrm{d}r^2 + g_{(5)x^ix^i}\mathrm{d}x^i\mathrm{d}x^i + R_4^2\sin^2\theta(r)\mathrm{d}\Omega_3^2,\\ =&\gamma_{(5)\alpha\beta}\mathrm{d}\xi^\alpha\mathrm{d}\xi^\beta + R_4^2\sin^2\theta(r)\mathrm{d}\Omega_3^2,\\ =&\gamma_{(8)\alpha\beta}\mathrm{d}\xi^\alpha\mathrm{d}\xi^\beta. \end{aligned} \tag{3.17}$$

The induced metric components in EF coordinates are

$$\gamma_{(5)\alpha\beta} = g_{(5)\mu\nu}\frac{\mathrm{d}x^\mu}{\mathrm{d}\xi^\alpha}\frac{\mathrm{d}x^\nu}{\mathrm{d}\xi^\beta} + R_4^2\theta'(r)^2\delta^r_\alpha\delta^r_\beta = g_{(5)\mu\nu}\delta^\mu_\alpha\delta^\nu_\beta + R_4^2\theta'(r)^2\delta^r_\alpha\delta^r_\beta. \tag{3.18}$$

The DBI action in the D7 brane worldvolume is,

$$\mathcal{S}_{D7} = -N_f T_7\int \mathrm{d}v\mathrm{d}r\mathrm{d}^3x\mathrm{d}^3\vartheta\times\ell_s^8\sqrt{-\gamma_{(8)}}, \tag{3.19}$$

where, $\gamma_{(8)} = \mathrm{Det}\left[\gamma_{(8)\alpha\beta}\right]$ is the determinant of the eight dimensional worldvolume metric (3.17) of the D7 brane. $T_7 = 1/(g_s\ell_s^8)$ is the tension of the D7 brane. As Ω_3 has the same symmetries as Ω_5 of the D3 brane background, these three spheres can be integrated out easily and the DBI action can be reduced into the following form,

$$\mathcal{S}_{D7} = -\frac{N_f R_4^3 V_{S^3}}{g_s}\int \mathrm{d}^5x\sin^3\theta(r)\sqrt{-\gamma_{(5)}}, \tag{3.20}$$

where, $\gamma_{(5)} = \mathrm{Det}\left[\gamma_{(5)\alpha\beta}\right]$ is the determinant of the five dimensional metric given in (3.18). The total bulk action in presence of N_f D7 flavor brane ($N_f \ll N_c$),

$$\begin{aligned}\mathcal{S}_{total} =& \mathcal{S}_{bulk} + \mathcal{S}_{D7},\\ =&\frac{1}{g_s^2}\int \mathrm{d}^5x\sqrt{-g_{(5)}}\left[V_{S^5}R_4^5\left(\mathcal{R}_{(5)} + \frac{12}{R_4^2}\right) - g_sN_fV_{S^3}R_4^3\sin^3\theta(r)\frac{\sqrt{-\gamma_{(5)}}}{\sqrt{-g_{(5)}}}\right],\\ =&\frac{V_{S^5}R_4^5}{g_s^2}\int \mathrm{d}^5x\sqrt{-g_{(5)}}\left[\left(\mathcal{R}_{(5)} + \frac{12}{R_4^2}\right) - \frac{n_f}{R_4^2}\sin^3\theta(r)\frac{\sqrt{-\gamma_{(5)}}}{\sqrt{-g_{(5)}}}\right], \end{aligned} \tag{3.21}$$

where, $V_{S^3} = 2\pi^2$ and $V_{S^5} = \pi^3$ and,

$$n_f = \frac{V_{S^3}}{V_{S^5}}g_sN_f = \frac{V_{S^3}}{4\pi V_{S^5}}R_4^4\frac{N_f}{N_c} \ll 1. \tag{3.22}$$

We call n_f the probe parameter or the flavor parameter as it is only proportional to the number of flavor N_f in YM theory. As we are in the probe limit, i.e., $n_f \ll 1$, this parameter

is considered as the perturbation parameter. Since this total action is invariant under the variation of the five-dimensional background metric $g_{(5)\mu\nu}$, we find Einstein's equation

$$\mathcal{R}_{(5)\mu\nu} - \frac{1}{2}\left(\mathcal{R}_{(5)} + \frac{12}{R_4^2}\right) g_{(5)\mu\nu} + \mathcal{T}^{flavor}_{\mu\nu} = 0. \tag{3.23}$$

The energy-momentum tensor due to the D7 brane is given as follows.

$$\begin{aligned}\mathcal{T}^{flavor}_{\mu\nu} &= -\frac{n_f}{R_4^2}\frac{\sin^3\theta(r)}{\sqrt{-g_{(5)}}}\frac{\delta}{\delta g^{\mu\nu}_{(5)}}\sqrt{-\gamma_{(5)}} \\ &= -\frac{n_f}{2R_4^2}\sin^3\theta(r) g_{(5)\mu\rho}g_{(5)\nu\sigma}\delta^\rho_\alpha\delta^\sigma_\beta\gamma^{\alpha\beta}_{(5)}\frac{\sqrt{-\gamma_{(5)}}}{\sqrt{-g_{(5)}}}.\end{aligned} \tag{3.24}$$

Here δ^α_μ indicates the Dirac delta function. If we take perturbation in the background metric $g_{(5)\mu\nu}$ of (3.7), the induced metric $\gamma_{(5)\alpha\beta}$ in (3.18) is also varied accordingly.

3.1.3 In the presence of Maxwell's Field

In the presence of Maxwell field $F_{\alpha\beta}$ along $\{v, r, \vec{x}\}$ with the flavors, the DBI action (3.19) in the D7 brane worldvolume is modified into the following form,

$$\begin{aligned}\mathcal{S}_{D7} &= -N_f T_7 \int \mathrm{d}^8x\sqrt{-\mathrm{Det}\left[\ell_s^2\gamma_{(8)\alpha\beta} + 2\pi\ell_s^2 F_{\alpha\beta}\right]}, \\ &= -\frac{N_f}{g_s}\int \mathrm{d}^8x\sqrt{-\mathrm{Det}\left[\gamma_{(8)\alpha\beta} + F_{\alpha\beta}\right]}, \\ &= -g_s^{-1}N_f R_4^3 V_{S^3}\int \mathrm{d}^5x\sqrt{-\gamma_{(5)}}\sin^3\theta(r)\mathcal{L}_8,\end{aligned} \tag{3.25}$$

where $\ell_s^2\gamma_{(8)\alpha\beta}$ is the pullback of the ten-dimensional background onto the D7 brane worldvolume. Note that 2π factor has been absorbed in $F_{\alpha\beta}$ and

$$\mathcal{L}_8 = \left[1 - \frac{1}{2}F_\alpha{}^\beta F_\beta{}^\alpha\right]^{1/2} \approx \left[1 - \frac{1}{4}F_\alpha{}^\beta F_\beta{}^\alpha\right],$$

The indices of the Maxwell field are raised/lowered with the D7 brane metric $\gamma_{(5)\alpha\beta}$, i.e., $F_\alpha{}^\beta = F_{\alpha\lambda}\gamma^{\lambda\beta}_{(5)}$. Now to find the energy-momentum tensor (3.24) with the presence of the

Maxwell field, we need to vary this action (3.25) w.r.t $g_{(5)\mu\nu}$

$$\frac{\Delta \mathcal{S}_{D7}}{\Delta g_{(5)\mu\nu}} = -\, g_s^{-1} N_f R_4^3 V_{S^3} \int \mathrm{d}^5 x \sin^3\theta(r) \sqrt{-\gamma_{(5)}} \times \left[\frac{1}{2}\left(1 - \frac{1}{4} F_\lambda{}^\gamma F_\gamma{}^\lambda\right) \gamma_{(5)}^{\alpha\beta} + \frac{1}{2} F^{\alpha\lambda} F_\lambda{}^\beta\right] \delta_\alpha^\mu \delta_\beta^\nu. \tag{3.26}$$

Therefore, the energy-momentum tensor is

$$\mathcal{T}^{\mu\nu}_{flavor} = -\,\frac{n_f}{2R_4^2} \sin^3\theta(r) \frac{\sqrt{-\gamma_{(5)}}}{\sqrt{g_{(5)}}} \left[\left(1 - \frac{1}{4} F_\lambda{}^\gamma F_\gamma{}^\lambda\right) \gamma_{(5)}^{\alpha\beta} + F^{\alpha\lambda} F_\lambda{}^\beta\right] \delta_\alpha^\mu \delta_\beta^\nu. \tag{3.27}$$

We have seen that the effective metric on the D7 brane due to the Maxwell field is $\gamma_{(8)\alpha\beta} + F_{\alpha\beta}$. Therefore the presence of an electric field modifies the location of the singularity.

3.1.4 Embedding equation

In the holographic picture, considering Maxwell's field on the flavored D7 brane is equivalent to considering the charged flavored quarks in the boundary Yang-Mills theory. We put a constant electric field E along the x_1 direction on the D7 brane. We can take one of the two configurations of the vector field A_μ given below which gives the same results in our case. (i) the Coulomb potential $A_v(x) = E\, x_1$. It gives the Maxwell field as,

$$F_{vx_1} = -\partial_{x_1} A_v = -E,$$

Or, (ii) a v dependent vector potential $A_{x_1} = -E\, v$ along x_1 direction. It gives the same Maxwell fields as above. Here we also add a current along x^1. So to apply the Maxwell potential, we can take either (i) $A_v = Ex^1$ & $A_{x^1} = \tilde{A}_x(r)$ or (ii) $A_{x^1} = -Ev + \tilde{A}_x(r)$. Now, the D7 brane action can be rewritten as,

$$\mathcal{S}_{D7} \sim \int dr\, \mathcal{L}.$$

$$\mathcal{L} = \frac{r^2 \sin^3\theta(r)}{R_4^3} \left[r^2 + \tilde{A}_x' \left(-2ER_4^2 + r^2 f(r) \tilde{A}_x'\right) + \left(-E^2 R_4^4 + r^4 f(r)\right) \theta'(r)^2\right]^{1/2}.$$

Here prime denotes the derivative with respect to r. Taking $E = E_0/R_4^2$, the Lagrangian becomes

$$\mathcal{L} = \frac{r^2 \sin^3\theta(r)}{R_4^3} \left[r^2 + \tilde{A}_x' \left(-2E_0 + r^2 f(r) \tilde{A}_x'\right) + \left(-E_0^2 + r^4 f(r)\right) \theta'(r)^2\right]^{1/2}. \tag{3.28}$$

From the above Lagrangian, it is clear that $\tilde{A}_x(r)$ is a cyclic coordinate, and hence the associated conserved current source J_0 is expressed as,

$$\frac{\partial \mathcal{L}}{\partial \tilde{A}'_x(r)} = J_0 \Rightarrow r^2 f(r)\tilde{A}'_x(r) = E_0 - R_4^3 J_0 \sqrt{\frac{(r^4 f(r) - E_0^2)\,(1 + r^2 f(r)\theta'(r)^2)}{r^6 f(r)\sin^6\theta - R_4^6 J_0^2}}. \tag{3.29}$$

Using this constraint, we can write the Lagrangian in the Legendre transformed form as

$$\begin{aligned}
\tilde{\mathcal{L}} =& \mathcal{L} - J_0 \tilde{A}'_x(r), \\
=& \frac{1}{r^2 f(r) R_4^3}\Big[-R_4^3 E_0 J_0 + \Big(\left\{r^4 f(r) - E_0^2\right\} \times \\
& \left\{1 + r^2 f(r)\theta'(r)^2\right\}\left\{r^6 f(r)\sin^6\theta - R_4^6 J_0^2\right\}\Big)^{1/2}\Big], \\
=& \frac{1}{r^2 f(r) R_4^3}\Big(\left\{r^4 f(r) - E_0^2\right\}\left\{1 + r^2 f(r)\theta'(r)^2\right\}\left\{r^6 f(r)\sin^6\theta - R_4^6 J_0^2\right\}\Big)^{1/2}.
\end{aligned} \tag{3.30}$$

In the last equation, we have dropped the term $-R_4^3 E_0 J_0$ as it is independent of the generalized coordinates. In other words, this $\theta(r)$ independent term is associated with a constant energy contribution in the D7 brane worldvolume. Now the final Lagrangian (3.30) is to be real. However, it has two factors – $r^4 f(r) - E_0^2$ and $r^6 f(r)\sin^6\theta - R_4^6 J_0^2$ – which can make the Lagrangian imaginary. The Lagrangian is real if either both factors are positive or negative. At finite electric field and current, both the factors are positive at large $r \to \infty$ and they decrease as we go to the smaller r regime. Then both factors become simultaneously zero at a particular point $r = r_0$. Here at this special cut-off point, the Lagrangian (3.30) vanishes. This point is also called as the position of vanishing locus [141, 142]. After that as $r < r_0$, both factors become negative which makes the Lagrangian real again. The location of the vanishing locus is at $r = r_0$ if

$$r_0^4 - r_h^4 - E_0^2 = 0, \tag{3.31}$$

$$r_0^6 f(r_0)\sin^6\theta(r_0) = R_4^6 J_0^2. \tag{3.32}$$

Again the effective open string metric on the probe brane is given by

$$\begin{aligned}\tilde{\gamma}_{(8)\alpha\beta} =& \gamma_{(8)\alpha\beta} + F_{\alpha\lambda}\gamma_{(8)}^{\lambda\nu}F_{\nu\beta} \\ =& \gamma_{(5)\alpha\beta} + F_{\alpha\lambda}\gamma_{(5)}^{\lambda\nu}F_{\nu\beta} + R_4^2\sin^2\theta(r)d\Omega_3^2\,,\end{aligned}$$

and the line element is

$$\begin{aligned}\tilde{ds}^2_{D7} =& -\frac{r^4f(r)-E_0^2}{R_4^2r^2}\mathrm{d}v^2 + \frac{r^4\left(r^4f(r)-E_0^2\right)\sin^6\theta}{R_4^2\left(r^6f(r)\sin^6\theta - R_4^6J_0^2\right)}\mathrm{d}x_1^2 + \frac{r^2}{R_4^2}\left(\mathrm{d}x_2^2+\mathrm{d}x_3^2\right) \\ &+2\left(1-\frac{E_0^2}{r^4f(r)}+\frac{R_4^3J_0E_0}{r^4f(r)}\sqrt{\frac{\left(r^4f(r)-E_0^2\right)\left(1+r^2f(r)\theta'(r)^2\right)}{r^6f(r)\sin^6\theta-R_4^6J_0^2}}\right)\mathrm{d}v\mathrm{d}r + R_4^2\left(\theta'(r)^2+\right. \\ &\left.\left(\frac{E_0}{r^3f(r)}-\frac{R_4^3J_0}{r^3f(r)}\sqrt{\frac{\left(r^4f(r)-E_0^2\right)\left(1+r^2f(r)\theta'(r)^2\right)}{r^6f(r)\sin^6\theta-R_4^6J_0^2}}\right)^2\right)\mathrm{d}r^2 + R_4^2\sin^2\theta\mathrm{d}\Omega_3^2. \quad (3.33)\end{aligned}$$

In the region $r < r_0$, according to the aforementioned discussion, the effective open string metric changes signature, as its vv-component becomes positive. So, it puts a further condition on the complete system and suggests to define an effective horizon at $r^4f(r)|_{r_0} = E_0^2$, i.e. $r_0 = (r_h^4 + E_0^2)^{1/4}$. In the following sections, this effective horizon will play a crucial role in chaos and pole-skipping. The AdS_5 blackhole background has the horizon at $r = r_h$. In the presence of the D7 brane and the Maxwell field, the background has to be back-reacted in principle. The back-reacted background is expected to have a new horizon around r_0. But, using the perturbative approximation ($N_f << N_c$), we have neglected the back-reaction. So, we don't find this effective horizon in the bulk metric. The effective horizon appears in the open string effective metric on the D7 brane. The above two conditions (3.31) & (3.32) give

$$r_0 = \left(r_h^4 + E_0^2\right)^{1/4}, \quad (3.34)$$

$$J_0 = R_4^{-3}E_0\left(r_h^4+E_0^2\right)^{1/4}\sin^3\theta_0, \quad (3.35)$$

and,

$$\tilde{A}'_x(r_0) = \frac{r_0^2}{E_0}\left[1-\sqrt{\frac{2r_0^4+2r_0^2E_0^2\theta'(r_0)^2}{2r_h^4+3\left(1+r_0\theta'(r_0)\cot\theta(r_0)\right)E_0^2}}\right]. \quad (3.36)$$

The above equation (3.35) relates the current density with the applied electric field, similar to Ohm's law. For weaker field ($E_0 \ll r_h^2$), $J_0 \propto E_0$, which is reminiscent of linear response theory. This field-induced current is the flow of the charged quarks in the direction parallel to the electric field. Therefore, the charged quark density distribution on dual field theory is varied with the applied field E_0.

Looking at the Lagrangian (3.30), one realises that the embedding angle $\theta(r)$ of the D7 brane in the D3 brane background is the only canonical variable in the effective D7 brane Lagrangian. Here, we take r as the parameter and derive the dynamical equation of $\theta(r)$ as,

$$\begin{aligned}
&\frac{d}{dr}\left[\frac{\theta'(r)}{1+r^2 f(r)\theta'(r)^2}\right] - \frac{3r^4\sin^5\theta\cos\theta}{r^6 f(r)\sin^6\theta - R_4^6 J_0^2} \\
&+ \frac{\theta'(r)}{1+r^2 f(r)\theta'(r)^2}\left[\frac{2r^3}{r^4 f(r) - E_0^2} + \frac{r\,(2-f(r))}{1+r^2 f(r)\theta'(r)^2}\left(\theta'(r)^2 + r^2 f(r)\theta'(r)\theta''(r)\right)\right. \\
&\left. + \frac{r^4\sin^5\theta}{r^6 f(r)\sin^6\theta - R_4^6 J_0^2}\left(r(2+f(r))\sin\theta + 3r^2 f(r)\theta'(r)\cos\theta\right)\right] = 0. \qquad (3.37)
\end{aligned}$$

The equation of motion of $\theta(r)$ given in (3.37) is a second-order non-linear differential equation. We know that $r\cos\theta(r)(= d(r))$ represents the separation between D3 and D7 brane. $r\sin\theta(r)(= \sqrt{r^2 - d^2})$ is the radius of the Ω_3 sphere on which the D7 is wrapped. Therefore, $d(r)$ should be regular at the horizon of the background geometry. It refers to the regularity condition of $\theta(r)$. Furthermore, the asymptotic behaviour of $\theta(r)$ is known to be holographically related to the quark mass m_q and its condensate c_q as follows,

$$d(r\to\infty) \approx m_q + \frac{c_q}{r^2} \quad \text{or} \quad \theta(r\to\infty) \approx \frac{\pi}{2} - \frac{m_q}{r} - \frac{c'}{r^3}, \qquad (3.38)$$

where, $c' = c_q + m^3/6$. Since this system preserves chiral symmetry, there is no non-zero mass with zero condensate.

Near the point $r = r_0$ of the constant energy, the regularity condition of $\theta(r)$ helps us to expand it in the Taylor series. This immediately gives the following relation

$$\theta'(r_0) = \frac{3r_0^3\cot\theta(r_0)}{2\,(2r_0^4 + E_0^2)} = \frac{3\,(r_h^4 + E_0^2)^{3/4}}{2\,(2r_h^4 + 3E_0^2)}\cot\theta_0, \qquad (3.39)$$

where θ_0 is the value of the embedding function at r_0. Now, the solution of $\theta(r)$ has to be found in two steps. In the first step, putting the boundary condition (3.39) and the value

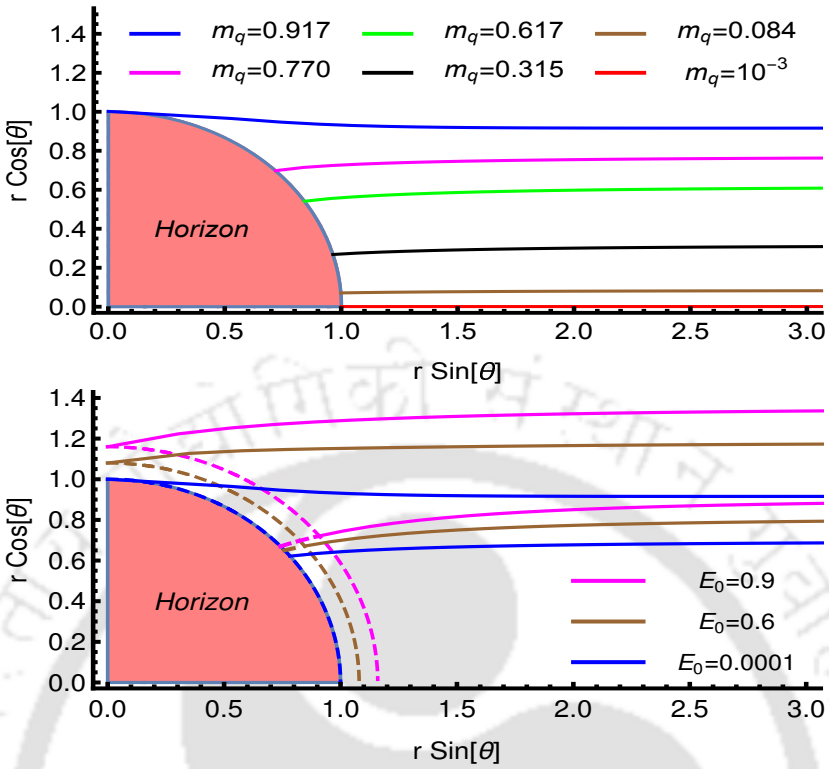

Figure 3.1: *Top*: Plotted the distance between D3 brane and D7 brane - $r\cos\theta$ and the radius of Ω_3 sphere - $r\sin\theta$ without electric field $E_0 = 0$ and $n_f = 1$. *Below*: Plotted the distance between D3 brane and D7 brane - $r\cos\theta$ and the radius of Ω_3 sphere - $r\sin\theta$ with different electric field values. The dashed lines are effective horizons at some specific values of E_0

$\theta(r_0)$, we solve the embedding function $\theta(r)$ from (3.37) in the range r_0 to ∞. In the next step, implementing the same boundary condition at r_0, we solve $\theta(r)$ from (3.37) in the range r_0 to r_h. In this way, we solve the embedding function for the whole range of the radial coordinate. From these solutions, we find the horizon value of the embedding function $\theta(r_h)$ depending on the boundary condition $\theta(r_0)$. We now solve numerically the equation (3.37) with two constraints, (3.38) and (3.39), using the above regularity condition. Once we have found the solution of $\theta(r)$, we can easily find the distance of the D7 brane from the D3 brane, $r\cos\theta(r)$ and the radius of the Ω_3 sphere on which the D7 brane is wrapped, $r\sin\theta(r)$. The different types of embedding of the D7 brane can be understood clearly from the plot of these two lengths presented in Figure 3.1. In the first of the two figures, we

plot $r\sin\theta$ vs. $r\cos\theta$ with zero electric field. The circular line represents the location of the black hole horizon. The different curves represent the embeddings for different quark masses. Since the background has a horizon at $r = r_h$, instead of the point $r = 0$, the effective distance of the flavor brane is measured from the surface of the horizon, which is a sphere of radius r_h. i.e., the distance of D7 brane from the horizon is $r\cos\theta - r_h$. We can have three situations: - (i) $r\cos\theta - r_h < 0$ signifying the fact that the D7 brane crosses the horizon and extends inside the horizon, i.e., *blackhole embedding*; (ii) $r\cos\theta - r_h = 0$ signifies that D7 brane just touches the horizon at a single point, i.e., *critical embedding*; and (iii) $r\cos\theta - r_h > 0$ signifies the fact that the D7 brane does not touch the horizon and is located above the horizon, i.e., *Minkowski embedding*. Here at the finite temperature, we start from the blackhole embedding and end at the critical embedding in the first plot of Figure 3.1. In the other plot, we turn on the electric field. We have plotted the critical embedding at three different values of the electric field: $E_0 = 0.0,\ 0.6\ \&\ 0.9$. The plot shows that with increasing electric field values, the effective horizon moves away from the original horizon and the quark mass of the corresponding embedding increases. The quark masses for the above three values of electric fields are $m_q = 0.9,\ 1.1\ \&\ 1.3$ accordingly. Therefore, the electric field increases the quark mass for critical embedding, i.e., the critical mass. With the electric field the type of embedding is identified with respect to $r = r_0$. So in the Minkowski embedding the D7-brane shrinks above r_0 and in the blackhole embedding the D7-brane crosses the vanishing locus $r = r_0$. We find two kinds of solutions in the blackhole embedding. The first kind is the solutions where the D7-branes are crossing $r = r_0$ and shrinking at a point before r_h. These solutions contain the conical singularity between the horizon and r_0. The second kind of solution is smooth. They smoothly cross the original horizon $r = r_h$ without encountering any singularity. We have found that smooth embedding occurs for the electric field value $E_0 < 0.86 r_h^2$. So for smooth embedding, we need to maintain an electric field smaller than this critical value $E_{\rm cr} \approx 0.86 r_h^2$.

So in our study, we will consider the weak electric field to ensure the smooth embedding. For a strong electric field, the system becomes complicated due to the presence of

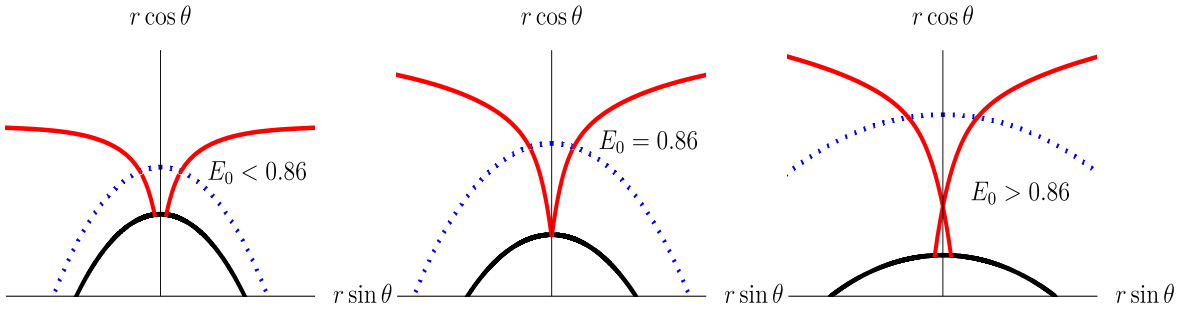

Figure 3.2: The plots of embedding function for different electric fields $E_0 < E_{cr}$, $E_0 = E_{cr}$ and $E_0 > E_{cr}$ at $r_h = 1$ and $\theta_0 = 0.1$. We find $E_{cr} = 0.86$.

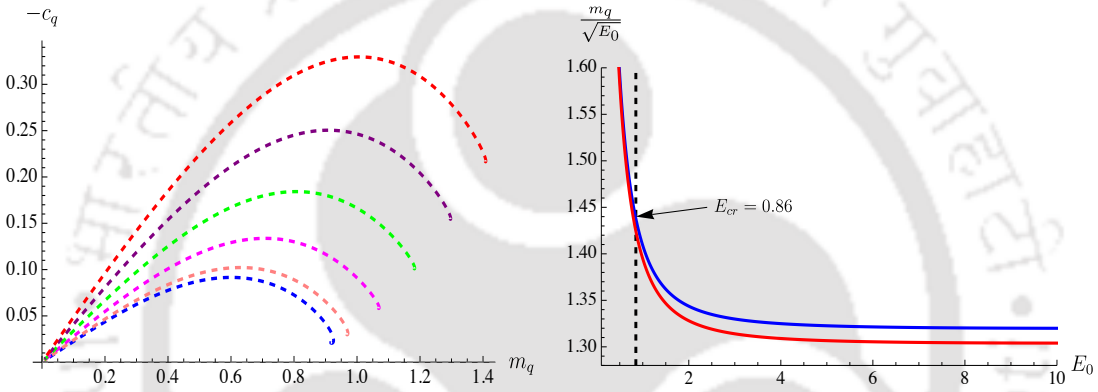

Figure 3.3: The condensate c_q vs the quark mass m_q with fixed temperature $T = 1/(\pi R_4^2)$ for different electric fields. From bottom, $E_0 = 0.0,\ 0.2,\ 0.4,\ 0.6,\ 0.8\ \&\ 1.0$. *Right* : Plot of $m_q/\sqrt{E_0}$ vs the electric field for two different values of embeddings.

those aforementioned singularities, and further backreaction will be important. We will work strictly in the perturbative limit.

Two important meson parameters namely the quark mass m_q and quark condensate c_q are numerically extracted from the asymptotic expansion of θ using (3.38). In Figure 3.3, we have plotted those quantities for different values of the electric field E_0. From the plot, we find $c_q = 0$ at $m_q = 0$ irrespective of E_0. The behaviour of the quark condensate is highly non-linear with increasing mass. At low quark mass m_q, the magnitude of c_q increases linearly. However, with increasing mass, c_q reaches maximum and then starts decreasing till the point of critical mass $m_q = m_q^{crit}$, where the meson starts to melt. Therefore, beyond

this mass value, the condensate does not exist. From the plot, we see that the critical mass m_q^{crit} increases with the increasing value of E_0 [141, 142]. The binding energy of mesons is expected to be proportional to the mass of its constituent quarks. Under the influence of an external electric field, the quark and anti-quark pair of the bound state meson experience Coulomb force in opposite directions, and that helps in the dissociation of the meson by decreasing its binding energy. Hence, in a stronger electric field background, meson needs higher binding energy to survive, which leads to a higher critical mass of the quark. In previous studies [141], we have also observed that this critical mass is proportional to $\sqrt{E_0}$. In Figure 3.3, we have plotted $\frac{m_q}{\sqrt{E_0}}$ with E_0 for two different values of $\theta = 0.09, 0.25$ with $r_h = 1$. These embedding values are less than the critical embedding. So, with these embeddings, we will not face the conical singularity problem. At a lower value of the electric field, we can see that there is no distinction between the embeddings. The difference becomes clear at higher values of the electric field. For different r_h, we have calculated the critical value of the electric field numerically. For $r_h = 0.9, E_{\text{cr}} = 0.75$ and for $r_h = 1.1, E_{\text{cr}} = 0.87$.

On the other hand, the inclusion of an electric field decreases the critical temperature of melting and the condensation parameter c_q is inversely scaled with temperature. This is the reason behind the increase of $-c_q$ with E_0. A more detailed explanation of this model can be found in [141, 142].

3.2 Pole-skipping and Characteristic parameters of Chaos

The primary goal of this work is to study the chaos in the $3+1$ dimensional flavored Yang-Mills theory. It is very common to calculate the Lyapunov exponent and butterfly velocity to measure the quantum chaos in such a model. In this context, one can get these parameters from the vv-component of the linearised Einstein equation. This method is well-known from various previous articles [86, 98]. Now, we employ this method in the above gravity background – the embedded probe D7 branes in black D3 brane metric. We take the following

perturbation in the background metric (3.7)

$$\bar{g}_{(5)\mu\nu} = g_{(5)\mu\nu} + \delta g_{\mu\nu}(r) e^{-i\omega v + ikx}, \tag{3.40}$$

where, the perturbation is assumed to propagate along x direction with frequency ω and momentum k. As the chaos is related to the energy density correlation function on the boundary theory, in the bulk, the corresponding perturbations need to have longitudinal polarization. These kinds of perturbation modes are also called the sound modes or scalar modes. Here, the sound modes metric perturbations are $\{\delta g_{ab},\, \delta g_{yy} + \delta g_{zz}\}$ where $a,\, b$ correspond to $v,\, r,\, x$. Without any loss of generality, we chose metric perturbations to be traceless, $\delta g_{yy} = \delta g_{zz} = -\delta g_{xx}/2$, which keeps $\theta(r)$ invariant. Further, we consider the gauge $\delta g_{r\mu} = 0$ for all μ. With this, the sound channel perturbation consists of only three independent components, $\{\delta g_{vv},\, \delta g_{vx},\, \delta g_{xx}\}$. Our main target is to look for the pole-skipping point associated with the metric perturbation variables. Therefore, we expand the metric perturbation near the effective horizon as follows,

$$\delta g_{\mu\nu} = \delta g^{(0)}_{\mu\nu} + \delta g^{(1)}_{\mu\nu}(r - r_0) + \cdots .$$

Upon using these near effective-horizon expansions into the vv-component of the linearised Einstein equation (3.23), we examine the coefficients of each order in $(r - r_0)$ expansion. The coefficients of zeroth order sound mode perturbations $\{\delta g^{(0)}_{vv},\, \delta g^{(0)}_{vx},\, \delta g^{(0)}_{xx}\}$ consists only two unknowns – ω and k resulting into following equation,

$$\begin{aligned} &8k^2 R_4^8 + \left(\sqrt{2E_0^2 + 4r_0^4} + 2r_0^2\right)\left(\frac{12 R_4^4 E_0^2}{r_0^4} - \frac{6i R_4^6 \omega}{r_0}\right) \\ &+ n_f \left[\left(\sqrt{2E_0^2 + 4r_0^4} + 2r_0^2\right)\left(\frac{2R_4^4 r_0^4}{E_0^2 + 2r_0^4} - 2r_0^4 + R_4^4\right) + 8r_0^6\right] \sin^3\theta_0 = 0 \end{aligned} \tag{3.41}$$

and, $$8kR_4^6\left(-3ir_h^4 + ir_0^4 + R_4^2 \omega r_0^3\right) = 0. \tag{3.42}$$

From these equations (3.42), we get,

$$\omega = i\frac{3r_h^4 - r_0^4}{R_4^2 r_0^3} = \frac{i}{R_4^2}\frac{2(\pi T R_4^2)^4 - E_0^2}{\left((\pi R_4^2 T)^4 + E_0^2\right)^{3/4}}, \tag{3.43}$$

where, we have used the relations $r_0^4 = r_h^4 + E_0^2$ and $r_h = \pi R_4^2 T$. Note that, from the right plot of Figure 3.3, we have already observed that $E_{cr} < r_h^2$. So, the allowed value of the electric field is always $E_0 < r_h^2$ which implies $E_0^2 \ll T^4$. Thus the shift due to the electric field term in the effective horizon is always very small compared to the blackhole horizon. Therefore, utilizing the relation given in (1.53), the Lyapunov exponent is calculated to be,

$$\begin{aligned}\lambda_L =& \frac{2(\pi T R_4^2)^4 - E_0^2}{R_4^2\left((\pi R_4^2 T)^4 + E_0^2\right)^{3/4}}\,, \\ =& 2\pi T\left[1 - \frac{5E_0^2}{4\pi^4 R_4^8 T^4} + \frac{33E_0^4}{32\pi^8 R_4^{16} T^8} + \mathcal{O}(E_0^5)\right]\,. \end{aligned} \tag{3.44}$$

The Lyapunov exponent in (3.44) is found to be affected by the electric field. The parameter R_4 is connected to the YM theory as $R_4^2 = \sqrt{g_{\rm YM}^2 N_c}$. So, from this Lyapunov exponent, we can see the dependence on N_c and $g_{\rm YM}$. In the absence of an electric field, we obtain the standard expression $\lambda_L = 2\pi T$, which saturates the MSS bound. Therefore, without the current source, the system is maximally chaotic. From (3.43), the Lyapunov exponent is found to be zero if $r_0^4 = 3r_h^4$ or $E_0^2 = 2\pi^4 R_4^8 T^4$, which sets the cut-off value of field $E_0 = \sqrt{2} r_h^2$. But this value is beyond the critical value E_0^{cr}. Further in our perturbative frame, the flavour density is too small as it is proportional to n_f. To keep the model consistent, the applied electric field E_0 should be small enough so that the induced current does not make much change in the charge distribution. So here the Lyapunov exponent can not be zero by tuning the electric field.

In the limit $E_0^2 << (\pi T R_4^2)^4$, we can write the above Lyapunov exponent (3.44) as,

$$\lambda_L \sim 2\pi T\left(1 - \frac{5E_0^2}{4\pi^4 R_4^8 T^4}\right) = 2\pi T\left(1 - \frac{5E_0^2}{4\pi^4 g_{\rm YM}^4 T^4 N_c^2}\right). \tag{3.45}$$

In Figure 3.4, we have plotted the Lyapunov exponent λ_L with the variation of the electric field. As the electric field E_0 increases, λ_L decreases monotonically. We have plotted the λ_L up to the critical value of the electric field only. As we have already discussed, beyond that critical value, we have conical solutions. So, we must have to avoid those solutions by restricting the electric field. Another point is, that turning on the electric field, pulls the quark/anti-quark pair apart, and lowers their binding energy. The plot, therefore, indicates an

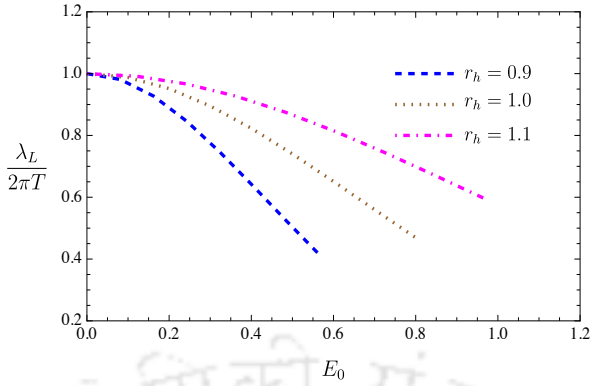

Figure 3.4: Plot of Lyapunov exponent λ_L vs electric field E_0 at three different temperature $\pi R_4^2 T = 0.9,\ 1.0\,\&\,1.1$ and $n_f = 1$.

interesting fact that as meson's binding energy decreases, the system becomes less chaotic with decreasing Lyapunov exponent.

The solution of k can be found from (3.42) which assumes the following form,

$$\begin{aligned} 8R_4^8 k^2 = &\left(\sqrt{2E_0^2 + 4r_0^4} + 2r_0^2\right)\left(-\frac{12R_4^4 E_0^2}{r_0^4} + \frac{6iR_4^6\omega}{r_0}\right) \\ &- n_f\left[\left(\sqrt{2E_0^2 + 4r_0^4} + 2r_0^2\right)\left(\frac{2R_4^4 r_0^4}{E_0^2 + 2r_0^4} - 2r_0^4 + R_4^4\right)\right. \\ &\left. + 8r_0^6\right]\sin^3\theta_0 \end{aligned} \tag{3.46}$$

Inserting the solution of ω into the above equation and expanding for small E_0, the solution of the momentum k can be written as follows,

$$\begin{aligned} k^2 = &-\frac{6r_h^2}{R_4^4} - \frac{3E_0^2}{4R_4^4 r_h^2} \\ &+ n_f\left(-\frac{r_h^2}{R_4^4} + \frac{E_0^2\left(r_h^4 - 3R_4^4\right)}{8r_h^2 R_4^8}\right)\sin^3\theta_0 + O\left(E_0^3/R_4^8\right) \end{aligned} \tag{3.47}$$

where, $\theta_0 \equiv \theta(r_0)$. The magnitude of momentum depends on the flavor parameter n_f and the electric field E_0. Without the probe D7 brane (i.e. $n_f = 0$ and $E_0 = 0$), we recover the standard result for pure AdS$_5$, $k^2 = -6\pi^2 T^2$. Unlike ω, the momentum receives a contribution from θ_0 which in turn leads to non-trivial quark mass m_q dependence, which is one of the important results of our present study. Given the above solutions for the pole-skipping momentum, the butterfly velocity can be calculated from the relation $v_b = \lambda_L/|k|$

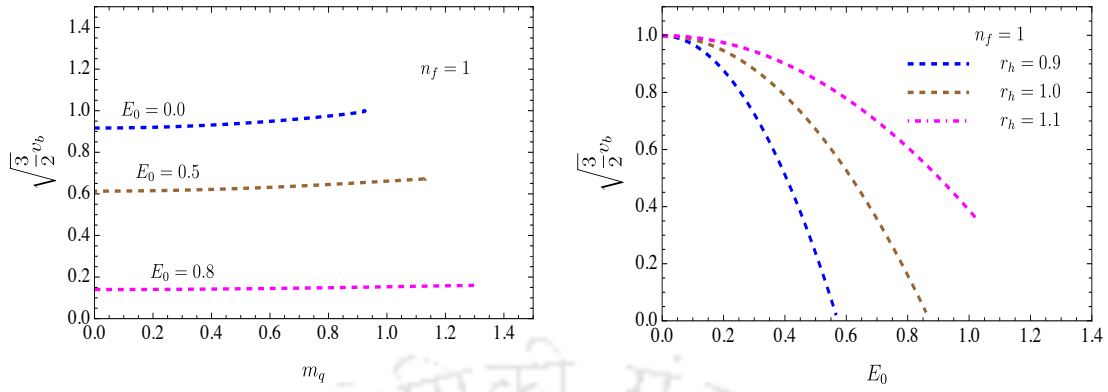

Figure 3.5: *Left*: The plot of butterfly velocity v_b vs quark mass m at three different fields $E_0 = 0.0,\ 0.5\ \&\ 0.8$ with fixed $T = 1/(\pi R_4^2)$ and $n_f = 1$. *Right*: The plot of butterfly velocity v_b vs electric field E_0 at $\theta_0 = 10^{-2}$ at three different temperature $\pi R_4^2 T = 0.9,\ 1.0\ \&\ 1.1$ and $n_f = 1$.

as,

$$v_b = \frac{r_0^2\left(2r_h^4 - E_0^2\right)\sqrt{3E_0^2 + 2r_h^4}\sqrt{\sqrt{6E_0^2 + 4r_h^4} - 2r_0^2}}{6\sqrt{6}E_0^3 R_4^4 r_0^3\left(3E_0^4 + 8E_0^2 r_h^4 + 4r_h^8\right)^{3/2}}\Big[-12E_0^2 R_4^4\left(3E_0^4 + 8E_0^2 r_h^4 + 4r_h^8\right)$$
$$+n_f \sin^3\theta_0\Big\{4r_0^{10}\left(2r_0^4 + E_0^2\right)\sqrt{6E_0^2 + 4r_h^4} - 12E_0^2 r_0^{12} + E_0^4 R_4^4 r_0^4$$
$$-2r_0^8\left(E_0^4 - 2E_0^2 R_4^4\right) - 16r_0^{16}\Big\}\Big] \tag{3.48}$$

At the small electric field expansion

$$v_b = \sqrt{\frac{2}{3}}\left[1 - \frac{21E_0^2}{16\pi^4 R_4^8 T^4} + \frac{n_f \sin^3\theta_0}{12}\left(-1 + \frac{E_0^2}{8R_4^4}\left(1 + \frac{17}{2\pi^4 R_4^4 T^4}\right)\right)\right] + O\left(E_0^3/R_4^6\right). \tag{3.49}$$

The butterfly velocity characterises how fast information scrambles in a system in the chaotic regime, and that turns out to be a function of the electric field, mass and current density of flavors in our study. We can see the effect in terms of YM theory by replacing R_4 in terms of $g_{\rm YM}$ and N_c. For pure AdS_5, the butterfly velocity is a numerical constant $\sqrt{\frac{2}{3}}$, which can be recovered from (3.48). In Figure 3.5, we represent the effect of flavor quark on the characteristic parameters of chaos. We plot the butterfly velocity v_b with the quark mass m_q for three different values of electric field, $E_0 = 0,\ 0.5\ \&\ 0.8$. For a fixed value of the electric

field, we find the butterfly velocity remains almost constant in the full range $0 \leq m_q \leq m_q^{crit}$. However, with increasing electric field, v_b decreases. The variation is almost the same as the Lyapunov exponent.

3.3 Master Equation

In the previous section, we have calculated the chaotic parameters from the vv component of Einstein's equation by perturbing the sound mode. In this section, we will analyze the perturbed modes by constructing a unique master equation from all the perturbed components of Einstein's equation as shown in [143]. In this D3-D7 background set-up, it would be noteworthy to study the dispersion relations at small ω, k. We can study these dispersion relations from the pole-skipping of retarded two-point function of the energy-momentum tensor [72, 76, 98]. Overall, these pole-skipping points unfold the relation between the boundary Green's function in the hydrodynamic limit and low energy perturbation with its near-horizon behaviour in the bulk. We perturb the background metric as $g_{\mu\nu} + \delta g_{\mu\nu}$, from which we compute the linearised coupled Einstein's equations. However, there exists a unique choice of gauge-invariant perturbation variable, which will be shown to reduce the perturbation equations into the unique form of the second-order master equation. The near-horizon behaviour of this master equation is enough to study the hydrodynamic dispersion relations. The complete solution of the perturbations comes from the master equation of the corresponding perturbation channel. The metric perturbation variables in a generic five-dimensional black hole can be classified into three classes: scalar or sound channel, vector or shear channel and tensor channel. We have chosen the wavenumber k to point along the x-direction. Then, we can write these perturbed channels as:

- Scalar or sound channel : δg_{vv}, δg_{vx}, δg_{xx} and $\delta g_{yy} + \delta g_{zz}$.
- Vector or shear channel : δg_{vy}, δg_{xy}, δg_{vz} and δg_{xz}
- Tensor channel : δg_{yz} .

We have imposed the radial gauge condition and trace-less condition, which we have thoroughly discussed in the previous section.

3.3.1 Sound Channel

The sound channel has three independent variables $\{\delta g_{vv},\, \delta g_{vx},\, \delta g_{xx}\}$. We can construct a gauge invariant master variable from these three variables,

$$\mathcal{Z}_{so}(r) = k^2\delta g_{vv}+2\omega k\delta g_{vx} + \omega^2\delta g_{xx} + \frac{k^2}{2}\left[2 - f(r) - \frac{\omega^2}{k^2}\right](-\delta g_{xx})\,,$$

which satisfies the unique master equation as follows,

$$\mathcal{Z}''_{so}(r) + \mathcal{P}_{so}(r,\omega,k) \times \mathcal{Z}'_{so}(r) + \mathcal{Q}_{so}(r,\omega,k) \times \mathcal{Z}_{so}(r) = 0. \tag{3.50}$$

The coefficients $\mathcal{P}_{so}$, $\mathcal{Q}_{so}$ are functions of r, ω and k. The detailed expressions of these coefficients are given in appendix C.8. To handle these large expressions, we have expanded them around $E_0 = 0$ and taken up to order of E_0^2. These coefficients consist of the flavor correction at the order of n_f. As $n_f \to 0$ and $E_0 \to 0$, the equation (3.50) reduces to the sound mode master equation of standard AdS_5. To obtain the pole-skipping points, we expand the master variable near the horizon as

$$\mathcal{Z}_{so}(r) = \sum_{n=0}^{\infty} Z_n \times (r - r_0)^n = Z_0 + Z_1 \times (r - r_0) + \cdots\,,$$

where Z_n are the non-zero finite constant coefficients. Consequently, the master equation around the horizon $r = r_0$ takes the following form,

$$\sum_{q=0}^{\infty}\left[\sum_{p=0}^{q+1} C_p^q\,(\omega,\, k) \times Z_p\right] \times (r - r_0)^q = 0, \tag{3.51}$$

where C_p^q depend on ω, k and other parameters of the system. At each order of $(r - r_0)$, the expression in the square bracket of (3.51) should vanish. It gives the relation between various Z_p. We can write it in the well-known matrix equation as discussed in [77, 78].

In this work, we discuss only the first-order pole-skipping point (ω_1, k_1), which comes from the equation (3.51) at the zeroth order term, i.e., $q = 0$, which gives

$$C_0^0(\omega,\, k) \times Z_0 + C_1^0(\omega,\, k) \times Z_1 = 0.$$

Since, Z_0 and Z_1 are non-zero and arbitrary, we must have $C_1^0(\omega_1,\, k_1) = 0$ and $C_0^0(\omega_1,\, k_1) = 0$. From the expansion of master equation (3.50) we get two equations given below,

$$r_h^2\left(2r_h - iR_4^2\omega_1\right) + \frac{E_0^2}{r_h^2}\left\{\left(r_h - iR_4^2\omega_1\right) + \omega_1^2\frac{3\left(2r_h - iR_4^2\omega_1\right)}{2\left(2k_1^2 - 3\omega_1^2\right)}\right\} = 0\,, \tag{3.52a}$$

$$\begin{aligned}
&6r_h^2 - R_4^4k_1^2 + r_h\left(2r_h + iR_4^2\omega_1\right)\frac{2k_1^2 + 9\omega_1^2}{2k_1^2 - 3\omega_1^2}\\
&+ n_f\frac{2R_4^4r_h^2\left(14k_1^2 - 9\omega_1^2\right) + r_h^6\left(10k_1^2 + 9\omega_1^2\right)}{12R_4^4\left(2k_1^2 - 3\omega_1^2\right)}\sin^3\theta_0\\
&+ \frac{E_0^2}{4r_h^3\left(2k_1^2 - 3\omega_1^2\right)^2}\left[\left(32r_h\left(8k_1^4 - 9k_1^2\omega_1^2\right) + iR_4^2\omega_1\left(92k_1^4 - 108k_1^2\omega_1^2 + 27\omega_1^4\right)\right)\right] +\\
&\qquad\qquad \mathcal{O}(n_f^2) = 0\,.
\end{aligned} \tag{3.52b}$$

Solving the above two equations simultaneously, we can evaluate the value of ω_1 and k_1. Here, we have assumed $2k_1^2 - 3\omega_1^2 \neq 0$ in evaluating these solutions.

Without D7 probe branes, $n_f = 0$ and $E_0 = 0$, the first-order pole-skipping point is located at $\omega_1 = -2ir_h/R_4^2$ and k_1 is given by the equation

$$6r_h^2 - R_4^4k_1^2 + 4r_h^2\frac{R_4^4k_1^2 - 18r_h^2}{R_4^4k_1^2 + 6r_h^2} = 0 \Rightarrow k_1^2 = \frac{2r_h^2}{R_4^4}\left(1 \pm 2i\sqrt{2}\right). \tag{3.53}$$

This solution matches with the known result obtained in [76, 86]. This result (3.53) also ensures the validity of our calculations.

With D7 brane (i.e., $n_f \neq 0$ and $E_0 = 0$), the first order pole-skipping occurs at $\omega_1 = -2ir_h/R_4^2$ and the equation of k_1 is

$$\begin{aligned}
&-12R_4^4\left(-4k_1^2R_4^4r_h^2 + 36r_h^4 + k_1^4R_4^8\right)\\
&+ n_fr_h^2\sin^3\theta_0\left(5k_1^2R_4^4r_h^4 + 36R_4^4r_h^2 - 18r_h^6 + 14k_1^2R_4^8\right) = 0,
\end{aligned}$$

from which k_1 can be solved and we get,

$$\begin{aligned}
k_1^2 = \frac{1}{24R_4^{12}}&\left(5n_fR_4^4r_h^6\sin^3\theta_0 + 2R_4^8r_h^2(24 + 7n_f\sin^3\theta_0)\right.\\
&\pm\left(R_4^8r_h^4(-18432R_4^8 + 384n_fR_4^4(8R_4^4 - r_h^4)\sin^3\theta_0\right.\\
&\left.\left.+n_f^2(14R_4^4 + 5r_h^4)^2\sin^6\theta_0)\right)^{1/2}\right).
\end{aligned} \tag{3.54}$$

We, therefore, find no effect of the flavor quarks on ω_1 as long as the Yang-Mills system contains only neutral meson states. However, the momentum value k_1 acquires non-trivial correction due to the presence of meson states. As the near-horizon value θ_0 appears in momentum k_1, we find that the momentum values are affected by the quark mass m_q.

With D7 brane and non-vanishing world volume electric field, we again can solve the above two equations (3.52a) and (3.52b) perturbatively in the small electric field limit and up to the first-order of n_f to find the first-order pole-skipping point.

$$\omega_1 = -\frac{2ir_h}{R_4^2} \pm \frac{R_4^6 E_0^2}{r_h^3}\left[\frac{1}{\sqrt{2}R_4^8} - \frac{n_f \sin^3\theta_0}{64R_4^{12}}\left(\left(\sqrt{2}\mp i\right) r_h^4 + 2\left(2\sqrt{2}\pm i\right) R_4^4\right)\right] + \mathcal{O}\left(E_0^3\right), \tag{3.55a}$$

$$k_1^2 = \frac{2\left(1\pm 2i\sqrt{2}\right) r_h^2}{R_4^4} + \frac{n_f r_h^2 \sin^3\theta_0}{24R_4^8}\left(\left(5\pm i\sqrt{2}\right) r_h^4 + 2\left(7\mp 4i\sqrt{2}\right) R_4^4\right) + \frac{R_4^4 E_0^2}{r_h^2}\left(\pm\frac{33+15i\sqrt{2}}{4R_4^8} + \frac{n_f \sin^3\theta_0}{768R_4^{12}}\left(\left(640\pm 263i\sqrt{2}\right) r_h^4 + 6\left(-32 \pm 89i\sqrt{2}\right) R_4^4\right)\right) + \mathcal{O}\left(E_0^3\right). \tag{3.55b}$$

To this end let us remind the reader that, previously, we have seen that the boundary Green's function related to the sound channel perturbations has given the pole-skipping points that are located in the upper half of the complex ω-plane. Therefore, those pole-skipping points can be directly related to the chaos parameters. However, from the master equation analysis, we get the pole-skipping points (3.55), that are located on the lower half of the complex ω-plane. These P-S points, therefore, cannot be related to the chaos parameters. However, it shows the same kind of non-uniqueness in the associated boundary Green's function. In the absence of the probe brane, the absolute value $|k_1^2| = 6r_h^2/R_4^4$ from (3.53) and $|v_b| = \sqrt{2/3}$ are the same for both of the upper and lower half-planes. However, perturbation modes are found to be related to the propagation and decay of the energy energy fluctuation in the boundary theory. The real and imaginary part of k_1 respectively gives diffusion and decay of energy density fluctuation in x direction. We can discuss the dispersion relation of hydrodynamic modes that pass through P-S points. We have noticed that the first-order P-S point is very close

to the hydrodynamic dispersion curve i.e., we can expect this point to satisfy the relation $\omega = -i\mathcal{D}_T k^2$. We indeed can define an effective thermal diffusion constant from the real part of k_1, as,

$$\mathcal{D}_T^{\text{eff}} = \frac{\text{Re}[i\omega_1]}{\text{Re}[k_1^2]} = \frac{1}{2\pi T} - n_f \frac{\pi^4 R_4^4 T^4 + 1}{48\pi T} \sin^3\theta_0 + \left(\frac{3}{8\pi^5 R_4^8 T^5} - n_f \frac{5\left(71\pi^4 R_4^4 T^4 - 6\right)}{3072\pi^5 R_4^8 T^5} \sin^3\theta_0 \right) E_0^2 + \mathcal{O}\left(E_0^3\right). \tag{3.56}$$

In the absence of the probe brane and the electric field, the thermal diffusion constant is found to be,

$$\mathcal{D}_T = \frac{1}{2\pi T} = \frac{3}{4\pi} \frac{v_b^2}{T}, \tag{3.57}$$

which is observed to be connected to the butterfly velocity [144]. The presence of the probe brane modifies the diffusion constant in a nontrivial manner.

3.3.2 Shear Channel

The perturbations in the direction transverse to the propagation direction are analysed in this section. These perturbation modes as a group belong to the shear channel. On the gauge theory side, these perturbations are the fluctuation of the momentum density. Using shear channel perturbations $\delta g_{vy}(r)$, $\delta g_{xy}(r)$, $\delta g_{vz}(r)$ and $\delta g_{xz}(r)$, we can construct two gauge invariant variables as $\mathcal{Z}_y = k\delta g_{vy} + \omega \delta g_{xy}$ and $\mathcal{Z}_z = k\delta g_{vz} + \omega \delta g_{xz}$. By manipulating the perturbed Einstein's component equations, we can construct the master equation for these gauge-invariant variables. The general form of the master equations can be written as,

$$\mathcal{Z}_{sh}''(r) + \mathcal{P}_{sh}(r,\omega,k) \times \mathcal{Z}_{sh}'(r) + \mathcal{Q}_{sh}(r,\omega,k) \times \mathcal{Z}_{sh}(r) = 0. \tag{3.58}$$

where, $\mathcal{Z}_{sh}(r) \equiv k\delta g_{vy}(r) + \omega \delta g_{xy}(r) \equiv k\delta g_{vz}(r) + \omega \delta g_{xz}(r)$. The coefficients are given in appendix C.9. Using the same method as the sound mode, we find the pole-skipping point from the near-horizon expansion.

In the small electric field limit, the equations for the pole-skipping points are,

$$2r_h^2\left(2r_h - iR_4^2\omega_1\right) + \frac{E_0^2\left(4r_h\left(k_1^2 + 2\omega_1^2\right) - iR_4^2\omega_1^3\right)}{\omega_1^2 r_h^2} = 0, \tag{3.59a}$$

and,

$$
\begin{aligned}
&-k_1^2 R_4^4+8r_h^2-\frac{iR_4^2 r_h\left(4k_1^2+7\omega_1^2\right)}{\omega_1}+\frac{1}{4}n_f r_h^2\sin^3\theta_0\left(2-\frac{r_h^4}{R_4^4}\right)\\
&+E_0^2\left[\frac{1}{4\omega_1^3 r_h^3}\left(32\omega_1 r_h\left(k_1^2+\omega_1^2\right)-iR_4^2\left(16k_1^4-12k_1^2\omega_1^2+7\omega_1^4\right)\right)\right.\\
&+\frac{n_f\sin^3\theta_0}{8R_4^4\omega_1^2 r_h^2\left(r_h^4+2R_4^4\right)}\left(4k_1^4\left(r_h^4\right.\right.\\
&\left.\left.\left.-2R_4^4\right)^2+\omega_1^2\left(-4R_4^4 r_h^4-3r_h^8+4R_4^8\right)\right)\right]=0. \qquad (3.59b)
\end{aligned}
$$

We can find the first-order pole-skipping point from the above equations. The approximate solutions in terms of the small n_f limit of the above equations are:

$$\omega_1\approx-\frac{2ir_h}{R_4^2}-in_f E_0^2\frac{2R_4^4-r_h^4}{8r_h^3R_4^6}\sin^3\theta_0+\mathcal{O}\left(E_0^3\right), \qquad (3.59c)$$

$$
\begin{aligned}
k_1^2\approx\frac{6r_h^2}{R_4^4}-n_f r_h^2\frac{2R_4^4-r_h^4}{4R_4^8}\sin^3\theta_0+\frac{E_0^2}{r_h^2}\left[\frac{69}{2R_4^4}+n_f\frac{15r_h^8-20R_4^4r_h^4-4R_4^8}{8R_4^8\left(r_h^4+2R_4^4\right)}\sin^3\theta_0\right]\\
+\mathcal{O}\left(E_0^3\right). \qquad (3.59d)
\end{aligned}
$$

In the absence of the flavor brane and the electric field, the first-order pole-skipping point matches with the previous result $\omega_1=-2i\pi T$, $k_1^2=6\pi^2T^2$ given in [76, 86]. From the above result, we can see the presence of probe D7 brane parameters.

Like the sound channel, the first-order pole-skipping point follows the hydrodynamic dispersion relation $\omega=-i\mathcal{D}_p k^2$ associated with the momentum transportation. Therefore, the corresponding momentum diffusion constant can similarly be calculated up to order E_0^2 as given below,

$$
\begin{aligned}
\mathcal{D}_p^{\text{eff}}&=\frac{i\omega_1}{k_1^2}\\
&=\frac{1}{3\pi T}+n_f\frac{2-\pi^4R_4^4T^4}{72\pi T}\sin^3\theta_0-\frac{E_0^2}{\pi^5R_4^8T^5}\left[\frac{23}{12}+n_f\frac{76-20\pi^4R_4^4T^4-5\pi^8R_4^8T^8}{144\left(2+\pi^4R_4^4T^4\right)}\sin^3\theta_0\right].
\end{aligned}
$$

In the absence of the probe brane and the electric field, the momentum diffusion constant is,

$$D_p=\frac{1}{3\pi T}=\frac{1}{2\pi}\frac{v_b^2}{T}. \qquad (3.59e)$$

It is very tempting to connect the momentum diffusion constant with the butterfly velocity [73]. However, in a physical sense, this relationship is not very well-motivated. A factor

of $3/4$ is missing in the diffusion constant calculated from the P-S point, whereas in the boundary theory, it comes out to be $\frac{1}{4\pi T}$ [145]. The presence of the probe brane modifies the diffusion constant up to higher orders of the electric field.

3.3.3 Tensor channel

Since the perturbation modes are assumed to propagate along the x-direction, the tensor mode will have polarization in the $y-z$ plane. Hence, $\delta g_{yz}(r)$ is the only perturbed component in this channel. Assuming $\mathcal{Z}_{ten} = \delta g_{yz}$, the master equation can be written in the following form,

$$\mathcal{Z}''_{ten}(r) + \mathcal{P}_{ten}(r,\omega,k) \times \mathcal{Z}'_{ten}(r) + \mathcal{Q}_{ten}(r,\omega,k) \times \mathcal{Z}_{ten}(r) = 0. \tag{3.60}$$

The coefficients are given in appendix C.10. Using the same method as the sound mode, we find the pole-skipping point from the near-horizon expansion.

The first-order pole-skipping point $(\omega_1,\ k_1)$ comes from the equations:

$$4r_h\left(E_0^2 + r_h^4\right) - iR_4^2\omega_1\left(E_0^2 + 2r_h^4\right) = 0, \tag{3.61a}$$

and,

$$8k_1^2R_4^8 + \frac{6iR_4^6\omega_1\left(E_0^2+4r_h^4\right)}{r_h^3} - \frac{n_f\sin^3\theta_0}{r_h^2}\left(2R_4^4\left(E_0^2+2r_h^4\right) - 3E_0^2r_h^4 - 2r_h^8\right) = 0. \tag{3.61b}$$

We, therefore, find the first-order pole-skipping point at

$$\omega_1 = -\frac{4ir_h}{R_4^2}\frac{r_h^4+E_0^2}{2r_h^4+E_0^2}, \tag{3.62a}$$

and,

$$k_1^2 = -\frac{3\left(4r_h^4+E_0^2\right)\left(r_h^4+E_0^2\right)}{r_h^2R_4^4\left(2r_h^4+E_0^2\right)} + \frac{n_f\sin^3\theta_0}{8r_h^2R_4^8}\left(2R_4^4\left(E_0^2+2r_h^4-3E_0^2r_h^4-2r_h^8\right)\right). \tag{3.62b}$$

In the absence of the flavor brane, we recover the result of pure AdS_5 [76, 86] from the above results (3.62a) & (3.62b) by putting $n_f = 0$ and $E_0 = 0$. This point is given as $\omega_1 = -2ir_h/R_4^2$ and $k_1^2 = -6r_h^2/R_4^4$.

The results for the neutral D7 brane can again be derived from the above results with $E_0 = 0$. It is given as

$$\omega_1 = -\frac{2ir_h}{R_4^2}, \qquad \text{and,} \quad k_1^2 = -\frac{6r_h^2}{R_4^4} + n_f \sin^3\theta_0 \frac{r_h^2\left(2R_4^4 - r_h^4\right)}{4R_4^8}. \tag{3.62c}$$

Whereas we have found the value of $(\omega_1,\, k_1)$ for charged D7 brane as given in (3.62a) and (3.62b). These results can be written with the small E_0 approximation as below,

$$\omega_1 = -\frac{2ir_h}{R_4^2} - \frac{iE_0^2}{r_h^3 R_4^2} + \mathcal{O}\left(E_0^3\right), \tag{3.62d}$$

$$\text{and,} \quad k_1^2 = -\frac{6r_h^2}{R_4^4} + n_f \sin^3\theta_0 \left(\frac{r_h^2\left(2R_4^4 - r_h^4\right)}{4R_4^8} + \frac{2R_4^4 - 3r_h^4}{8r_h^2 R_4^8} E_0^2\right) + \mathcal{O}\left(E_0^3\right). \tag{3.62e}$$

From the above result, we can conclude that, in the presence of the charged probe D7 brane, we get the effect of the effective horizon on the pole-skipping points. Momentum value is affected by the near-horizon (effective) value of the radius of Ω_3 sphere.

In this chapter, we have studied the chaotic behaviour of a holographic QCD system in the presence of an external electric field by pole-skipping analysis. The Lagrangian of the probe brane vanishes at some special radial distance away from the D3 brane horizon, which will act as the effective horizon of the open-string induced metric on the D7 brane world volume. The emergence of such an effective horizon is expected to give rise to non-trivial effects, and indeed alter the chaos dynamics of the boundary theory in terms of characteristic parameters (λ_L, v_b). Further, the probe branes can support the background Maxwell's field, and in the dual theory that will correspond to interacting charged flavors with the electric field. However, for the perturbative consideration, we must maintain the electric field in a very small range. This configuration is expected to add additional characteristic changes in the diagnostic parameters of chaos. Without the flavor D7 branes, a stack of black D3 branes in supergravity limit gives rise to an AdS-blackhole background in the bulk, corresponding to the Yang-Mills theory on the boundary. In the paper [38], it was first shown that the AdS black holes are maximally chaotic, and hence the Lyapunov exponent of the boundary theory saturates the Maldacena-Shenker-Stanford (MSS) bound [40]. In the presence of Maxwell's field in the world volume of probe D7 brane, we found the dual theory to be no

longer maximally chaotic, and the Lyapunov exponent depends on the electric field and the butterfly velocity depends on both the electric field and the number of flavors N_f in the dual system. In this work, we have explicitly shown how the electric field affects the Lyapunov exponent by pole-skipping analysis and this exponent obeys the MSS bound.

Non-trivial dependence of the chaotic parameters on the background electric field can be understood in terms of the behaviour of the meson states under the field. The light quark/anti-quark bound state in the boundary theory gives rise to the meson spectrum. The mesons are charged neutral in this case. But the constituent quark and anti-quark are positively and negatively charged respectively. Without any external electric field, the neutral meson states will not get affected in their probe limit. But, in the presence of an external electric field, the quark/anti-quark pair of mesons separates away by reducing its binding energy. Further, these charged quarks can have strong interaction with the background gluons in this situation. The motion of the neutral particle in the neutral background is more chaotic than the motion of the charged particle in the charged background. Because in the presence of the background charge, the charged particle encounters restoring drag due to Coulomb's interaction. Therefore the chaotic behaviour is expected to reduce due to the applied electric field. Further, the corresponding Lyapunov exponent is affected by the electric field. All these new physical effects can strongly influence the Yang-Mills dynamics. Lowering the binding energy causes the mesons to melt at a lower value of temperature, and at that point, the characteristic parameters of the chaos reduce. These new features influencing quantum chaos have been discussed in this present literature.

Apart from deriving the parameter of the chaos, we further calculate the P-S points associated with the hydrodynamic modes. With the choice of gauge invariant variables, we have constructed the master equations for sound, shear, and tensor channels perturbation variables [143]. Expanding those equations near the effective horizon induced by the D7 brane, we have again calculated the P-S points in all three channels and discussed their relation with hydrodynamic transport and their dependence on the tuning parameters such as external electric field E_0, the number of flavors N_f and quark mass m_q.

So far in this thesis, we have used pole-skipping analysis only to study the chaotic behaviour of a system. But, there are various methods to investigate the chaotic properties. In the next chapter, we will discuss three methods of chaos computation in a non-relativistic background and show an equivalence among all those methods.

Chapter 4

An equivalence of three butterflies in Lifshitz background

Holographic duality can also be extended as general gauge/gravity duality where the field theory breaks conformal invariance and its dual geometry is eventually a non-AdS one. A class of nonrelativistic Lifshitz field theories are such theories that follow Lifshitz scaling symmetry

$$t \to \Omega^{\xi} t, \quad \vec{x} \to \Omega \vec{x}, \tag{4.1}$$

characterized by the dynamical critical exponent $\xi \in \mathbb{R}$, $\xi \geq 1$. Such QFTs break Lorentz invariance due to the presence of an anisotropic scale factor along the temporal direction and thus do not adhere to CFT. The holographic dual of Lifshitz field theories is the nonrelativistic Lifshitz geometry which shares similar scale symmetry [146–150]. Exploration of such theories finds its significance in the context of the correlation between high energy physics and condensed matter physics due to the fact that these theories, especially for $\xi = 2$, are directly related to strongly correlated electron systems. A series of research for rigorous understanding of such field theories have been going on over the last decade by implementing various perspectives [151–155]. We explore the butterfly effect in asymptotically Lifshitz black holes by calculating butterfly velocity and the Lyapunov exponent via three distinct methods–entanglement wedge method, OTOC computation and pole-skipping. Our comparative analysis delivers an exact matching of the results obtained from these methods. This

eventually demonstrates the equivalence between these methods for deriving quantum chaos for an asymptotically Lifshitz black hole.

In addition, we also elucidate some of the chaotic features, to name, the eikonal bulk phase shift in the heavy-heavy-light-light gravitational scattering and the Lyapunov exponent, from the classical perspective. Classically, the eikonal phase is known to be related to the deflection angle of the null geodesic of a gravity background [156–158]. It also finds its own significance in the AdS/CFT holography, see [159–161] for review. In [162], the bulk eikonal phase shift for the heavy-heavy-light-light particle scattering in the asymptotically AdS black hole is found to be dual to the OTOCs in the Regge limit of the corresponding dual conformal field theory. Moreover, there is evidence of classical/quantum correspondence in different chaotic one-body or two-body quantum systems where the classical Lyapunov exponent can be exactly extracted from the growth rate of the OTOCs [163, 164]. In light of such studies, we wish to understand a suitable connection of the classical bulk phase with the phase factor in the OTOCs of our chosen system, as well as, propose an empirical relation between the temperature of the system and the turning point of the null geodesic in that system for any fixed value of the anisotropy parameter ξ by calculating the classical Lyapunov exponent. To compute for eikonal phase shift, the null geodesic equation plays a dominant role in determining the impact parameter, often taken as the ratio of conserved momenta to conserved energy, which eventually affects the nature of the eikonal phase. For real and imaginary eikonal phases, one must obtain elastic and completely nonelastic gravitational scattering respectively. Here in this work, we also present how the anisotropy of our chosen gravity background causes different kinds of eikonal phases that result in different types of scatterings when we gradually shift the extrema of the null geodesic from near boundary to near horizon limit. Added to this, we verify the eikonal phase using the WKB approximation of the equation of motion of a scalar field. Specifically, we examine for a probable matching of the eikonal phase yielded from both methods. Furthermore, we wish to briefly exhibit the classical nature of the Lyapunov exponent in the anisotropic background and its consistency with the restrictions that we must impose on the choices of the extrema for the validity of

our study.

4.1 Asymptotically Lifshitz black hole

In this section, we briefly revisit the black hole geometries that asymptote the nonrelativistic planar Lifshitz background. Such black holes were first developed in [165] for $d = 2,\ \xi = 2$. These black hole solutions are found to consistently satisfy the equations of motion of the Einstein-Proca type gravity theories with the inclusion of a massive vector field [166],

$$\mathcal{S} = \frac{1}{2\kappa^2}\int d^{d+1}x\sqrt{-g}\left[\mathcal{R} - 2\Lambda - \frac{1}{4}F_{\mu\nu}F^{\mu\nu} - \frac{1}{2}m^2A_\mu A^\mu\right], \qquad F_{\mu\nu} = \partial_\mu A_\nu - \partial_\nu A_\mu\,. \tag{4.2}$$

Here, for any (d+1) dimensional Lifshitz black hole, the cosmological constant Λ must be a negative quantity that depends on the anisotropy index ξ as $\Lambda = \frac{d-1}{2(d+1)}\mathcal{R}(\xi)$. Again, $F_{\mu\nu}$ is the electromagnetic field strength. The appearance of a massive vector field with mass m in the above action causes the breaking of the Lorentz invariance in the corresponding metric. The generic form of the $(d+1)$ dimensional Lifshitz black hole solution of the above action can be written as,

$$ds^2 = \frac{R^2}{z^2}\left[-\frac{R^{2(\xi-1)}}{z^{2(\xi-1)}}f(z)dt^2 + d\vec{x}_{d-1}^2 + \frac{dz^2}{f(z)}\right], \qquad f(z) = 1 - \left(\frac{z}{z_h}\right)^{d-1+\xi}. \tag{4.3}$$

R is the AdS radius, z is the radial coordinate and z_h is the black hole horizon. This geometry asymptotically reaches the planar Lifshitz spacetime

$$ds^2 = \frac{R^2}{z^2}\left[-\frac{R^{2(\xi-1)}}{z^{2(\xi-1)}}dt^2 + d\vec{x}_{d-1}^2 + dz^2\right]. \tag{4.4}$$

Similarly as the planar Lifshitz spacetime, the Lifshitz black hole geometry also follows anisotropic scaling along the time and space directions

$$t \to \Omega^\xi t,\ \ z \to \Omega z,\ \ \vec{x} \to \Omega\vec{x}\,, \tag{4.5}$$

that breaks the Lorentz invariance. Equation (4.3) describes a one-parameter family of linearly charged Lifshitz black holes that are thermodynamically stable and become extremal at the vanishing size [167]. The thermodynamics of such an asymptotically Lifshitz black hole can be reproduced from the holographic renormalization of the gravity theory represented by the action (4.2) [153]. The legitimate dual field theory that lives on the boundary of Lifshitz black hole geometry is the finite temperature version of the non-relativistic Lifshitz field theories. When we take 2D thermal CFT, the flat boundary that accommodates the CFT is compactified along the time direction and becomes a cylinder. This compactification is done by taking $t \to t + \beta$, where β gives the circumference of the compactifying circle. Thus β acquires the dimension of length. Now, let us consider a similar compactification of the boundary in the case of thermal LFT for which the dimension of time is [length]$^{\xi}$ due to Lifshitz scaling. Thus if we take $t \to t + \tilde{\beta}$ with the analogy of thermal CFT for the compactification, then $\tilde{\beta}$ should have the dimension of time. Thus we can assume the inverse temperature of thermal LFT as $\tilde{\beta} = \beta^{\xi}$, where β is the inverse temperature of the thermal CFT. Hence, in the dual bulk side, the temperature of the Lifshitz black hole will also be $T = \frac{1}{\beta^{\xi}}$. The temperature of the black hole is given by

$$T = \frac{1}{z_h^{\xi}} \frac{d-1+\xi}{4\pi} = \frac{1}{\beta^{\xi}} \equiv \frac{1}{\tilde{\beta}} \,. \tag{4.6}$$

Note that, $\tilde{\beta}$ has dimension of length. For maintaining simplicity in our further calculations, we will denote $\tilde{\beta}$ as β. In the next section, we start with the $(d+1)$-dimensional Lifshitz black hole geometry given in (4.3) to analyse the chaotic features via a quantum approach.

4.2 Analyses of quantum chaos

In this section, we will show the explicit calculations of the three methods that we are interested in to study the chaotic parameters. Our focus is to compare these results and see the similar dependence of the chaotic parameters on the anisotropy.

4.2.1 Entanglement wedge method

In AdS/CFT correspondence, entanglement wedge reconstruction [168–170] depicts that all the information of the entanglement wedge in the bulk lies in the boundary region. When we perturb the boundary state by a local operator and let the system evolve, then the information gets scrambled in the whole space at a late time. This information propagates outward with a constant velocity. The whole scenario has a bulk description. Perturbing the boundary means probing a particle close to the asymptotic boundary, which is falling toward the black hole in the bulk. This particle then follows a trajectory that reaches inside the extremal surface, also known as the Ryu-Takayanagi(RT) surface [171]. As the trajectory of the particle changes, the RT surface changes its shape. At late time, this RT surface reaches up to the near-horizon region of the black hole with a constant velocity – butterfly velocity (v_B). This method is very well-known for extracting the butterfly velocity [172]. In higher-derivative gravity theories also, this method is well understood [173]. In our work, we employ this method to calculate the butterfly velocity in the Einstein-Proca-type Lifshitz gravity theory. The action of such theories contains a massive vector field that breaks Lorentz symmetry[174]. It is very motivating to study the chaotic properties of such a theory.

We aim in this subsection to find the butterfly velocity with the entanglement wedge method. For this, we need to calculate the size of the smallest boundary region whose entanglement wedge encloses the infalling particle as shown in Figure 4.1. In this pictorial description, we can see that $z = 0$ is the boundary and $z = 1$ is the horizon of the black hole. A particle (shown by the red dot) is on the RT surface (shown by the light teal portions) bounded by the boundary region. In general, the RT surface location is determined by extremizing the holographic entanglement entropy functional. We can write the entropy functional as,

$$S_{\text{EE}} = 2\pi \int \mathrm{d}^{d-1}y\sqrt{\gamma}\,, \tag{4.7}$$

where γ is the determinant of the induced metric and y is the set of coordinates on an appropriate codimension-2 surface.

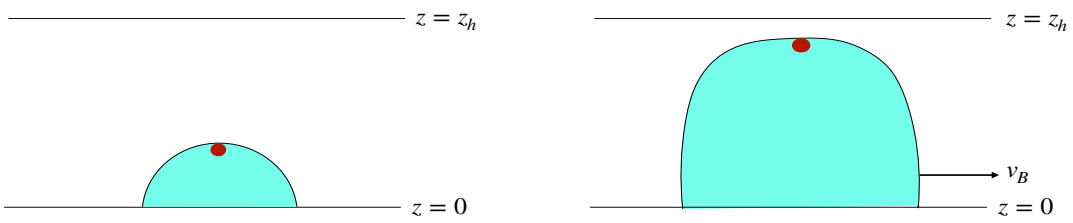

Figure 4.1: A particle (red dot) is enclosed in the RT surface (light teal)

Now, we will use background (4.3) for this wedge method. At a constant t hypersurface ($\mathrm{d}t = 0$) and parameterizing z as $z(r)$ with assumption $r = |x^i|$, we can write the induced metric as,

$$\gamma_{\alpha\beta}\,\mathrm{d}x^\alpha \mathrm{d}x^\beta = \frac{R^2}{z^2}\left[\left(1+\frac{z'^2}{f(z)}\right)\mathrm{d}r^2 + r^2\mathrm{d}\Omega_{d-2}^2\right]. \tag{4.8}$$

Note that in the (4.3), the near-horizon limit is achieved by $z = z_h$ limit and the boundary limit is achieved by $z = 0$ limit. As we will work with the near-horizon region, we define the RT surface in the $z = z_h$ limit by,

$$z(r) = z_h - \epsilon\, y(r)^2, \tag{4.9}$$

where we parameterize the near-horizon limit($z = z_h$) with a new function $y(r)$. The coefficient $\epsilon\,(>0)$ is a very small number and the function $y(r)$ is the RT profile, which we will solve from the RT equation by performing a Taylor series expansion around $\epsilon = 0$. Now, expanding the induced metric up to order ϵ, we get,

$$\begin{aligned}\gamma_{\alpha\beta}\,\mathrm{d}x^\alpha \mathrm{d}x^\beta &= R^2\left[\left(\frac{4\,\epsilon^2 y^2 y'^2}{(z_h-\epsilon\,y^2)^2 f_1(z_h-z)}+\frac{1}{(z_h-\epsilon\,y^2)^2}\right)\mathrm{d}r^2+\frac{r^2}{(z_h-\epsilon\,y^2)^2}\mathrm{d}\Omega_{d-2}^2\right],\\ &= \frac{R^2}{z_h^2}\left[\left(1+\frac{2\epsilon}{z_h}(y^2+\frac{2}{f_1}y'^2)\right)\mathrm{d}r^2 + r^2(1+\frac{2\epsilon}{z_h}y^2)\mathrm{d}\Omega_{d-2}^2+\mathcal{O}(\epsilon^2)\right],\end{aligned} \tag{4.10}$$

where we Taylor expand the factor $f(z)$ near the horizon up to the first order as $f(z) \approx f_1(z_h - z)$. The determinant of the induced metric is given by,

$$\sqrt{\gamma} = \frac{R^2 r^{d-2}}{z_h^{d-1}}\left[1+\frac{\epsilon}{z_h}\left((d-1)y(r)^2+\frac{2}{f_1}z_h y'(r)^2\right)\right]+\mathcal{O}(\epsilon^2)\,. \tag{4.11}$$

Now, we can write the RT equation by varying the above equation with respect to $y(r)$. Keeping terms only up to order ϵ, we get,

$$(d-1)y(r) - \frac{2z_h}{f_1}\left(y''(r) + (d-2)\frac{y'(r)}{r}\right) = 0\,. \tag{4.12}$$

Solving this second-order differential equation, we get,

$$y(r) = r^{-n}\left[\mathrm{J}_n(\mu r) + \mathrm{Y}_n(\mu r)\right]\,, \tag{4.13}$$

where J_n and Y_n are the Bessel functions of first kind and second kind respectively. In the above equation,

$$n = \frac{1}{2}(d-3), \qquad\qquad |\mu| = \sqrt{\frac{(d-1)(d-1+\xi)}{2{z_h}^2}}\,. \tag{4.14}$$

Here, the scaling parameter μ is behaving as the momentum. From the eq. (4.9), we can see that near the horizon z_h, the function $y(r)$ takes the form of 0. So, we will see the form of these Bessel functions near $r = 0$. At this vicinity, both these Bessel functions will behave as $\sim \mu^n$. Following [173], where the authors have calculated the butterfly velocity with an exponential ansatz, here in this paper, we have prescribed a more general result for calculating butterfly velocity without taking any ansatz.

The surface enclosing the particle is approaching the horizon at a constant speed, termed as butterfly velocity (v_B). We assume that at each point in time, the tip of the RT surface touches the particle which is visualised by demanding $y(r=0,t) \sim e^{-\frac{2\pi}{\beta}t}$. Therefore, with the value of μ, we can calculate the butterfly velocity as,

$$v_B = \frac{2\pi}{\beta|\mu|} = \frac{2\sqrt{2}\pi z_h}{\beta\sqrt{(d-1)(d-1+\xi)}}\,. \tag{4.15}$$

So, the butterfly velocity v_B at horizon becomes,

$$v_B = z_h^{1-\xi}\sqrt{\frac{d-1+\xi}{2(d-1)}}\,. \tag{4.16}$$

This is the butterfly velocity for a $d+1$- dimensional Lifshitz black hole. In $\xi \to 1$ limit, we are getting the planar black hole result $v_B = \sqrt{\frac{d}{2(d-1)}}$. So, the anisotropy affects the

butterfly velocity nontrivially. Butterfly velocity characterizes the propagation of chaos in a local system. It has been observed previously that the chaotic feature of the Lifshitz invariant system increases for large ξ values, in other words, for large anisotropy[175–177]. From the expression of v_B that we get, it is obvious that v_B increases monotonically with ξ for any fixed dimension of the bulk. Thus, the chaotic feature of the asymptotic Lifshitz black hole monotonically increases with larger anisotropy which is consistent from the previous results. Furthermore, we can substitute for z_h in terms of T in the equation (4.16) by using (4.6) so that

$$v_b = (4\pi T)^{\frac{\xi-1}{\xi}} \frac{1}{\sqrt{2(d-1)}} (d-1+\xi)^{\frac{2-\xi}{2\xi}} \tag{4.17}$$

Therefore, for any fixed $\xi > 1$, the butterfly velocity is found to be a monotonically increasing function of the Lifshitz black hole temperature T. However, in the absence of anisotropy for $\xi = 1$, v_b becomes independent of the temperature which is consistent with the case for the usual asymptotically AdS black hole.

4.2.2 Out-of-Time-Ordered correlators

In this subsection, we will study the out-of-time-ordered correlator (OTOC) for thermal Lifshitz field theory dual to a linearly charged asymptotically Lifshitz black hole. It is convenient to study the OTOC in the Kruskal-Szekeres form of the bulk metric, which smoothly covers the globally extended space-time. In Kruskal geometry, the OTOC can be interpreted as the two-particle gravitational scattering amplitude of particles moving along the two horizons [39, 40, 50, 66]. We shall compute the OTOC in the specific dual-field theory in the form given as

$$\langle \hat{W}(t_2, x_2)\hat{V}(t_1, x_1)\hat{W}(t_2, x_2)\hat{V}(t_1, x_1)\rangle_\beta \,, \tag{4.18}$$

where we consider $t_2 - t_1 >> \beta$. The particles that participate in the gravitational scattering process are the operators $\hat{W}$ and $\hat{V}$, which are inserted in the dual thermofield double (TFD) state. Though the quantity (4.18) is one-sided, our whole computation of the OTOC has been done in a two-sided geometry. So far, the OTOC via the gravitational scattering process has

been explored with various black hole backgrounds [39, 40, 50, 51, 66, 74, 85, 178–183]. In our work, we have calculated this quantity (4.45) for a linearly charged asymptotically Lifshitz black hole with arbitrary anisotropy. In the Lifshitz background, the authors of [184] have calculated the scrambling time, though the background they worked with is slightly different from ours. Moreover, OTOCs for a generic holographic bulk including specific classes of anisotropic black holes are also derived analytically in [176, 185]. Here, we have provided an explicit derivation of the double-sided Kruskal-Szekeres form of the Lifshitz black hole and analytically developed the OTOCs. We will show that our constructed OTOCs are consistent with those found for the generic holographic dual gravity theories. We will use these OTOCs to subsequently calculate the Lyapunov exponent and butterfly velocity in the two-sided geometry, which yields interesting results.

Kruskal extension

To study the out-of-time-ordered correlators, let us first construct the Kruskal extension of the (2+1) dimensional Lifshitz black hole. We will start with the metric (4.3), but replacing $z = 1/r$ and considering the AdS radius to be 1 for simplicity,

$$\mathrm{d}s^2 = -r^{2\xi} f(r)\mathrm{d}t^2 + \frac{1}{r^2}\frac{\mathrm{d}r^2}{f(r)} + r^2\,\mathrm{d}x^2 \ , \tag{4.19}$$

and the blackening factor $f(r)$ is given by,

$$f(r) = 1 - \left(\frac{r_h}{r}\right)^{1+\xi} \ . \tag{4.20}$$

r is the radial coordinate and r_h is the black hole horizon in the emblackening factor $f(r)$. In [186, 187], nonlinearly charged Lifshitz black holes with one and two horizons are obtained with the Eddington-Finkelstein form of the metric. In this case, nonlinearity appears in the blackening factors, and it is characterized by using some extra parameters along with the dynamical exponent ξ of the Lifshitz black hole. Single horizons and double horizons for such black holes are obtained by using specific parametric conditions. However, for the metric in (4.19), we will construct an explicit form of the linearly charged thermal Lifshitz

black hole with double horizons by using the Kruskal-Szekeres coordinates. To work in these coordinates, we transform,

$$u = e^{\frac{\alpha}{2}(r_* - t)}, \quad v = e^{\frac{\alpha}{2}(r_* + t)}, \tag{4.21}$$

where α is a function of r_h that relates with the finite temperature T of the black hole as $\alpha \equiv 2\pi T$. The tortoise coordinate r_* will play a very crucial role in defining the smooth horizon in the (u, v) coordinate. We define,

$$r_*(r) = \int \frac{\mathrm{d}r}{r^{1+\xi} f(r)} = \int \frac{\mathrm{d}r}{r^{1+\xi}\left[1 - \left(\frac{r_h}{r}\right)^{1+\xi}\right]}. \tag{4.22}$$

Integrating equation (4.22), we get,

$$r_*(r) \approx \frac{r^{-\xi}}{\xi(1+\xi)}\, {}_2F_1\left(1, -\xi, 1-\xi, \frac{r}{r_h}\right). \tag{4.23}$$

We consider $f(r) = (r - r_h) f'(r_h)$ while solving the above equation. Now, taking the near-horizon limit ($r \to r_h$) of the whole solution, we get,

$$r_* \approx \frac{1}{r_h^{\xi}(1+\xi)} \log\left(\frac{r - r_h}{r_h}\right). \tag{4.24}$$

As there is a relation between (u, v) coordinate and r_* (from (4.21)), we can easily write,

$$uv = e^{\alpha r_*} \approx \left(\frac{r - r_h}{r_h}\right). \tag{4.25}$$

This equation allows us to claim that the $uv = 0$ is the same limit as the $r = r_h$. This result will be quite helpful for the analysis afterwards. Writing the metric (4.19) in terms of the null coordinates u and v, we get

$$\mathrm{d}s^2 = \frac{4r(u,v)^{2\xi}}{\alpha^2 uv} f(r(u,v))\mathrm{d}u\,\mathrm{d}v + r(u,v)^2\,\mathrm{d}x^2 = 2A(u,v)\mathrm{d}u\,\mathrm{d}v + B(u,v)\mathrm{d}x^2. \tag{4.26}$$

In this Kruskal geometry, $uv = 0$ is defined as the horizon, singularity is at $uv = 1$ and both left/right boundaries are located at $uv = -1$. This unperturbed background will obey Einstein's equation which is of the form,

$$E_{\mu\nu} = \kappa T_{\mu\nu}. \tag{4.27}$$

Here, $E_{\mu\nu}$ is the Einstein tensor, $\kappa = 8\pi G_N$ is a constant related to the Newton's constant G_N and $T_{\mu\nu}$ is the stress-energy tensor which is of the form,

$$T_0^{\text{matter}} = 2T_{uv}\mathrm{d}u\mathrm{d}v + T_{uu}\mathrm{d}u^2 + T_{vv}\mathrm{d}v^2 + T_{xx}\mathrm{d}x^2\,. \tag{4.28}$$

It is worth mentioning that this stress tensor accounts for the cosmological constant and is consistent with the Ricci tensor of the unperturbed background. For the unperturbed Einstein equation, solving T_{uu}, T_{vv} and T_{uv}, we get,

$$T_{uu} = \frac{1}{4A(u,v)B(u,v)^2}\left[A(u,v)\partial_u B(u,v)^2 + 2B(u,v)\left(\partial_u A(u,v)\partial_u B(u,v)\right.\right. \\ \left.\left. - A(u,v)\partial_u^2 B(u,v)\right)\right]\,, \tag{4.29a}$$

$$T_{uv} = \frac{1}{4B(u,v)^2}\left[2B(u,v)\partial_u\partial_v B(u,v) - \partial_v B(u,v)\partial_u B(u,v)\right]\,, \tag{4.29b}$$

$$T_{vv} = \frac{1}{4A(u,v)B(u,v)^2}\left[A(u,v)\partial_v B(u,v)^2 + 2B(u,v)\left(\partial_v A(u,v)\partial_v B(u,v)\right.\right. \\ \left.\left. - A(u,v)\partial_v^2 B(u,v)\right)\right]\,. \tag{4.29c}$$

Gravitational backreaction due to shock wave

In the previous subsection, we constructed a two-sided Lifshitz black hole geometry in a (2+1) - dimensional background. This section aims to study the back-reacted metric due to a null pulse of energy localized along the $v = 0$ horizon. In the bulk-boundary picture, this means we have inserted an operator in the boundary thermal state at some past time t and let it evolve. Inserting an operator in the boundary leads to releasing a perturbation close to the boundary, which falls into the bulk. From the point of view of the $t = 0$ slice, the energy of this perturbation is exponentially increasing with time t [38]. Thus, we can approximate this perturbation as a null pulse of energy E localized at the $v = 0$ horizon along the u-direction. We must consider the back-reaction of this null pulse in the two-sided geometry. We consider the following form of the stress-tensor localised at $v = 0$,

$$T_{vv}^{\text{shock}} = E\exp\left(\frac{2\pi t}{\beta}\right)\delta(v)\delta(x)\,. \tag{4.30}$$

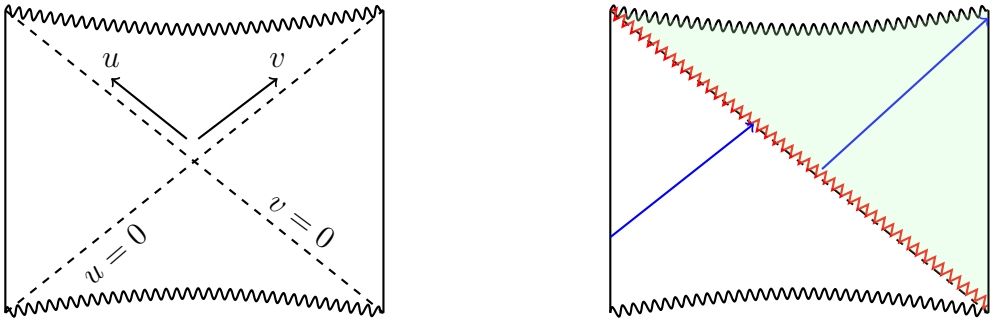

Figure 4.2: *Left:* Penrose diagram of two-sided geometry. *Right:* A shock wave (red zigzag line) localised along $v = 0$ causes a discontinuity of the $u = 0$ horizon (the blue arrow)

The shock wave localised at $v = 0$ horizon is indeed splitting the causal past (white) and future (green) of v. The metric in the green region will change while in the white region, it will remain the same. In the Penrose diagram, we can clearly see the shift along the v-direction. We can write the form of the shift in the following way:

$$\bar{u} = u + \Theta(v)\eta(u, v, x) \rightarrow \mathrm{d}u = \mathrm{d}\bar{u} - \eta(u, v, x)\delta(v)\mathrm{d}v\,, \tag{4.31}$$

$$\bar{v} = v\,, \qquad \bar{x} = x\,. \tag{4.32}$$

Our goal is to calculate the form of the function $\eta(u, v, x)$ – the shockwave profile. Note that the Heaviside step function $\Theta(v)$ is present to ensure that only the causal future of the pulse is affected by its presence. In terms of these new coordinates $(\bar{u}, \bar{v}, \bar{x})$, we can write the metric as,

$$\mathrm{d}s^2 = 2A(\bar{u}, \bar{v})\mathrm{d}\bar{u}\mathrm{d}\bar{v} + B(\bar{u}, \bar{v})\mathrm{d}\bar{x}^2 - 2A(\bar{u}, \bar{v})\eta(u, v, x)\delta(\bar{v})\mathrm{d}\bar{v}^2\,. \tag{4.33}$$

With this back-reacted form of the metric, we need to calculate a form of $\eta(u, v, x)$ which will obey eq.(4.27). In the above metric,

$$A(\bar{u}, \bar{v}) = \frac{2r(\bar{u}, \bar{v})^{2\xi}}{\alpha^2\bar{u}\bar{v}} f(r(\bar{u}, \bar{v})), \qquad B(\bar{u}, \bar{v}) = r(\bar{u}, \bar{v})^2\,, \tag{4.34}$$

where we have expressed the radial coordinate r in terms of (u, v). Now, for the perturbed background, we wish to calculate the stress tensor. The stress tensor for the matter part reads

as

$$T^{\text{matter}}_{\mu\nu} = 2\left[T_{\bar{u}\bar{v}} - 2T_{\bar{u}\bar{u}}\eta(\bar{u},\bar{v},x)\delta(\bar{v}]\,\mathrm{d}\bar{u}\mathrm{d}\bar{v} + \left[T_{\bar{v}\bar{v}} + T_{\bar{u}\bar{u}}\eta(\bar{u},\bar{v},x)^2\delta(\bar{v})^2\right.\right. \\ \left.\left. -2T_{\bar{u}\bar{v}}\eta(\bar{u},\bar{v},x)\delta(\bar{v})\right]\mathrm{d}\bar{v}^2 + T_{\bar{u}\bar{u}}\mathrm{d}\bar{u}^2 + T_{\bar{x}\bar{x}}\mathrm{d}\bar{x}^2\,. \tag{4.35}$$

We will drop the bar convention for further analyses so that the result looks simpler. Now, we will solve the back-reacted Einstein's equation which is of the form :

$$E_{\mu\nu} = \kappa\left(T^{\text{matter}}_{\mu\nu} + T^{\text{shock}}_{\mu\nu}\right)\,. \tag{4.36}$$

The expressions of $T^{\text{matter}}_{\mu\nu}$ and $T^{\text{shock}}_{\mu\nu}$ is given by (4.35) and (4.30) respectively. Solving the vv component of the perturbed Einstein equation, we get,

$$\left[\partial_x^2 - \frac{1}{A(u,v)}\partial_u\partial_v B(u,v)\right]\eta(u,v,x) - \frac{8\pi G_N E\, B(u,v)}{A(u,v)}e^{2\pi t/\beta}\delta(v)\delta(x) = 0\,, \\ \Rightarrow \left[\partial_x^2 - \mathcal{M}(u,v)^2\right]\eta(u,v,x) = e^{\frac{2\pi}{\beta}(t-t_*)}\delta(v)\delta(x)\,. \tag{4.37}$$

Where,

$$\mathcal{M}(u,v) = \sqrt{\frac{\partial_u\partial_v B(u,v)}{A(u,v)}}\,, \qquad t_*(u,v) = \frac{\beta}{2\pi}\log\left(\frac{A(u,v)}{8\pi G_N E\, B(u,v)}\right)\,. \tag{4.38}$$

The function $t_*(u,v)$ has some physical meaning, which we will discuss in the upcoming part. After implementing the values of $A(u,v)$ and $B(u,v)$ to $t_*(u,v)$, it will take a constant form. We can see that the shockwave profile $\eta(u,v,x)$ is obeying an ODE which we can solve easily. In writing the above equation, we assume, $T_{uu} = 0$ near the $v = 0$ horizon [51]. Our task is to solve the equation (4.37) near the horizon. Near the horizon ($v = 0$ or $r = r_h$),

$$A(u,v)|_{v=0} = \frac{8}{1+\xi}, \qquad \partial_u\partial_v B(u,v)|_{v=0} = 4r_h^2\,. \tag{4.39}$$

In taking the derivative of $B(u,v)$ with u and v, we have used the relation (4.25) and performed a chain rule differentiation with r_*. Now, implementing the above two expressions into (4.38), we get,

$$\mathcal{M}(u,v)|_{v=0} = \sqrt{\frac{{r_h}^2(1+\xi)}{2}}\,, \qquad t_* = \frac{\beta}{2\pi}\log\left(\frac{1}{\pi G_N E(1+\xi)r_h^2}\right)\,, \tag{4.40}$$

where we have considered $r_h = 1$. The constant t_* is called the scrambling time, which is dependent on the anisotropy index ξ. Near the horizon, the equation (4.37) becomes,

$$\left[\partial_x^2 - \frac{{r_h}^2(1+\xi)}{2}\right]\eta(x) = e^{\frac{2\pi}{\beta}(t-t_*)}\delta(x)\,. \tag{4.41}$$

To solve this, first, we will solve the homogeneous equation and get,

$$\eta(x) = \begin{cases} c_1 e^{\mathcal{M}x} + c_2 e^{-\mathcal{M}x} & \text{for } x > 0\,, \\ c_3 e^{\mathcal{M}x} + c_4 e^{-\mathcal{M}x} & \text{for } x < 0\,. \end{cases} \tag{4.42}$$

Now, to solve the non-homogeneous equation, we will check the discontinuity of the first derivative of the solution and get,

$$\eta'(\epsilon) - \eta'(-\epsilon) = e^{\frac{2\pi}{\beta}(t-t_*)}\,, \tag{4.43}$$

where, ϵ is a small parameter $\epsilon \to 0$. Imposing the continuity of the solution at $x = 0$ and with the discontinuity equation (4.43), we get a relation between the coefficients as,

$$c_1 - c_3 = c_4 - c_2 = \frac{4\sqrt{2}e^{\frac{2\pi}{\beta}(t-t_*)}}{r_h((1+\xi)^{3/2}}\,. \tag{4.44}$$

We will choose $c_2 = c_3 = 0$ and the final solution for the shock will be,

$$\eta(t,x) = \frac{4\sqrt{2}}{r_h((1+\xi)^{3/2}} e^{\frac{2\pi}{\beta}(t-t_*-\frac{\beta\mathcal{M}}{2\pi}x)}\,. \tag{4.45}$$

This shockwave profile will completely determine the four-point out-of-time ordered function - OTOC. We can identify the commutator $C(t,x)$ in equation (1.41) with the shockwave profile $\eta(t,x)$ and write,

$$\lambda_L = 2\pi T\,, \qquad\qquad v_B = r_h^{\xi-1}\sqrt{\frac{1+\xi}{2}}\,. \tag{4.46}$$

This Lyapunov exponent agrees with our results of the entanglement wedge method. For the butterfly velocity, this result is found to be the same as obtained from the entanglement wedge result for $d = 2$ in (4.16). Thus, we can claim that these two methods are congruent for a reliable study of chaos in Lifshitz background.

4.2.3 Pole-skipping

In this subsection, we wish to study the retarded energy density correlation function $G^{\rm R}_{T_{00}T_{00}}(\omega, k)$ near the pole-skipping point. This correlation function can be calculated by perturbing the gravitational background (4.3) and imposing ingoing boundary conditions at the black hole horizon. To perform the pole-skipping analysis, it is customary to work with Eddington-Finkelstein coordinates, defined by

$$v = t + r_*, \qquad \frac{{\rm d}r_*}{{\rm d}r} = \frac{1}{r^{1+\xi} f(r)}\,, \tag{4.47}$$

where v is the null coordinate and r_* is the tortoise coordinate. With the above coordinate system, the background metric (4.3) is transformed into

$${\rm d}s^2 = -r^{2\xi} f(r) {\rm d}v^2 + 2r^{\xi-1} {\rm d}v{\rm d}r + r^2 {\rm d}x^2\,. \tag{4.48}$$

For our current analysis, we choose the gravity background as the (2+1)-D Lifshitz black hole. Now, to calculate the energy density correlation function, we must perturb the background metric - specifically the sound modes (longitudinal modes). We perturb the background metric as,

$$g_{\mu\nu} \to g_{\mu\nu} + \delta g_{\mu\nu}(r) e^{-i\omega v + ikx}\,. \tag{4.49}$$

Here we perform a Fourier transformation to the perturbed mode and choose the wavenumber k along the x-direction. Then, the sound modes will be–

$$\delta g_{vv}, \delta g_{vx}, \delta g_{vr}, \delta g_{rr}, \delta g_{rx}, \delta g_{xx}\,. \tag{4.50}$$

As the wave points along the x- direction, sound modes are the modes that are only along the (v, r, x) directions. But, imposing radial gauge condition $\delta g_{r\mu} = 0$ and traceless ness condition $g^{\mu\nu}\delta g_{\mu\nu} = 0$, we get some redundant modes and left with–

$$\delta g_{vv}, \delta g_{vx}\,. \tag{4.51}$$

The retarded energy density Green's function is governed by the perturbed equations that are regular at the horizon in ingoing EF coordinates. So, we Taylor expand the modes near the

horizon as,

$$\delta g_{\mu\nu}(r) = \delta g^{(0)}_{\mu\nu} + (r - r_h)\delta g^{(1)}_{\mu\nu} + \dots , \tag{4.52}$$

Perturbing the sound modes of the background and imposing the regularity condition (4.52) near the black hole horizon, we can achieve the expanded form of Einstein's equations near the horizon. Our goal is to check whether we get the results of chaos obtained in the previous subsections. For field δg_{vv}, the associated equation of motion is $\delta E_{vv} = \delta T_{vv}$. But, the perturbation to stress tensor δT_{vv} does not vanish necessarily, while δT^r_v vanishes at the horizon [72, 105]. Keeping this in mind, we will set $\delta T^r_v = 0$ to calculate the pole-skipping point connected to chaos. Expanding this equation near the black hole horizon, we get,

$$\left[k^2 - i\omega r_h^{2-\xi}\right] \delta g^{(0)}_{vv} + k\left[-ir_h^{\xi}(1+\xi) + 2\omega\right] \delta g^{(0)}_{vx} = 0\,. \tag{4.53}$$

This equation represents a constraint relation between the near-horizon coefficients. At some specific value $\omega = \omega_* = \frac{i}{2} r_h^{\xi}(1+\xi)$, coefficient of $\delta g^{(0)}_{vx}$ is 0. So, at this specific value of ω, we get,

$$\left[k^2 + \frac{1}{2} r_h^2\,(1+\xi)\right] \delta g^{(0)}_{vv} = 0\,. \tag{4.54}$$

For general k, this equation gives rise to $\delta g^{(0)}_{vv} = 0$. However, at $k = k_*$, this equation is automatically satisfied. That means, at these specific values of ω and k, δT^r_v is automatically zero. Consequently, they will not impose any constraint on the near-horizon coefficients $\delta g^{(0)}_{vv}$ and $\delta g^{(0)}_{vx}$. The frequency (ω_*) and momentum (k_*) define the pole-skipping point. At the pole-skipping point, we thus get,

$$\omega_* = \frac{i}{2} r_h^{\xi}(1+\xi)\,, \qquad k_*^2 = -\frac{1}{2} r_h^2\,(1+\xi)\,. \tag{4.55}$$

Writing r_h in terms of temperature as $r_h = \left(\frac{4\pi T}{1+\xi}\right)^{1/\xi}$, we can express ω and k in terms of the temperature of the black hole. One can therefore calculate the Lyapunov exponent and butterfly velocity from (1.53) as,

$$\lambda_L = 2\pi T\,, \qquad\qquad v_B = r_h^{\xi-1}\sqrt{\frac{1+\xi}{2}}\,. \tag{4.56}$$

respectively. Note that the butterfly velocity (v_B) is a positive real quantity. So, we will take the absolute value of momentum while calculating v_B, i.e. $v_B = \frac{|\omega_*|}{|k_*|}$. From the above expression, it is obvious that both the Lyapunov exponent and butterfly velocity assume the same forms as those achieved in the previous subsections. Henceforth, we claim that all three methods to compute the chaotic features are equivalently reliable. These methods also give consistent results in higher orders. One can check it explicitly.

One can note that, for the class of hyperscale violating Lifshitz backgrounds, the metric components in the near-horizon limit involve a hyperscale violating parameter θ on top of Lifshitz scaling. This causes a nontrivial appearance of this parameter in different chaotic measures. Thus, using the above three computational methods, one can expect equivalent θ-dependent expressions of v_B and λ_L for the hyperscale violating class of Lifshitz gravity background. Moreover, it has been found in [176] that the Lifshitz geometry can be obtained in the IR zone when the AdS background in UV undergoes a holographic renormalisation group (RG) flow. Thus, the conformality of the UV theory is broken in the IR due to the appearance of $\xi \neq 1$. Subsequently, a distinct confinement/deconfinement like critical phase transition scenario occurs when ξ attains the values such that $\xi \neq 1$. Therefore, the anisotropy parameter ξ is somewhat suggestive of the critical phase transition temperature during the RG flow. As in our case, v_B and λ_L derived from each of the aforementioned methods are nontrivial functions of ξ, and this anisotropic index is related to the black hole temperature T via (4.6). Added to this, it has been observed for each of the above studies that v_B and λ_L pick the expressions of those for AdS black hole when $\xi = 1$. This makes us claim that a critical phase transition under the holographic RG flow can be traced out from the chaotic features analysed by using all these equivalent frameworks.

4.3 Analysis of classical chaos

Here we elucidate a parallel survey of some of the chaos properties, to be precise, eikonal phase shift and Lyapunov exponent, at the classical level. We will show that the bulk phase shift may be written in terms of the leading order of the series expansion of the exponential growth rate of the quantum OTOCs. Similarly as in conformal case [188], the bulk phase shift happens to be a hypergeometric function though it nontrivially depends on the anisotropy parameter ξ for our case. Also, we will compute the Lyapunov exponent at the classical level and check any possible relevance of the same with the λ_L computed by using the three different methods of quantum chaos.

4.3.1 Null geodesic

The anatomy of the null geodesics for our specified background and the corresponding turning points adequately serve the purpose of calculating both eikonal bulk phase shift as well as Lyapunov exponent in the classical sense. In the case of our chosen gravity background, the presence of arbitrary anisotropy parameter ξ causes an arbitrary number of positive real roots of the null geodesics depending on the value of ξ. Moreover, all of those roots contain a nontrivial dependency on z_h and γ. Before computing the phase shift and Lyapunov exponent, here we will present of a quantitative evaluation of the null geodesics and their turning points in our framework. To carry out the eikonal phase shift in the bulk following, here we will first enunciate the details of the null geodesic for our chosen background. The bulk phase shift for a particle described by a plane wave is given by [162, 189]

$$\delta \equiv -p.(\Delta x)\,, \tag{4.57}$$

where, p denotes the components of the conserved momentum vector and Δx gives the deflections in the corresponding bulk directions. For our metric in equation (4.3) in 2+1 dimension, the conserved energy and momentum are given by

$$p_t = \frac{1}{z^{2\xi}} f(z) \frac{\partial t}{\partial s}\,, \quad p_x = \frac{1}{z^2} \frac{\partial x}{\partial s}\,, \tag{4.58}$$

s being the intrinsic affine parameter. These conserved quantities correspond to the two killing vectors ∂_t and ∂_x of our chosen metric during a heavy-heavy-light-light 2-particle scattering, it is convenient to consider that the highly boosted particle consists of large values of conserved momenta. We introduce a parameter $\gamma = \frac{p_x}{p_t}$ which often serves as the impact parameter of the corresponding scattering process. The null geodesic equation is given by

$$g_{\mu\nu}\dot{x}^\mu\dot{x}^\nu = 0\,, \tag{4.59}$$

which yields

$$\dot{z}^2 = (p_t)^2 z^{2\xi+2} - (p_x)^2 z^4 f(z)\,. \tag{4.60}$$

At the turning point $z = z_0$, z attains extreme value for which we can set $\dot{z}|_{z=z_0} = 0$. Hence, the values of turning points z_0 should satisfy the relation

$$z_0^{2\xi-2} + \frac{\gamma^2}{z_h^{\xi+1}} z_0^{\xi+1} - \gamma^2 = 0\,. \tag{4.61}$$

The equation (4.61) is a polynomial of either integer order or fractional order, depending on the values of the critical exponent ξ. Thus the valid roots of this equation for our approach are all positive real values such as $z_0 = f(z_h, \gamma)$ that lie within the singularity and the boundary of the bulk geometry. At this stage, some further crucial remarks on the turning point follow immediately:

- Let us take the assumption that the energy p_t is much greater than the momentum p_x, i.e., $\gamma \gg 1$. With this assumption, taking $z_0 = 1$ equation (4.61) gives,

$$\gamma = \sqrt{\frac{z_h^{\xi+1}}{z_h^{\xi+1} - 1}}\,. \tag{4.62}$$

  It is obvious from the above expression that for any arbitrary value of z_h in between $z_h \to 0$ and $z_h \to \infty$, the condition $\gamma \gg 1$ is not satisfied.

- If $\gamma = 1$, i.e., $p_x = p_t$, then the equation (4.61) is not satisfied with $z_0 = 1$.

- Again, for $z_h = 1$, $z_0 = 1$ is not a solution of the null geodesic equation for any arbitrary value of γ.

- The condition (4.62) clearly tells us that, for $z_0 = 1$ as a solution, p_x cannot be less than p_t. Hence, with $p_x < p_t$, we must have $z_0 \neq 1$.

- For any arbitrary value of p_x and p_t; $z_0 = 0$ does not satisfy the geodesic equation.

From the above conditions, it is evident that $z_0 = 1$, i.e., the horizon for our case and $z_0 = 0$, i.e., the boundary are not included in the consistent solutions of the null geodesic equation in our present study. For the relativistic asymptotically AdS black hole with $\xi = 1$, the above procedure gives the null geodesic equation as

$$\dot{z} = z_0^2 p_t \sqrt{1 - (1 - \frac{z_0^2}{z_h^2})\gamma^2} \tag{4.63}$$

For any arbitrary impact parameter γ, the turning point of this geodesic can be obtained only at $z_0 = 0$. Even for the relativistic case, the null geodesic equation is not satisfied if the corresponding turning point is at the horizon. So, for both the relativistic AdS and nonrelativistic Lifshitz black hole, the above method does not support the exact horizon of the geometry to carry out the expressions of the classical eikonal phase shift and Lyapunov exponent.It is nevertheless worth mentioning that one may carry out a polynomial distribution by using a suitable numerical approach to see what values of z_0 the equation (4.61) can accommodate as its valid solution. We keep this computation for future extensions of our work.

4.3.2 Eikonal phase shift

With the above analysis, here we will exhibit an explicit computation of eikonal phase shift at the turning points z_0 as a nontrivial function of z_0 and ξ. With p_t and p_x as the conserved energy and momentum for our system, the expression of the bulk phase shift takes the form as

$$\delta \equiv p_t(\Delta t) - p_x(\Delta x)\,. \tag{4.64}$$

It is worth noting that the growth rate of the OTOCs found in the limit $u = 0,\ v = 0,\ t_2 - t_1 >> 1$(i.e., the Regge limit for any double-sided Kruskal geometry) in section

4.2.2 is $\frac{2\pi}{\beta}\left(t - t_* - \frac{\beta\mathcal{M}x}{2\pi}\right)$, where β, t_* and $\mathcal{M}$ are nontrivial functions of ξ. For any fixed ξ, these quantities become constants. Let us assume that $t - t_* \sim \Delta t$ and the corresponding deflection occurs as $\Delta x \sim (x - 0)$, then the OTOC growth rate represents the bulk phase shift for a 2-particle heavy-heavy-light-light scattering. With this scenario, we can infer that the conserved momenta p_x, energy p_t and hence impact parameter γ can be expressed non-trivially in terms of β, t_* and $\mathcal{M}$, or in other words, in terms of ξ. The deflections along the time and space directions can be found respectively from the expressions of p_t and p_x in (2.41) and the null geodesic equation (4.60) as

$$\Delta t = 2\int_0^{z_0} \frac{z^{2\xi-1}\mathrm{d}z}{f(z)\sqrt{z^{2\xi} - \gamma^2 z^2 f(z)}} = 2a^{\frac{3}{2}}\int_0^{z_0} \frac{z^{2\xi-1}\mathrm{d}z}{(a - z^{\xi+1})\sqrt{(az^{2\xi} - a\gamma^2 z^2 + \gamma^2 z^{\xi+3})}}\,, \tag{4.65}$$

and

$$\Delta x = 2\int_0^{z_0} \frac{\gamma z\,\mathrm{d}z}{\sqrt{z^{2\xi} - \gamma^2 z^2 f(z)}} = 2a^{\frac{1}{2}}\gamma\int_0^{z_0} \frac{z\,\mathrm{d}z}{\sqrt{(az^{2\xi} - a\gamma^2 z^2 + \gamma^2 z^{\xi+3})}}\,, \tag{4.66}$$

where, $a = z_h^{\xi+1}$. Because of the intricate structure of the above integrands, we assume two limiting cases to derive it. Firstly we take the near-boundary zone where $z \ll z_h$. Substituting (4.65) and (4.66) in the expression of the eikonal shift and simplifying, we get for the near boundary zone,

$$\delta \sim \int_0^{z_0} \sqrt{z^{2\xi-2} - \gamma^2(1-\epsilon)}\mathrm{d}z \approx p_t\int_0^{z_0} \sqrt{z^{2\xi-2} - \gamma^2}\mathrm{d}z\,, \tag{4.67}$$

where, $\left(\frac{z}{z_h}\right)^{\xi+1} = \epsilon \ll 1$ for $\xi \geq 1$. Now defining a new integration variable $y = \frac{z}{z_0}$ the bulk phase shift is given by

$$\delta \sim \int_0^1 z_0\sqrt{z_0^{2\xi-2}y^{2\xi-2} - \gamma^2}\mathrm{d}y \approx i\gamma z_0\,{}_2F_1\left(-\frac{1}{2}, \frac{1}{2\xi-2}; \frac{2\xi-1}{2\xi-2}; \frac{z_0^{2\xi-2}}{\gamma^2}\right)\,. \tag{4.68}$$

On the other hand, we take the near horizon regime where $z \approx z_h$. In this regime, we can take two liming cases for the impact parameter γ. When the energy p_t is much greater than the momentum p_x, i.e., $\gamma < 1$, the eikonal phase shift in near horizon case gives

$$\delta = \frac{z_0^\xi}{\xi(\xi+1)}\,{}_2F_1\left(1, \xi; \xi+1; \frac{z_0}{z_h}\right) = \frac{z_0^\xi}{\xi(\xi+1)}\,{}_2F_1\left(1, \xi; \xi+1; z_0\right)\,. \tag{4.69}$$

Again for the small energy limit, i.e., $p_x \geq p_t$, the impact parameter $\gamma \geq 1$. This, in the near horizon zone, produces,

$$\delta = -\frac{4\gamma\left(\sqrt{z_0 - z_h} - \sqrt{-z_h}\right)\sqrt{z_h}p_t}{\sqrt{\xi+1}} = -\frac{4\gamma\left(\sqrt{z_0 - 1} - i\right)p_t}{\sqrt{\xi+1}}\,. \tag{4.70}$$

where we choose $z_h = 1$ in the above expression for the sake of simplicity of our derivation. It is well-known in the backdrop of gravitational scattering that the real and imaginary nature of the eikonal phase shift respectively represent elastic and inelastic scattering. Thus our study of the classical eikonal phase clearly reveals that the nature of the gravitational scattering between the heavy-heavy-light-light particle collision in the Lifshitz black hole depends on the different regimes taken for the radial coordinate z along with the choices of the impact parameter. For the near boundary case and the large impact parameter limit in the near horizon zone, the imaginary eikonal phase shift implies completely inelastic collisions whereas the small impact parameter limit in the near horizon zone gives real values of δ that stand for elastic scattering. For elastic scattering in near-horizon limit, the phase shift assumes a hypergeometric function which is similar to the case with Regge behaviour of CFT although here, due to the anisotropy of the chosen background, the hypergeometric function depends nontrivially on ξ. Hypergeometric function with ξ-dependence has also been achieved inelastic scattering in the near-boundary zone. Nevertheless, all the δ's derived in these limits inevitably happen to be nontrivial functions of the anisotropy index ξ. This allows one to speculate about the dependencies of absorption cross-sections of the above scatterings on the finite anisotropy present in the black hole background.

Again, we use a WKB approximation to verify the consistency of the eikonal phase. Inserting the expressions of time and space deflections in (4.64), we can write,

$$\delta = 2p_t \int_0^{z_0} \frac{\sqrt{z^{2\xi} - \gamma^2 z^2 f(z)}}{z f(z)}\,\mathrm{d}z\,. \tag{4.71}$$

One may check the emergence of the above eikonal phase via WKB approximation of the solution of the equation of motion of a scalar field. To do this, consider a heavy scalar field ϕ propagating in the chosen Lifshitz background. In the background (4.3), the Klein-Gordon

equation of the scalar can be written as

$$z^2 f(z)\partial_z^2\phi + z^2\partial_x^2\phi + z^2 f'(z)\partial_x^2\phi - \frac{z^{2\xi}}{f(z)}\partial_t^2\phi - z^\xi f(z)\partial_z\phi + m^2 z^{2+\xi}\phi = 0\,. \tag{4.72}$$

Performing a Fourier transformation as

$$\phi = \tilde{\phi}(z)\, e^{i(-p_t t + p_x x)}\,,$$

and taking an ansatz,

$$\tilde{\phi}(z) = e^{ip_t\chi(z)}\,, \tag{4.73}$$

we can solve for $\chi(z)$. With the large energy ($p_t >> 1$) limit, the EOM boils down to,

$$(\partial_z\chi(z))^2 = \frac{z^{2\xi} - \gamma^2 z^2 f(z)}{z^2 f^2(z)}\,. \tag{4.74}$$

Now, taking the positive term of $\partial_z\chi(z)$, we perform an integration and get a solution of $\chi(z)$ as

$$\chi(z) = \int_0^{z_0} \frac{\sqrt{z^{2\xi} - \gamma^2 z^2 f(z)}}{z f(z)}\,\mathrm{d}z\,. \tag{4.75}$$

where the terms of order $\mathcal{O}(p_t^{-1})$ can be ignored at large energy limit. This is indeed the leading term of the solution. We can see that the WKB approximation of the solution gives us the exact eikonal phase we recovered in (4.71) at leading order.

4.3.3 Lyapunov exponent

The Lyapunov exponent (λ_L) is one of the key measures in understanding chaotic systems in classical phase space. It quantifies the rate at which the nearby trajectories diverge and provides information on the system's sensitivity to initial conditions. A positive Lyapunov exponent signifies a chaotic system. Mathematically,

$$\delta X(t) = \delta X(0) e^{\lambda_L t}\,,$$

where δX represents the separation between two nearby trajectories. In their study [190], the authors established a connection between the Lyapunov exponent and the effective potential

in the radial motion for both massive and massless particles. Building on this framework, we aim to calculate the Lyapunov exponent for a 2+1-dimensional planar Lifshitz black hole in this subsection. Recently, [191] conducted a similar analysis in the context of equatorial hyperscaling-violating black holes, treating Lifshitz black holes as a specific case within their study. For a circular geodesic, the Lyapunov exponent in terms of the second derivative of the effective potential V_{eff} for radial motion is given by [190],[191]

$$\lambda_L = \sqrt{-\frac{V''_{eff}}{2\dot{t}^2}}\,. \tag{4.76}$$

Now, for a massless particle, the geodesic equation is given in equation (4.60) from which we can calculate the effective potential

$$V_{eff}(z) = \dot{z}^2 = (p_t)^2 z^{2\xi+2} - (p_x)^2 z^4 f(z)\,. \tag{4.77}$$

Where t is the coordinate time. At the turning point $z = z_0$, the condition on circular orbit, i.e., $V_{eff}(z_0) = 0$ and $V'_{eff}(z_0) = 0$ yield

$$\frac{p_t^2}{p_x^2} = z_0^{2-2\xi} f_0\,, \tag{4.78}$$

and

$$z_0 f'_0 = 2(\xi - 1) f_0\,, \tag{4.79}$$

where $f_0 = f(z_0)$. Upon substituting equations (4.78) and (4.79) in equation (4.77) we get

$$V''_{eff}(z_0) = -z_0^2 p_x^2 \left(z_0^2 f''_0 - 2f_0\left(2\xi^2 - 5\xi + 3\right)\right)\,. \tag{4.80}$$

Now, utilizing equations (2.41) and (4.80) within equation (4.76), we derive the Lyapunov exponent for the null circular geodesic

$$\lambda_L = \sqrt{\frac{f_0\left(z_0^2 f''_0 - 2f_0\left(2\xi^2 - 5\xi + 3\right)\right)}{2z_0^{2\xi}}}\,. \tag{4.81}$$

Since an unstable circular geodesic meets the condition $V''_{eff} < 0$, it follows from equations (4.80) and (4.81) that λ_L is real whenever the orbit is unstable. From equation (4.81), it is

clear that in AdS spacetime, when the anisotropic parameter $\xi = 1$, the Lyapunov exponent depends on z_0 and z_h. For a horizon radius of $z_h = 1$, the Lyapunov exponent indicates unstable orbits when $z_0 > 1$. In the near horizon limit, the Taylor expansion of the function $f(z_0)$ around $z_0 = z_h$ gives

$$f_0 = f(z_0) = -\left[\frac{(1+\xi)}{z_h}(z_0 - z_h) + \frac{\xi(\xi+1)}{2z_h^2}(z_0 - z_h)^2 + \mathcal{O}(z_0 - z_h)^3\right].$$

From this expression, we get

$$f'(z_0) = -\left[\frac{(1+\xi)}{z_h} + \frac{\xi(\xi+1)}{2z_h^2}(z_0 - z_h) + \mathcal{O}(z_0 - z_h)^2\right],$$

and

$$f''(z_0) = -\frac{\xi(\xi+1)}{2z_h^2}(z_0 - z_h) + \mathcal{O}(z_0 - z_h).$$

Substituting all these expressions in the equation (4.81) and simplifying we get

$$\lambda_L = \frac{(1+\xi)}{z_0^{\xi}\sqrt{2}}\left[a(\xi) + b(\xi)\frac{z_0}{z_h} + \mathcal{O}\left(\frac{z_0^2}{z_h^2}\right)\right]. \tag{4.82}$$

where,

$$\begin{aligned} a(\xi) &= 2\left(1 - \frac{\xi}{2}\right)(1-\xi)(2\xi - 3), \\ b(\xi) &= 2(3 - 2\xi)(\xi - 1)^2, \\ c(\xi) &= 2\xi(\xi-1)(2\xi-3) - \xi\left(1 - \frac{\xi}{2}\right)(1+\xi) \end{aligned} \tag{4.83}$$

and others coefficients are also the functions of ξ. Now using the expression of temperature of the Lifshitz black hole in (4.6) we get from (4.82),

$$\lambda_L = 2\sqrt{2}\pi T\left[a(\xi)\left(\frac{z_h}{z_0}\right)^{\xi} + b(\xi)\left(\frac{z_h}{z_0}\right)^{\xi-1} + \mathcal{O}\left[\left(\frac{z_h}{z_0}\right)^{\xi-2}\right]\right]. \tag{4.84}$$

It is thus obvious that the classical Lyapunov exponent is also directly proportional to T similar to the bound found for the Lyapunov exponent obtained in the three methods of quantum chaos discussed above for the asymptotically Lifshitz black hole. Therefore, to acquire the scenario of classical/quantum correspondence in our study, we get the relation

$$a(\xi)\left(\frac{z_h}{z_0}\right)^{\xi} + b(\xi)\left(\frac{z_h}{z_0}\right)^{\xi-1} + \mathcal{O}\left[\left(\frac{z_h}{z_0}\right)^{\xi-2}\right] = \frac{1}{\sqrt{2}}, \tag{4.85}$$

that must be satisfied by a specific power series of $\left(\frac{z_h}{z_0}\right)^{\xi}$.

In this Chapter, we undergo a comparative analysis of three different holography-based approaches, namely, entanglement wedge reconstruction, out-of-time-ordered correlators and pole-skipping, of studying quantum chaos to understand their plausible equivalence in the asymptotically Lifshitz black hole with arbitrary anisotropy index. In the entanglement wedge method, we construct an extremal hypersurface as a constant time slice, famously called Ryu-Takayanagi surface, that extracts out the butterfly velocity at late time. The butterfly velocity occurs to have monotonically increasing behaviour with both the anisotropy index and the finite temperature of the chosen background. For the unit anisotropy index, it expectantly reduces to that for the planar AdS black hole. For the derivation of OTOCs, we explicitly construct the double-sided Kruskal geometry corresponding to the asymptotically Lifshitz black hole. We introduce a gravitational shockwave backreacting in the Kruskal version of our background. Subsequently, the functional form of the shockwave occurs to be exponential and gives rise to the OTOCs. It further shows that the system is chaotic and the rate of chaotic growth is specified by the Lyapunov exponent. Such a scenario is somewhat consistent with the previously obtained scenario for any generic perturbed holographic two-sided gravity background. The butterfly velocity and Lyapunov exponent obtained from the shockwave profile are exactly similar to those from the entanglement wedge method. Finally, in the method of pole-skipping, we again observe the exact same dependency of butterfly velocity as well as the Lyapunov exponent on the anisotropy. As a consequence of such exact matching of these salient chaotic features, we claim that all these chosen methods are equivalent and definitive to understanding chaos for the class of asymptotically Lifshitz black holes at the quantum level.

This Chapter deals with an extensive study of chaos in Lifshitz background by these three methods and shows an equivalence among them. Our results show that the butterfly velocity increases with an increase in the anisotropy of the background and this velocity becomes temperature dependent. Further, we have shown a classical chaos study of the same

background by the geodesic instability analysis. We further calculate the eikonal phase shift and comment on the nature of the scattering process at different regimes of the bulk. We further aim to study a classical/quantum correspondence of chaos in this background.

Chapter 5

Discussions

The second chapter is a collection of two of our research works. In the first work, we studied the pole-skipping phenomena in non-extremal gravity theory in the presence of the Scalar-Gauss-Bonnet interaction. We have considered a four-dimensional Schwarzchild-AdS black hole solution as the holographic bulk theory. On the boundary, we have a finite temperature conformal theory. The interaction is sourced by an operator of dimension Δ of the boundary theory, which is dual to the scalar field ϕ in the bulk. In the Einstein action, the interaction term is added perturbatively (2.1). In the perturbative approximation, this external scalar source does not affect the original bulk solution but makes a nontrivial contribution in the linearised field equations (2.5). We have found that k of the pole-skipping points (ω, k) corresponding to the scalar field and metric perturbation have been affected by the external scalar source $\mathcal{O}_s$ in both quantizations, whereas ω remains unchanged. Unlike the unperturbed model, the minimally coupled scalar ϕ has contained both real and imaginary k in the pole-skipping points. As the source is increased, the points of the imaginary k plane have moved into the real k plane. We have presented these facts pictorially in Figure 2.2. In Schwarzchild-AdS$_4$ without external effect [76], k is always real in the shear mode. Here we have found that the shear mode k can have both real and imaginary values depending on the effect of the scalar source. We have analytically found the effect of the interaction on the poles located at $\omega_n = -2in\pi T$ and corresponding $k \sim T$ which are given in (2.14) and higher order momentum values of shear mode. The first order pole-point k_1^2 is always greater than $3r_0^2$ for $\zeta = \phi$, ϕ^2, ϕ^3 & ϕ^4 and has decreased for other higher powers of ϕ. However,

for the second and other higher orders of pole-skipping, k^2 has always decreased with the increasing source for all positive integer powers of ϕ in $\zeta(\phi)$. These have been shown in Figure 2.3. Here, the increase (or decrease) of real k implies a slow (or fast) rate of momentum transportation in shear mode and the imaginary k means the exponential decay of the momentum density. As a result, when positive k_1^2 has increased with the increasing source $\mathcal{O}_s$, the mobility of the corresponding modes has decreased. Thus the decreasing mobility has decreased the value of diffusion coefficient $\mathcal{D}_s$. In Figure 2.4, we have presented this consistent behaviour of diffusion coefficient. At $\mathcal{O}_s \to 0$, k_1^2 is at a minimum value, and therefore, momentum flow is maximum which has given the maximum value of $\mathcal{D}_s$. So, due to the effect of the external source, the flow of momentum in shear mode has decreased for $p \leq 4$, otherwise, it has increased. The 1st-order pole-skipping point lies in the dispersion curve.

In the sound mode, the first three pole-skipping points have been derived from the master equation as $\omega_n = -2\pi i n T$ and corresponding $k_n \sim T$ is given in (2.18a) and (2.18b). In the non-perturbative case where either $\lambda \to 0$ or $\mathcal{O}_s \to 0$, our results have reduced into the pole-skipping points of pure Schwarzchild-AdS$_4$ background [76], i.e, $k_n^4 = -9nr_0^4$. It gives a complex value (of equal real and imaginary parts) of k. As the source is turned on, we have found that an imaginary part has been added with the negative real part of k^4. It means the real and imaginary parts of k are no longer equal. We have shown all of these in Figure 2.6. From the OTOC calculation in the last section, we have found the Lyapunov exponent $\lambda_L = i\omega = 2\pi T$ and the butterfly velocity $v_b = \frac{\sqrt{3}}{2}$ where $\omega_* = 2i\pi T$ and $k_* = \pm\frac{4}{\sqrt{3}} i\pi T$. These results have been further verified with a different approach by analyzing the power series solution of the sound mode master equation near the horizon. Therefore $(\omega_*,\ k_*)$ is considered as the lowest order pole-skipping point in sound mode instead of $(\omega_1,\ k_1)$. So the pole-skipping points of sound mode are $(\omega_*,\ k_*)$, $(\omega_1,\ k_1)$, $(\omega_2,\ k_2)$, $(\omega_3,\ k_3)$ and so on. The pole-skipping points $(\omega,\ k)$ describe the flow of energy density. Here k has both the real and imaginary parts. It signifies that the real part is associated with the flow of the energy density in longitudinal mode whereas the imaginary part of k is related to the exponential decay of

the energy density. Therefore with the effect of interaction, when the energy density diffusion has increased, the exponential decay has decreased and vice-versa. It would be interesting to study these flows and decays quantitatively. It would be very interesting to calculate the bulk-boundary Green's function with the set-up of this paper and calculate the pole-skipping points from Green's function.

In this work, we have found some non-trivial effects of the interaction on the sound mode and shear mode. We have not found any effect on the chaotic behaviour. The reason is mainly the perturbative approach to the interaction term. If one considers the backreaction of the interaction, the Lyapunov exponent and the butterfly velocity are expected to be affected by the interaction. With backreaction, one can expect k_* and k_1 to be equal in the sound mode.

In the second work, we have studied the P-S phenomenon with 2 types of couplings: dipole and Yukawa, where we have probed a scalar field, which can be real or charged. We have investigated the behaviour of fermionic P-S points with increasing temperature up to the critical temperature (T_c) of the background scalar field. We have checked that after crossing the critical value of the temperature, the P-S points saturate at the mass value of fermion and for massless fermions, P-S points vanish after crossing T_c. For real scalar coupling, the momentum values are $\propto\ (T_c - T)^{1/2}$, while for charged scalar coupling, the momentum values are $\propto\ (T_c - T)$. We have checked our results upto third order pole-skipping. It would be very interesting to see the effect of couplings in other backgrounds with different interaction terms. Our question was: what does it mean when the line of poles and zeros intersect for a real condensed matter system? The poles of the Green's function typically define the Fermi surface. An interesting example is the well-known condensed matter system Mott insulator. In those systems, when the system undergoes from metal to insulator transition such phenomenon of pole-skipping happens. At the transition point, fermionic Green's function simultaneously has pole and zeros, where the Fermi surface disappears and zero surface appears[131]. In this work, we have tried to interpret the meaning of pole-skipping points in a novel way by perturbing the fermions. Pole-skipping points are the points of intersection of

lines of poles and zeroes of Green's function. In a condensed matter system, a line of poles means the appearance of the Fermi surface, while a line of zeroes means Green's function is zero. The fermionic Green's function is zero means the system is not giving any response to the fermionic perturbations. Or, in a mathematical sense, we can say that the density of states is zero, meaning there are no available energy states to occupy for the electrons. We can think of the pole-skipping point as the transiting point where the fermi surface overlaps with a surface where electrons are tightly bound. In terms of physical properties, at that point, conducting and insulating phases overlap. Therefore, it could be interesting to investigate those systems from the perspective of holographic P-S phenomena. This we leave for our future studies.

In Chapter 3, we have studied the D3-D7 brane system in the supergravity limit, where the dual theory is a strongly coupled Yang-Mills gauge theory at finite temperature with light quark flavors. In bulk, a stack of D3 branes creates the black hole gravitational background, while D7 branes are considered to be probing this background with an electric field on their world volume. This type of boundary theory can be viewed as a model for unquenched QCD. Within this framework, we have computed pole-skipping points which are claimed to be connected with quantum chaotic parameters on the boundary theory [100]. Specifically, we have calculated two well-known characteristic parameters of chaotic systems: the Lyapunov exponent and the butterfly velocity. Additionally, we have examined how these parameters depend on external electric fields and quark masses. Another diagnostic to study the chaotic properties in both bulk/boundary theories is OTOC. The computation of OTOC in this set-up would be very interesting. In [192], the authors have computed OTOC in the D3-D5 brane set-up and argued that the Lyapunov exponent would increase in the presence of an electric field. In a perturbative limit, we have observed that the electric field is decreasing the chaotic exponent up to some critical value of the electric field. The OTOC computation in D3-D7 brane systems in the presence of an external electric or magnetic field is beyond the scope of this present work, and we are presently working on this important issue.

In the absence of the electric field, we have found that the Lyapunov exponent is $2\pi T$,

which indicates a maximally chaotic system similar to the flavor-less theory. However, the butterfly velocity has an implicit dependence on the flavor mass. The presence of an electric field deviates the system from maximal chaos. As one increases the electric field, the Lyapunov exponent decreases, and that has been displayed in Figure 3.4. We have calculated a bound of the electric field up to which the Lyapunov exponent decreases. Beyond that value, solutions are not regular. So, this study is valid up to that critical value of the electric field. We further evaluated the butterfly velocity and presented it pictorially in Figure 3.5. Analytically, we have found in (3.48) that v_b depends on both the quark mass (through θ_0) and the electric field. We have observed that the butterfly velocity is insensitive to the quark mass but changes significantly in terms of the background electric field as expected due to its effect on the binding energy of the quark/anti-quark bound state. The most interesting observation is that there exists a critical electric field up to which both (λ_L, v_b) decreases indicating the fact that the system under consideration becomes less chaotic for a sufficiently strong electric field. Due to strong pull under the electric field $(E > E^*)$, the meson state dissociates into two separate charged quarks. In the presence of a strong electric field, we have a system of Yang-Mills gauge fields and dissociated quarks showing less chaotic behaviour than the system with zero electric fields. It would be interesting to study this further. We have further analyzed the first-order pole-skipping points for gauge invariant gravitational perturbation using the master equations for the sound, shear, and tensor channels. We have calculated the pole-skipping points in the small external electric field limit. It was argued in [86, 97, 98] that in the perturbative limit, ω values generically do not receive any contribution. However, our analysis reveals that this is indeed not true. For stringy brane systems, even in the probe limit the world volume electric field can give rise to non-trivial correction to the pole-skipping frequency ω, and this is precisely due to the appearance of effective horizon outside the actual horizon of the black D3 brane. Pole-skipping points associated with the gauge invariant gravitational perturbations in the bulk correspond to dual hydrodynamic dispersion relation. Using this dual interpretation, we further computed the associated modified hydrodynamic transport coefficients, namely, thermal diffusion $\mathcal{D}_T$ and momentum diffusion

$\mathcal{D}_p$ constant. However, our entire analysis is within the probe limit. It would be interesting to investigate pole-skipping phenomena considering the back-reaction of those probe branes [193].

In Chapter 4, we have studied chaotic properties of a Lifshitz black hole with anisotropy by three holography-based approaches, namely, entanglement wedge reconstruction, out-of-time-ordered correlators and pole-skipping [114]. Our computations have been mainly done in the bulk of Lifshitz space-time. The results of this work show that the entanglement wedge, OTOC and pole-skipping show the same Lyapunov exponent and butterfly velocity. The butterfly velocity is dependent on temperature of the field theory as $T^{1-\frac{1}{\xi}}$, where ξ is the anisotropy of the background. This says that as anisotropy increases, the growth of operator increases in physical space. The three methods are based on near-horizon analysis of the background. The entanglement wedge method says how the RT surface is approaching the horizon. From the shock wave method (OTOC), we see the amount of discontinuity in one horizon due to the presence of a localised shock wave. The third method, pole-skipping is based on a sound mode analysis in bulk. Basically, we are computing the geodesic equations from all these methods. So, it is expected to get the same results from all of them. One can trust any of the methods to study the chaotic behaviour of a thermal background.

We demonstrate a further investigation of the eikonal phase shift due to heavy-heavy-light-light gravitational scattering and compute the Lyapunov exponent, at the classical level, by using the bulk metric both in near-boundary and near-horizon regimes. A detailed study of the associated null geodesics serves this purpose. We infer a compatible connection of the quantum OTOCs in the leading order of the series expansion of its exponential form with the classical eikonal phase shift in the bulk. This reveals that the leading order term of OTOCs at the classical level can be studied as nontrivial functions of the turning point of the null geodesic as well as the anisotropy index. Interestingly, due to the presence of arbitrary anisotropy in our case, the eikonal phase becomes real or imaginary depending on the near-horizon and near-boundary limits of the black hole and the impact parameter. This may allow one to explore the absorption cross-section for both elastic and inelastic scatter-

ings in terms of the arbitrary anisotropy index of the asymptotically Lifshitz black hole. We successfully verified the eikonal phase by using the WKB approximation of the solution of the Klein-Gordon equation, at least up to the leading order. The classical Lyapunov exponent also appears to be a nontrivial function of the anisotropy index ξ. It is observed that, in the near-horizon limit, there occurs an emergent classical/quantum correspondence for the class of Lifshitz theories for a specific convergent power series of $\left(\frac{z_h}{z_0}\right)^{\xi}$ with ξ-dependent coefficients and the series must converge at $\frac{1}{\sqrt{2}}$ to achieve an exact matching between classical and quantum Lyapunov exponents. In addition to these, we further remark on some obvious restrictions on the possible extrema of the null geodesics, where we obtain inconsistent natures of classical eikonal phase shift and Lyapunov exponent. It would be further interesting to explore the possible connection between these two results, which may eventually lead to classical/quantum correspondence in the context of chaos in Lifshitz black hole. As potential future research, it would be rather fascinating to have a more elaborate investigation of the classical/quantum correspondence in the context of a generic class of holographic Lifshitz theories. One can also go for an explicit evaluation of the OTOCs from the systematic construction of the dual thermofield double states of the finite temperature Lifshitz field theory, and subsequently study different chaotic features on the field theory side. We hope to come back with some of these ideas in the near future.

Appendix A

In Chapter 2, we studied the effect of higher derivative terms on the pole-skipping points. The master equations we constructed in section 2.2 had various coefficients dependent on ω, k and $\phi(r_0)$. In this section of the appendix, we have shown the coefficients of the master equations for both shear and sound channels.

A.1 Coefficient of Master Equation: Shear Channel

Three coefficients of the master equation can be written in the linear order of the perturbation parameter λ

$$\begin{aligned}
\mathcal{M}_{sh}(r) &= \mathcal{M}^{(0)}_{sh} + \lambda\mathcal{M}^{(1)}_{sh} + \mathcal{O}(\lambda^2) \\
\mathcal{P}_{sh}(r) &= \mathcal{P}^{(0)}_{sh} + \beta^2\mathcal{P}^{(\phi)}_{sh} + \lambda\mathcal{P}^{(1)}_{sh} + \mathcal{O}(\lambda^2) \\
\mathcal{Q}_{sh}(r) &= \mathcal{Q}^{(0)}_{sh} + \beta^2\mathcal{Q}^{(\phi)}_{sh} + \lambda\mathcal{Q}^{(1)}_{sh} + \mathcal{O}(\lambda^2)
\end{aligned}$$

We have found the above functions as follows.

$$\mathcal{M}^{(0)}_{sh} = r^2 f(r) \tag{5.1}$$

$$\mathcal{P}^{(0)}_{sh} = \frac{\omega f(r)\left(5r\omega + 2ik^2\right) - 8k^2 r f(r)^2 + \omega^2(3r - 2i\omega)}{\omega^2 - k^2 f(r)} \tag{5.2}$$

$$\mathcal{Q}^{(0)}_{sh} = \frac{-10k^2r^2f(r)^2 + f(r)\left(k^4 + 9ik^2r\omega + 4r^2\omega^2\right) + \omega\left(k^2(-\omega - 3ir) + 6r\omega(r - i\omega)\right)}{r^2\left(\omega^2 - k^2 f(r)\right)} \tag{5.3}$$

and

$$\mathcal{M}_{sh}^{(1)} = 0 \tag{5.4}$$

$$\mathcal{P}_{sh}^{(1)} = \frac{r^2 f(r)}{\left(\omega^2 - k^2 f(r)\right)^2}\left[r\zeta''(r)\left(\omega^2 - k^2 f(r)\right)\left(f(r)\left(2k^2 f(r) + \omega^2\right) - 3\omega^2\right) + \zeta'(r)\left(f(r)\right.\right.$$
$$\left.\left.\left(k^2 f(r)\left(4k^2 f(r) - 6k^2 - 11\omega^2\right) + 24k^2\omega^2 - 2\omega^4\right) - 9k^2\omega^2\right) - \omega\mathcal{F}\right] \tag{5.5}$$

$$\mathcal{Q}_{sh}^{(1)} = \frac{1}{r\left(\omega^2 - k^2 f(r)\right)^2}\left[r\zeta''(r)\left(\omega^2 - k^2 f(r)\right)\left(f(r)\left(\omega^2\left(4k^2 - ir\omega\right) - 2k^2 f(r)\left(-3r^2 f(r)\right.\right.\right.$$
$$+k^2 + 3r^2 + ir\omega + \omega^3(-2\omega + 3ir)\Big) + \zeta'(r)\Big(f(r)\Big(f(r)\Big(-k^2 f(r)\Big(-14k^2 r^2 f(r) + 3k^4$$
$$+4k^2 r(6r + i\omega) + 34r^2\omega^2\Big) + 3k^6 + 6k^4\left(3r^2 + ir\omega + \omega^2\right) + k^2 r\omega^2(72r + 11i\omega)$$
$$\left.\left.+2r^2\omega^4\right) + \omega^2\left(-6k^4 - 3k^2\left(18r^2 + 8ir\omega + \omega^2\right) + 2r\omega(-6r + i\omega)\right)\right) + 3\omega^3\left(6r^2\omega\right.$$
$$\left.\left.+k^2(\omega + 3ir)\right)\right) + ir\left(2\omega^2 - f(r)\left(k^2 - 2ir\omega\right)\right)\mathcal{F}\Big] \tag{5.6}$$

where,

$$\mathcal{F} = 6k^2 r^2\omega(f(r) - 1)\left[r(f(r) - 3)f(r)\zeta''(r) - 3((f(r) - 2)f(r) + 3)\zeta'(r)\right]^2 / \left[r\zeta''(r)\left(f(r)\right.\right.$$
$$\left(f(r)\left(k^2 - 3ir\omega\right) - 3k^2 + 3ir\omega\right) - 18ir\omega\Big) - 3\zeta'(r)\Big((f(r) - 2)f(r)\left(k^2 - ir\omega\right)$$
$$\left.+3\left(k^2 + 3ir\omega\right)\right) + ir^3\omega(f(r) - 3)f(r)\zeta'''(r)\Big]$$

$$\mathcal{P}_{sh}^{(\phi)} = \frac{1}{(\omega^2 - k^2 f(r))^3\Xi}\left(-3k^2 r^5\omega(f(r) - 1)f(r)^3\phi'(r)^3\left(i\omega f(r)\left(4\omega^2 f(r)^2\left(\omega^2\right.\right.\right.$$
$$\left.-k^2 f(r)\right)\zeta''(r)\phi''(r)^2 r^4 + 4\omega f(r)\left(3r\omega^3 + \left(3r\omega(\omega - 4ir) - k^2(3r + i\omega)\right)f(r)\omega\right.$$
$$\left.+i\left(k^4 + 3ir\omega k^2 + 4r^2\omega^2\right)f(r)^2\right)\phi'(r)\zeta''(r)\phi''(r)r^2 + \phi'(r)^2\left(\left(9r^2\omega^4 + 3r\left(6r\omega^2\right.\right.\right.$$
$$\left.\left.-k^2(3r + 2i\omega)\right)f(r)\omega^2 + \left((6ir - \omega)k^4 - 6r(5r + i\omega)\omega k^2 + 3r^2\omega^2(3\omega - 20ir)\right)f(r)^2\omega\right.$$
$$\left.\left.+\left(k^6 + 6ir\omega k^4 - 5r^2\omega^2 k^2 + 36ir^3\omega^3\right)f(r)^3\right)\zeta''(r) - 4ir^4\omega^3(f(r) - 3)f(r)^2\zeta^{(3)}(r)\right)\Big)r^2$$
$$+\zeta'(r)\left(4\omega^2 f(r)^2\left((3ir + \omega)\omega^3 + \left(k^4 + ir\omega k^2\right)f(r)^2 + i\left(k^2(3r + 2i\omega)\omega - 7r\omega^3\right)f(r)\right)\right.$$
$$\phi''(r)^2 r^4 + 4\omega f(r)\left(3r(3ir + \omega)\omega^4 + \left(i\left(9r^2 + 3i\omega r - \omega^2\right)k^2 + 3r\omega\left(12r^2 - 4i\omega r\right.\right.\right.$$
$$\left.\left.+\omega^2\right)\right)f(r)\omega^2 + \left((6r + 2i\omega)k^4 + r(12ir - 13\omega)\omega k^2 - 3r^2(8r + 7i\omega)\omega^2\right)f(r)^2\omega + \left(-ik^6\right.$$
$$\left.+4r\omega k^4 + 3ir^2\omega^2 k^2 + 12r^3\omega^3\right)f(r)^3\Big)\phi'(r)\phi''(r)r^2 + \left(9r^2(3ir + \omega)\omega^5 + 3r\left(i\left(9r^2\right.\right.\right.$$
$$\left.\left.-2\omega^2\right)k^2 + 3r\omega\left(24r^2 - i\omega r + 2\omega^2\right)\right)f(r)\omega^3 + \left(\left(27r^2 + 9i\omega r - \omega^2\right)k^4 + 3ir\omega\left(9r^2\right.\right.$$

$$+20i\omega r-2\omega^2\big)k^2+9r^2\omega^2\left(-4r^2-11i\omega r+\omega^2\right)\big)f(r)^2\omega^2+\big((2\omega-9ir)k^6$$
$$+r(42r+19i\omega)\omega k^4+3r^2(23ir-20\omega)\omega^2k^2-3r^3(32r+21i\omega)\omega^3\big)f(r)^3\omega$$
$$-\left(k^8+7ir\omega k^6-15r^2\omega^2k^4+3ir^3\omega^3k^2-84r^4\omega^4\right)f(r)^4\big)\phi'(r)^2\big)\big)\big)$$

$$\mathcal{Q}_{sh}^{(\phi)}=\frac{r^3f(r)\phi'(r)^2}{(\omega^2-k^2f(r))^3\Xi}\big(3k^2r^2\omega(f(r)-1)\left(\left(k^2-2ir\omega\right)f(r)-2\omega^2\right)\phi'(r)\left(4\omega^2f(r)^2\left(\omega^2\right.\right.$$
$$-k^2f(r)\big)\zeta''(r)\phi''(r)^2r^4+4\omega f(r)\left(3r\omega^3+\left(3r\omega(\omega-4ir)-k^2(3r+i\omega)\right)f(r)\omega\right.$$
$$+i\left(k^4+3ir\omega k^2+4r^2\omega^2\right)f(r)^2\big)\phi'(r)\zeta''(r)\phi''(r)r^2+\phi'(r)^2\left(\left(9r^2\omega^4+3r\left(6r\omega^2\right.\right.\right.$$
$$-k^2(3r+2i\omega)\big)f(r)\omega^2+\big((6ir-\omega)k^4-6r(5r+i\omega)\omega k^2+3r^2\omega^2(3\omega$$
$$-20ir)\big)f(r)^2\omega+\left(k^6+6ir\omega k^4-5r^2\omega^2k^2+36ir^3\omega^3\right)f(r)^3\big)\zeta''(r)-4ir^4\omega^3(f(r)$$
$$-3)f(r)^2\zeta^{(3)}(r)\big)\big)f(r)^2+\zeta'(r)\left(8\omega^3(f(r)-3)f(r)^3-k^2f(r)\right)^3\phi''(r)^3r^6\left(\omega^2\right.$$
$$+12i\omega^2f(r)^2\left(9ir\omega^7+\big((21ir-4\omega)k^4+\omega\left(6r^2-6i\omega r+\omega^2\right)k^2-3ir\omega^4\right)f(r)^2\omega^3\right.$$
$$+2k^4r\left(2ik^2-r\omega\right)f(r)^5\omega+k^2\big((5\omega-6ir)k^4-2\omega\left(-3r^2-11i\omega r+\omega^2\right)k^2$$
$$-20r^2\omega^3\big)f(r)^3\omega+\left(-2k^8+\omega(\omega-10ir)k^6-r(4r+7i\omega)\omega^2k^4+14r^2\omega^4k^2\right)f(r)^4$$
$$+\left(6ir\omega^7+k^2(\omega-30ir)\omega^5\right)f(r)\big)\phi'(r)\phi''(r)^2r^4-6\omega f(r)\left(27r^2\omega^8+3r\left(15r\omega^2\right.\right.$$
$$-k^2(33r+2i\omega)\big)f(r)\omega^6+\big(\left(45r^2+30i\omega r+\omega^2\right)k^4+3ir\omega\left(36r^2+27i\omega r\right.$$
$$-4\omega^2\big)k^2+9r^2\omega^4\big)f(r)^2\omega^4-\big(\left(9r^2+18i\omega r+\omega^2\right)k^6+3\omega\left(36ir^3-37\omega r^2-4i\omega^2r\right.$$
$$+\omega^3\big)k^4+3r\omega^2\left(48r^3+52i\omega r^2+3\omega^2r+2i\omega^3\right)k^2+9r^2\omega^6\big)f(r)^3\omega^2+k^2\left((6ir\right.$$
$$-\omega)k^6+\omega\left(-63r^2-44i\omega r+7\omega^2\right)k^4+r\omega^2\left(108ir^2+103\omega r+30i\omega^2\right)k^2$$
$$+3r^2\omega^3\left(80r^2+60i\omega r-9\omega^2\right)\big)f(r)^4\omega+k^2\left(k^8-2ir\omega k^6+19r^2\omega^2k^4+36ir^3\omega^3k^2\right.$$
$$+48r^4\omega^4\big)f(r)^6+k^2\left(k^8+5(4ir-\omega)\omega k^6-r(19r+10i\omega)\omega^2k^4+r^2(-36ir\right.$$
$$-43\omega)\omega^3k^2-12r^3(12r+11i\omega)\omega^4\big)f(r)^5\big)\phi'(r)^2\phi''(r)r^2+\left(-81r^3\omega^9\right.$$
$$+27r^2\left(k^2(12r+i\omega)-8r\omega^2\right)f(r)\omega^7-9r\left(\left(9r^2+18i\omega r+\omega^2\right)k^4\right.$$
$$+9ir\omega\left(14r^2+6i\omega r-\omega^2\right)k^2+18r^2\omega^4\big)f(r)^2\omega^5+3k^2\left(i\left(9r^2+\omega^2\right)k^4\right.$$
$$+6r\left(45ir^3-30\omega r^2-6i\omega^2r+\omega^3\right)k^2+27r^2\omega\left(16r^3+16i\omega r^2+2\omega^2r\right.$$
$$+i\omega^3\big)\big)f(r)^3\omega^4-\big((9r+6i\omega)k^8+\left(-378r^3-243i\omega r^2+18\omega^2r+5i\omega^3\right)k^6$$

$$
\begin{aligned}
&+27r\omega\left(28ir^3+18\omega r^2+6i\omega^2 r-\omega^3\right)k^4+9r^2\omega^2\left(168r^3+20i\omega r^2-18\omega^2 r\right.\\
&\left.-3i\omega^3\right)k^2-27r^3\omega^6\Big)f(r)^4\omega^3+3k^2\left(ik^8+\left(-48ir^2+22\omega r+4i\omega^2\right)k^6\right.\\
&+r\omega\left(42r^2+119i\omega r-30\omega^2\right)k^4+12ir^2\omega^2\left(2r^2+15i\omega r-6\omega^2\right)k^2\\
&\left.-6r^3\omega^3\left(20r^2+48i\omega r-9\omega^2\right)\right)f(r)^5\omega^2+3k^2\left(-(10r+3i\omega)k^8+r\omega(17\omega\right.\\
&-32ir)k^6+r^2(18r+7i\omega)\omega^2k^4+9r^3\omega^3(4ir+13\omega)k^2+6r^4(60r\\
&\left.+49i\omega)\omega^4\right)f(r)^6\omega+2ik^2\left(k^{10}+3ir\omega k^8+12r^2\omega^2k^6+63ir^3\omega^3k^4\right.\\
&\left.-117r^4\omega^4k^2+252ir^5\omega^5\right)f(r)^7\Big)\phi'(r)^3\Big)\Big).
\end{aligned}
$$

$$
\Xi = (3r\omega-(ik^2+3r\omega)f(r))\phi'(r)+2r^2\omega f(r)\phi''(r).
$$

Here the ζ function takes its appropriate form as mentioned earlier. After the near-horizon analysis of the master equation, we found the first pole-skipping point (ω_1, k_1) at $\omega_1 = -\frac{3}{2}ir_0$ and

$$
\begin{aligned}
k_1^2-3r_0^2-\frac{9\beta^2\xi r_0^2\phi(r_0)^2\left(r_0^2(3\xi+4p)-2k^2p\right)}{p\left(2k^2p+3r_0^2(3\xi+4p)\right)}+\frac{3\lambda\xi\phi(r_0)^p}{\left(2k^2p+3r_0^2(3\xi+4p)\right)^2}\left[-4k^6p^2+12k^4pr_0^2((\xi-12)p\right.\\
\left.-3\xi)+9k^2r_0^4\left(-9\xi^2+16(3\xi-10)p^2+12(\xi-10)\xi p\right)+27\xi r_0^6(3\xi+4p)^2\right]=0
\end{aligned}
\tag{5.7}
$$

Similarly, one can find the higher-order pole-skipping points by performing the near-horizon expansion of the master equation. Here, by considering the negligible value of the β parameter, one can get the master equation with interaction only. However, in the shear mode case, to get the previous result (2.14), one needs to ignore the β^2 term from the starting point.

A.2 Coefficient of Master Equation: Sound Channel

Three coefficients of the master equation can be written in the linear order of the perturbation parameter λ

$$
\mathcal{M}_{so}(r) = \mathcal{M}_{so}^{(0)}+\lambda\mathcal{M}_{so}^{(1)}+\mathcal{O}(\lambda^2)
$$

$$\mathcal{P}_{so}(r) = \mathcal{P}_{so}^{(0)} + \beta^2\mathcal{P}_{so}^{\phi} + \lambda\mathcal{P}_{so}^{(1)} + \mathcal{O}(\lambda^2)$$
$$\mathcal{Q}_{so}(r) = \mathcal{Q}_{so}^{(0)} + \beta^2\mathcal{Q}_{so}^{\phi} + \lambda\mathcal{Q}_{so}^{(1)} + \mathcal{O}(\lambda^2)$$

where,

$$\mathcal{M}_{so}^{(0)} = r^4 f(r) \tag{5.8}$$

$$\mathcal{P}_{so}^{(0)} = \frac{r^2\left(f(r)\left(11k^2rf(r)+2k^2(6r-i\omega)-20r\omega^2\right)+\left(3k^2-4\omega^2\right)(3r-2i\omega)\right)}{k^2f(r)+3k^2-4\omega^2} \tag{5.9}$$

$$\mathcal{Q}_{so}^{(0)} = \frac{1}{k^2f(r)+3k^2-4\omega^2}\left(-f(r)\left(-25k^2r^2f(r)+k^4+12k^2r(r+i\omega)+16r^2\omega^2\right)-3k^4 + k^2(9r+2i\omega)(3r-2i\omega)-24r\omega^2(r-i\omega)\right) \tag{5.10}$$

$$\mathcal{P}_{so}^{\phi} = \left[2k^2rf(r)^2\left(r\phi'(r)^2\left(k^2rf(r)^2\left(k^4-4k^2r(3r+i\omega)+16r^2\omega^2\right)-2f(r)\left(k^6(6r+i\omega)\right.\right.\right.\right.$$
$$\left.\left.\left.\left.-2k^4r\left(9r^2+3ir\omega+2\omega^2\right)+8k^2r^2\omega^2(6r+i\omega)-32r^3\omega^4\right)+k^2\left(3k^2-4\omega^2\right)\left(4r\omega^2\right.\right.\right.\right.$$
$$\left.\left.\left.\left.-k^2(3r+2i\omega)\right)\right)-4m^2\phi(r)^2\left(k^2rf(r)\left(-4r\omega^2+k^2(3r+i\omega)\right)+3k^6-k^4\left(9r^2\right.\right.\right.$$
$$\left.\left.\left.+3ir\omega+2\omega^2\right)+4k^2r\omega^2(6r+i\omega)-16r^2\omega^4\right)\right)\Big] \Big/ \left\{\left(k^2+2ir\omega\right)\left(k^2f(r)+3k^2-4\omega^2\right)^3\right\}$$

$$\mathcal{Q}_{so}^{\phi} = -\Big[r\phi'(r)^2\left(2k^4r^3f(r)^4\left(-9k^4+6k^2r(20r+7i\omega)-160r^2\omega^2\right)+k^2rf(r)^3\left(k^8\right.\right.$$
$$\left.\left.+2k^6r(93r+17i\omega)-4k^4r^2\left(108r^2+39ir\omega+20\omega^2\right)+48k^2r^3\omega^2(20r+3i\omega)-512r^4\omega^4\right)\right.$$
$$+k^2f(r)^2\left(-k^8(9r+2i\omega)+6k^6r\left(27r^2+9ir\omega+2\omega^2\right)+4ik^4r^2\omega\left(63r^2+144ir\omega-32\omega^2\right)\right.$$
$$\left.+96k^2r^3\omega^3(4\omega-7ir)+448ir^4\omega^5\right)+f(r)\left(3k^2-4\omega^2\right)\left(-k^8(15r+4i\omega)+2k^6r\left(9r^2\right.\right.$$
$$\left.\left.-3ir\omega+10\omega^2\right)+12ik^4r^2\omega\left(3r^2+10ir\omega-2\omega^2\right)+96k^2r^3\omega^3(\omega-ir)+64ir^4\omega^5\right)$$
$$\left.-k^4\left(3k^2-4\omega^2\right)^2(3r+2i\omega)\left(k^2+2ir\omega\right)\right)+2m^2\phi(r)^2\left(k^4r^2f(r)^3\left(k^4+6k^2r(20r+7i\omega)\right.\right.$$
$$\left.\left.-160r^2\omega^2\right)+k^2rf(r)^2\left(k^6(105r-2i\omega)-2k^4r\left(108r^2+39ir\omega+32\omega^2\right)+24k^2r^2\omega^2(20r\right.$$
$$\left.+3i\omega)-256r^3\omega^4\right)+f(r)\left(-6k^{10}+k^8\left(27r^2-24ir\omega+4\omega^2\right)+2ik^6r\omega\left(63r^2+84ir\omega\right)\right.$$
$$\left.+8\omega^2+16k^4r^2\omega^3(8\omega-21ir)+224ik^2r^3\omega^5\right)-\left(3k^2-4\omega^2\right)\left(6k^8-k^6\left(9r^2+6ir\omega+4\omega^2\right)\right.$$
$$\left.+2k^4r\omega\left(-9ir^2+30r\omega+4i\omega^2\right)+48ik^2r^2\omega^3(r+i\omega)-32ir^3\omega^5\right)\Big)\Big] \Big/$$
$$\left\{2r^2\left(k^2+2ir\omega\right)\left(k^2f(r)+3k^2-4\omega^2\right)^3\right\}$$

$$\mathcal{M}_{so}^{(1)} = 0 \tag{5.11}$$

$$\mathcal{P}_{so}^{(1)} = \frac{r^2 f(r)}{(2ir\omega + k^2)\left(k^2 f(r) + 3k^2 - 4\omega^2\right)^3}\Big[r^3\zeta''(r)\Big\{f(r)\Big(k^2 f(r)\Big(k^2 f(r)^2\Big(9k^4 + 2k^2 r(-24r + 25i\omega) + 64r^2\omega^2\Big) + 2f(r)\Big(-27k^6 + 6k^4\Big(24r^2 - 9ir\omega + 11\omega^2\Big) + 4k^2 r\omega^2(-72r + 17i\omega) + 128r^2\omega^4\Big) + 12\Big(3k^2 - 4\omega^2\Big)\Big(2k^4 + k^2\Big(-12r^2 - 4ir\omega + 3\omega^2\Big) + 2r\omega^2(8r + 3i\omega)\Big)\Big) + 2\Big(3k^2 - 2\omega^2\Big)\Big(3k^2 - 4\omega^2\Big)^2\Big(k^2 + 2ir\omega\Big)\Big) - 3\Big(3k^2 - 4\omega^2\Big)^3\Big(k^2 + 2ir\omega\Big)\Big\} + 4\zeta'(r)\Big\{f(r)\Big(k^2 f(r)\Big(r^2 f(r)\Big(-k^2 f(r)\Big(5k^4 + 3k^2 r(-12r + 7i\omega) + 48r^2\omega^2\Big) + 9k^6 + k^4\Big(-180r^2 + 33ir\omega - 26\omega^2\Big) + 4k^2 r\omega^2(96r + 5i\omega) - 192r^2\omega^4\Big) + 3k^8 + 4k^6\Big(36r^2 + 6ir\omega - \omega^2\Big) + k^4 r\Big(324r^3 + 243ir^2\omega - 324r\omega^2 - 32i\omega^3\Big) - 8k^2 r^2\omega^2\Big(90r^2 + 81ir\omega - 34\omega^2\Big) + 48r^3\omega^4(8r + 9i\omega)\Big) + \Big(3k^2 - 4\omega^2\Big)\Big(3k^8 - k^6\Big(63r^2 + 4\omega^2\Big) - k^4 r\Big(108r^3 + 171ir^2\omega - 126r\omega^2 + 8i\omega^3\Big) + 8k^2 r^2\omega^2\Big(18r^2 + 27ir\omega - \omega^2\Big) - 16ir^3\omega^5\Big)\Big) + 9k^2 r^2\Big(3k^2 - 4\omega^2\Big)^2\Big(k^2 + 2ir\omega\Big)\Big\}\Big] \tag{5.12}$$

$$\mathcal{Q}_{so}^{(1)} = -\frac{1}{r\left(2ir\omega + k^2\right)\left(f(r)k^2 + 3k^2 - 4\omega^2\right)^3}\Big[\Big\{\omega(3r + 2i\omega)\Big(2r\omega - ik^2\Big)\Big(3k^2 - 4\omega^2\Big)^3 + f(r)\Big(f(r)\Big(f(r)\Big(-3k^8 + 18\Big(-19r^2 - 2i\omega r + \omega^2\Big)k^6 + 4r(3r - i\omega)\Big(108r^2 + 99i\omega r - 26\omega^2\Big)k^4 - 8r^2\omega^2\Big(360r^2 + 234i\omega r - 85\omega^2\Big)k^2 + 32r^3\omega^4(48r + 35i\omega) + f(r)\Big(3k^8 + r(180r + 23i\omega)k^6 - 2r^2\Big(576r^2 - 108i\omega r + 257\omega^2\Big)k^4 + 64r^3\omega^2(30r - i\omega)k^2 - r^2\Big(43k^4 + 6r(41i\omega - 40r)k^2 + 320r^2\omega^2\Big)f(r)k^2 - 512r^4\omega^4\Big)\Big) - \Big(3k^2 - 4\omega^2\Big)\Big(9k^6 + 6\Big(18r^2 + 3i\omega r - 7\omega^2\Big)k^4 + 8ir\omega\Big(45r^2 + 42i\omega r - 11\omega^2\Big)k^2 + 8r^2\omega^3(\omega - 60ir)\Big)\Big)k^2 + \Big(k^2 + 2ir\omega\Big)\Big(3k^2 - 4\omega^2\Big)^2\Big(3k^4 + \Big(9r^2 - 18i\omega r + 14\omega^2\Big)k^2 - 4ir\omega^3\Big)\Big)\Big\}\zeta''(r)r^3 + \Big\{\Big(k^2 + 2ir\omega\Big)\Big(3k^6 + 2\omega(-3ir - 2\omega)k^4 - 6r^2\Big(9r^2 + 6i\omega r - 2\omega^2\Big)k^2 + 72r^4\omega^2\Big)\Big(3k^2 - 4\omega^2\Big)^2 + f(r)\Big(2\Big(3k^2 - 4\omega^2\Big)\Big(3k^{10} + \Big(63r^2 + 18i\omega r - 4\omega^2\Big)k^8 - r\Big(189r^3 + 18i\omega r^2 + 66\omega^2 r + 28i\omega^3\Big)k^6 + 2r^2\omega\Big(-297ir^3 + 315\omega r^2 + 6i\omega^2 r + 28\omega^3\Big)k^4 + 8ir^3\omega^3\Big(63r^2 + 18i\omega r + 4\omega^2\Big)k^2 + 32r^4\omega^5(6ir + \omega)\Big) + f(r)\Big(3k^{12} + \Big(-90r^2 + 36i\omega r - 4\omega^2\Big)k^{10} + 12r\Big(171r^3 + 63i\omega r^2 + 24\omega^2 r - 4i\omega^3\Big)k^8 + 4r^2\Big(972r^4 + 1971i\omega r^3$$

$$-1863\omega^2r^2-186i\omega^3r-32\omega^4\big)k^6-32r^3\omega^2\left(270r^3+531i\omega r^2-243\omega^2r-i\omega^3\right)k^4$$
$$+64r^4\omega^4\left(72r^2+132i\omega r-13\omega^2\right)k^2+2r^2f(r)\left(3\left(-15k^8-2\left(186r^2+37i\omega r-9\omega^2\right)k^6\right.\right.$$
$$+2r\left(-396r^3-417i\omega r^2+339\omega^2r+50i\omega^3\right)k^4+8r^2\omega^2\left(180r^2+232i\omega r-73\omega^2\right)k^2$$
$$-64r^3(8r+13i\omega)\omega^4\big)+f(r)\left(-3k^8+r(21r-20i\omega)k^6+2r^2\left(684r^2-24i\omega r+43\omega^2\right)k^4\right.$$
$$-8r^3(300r+91i\omega)\omega^2k^2+r^2\left(47k^4+12r(17i\omega-30r)k^2+480r^2\omega^2\right)f(r)k^2$$
$$\left.\left.+768r^4\omega^4\big)\big)k^2+256ir^5\omega^7\big)\big)\right\}\zeta'(r)\Big] \tag{5.13}$$

After near horizon analysis of the master equations we find the first pole skipping point at $\omega_1=-\frac{3}{2}ir_0$ and

$$k_1^4+9r_0^4-\lambda\frac{\xi\left(-k_1^6+9(\xi+3)k_1^2r_0^4+27\xi r_0^6\right)\phi(r_0)^p}{r_0^2}$$
$$-\frac{\beta^2\xi\phi(r_0)^2\left(k_1^6(\xi+2p)+3k_1^4r_0^2(\xi-3p)-36pk_1^2r_0^4-27pr_0^6\right)}{p^2\left(k_1^2+3r_0^2\right)}=0, \tag{5.14}$$

Similarly one can find higher-order pole-skipping points. Since β and λ are two independent perturbative parameters, we can choose to observe the matter field's effect or the scalar-Gauss-Bonnet interaction's effect by switching the particular ranges of these parameters. For example, $\lambda\ll\beta^2\ll1$ helps us to neglect the interaction effect and to consider the effect of matter stress-tensor only. However here we have considered the opposite one.

Appendix B

B.3 Dirac equations for various couplings

As discussed in Section 3 of Chapter 2, with various forms of coupling, we can write the Dirac component equations. Imposing the spinor decomposition mentioned in the paper, we can get the component equations.

- **Dipole coupling :** When $\zeta(\phi) = -ip\phi\not{F}$ (here, $\not{F} = \frac{1}{2}\Gamma^{ab}e_a^M e_b^N F_{MN}$), then summing over the indices, we get, $\zeta(\phi) = -ip\phi(r)A_v'(r)\Gamma^{\underline{v}}$.

$$r^2 f(r)\partial_r\psi_+^+ + \Gamma^{\underline{v}}\left[-i\omega + \frac{r^2 f'(r)}{4} - iqA_v(r) + \frac{mr(1-f(r))}{2} + \frac{ik(1+f(r))}{2}\right.$$
$$\left.-\frac{ipr\phi(r)A_v'(r)(1+f(r))}{2}\right]\psi_-^- + \left[-i\omega + \frac{r^2 f'(r)}{4} + \frac{3rf(r)}{2} - iqA_v(r)\right.$$
$$\left.-\frac{mr(1+f(r))}{2} - \frac{ik(1-f(r))}{2} + \frac{ipr\phi(r)A_v'(r)(1-f(r))}{2}\right]\psi_+^+ = 0 \qquad (5.15a)$$
$$r^2 f(r)\partial_r\psi_-^- - \Gamma^{\underline{v}}\left[-i\omega + \frac{r^2 f'(r)}{4} - iqA_v(r) - \frac{mr(1-f(r))}{2} - \frac{ik(1+f(r))}{2}\right.$$
$$\left.+\frac{ipr\phi(r)A_v'(r)(1+f(r))}{2}\right]\psi_+^+ + \left[-i\omega + \frac{r^2 f'(r)}{4} + \frac{3rf(r)}{2} - iqA_v(r)\right.$$
$$\left.+\frac{mr(1+f(r))}{2} + \frac{ik(1-f(r))}{2} - \frac{ipr\phi(r)A_v'(r)(1-f(r))}{2}\right]\psi_-^- = 0 \qquad (5.15b)$$

  We can easily get the other two component equations for ψ_+^- and ψ_-^+ by replacing $k \to -k$ in (5.15a) and (5.15b).

- **Yukawa coupling :** When $\zeta(\phi) = g\phi(r)$, then, the Dirac component equations we get as,

$$r^2 f(r)\partial_r\psi_+^+ + \Gamma^{\underline{v}}\left[-i\omega + \frac{r^2 f'(r)}{4} - iqA_v(r) + \frac{mr(1-f(r))}{2} + \frac{ik(1+f(r))}{2}\right.$$

$$+\frac{gr\phi(r)(1-f(r))}{2}\Big]\psi_-^- + \Big[-i\omega + \frac{r^2 f'(r)}{4} + \frac{3rf(r)}{2} - iqA_v(r)$$
$$-\frac{mr(1+f(r))}{2} - \frac{ik(1-f(r))}{2} - \frac{gr\phi(r)(1+f(r))}{2}\Big]\psi_+^+ = 0 \tag{5.16a}$$

$$r^2 f(r)\partial_r\psi_-^- - \Gamma^v\Big[-i\omega + \frac{r^2 f'(r)}{4} - iqA_v(r) - \frac{mr(1-f(r))}{2} - \frac{ik(1+f(r))}{2}$$
$$-\frac{gr\phi(r)(1-f(r))}{2}\Big]\psi_+^+ + \Big[-i\omega + \frac{r^2 f'(r)}{4} + \frac{3rf(r)}{2} - iqA_v(r)$$
$$+\frac{mr(1+f(r))}{2} + \frac{ik(1-f(r))}{2} + \frac{gr\phi(r)(1+f(r))}{2}\Big]\psi_-^- = 0 \tag{5.16b}$$

We can easily get the other two component equations for ψ_+^- and ψ_-^+ by replacing $k \to -k$ in (5.16a) and (5.16b).

B.4 Detailed pole-skipping analysis for Dipole coupling (real) case

To calculate the pole-skipping points, we expand the spinors around the horizon as,

$$\psi_+^+ = \sum_{j=0}^{\infty}(\psi_+^+)^j(r-r_0)^j, \qquad \psi_- = \sum_{j=0}^{\infty}(\psi_-^-)^j(r-r_0)^j \tag{5.17}$$

We have to expand the gauge field A_v, $f(r)$ and ϕ also around the horizon as[1]

$$\begin{cases} f(r) & = f(r_0) + (r-r_0)f'(r_0) + \ldots \\ A_v(r) & = A_v(r_0) + (r-r_0)A_v'(r_0) + \ldots \\ \phi(r) & = \phi(r_0) + (r-r_0)\phi'(r_0) + \ldots \end{cases} \tag{5.18}$$

Expanding the Dirac equations (5.15a) and (5.15b) around the horizon as,

$$\mathcal{D}_+^+ = \sum_{j=0}^{\infty}(\mathcal{D}_+^+)^j(r-r_0)^j, \qquad \mathcal{D}_-^- = \sum_{j=0}^{\infty}(\mathcal{D}_-^-)^j(r-r_0)^j \tag{5.19}$$

To calculate the zeroth order pole-skipping points, we expand (5.15a) near horizon upto zeroth order and get,

$$(\mathcal{D}_+^+)^{(0)} = \left(-i\omega + \frac{{r_0}^2 f'(r_0)}{4} + \frac{mr_0}{2} + \frac{ik}{2} - \frac{ipr_0\phi(r_0)A_v'(r_0)}{2}\right)(\psi_-^-)^{(0)}$$

[1] the emblackening factor $f(r)$ and gauge field $A_v(r)$ vanishes at the horizon.

$$+\left(-i\omega+\frac{{r_0}^2 f'(r_0)}{4}-\frac{mr_0}{2}-\frac{ik}{2}+\frac{ipr_0\phi(r_0)A_v'(r_0)}{2}\right)(\psi_+^+)^{(0)}=0 \quad (5.20a)$$

In the same way, we expand (5.15b) upto zeroth order and get,

$$\begin{aligned}(\mathcal{D}_-^-)^{(0)} =&-\left(-i\omega+\frac{{r_0}^2 f'(r_0)}{4}-\frac{mr_0}{2}-\frac{ik}{2}+\frac{ipr_0\phi(r_0)A_v'(r_0)}{2}\right)(\psi_+)^{(0)}\\ &+\left(-i\omega+\frac{{r_0}^2 f'(r_0)}{4}+\frac{mr_0}{2}+\frac{ik}{2}-\frac{ipr_0\phi(r_0)A_v'(r_0)}{2}\right)(\psi_-)^{(0)}=0 \quad (5.20b)\end{aligned}$$

To calculate the pole-skipping points, we make the coefficients of $(\psi_+^+)^{(0)}$ and $(\psi_-^-)^{(0)}$ zero and extract the frequency and associated momentum as,

$$\omega_0=-\pi i T, \qquad k=imr_0+p\mu\phi(r_0) \quad (5.21)$$

So, this (ω_0, k) is the zeroth order pole-skipping point. We will get another pole-skipping point from the other two component equations simply by replacing $k\to -k$.

$$\omega_0=-\pi i T, \qquad k=-imr_0-p\mu\phi(r_0) \quad (5.22)$$

The additional term we got is dependent on coupling parameter p, a chemical potential μ and the value of the scalar field at the horizon $\phi(r_0)$. We have discussed the effect of this additional term in section 3 of the paper.

To get the higher-order pole-skipping points, we have to expand the 1st-order Dirac equations up to higher orders. For that, we will follow a matrix formalism to extract the pole-skipping points. Now, expanding the Dirac equation in the first order, we will get two equations containing the coefficients of $(\psi_+^+)^1, (\psi_-^-)^1, (\psi_+^+)^0$ and $(\psi_-^-)^0$. Then, we will form a 2×2 matrix of the coefficients. We can write the equations in a matrix form as,

$$\begin{pmatrix}(\mathcal{D}_+^+)^1\\(\mathcal{D}_-^-)^1\end{pmatrix}=\tilde{\mathcal{A}}^{11}\begin{pmatrix}(\psi_+^+)^1\\(\psi_-^-)^1\end{pmatrix}+\tilde{\mathcal{A}}^{10}\begin{pmatrix}(\psi_+^+)^0\\(\psi_-^-)^0\end{pmatrix}=0 \quad (5.23)$$

Where,

$$\tilde{\mathcal{A}}^{11}=\begin{pmatrix}5\pi T-i\omega-\frac{mr_0}{2}-\frac{ik}{2}+\frac{ipr_0\phi(r_0)A_v'(r_0)}{2} & \left(-i\omega+\pi T+\frac{mr_0}{2}+\frac{ik}{2}-\frac{ipr_0\phi(r_0)A_v'(r_0)}{2}\right)\\ -\left(-i\omega+\pi T-\frac{mr_0}{2}-\frac{ik}{2}+\frac{ipr_0\phi(r_0)A_v'(r_0)}{2}\right) & 5\pi T-i\omega+\frac{mr_0}{2}+\frac{ik}{2}-\frac{ipr_0\phi(r_0)A_v'(r_0)}{2}\end{pmatrix} \quad (5.24)$$

and, $\tilde{\mathcal{A}}^{10}$ is dependent on k only. We can clearly see that $\det\tilde{\mathcal{A}}^{11} = 8\pi T(3\pi T - i\omega)$ which disappears at $\omega = -3\pi iT$. To calculate associated momentum, we have to rewrite $(\mathcal{D}_+^+)^0, (\mathcal{D}_+^+)^1$ and $(\mathcal{D}_-^-)^1$ at $\omega = -3\pi iT$ and we can construct a 3×3 matrix out of the co-efficients of $(\psi_+^+)^0, (\psi_-^-)^1$ and ψ_c^1 where $\psi_c^1 = (\psi_+^+)^1 - \Gamma^{\underline{v}}(\psi_-^-)^1$. We can express the matrix form as,

$$\begin{pmatrix}(\mathcal{D}_+^+)^0\\(\mathcal{D}_+^+)^1\\(\mathcal{D}_-^-)^1\end{pmatrix} = \tilde{\mathcal{A}}_1(\omega_1,k)\begin{pmatrix}(\psi_+^+)^0\\(\psi_-^-)^0\\\psi_c^1\end{pmatrix} = \begin{pmatrix}\tilde{\mathcal{A}}^{00}_{++} & \tilde{\mathcal{A}}^{00}_{+-} & 0\\ \tilde{\mathcal{A}}^{10}_{++} & \tilde{\mathcal{A}}^{10}_{+-} & \tilde{\mathcal{A}}^{11}_{+}\\ \tilde{\mathcal{A}}^{10}_{-+} & \tilde{\mathcal{A}}^{10}_{--} & \tilde{\mathcal{A}}^{11}_{-}\end{pmatrix}\begin{pmatrix}\psi_+^0\\\psi_-^0\\\psi_c^1\end{pmatrix} = 0 \tag{5.25}$$

We can evaluate the associated momentum at which $\det\tilde{\mathcal{A}}_1(\omega_1,k)$ vanishes. To see the associated momentum with $\omega = -3\pi iT$, we evaluate the above matrix (5.25) at $\omega = -3\pi iT$ In this way, we have extracted the pole-skipping points up to many orders. We can clearly see that these ω's are fermionic matsubara frequencies at various orders; $\omega = \omega_n = -2\pi iT(n+\frac{1}{2})$.

$$\omega_1 = -3\pi iT \tag{5.26}$$

$$k_{1a} = \frac{ir_0}{3T}\left(2^{-1/3}A + T\left(m - \frac{3ip\mu\phi(r_0)}{r_0}\right) + \frac{4^{2/3}T^2B}{r_0A}\right) \tag{5.27}$$

$$k_{1b} = -\frac{ir_0}{3T}\left(4^{-2/3}(1-\sqrt{3i})A - T\left(m - \frac{3ip\mu\phi(r_0)}{r_0}\right) + \frac{2^{1/3}(1+\sqrt{3i})T^2B}{r_0A}\right) \tag{5.28}$$

$$k_{1c} = -\frac{ir_0}{3T}\left(4^{-2/3}(1+\sqrt{3i})A - T\left(m - \frac{3ip\mu\phi(r_0)}{r_0}\right) + \frac{2^{1/3}(1-\sqrt{3i})T^2B}{r_0A}\right) \tag{5.29}$$

$$B = (-9+2m^2)r_0 + 18\pi T + 3iq\mu \tag{5.30}$$

$$A = r_0^{-2/3}\Bigg[-12mr_0BT^3 - 2m^2r_0 - 9\pi T - \frac{27}{4}ip\mu\phi(r_0)r_0T^3(m_\phi^2+\phi(r_0)^2-4\pi T) + 4ir_0^{1/2}T^3\left(2B^3 - Bm + 2m^3r_0 + 9m\pi T - \frac{27}{4}ip\mu\phi(r_0)T^3(m_\phi^2+\phi(r_0)^2-4\pi T)\right)^{1/2}\Bigg]^{1/3} \tag{5.31}$$

So, these are the 1st order pole-skipping points. we get 3 associated momentum values in 1st order. We can see from the momentum values that they are directly proportional to $\phi(r_0)$ which means $(T_c - T)^{1/2}$. So, up to higher orders, they obey the power law. From the Figure2.10 also, it is evident.

B.5 Higher order momentum values for Yukawa coupling (real)

With the same method described above, we can calculate the 1st-order P-S points for Yukawa coupling. We observe that, $\omega_1 = -3\pi i T$ while k_1 takes 3 values as

$$\omega_1 = -3\pi i T \tag{5.32a}$$

$$k_{1a} = \frac{ir_0}{3T}\left(\frac{Z}{r_0} + (m + g\phi(r_0))T + \frac{2Y}{Z}T^2\right) \tag{5.32b}$$

$$k_{1b} = \frac{ir_0}{3T}\left(-\frac{(1-\sqrt{3}i)Z}{2r_0} + (m + g\phi(r_0))T - \frac{(1+\sqrt{3}i)Y}{Z}T^2\right) \tag{5.32c}$$

$$k_{1c} = \frac{ir_0}{3T}\left(-\frac{(1+\sqrt{3}i)Z}{2r_0} + (m + g\phi(r_0))T - \frac{(1-\sqrt{3}i)Y}{Z}T^2\right) \tag{5.32d}$$

$$Y = (-9 + 2m^2)r_0 + 18\pi T + 3iq\mu + 4gmr_0\phi(r_0) + 2g^2 r_0\phi^2(r_0) \tag{5.32e}$$

$$\begin{aligned} Z = \big(&2mr_0^2T^3(Y + 3(12r_0 - 2m^2r_0 - 15\pi T - 4iq\mu) - 16gmr_0\phi(r_0) - 14g^2r_0\phi^2(r_0) \\ &+27\frac{g}{m}\phi(r_0)(r_0 - \pi T) - 9i\frac{g}{m}q\mu\phi(r_0) - 4\frac{g^3}{m}r_0\phi^3(r_0) + \frac{27g}{4m}r_0\phi(r_0)(m_\phi^2 + \phi^2(r_0))) \\ &+\frac{1}{2}r_0^{3/2}T^3(-32Y^3 + r_0\big(4m(r_0(-27 + 4m^2) + 27\pi T + 9iq\mu) + 3g(4(-9r_0 + 4m^2r_0 \\ &+9\pi T + 3iq\mu) - 9r_0m_\phi^2)\phi(r_0) + 48g^2mr_0\phi^2(r_0) + g(-27 + 16g^2)r_0\phi^3(r_0)\big)^2)\big)^{1/3} \end{aligned} \tag{5.32f}$$

The momentum values are proportional to $\phi(r_0)$ here also. So, they will obey the power law as $(T_c - T)^{1/2}$. So, we have checked that up to the first order, P-S points obey $(T_c - T)^{1/2}$ law near critical temperature for a theory with massless fermions propagating in a charged black hole background, with real dipole and Yukawa coupling. We have explicitly discussed this in subsection 3.1.1.

B.6 Dirac component equations for charged Dipole coupling

With charged Dipole coupling, decomposing the Dirac equation into components, we can write,

$$r^2 f(r)\partial_r\psi_+^+ + \Gamma^{\underline{v}}\left[-i\omega + \frac{r^2 f'(r)}{4} - iqA_v(r) + \frac{mr(1-f(r))}{2} + \frac{ik(1+f(r))}{2} - \frac{ipr|\tilde{\phi}|^2 A_v'(r)(1+f(r))}{2}\right]\psi_-^- + \left[-i\omega + \frac{r^2 f'(r)}{4} + \frac{3rf(r)}{2} - iqA_v(r) - \frac{mr(1+f(r))}{2} - \frac{ik(1-f(r))}{2} + \frac{ipr|\tilde{\phi}|^2 A_v'(r)(1-f(r))}{2}\right]\psi_+^+ = 0 \tag{5.33a}$$

$$r^2 f(r)\partial_r\psi_-^- - \Gamma^{\underline{v}}\left[-i\omega + \frac{r^2 f'(r)}{4} - iqA_v(r) - \frac{mr(1-f(r))}{2} - \frac{ik(1+f(r))}{2} + \frac{ipr|\tilde{\phi}|^2 A_v'(r)(1+f(r))}{2}\right]\psi_+^+ + \left[-i\omega + \frac{r^2 f'(r)}{4} + \frac{3rf(r)}{2} - iqA_v(r) + \frac{mr(1+f(r))}{2} + \frac{ik(1-f(r))}{2} - \frac{ipr|\tilde{\phi}|^2 A_v'(r)(1-f(r))}{2}\right]\psi_-^- = 0 \tag{5.33b}$$

The other two component equations can be obtained by replacing $k \to -k$ in the above two equations. Expanding these equations near the black hole horizon and applying the method discussed in (B.4), we can calculate P-S points up to any order. We have checked that the behaviour of momentum values for this case is proportional to $(T_c - T)$ which is different from the real coupling case. We have calculated the P-S points in section 3.2. The ω values are not different from the fermionic Matsubara frequencies, but the momentum values change with the coupling. We have shown the numerical behaviour of these higher-order points in Figure 5.

B.7 Dirac component equations for charged Yukawa coupling

With charged Yukawa coupling, decomposing the Dirac equation into components, we can write,

$$r^2 f(r)\partial_r \psi_+^+ + \Gamma^{\underline{v}} \left[-i\omega + \frac{r^2 f'(r)}{4} - iqA_v(r) + \frac{mr(1-f(r))}{2} + \frac{ik(1+f(r))}{2} + \frac{gr|\tilde{\phi}|^2(1-f(r))}{2} \right] \psi_-^- + \left[-i\omega + \frac{r^2 f'(r)}{4} + \frac{3rf(r)}{2} - iqA_v(r) - \frac{mr(1+f(r))}{2} - \frac{ik(1-f(r))}{2} - \frac{gr|\tilde{\phi}|^2(1+f(r))}{2} \right] \psi_+^+ = 0 \tag{5.34a}$$

$$r^2 f(r)\partial_r \psi_-^- - \Gamma^{\underline{v}} \left[-i\omega + \frac{r^2 f'(r)}{4} - iqA_v(r) - \frac{mr(1-f(r))}{2} - \frac{ik(1+f(r))}{2} - \frac{gr|\tilde{\phi}|^2(1-f(r))}{2} \right] \psi_+^+ + \left[-i\omega + \frac{r^2 f'(r)}{4} + \frac{3rf(r)}{2} - iqA_v(r) + \frac{mr(1+f(r))}{2} + \frac{ik(1-f(r))}{2} + \frac{gr|\tilde{\phi}|^2(1+f(r))}{2} \right] \psi_-^- = 0 \tag{5.34b}$$

The other two component equations can be obtained by replacing $k \to -k$ in the above two equations. With the matrix method, we can calculate the P-S points. Here also, ω values are just the fermionic Matsubara frequencies, only the momentum value changes. The behaviour of momentum values for this case is also proportional to $(T_c - T)$.

Appendix C

In the Chapter 3, we studied the phenomenon of pole-skipping in D3-D7 brane systems in presence of external electric field. We constructed master equations for each channel of gravitational perturbations. In this appendix, we have written the co-efficients of the master equations obtained from various channels.

C.8 Sound mode

The coefficients of master equation (3.50) can be expressed as,

$$\mathcal{P}_{so}(r,\omega,k) = P_0(r,\omega,k) + n_f P_1(r,\omega,k), \tag{5.35a}$$

$$\mathcal{Q}_{so}(r,\omega,k) = Q_0(r,\omega,k) + n_f Q_1(r,\omega,k). \tag{5.35b}$$

Now,

$$P_0 = \frac{-f(r)\left(3r\omega^2+2k^2\left(r+iR_4^2\omega\right)\right)+9k^2rf(r)^2+2\left(2k^2-3\omega^2\right)\left(2r-iR_4^2\omega\right)}{r^2f(r)\left(k^2f(r)+2k^2-3\omega^2\right)}, \tag{5.35c}$$

$$Q_0 = \left[-k^2f(r)\left(k^2R_4^4+32r^2+11irR_4^2\omega\right)+16k^2r^2f(r)^2-2k^4R_4^4+k^2\left(16r^2\right.\right.$$
$$\left.\left.+2irR_4^2\omega+3R_4^4\omega^2\right)+9irR_4^2\omega^3\right] / \left\{r^4f(r)\left(k^2f(r)+2k^2-3\omega^2\right)\right\}, \tag{5.35d}$$

$$\begin{aligned} P_1 = {} & 2ik^2\sin^3\theta(r)\left[k^4\left(18E_0^2r^5f(r)^4-3r^4f(r)^3\left(10E_0^2r+3iE_0^2R_4^2\omega+24rR_4^4\right)+2f(r)^2\left(6R_4^4\right.\right.\right. \\ & \left(3E_0^2r+10r^5\right)+15E_0^2r^5-7iE_0^2r^4R_4^2\omega+2iE_0^2R_4^6\omega\Big)+f(r)\left(-12R_4^4\left(5E_0^2r+4r^5\right)\right. \\ & \left.-30E_0^2r^5+4iE_0^2r^4R_4^2\omega+4iE_0^2R_4^6\omega\right)+4E_0^2\left(3r^5-2ir^4R_4^2\omega+6rR_4^4-2iR_4^6\omega\right)\Big) \\ & -3k^2\omega^2\left(5E_0^2r^5f(r)^4+r^4f(r)^3\left(-17E_0^2r+2iE_0^2R_4^2\omega-20rR_4^4\right)+f(r)\left(-2R_4^4\left(17E_0^2r\right.\right.\right. \\ & \left.\left.\left.+24r^5\right)-17E_0^2r^5+10iE_0^2r^4R_4^2\omega+4iE_0^2R_4^6\omega\right)+f(r)^2\left(2R_4^4\left(5E_0^2r+34r^5\right)+17E_0^2r^5\right. \end{aligned}$$

$$-2iE_0^2r^4R_4^2\omega\big)+4E_0^2\left(3r^5-ir^4R_4^2\omega+6rR_4^4-iR_4^6\omega\right)\big)-9r\omega^4\left(3E_0^2r^4f(r)^3-r^3f(r)^2\right.$$
$$\left(3E_0^2r+2iE_0^2R_4^2\omega+12rR_4^4\right)+3f(r)\left(2R_4^4\left(E_0^2+2r^4\right)+E_0^2r^4-iE_0^2r^3R_4^2\omega\right)$$
$$\left.-3E_0^2\left(r^4+2R_4^4\right)\right)\Big]\Big/\left\{r^3R_4^6\left(k^2(f(r)+2)-3\omega^2\right)^3\left(3r\omega\left(4rf(r)-2r-iR_4^2\omega\right)\right.\right.$$
$$\left.\left.-k^2R_4^2\left(3irf(r)-2ir+R_4^2\omega\right)\right)\right\}, \tag{5.35e}$$

$$Q_1=i\sin^3\theta(r)\Big[4k^2r\left(132r+7iR_4^2\omega\right)+3k^4R_4^4-504r^2\omega^2\big)+E_0^2R_4^2\left(2k^2-3\omega^2\right)^2$$
$$\left(2r+iR_4^2\omega\right)\left(2k^4\left(5r^4R_4^2+2R_4^6\right)+3k^2\omega\left(10ir^5+3r^4R_4^2\omega+4irR_4^4+6R_4^6\omega\right)\right.$$
$$+27ir\omega^3\left(r^4+2R_4^4\right)\big)-3k^2r^4f(r)^5\left(2k^4r\left(8R_4^4\left(132r^2-E_0^2\omega^2\right)+312E_0^2r^2+147i\mathrm{E}0^2rR_4^2\omega\right.\right.$$
$$\left.\left.+56irR_4^6\omega\right)+12k^2r^2\omega^2\left(2E_0^2r+19iE_0^2R_4^2\omega-168rR_4^4\right)+k^6\left(16E_0^2rR_4^4+iE_0^2R_4^6\omega+12rR_4^8\right)\right.$$
$$\left.-576E_0^2r^3\omega^4\right)+f(r)^3\left(k^8R_4^4\left(R_4^4\left(96r^5-176E_0^2r\right)+208E_0^2r^5-2iR_4^6\omega\left(11E_0^2-36r^4\right)\right.\right.$$
$$\left.\left.+161iE_0^2r^4R_4^2\omega\right)-54k^2r^3\omega^4\left(32E_0^2r^4+53iE_0^2r^3R_4^2\omega-4R_4^4\left(5E_0^2r^2\omega^2+16E_0^2-32r^4\right)\right.\right.$$
$$\left.\left.+152ir^3R_4^6\omega\right)+9k^4r^2\omega^2\left(152E_0^2r^5+380iE_0^2r^4R_4^2\omega-iR_4^6\omega\left(25E_0^2r^2\omega^2+184E_0^2\right.\right.\right.$$
$$\left.\left.\left.-1176r^4\right)-16rR_4^4\left(3E_0^2r^2\omega^2+E_0^2+4r^4\right)+56r^3R_4^8\omega^2\right)-6k^6r\left(312E_0^2r^6+123iE_0^2r^5R_4^2\omega\right.$$
$$\left.-16R_4^8\omega^2\left(3E_0^2-7r^4\right)+2irR_4^6\omega\left(7E_0^2r^2\omega^2-E_0^2+348r^4\right)+48R_4^4\left(2E_0^2r^4\omega^2+13E_0^2r^2\right.\right.$$
$$\left.\left.+4r^6\right)+18ir^3R_4^{10}\omega^3\right)+324r^6\omega^6\left(6E_0^2r-7iE_0^2R_4^2\omega+24rR_4^4\right)\big)+f(r)\left(2k^2-3\omega^2\right)$$
$$\left(E_0^2\left(k^6\left(224r^5R_4^4+30ir^4R_4^6\omega+224rR_4^8-36iR_4^{10}\omega\right)+3ik^4R_4^2\omega\left(28r^6+144ir^5R_4^2\omega\right.\right.\right.$$
$$\left.\left.+r^2R_4^4\left(r^2\omega^2-136\right)+80irR_4^6\omega+34R_4^8\omega^2\right)+18k^2r\omega^2\left(40r^6+13ir^5R_4^2\omega\right.\right.$$
$$\left.\left.+4r^2R_4^4\left(r^2\omega^2+20\right)+42irR_4^6\omega-8R_4^8\omega^2\right)-324r^2\omega^4\left(r^4+2R_4^4\right)\left(2r-iR_4^2\omega\right)\right)$$
$$+12r^4R_4^6\left(2k^2-3\omega^2\right)^2\left(2r+iR_4^2\omega\right)\left(k^2R_4^2+3ir\omega\right)\big)+f(r)^4\left(E_0^2r\left(108k^2r^5\omega^4\right.\right.$$
$$\left.\left.\left(16r+35iR_4^2\omega\right)+k^8\left(-7r^4R_4^4+30ir^3R_4^6\omega+2R_4^8\right)+3k^6r\left(624r^5-152ir^4R_4^2\omega\right.\right.\right.$$
$$\left.\left.\left.+iR_4^6\omega\left(17r^2\omega^2+152\right)+32rR_4^4\left(r^2\omega^2+33\right)\right)-18k^4r^2\omega^2\left(76r^4+7ir^3R_4^2\omega\right.\right.\right.$$
$$\left.\left.\left.+3R_4^4\left(9r^2\omega^2+56\right)\right)-1944r^6\omega^6\right)+12k^2r^4R_4^4\left(2k^4r\left(312r^2+15irR_4^2\omega-4R_4^4\omega^2\right)\right.$$
$$\left.+12k^2r^2\omega^2\left(2r+7iR_4^2\omega\right)+k^6\left(16rR_4^4+iR_4^6\omega\right)-576r^3\omega^4\right)\big)+3f(r)^2\left(E_0^2\left(k^8\left(40r^5R_4^4\right.\right.\right.$$
$$\left.\left.+66ir^4R_4^6\omega-48rR_4^8-28iR_4^{10}\omega\right)+9k^2r^2\omega_1^4\left(64r^5-136ir^4R_4^2\omega_1+iR_4^6\omega_1\left(11r^2\omega^2+184\right)\right.\right.$$
$$\left.\left.+32rR_4^4\left(3r^2\omega^2+4\right)\right)+k^6\left(96r^7+204ir^6R_4^2\omega-ir^2R_4^6\omega\left(131r^2\omega^2-408\right)\right.\right.$$

$$+8r^3R_4^4\left(13r^2\omega^2+24\right)+288rR_4^8\omega^2+50iR_4^{10}\omega^3\big)+6k^4r\omega^2\left(8r^6+33ir^5R_4^2\omega\right.$$
$$-irR_4^6\omega\left(r^2\omega^2+230\right)+R_4^4\left(16r^2-119r^4\omega^2\right)-54R_4^8\omega^2\big)-27r^3\omega^6\left(24r^4-46ir^3R_4^2\omega\right.$$
$$\left.+R_4^4\left(11r^2\omega^2+48\right)\right)\big)-4r^4R_4^4\left(2k^2-3\omega^2\right)\left(ik^4R_4^2\omega\left(-68r^2+32irR_4^2\omega+9R_4^4\omega^2\right)\right.$$
$$+30k^2r^2\omega^2\left(8r+iR_4^2\omega\right)+k^6\left(32rR_4^4-6iR_4^6\omega\right)+108r^2\omega^4\left(-2r+iR_4^2\omega\right)\big)\big)\big]\,/$$
$$\left\{12r^6R_4^6f(r)^2\left(k^2(f(r)+2)-3\omega^2\right)^3\left(3r\omega\left(4rf(r)-2r-iR_4^2\omega\right)-k^2R_4^2\left(3irf(r)\right.\right.\right.$$
$$\left.\left.\left.-2ir+R_4^2\omega\right)\right)\right\}. \tag{5.35f}$$

C.9 Shear mode

The coefficients of master equation (3.58) can be expressed as,

$$\mathcal{P}_{sh}(r,\omega,k) = P_0(r,\omega,k)+n_fP_1(r,\omega,k), \tag{5.36a}$$
$$\mathcal{Q}_{sh}(r,\omega,k) = Q_0(r,\omega,k)+n_fQ_1(r,\omega,k), \tag{5.36b}$$

where these Ps and Qs are given below.

$$P_0 = \frac{-\omega f(r)\left(5r\omega+2ik^2R_4^2\right)+9k^2rf(r)^2-4r\omega^2+2iR_4^2\omega^3}{r^2f(r)\left(k^2f(r)-\omega^2\right)}, \tag{5.36c}$$
$$Q_0 = \left[12k^2r^2f(r)^2-f(r)\left(k^4R_4^4+11ik^2rR_4^2\omega+4r^2\omega^2\right)+\omega\left(irR_4^2\left(4k^2+7\omega^2\right)\right.\right.$$
$$\left.\left.+k^2R_4^4\omega-8r^2\omega\right)\right]/\left\{r^4f(r)\left(k^2f(r)-\omega^2\right)\right\}, \tag{5.36d}$$

$$P_1=-\left[ik^2\omega^2(f(r)-1)\sin^3(\Theta(r))\left(2R_4^4\left(E_0^2-2r^4f(r)\right)+E_0^2r^4\left(f(r)^2+1\right)\right)^2\right]/\left\{r^3R_4^6\right.$$
$$\left(\omega^2-k^2f(r)\right)^2\left(-r\omega\left(2R_4^4\left(5f(r)\left(E_0^2-2r^4f(r)\right)-4E_0^2\right)+E_0^2r^4(f(r)(f(r)\right.\right.$$
$$\left.\left.(f(r)+4)+9)-4)\right)+ik^2R_4^2f(r)\left(2R_4^4\left(E_0^2-2r^4f(r)\right)+E_0^2r^4\left(f(r)^2+1\right)\right)\right)\Big\}\,, \tag{5.36e}$$

$$Q_1=\left[i\sin^3(\theta(r))\left(2R_4^4\left(E_0^2-2r^4f(r)\right)+E_0^2r^4\left(f(r)^2+1\right)\right)\left(ik^4rR_4^2\omega f(r)^2\left(2R_4^4\left(f(r)\left(9E_0^2\right.\right.\right.\right.$$
$$\left.\left.\left.\left.-18r^4f(r)+8r^4\right)-8E_0^2\right)+E_0^2r^4\left(5f(r)^3+13f(r)-8\right)\right)+k^2R_4^4\omega^4f(r)\left(2R_4^4\left(E_0^2\right.\right.\right.$$

$$-2r^4f(r)\big) + E_0^2r^4\left(f(r)^2+1\right)\big) - 2ik^2rR_4^2\omega^3f(r)\left(2R_4^4\left(f(r)\left(9E_0^2 - 18r^4f(r) + 8r^4\right)\right.\right.$$
$$\left.-8E_0^2\right) + E_0^2r^4\left(5f(r)^3 + 13f(r) - 8\right)\big) + k^6R_4^4f(r)^3\left(2R_4^4\left(E_0^2 - 2r^4f(r)\right) + E_0^2r^4\left(f(r)^2\right.\right.$$
$$\left.+1)\right) + 2k^2\omega^2f(r)^2\left(2R_4^4\left(E_0^2 - 2r^4f(r)\right) + E_0^2r^4\left(f(r)^2+1\right)\right)\left(4r^2(f(r)-1) - k^2R_4^4\right)$$
$$+irR_4^2\omega^5\left(2R_4^4\left(5f(r)\left(E_0^2 - 2r^4f(r)\right) - 4E_0^2\right) + E_0^2r^4(f(r)(f(r)(f(r)+4)+9) - 4)\right)\big]$$
$$/\left\{4r^6R_4^6f(r)^2\left(\omega^2 - k^2f(r)\right)^2\left(r\omega\left(2R_4^4\left(5f(r)\left(E_0^2 - 2r^4f(r)\right) - 4E_0^2\right) + E_0^2r^4(f(r)(f(r)\right.\right.\right.$$
$$\left.\left.(f(r)+4)+9) - 4)) - ik^2R_4^2f(r)\left(2R_4^4\left(E_0^2 - 2r^4f(r)\right) + E_0^2r^4\left(f(r)^2+1\right)\right)\right)\right\}. \tag{5.36f}$$

C.10 Tensor mode

The coefficients of master equation (3.58) can be expressed as,

$$\mathcal{P}_{ten} = \frac{rf(r) + 4r - 2iR_4^2\omega}{r^2f(r)}, \tag{5.37a}$$

$$\mathcal{Q}_{ten} = -\frac{k^2R_4^4 + 3irR_4^2\omega}{r^4f(r)} + n_f\left[\frac{\sin^3\theta(r)}{r^2f(r)}\right.$$
$$\left.-\frac{r^5f(r)^2 + \left(r - r_h\sin^3\theta_0\right)\left(r^4 + r^3r_h\sin^3\theta_0 + 2R_4^4\right)}{4r^7R_4^4f(r)^2}E_0^2\sin^3\theta(r)\right]. \tag{5.37b}$$

Bibliography

[1] R.P. Kerr, *Gravitational field of a spinning mass as an example of algebraically special metrics*, *Phys. Rev. Lett.* **11** (1963) 237.

[2] W. de Sitter, *On the relativity of inertia: Remarks concerning einstein's latest hypothesis*, *Proceedings of the Royal Netherlands Academy of Arts and Sciences* **19** (1917) 1217.

[3] J. Droste and W. de Sitter, *On the curvature of space*, *Proceedings of the Royal Netherlands Academy of Arts and Sciences* **19** (1917) 447.

[4] B.S. DeWitt, *Quantum theory of gravity. i. the canonical theory*, *Physical Review* **160** (1967) 1113.

[5] A. Strominger, *AdS(2) quantum gravity and string theory*, *JHEP* **01** (1999) 007 [hep-th/9809027].

[6] S.W. Hawking, *The quantum state of the universe*, *Physics Letters B* **73** (1980) 305.

[7] C. Kiefer, *Quantum gravity: General introduction and recent developments*, *Annalen Phys.* **15** (2005) 129 [gr-qc/0508120].

[8] J.M. Maldacena, *The Large N limit of superconformal field theories and supergravity*, *Adv. Theor. Math. Phys.* **2** (1998) 231 [hep-th/9711200].

[9] S.S. Gubser, I.R. Klebanov and A.M. Polyakov, *Gauge theory correlators from noncritical string theory*, *Phys. Lett. B* **428** (1998) 105 [hep-th/9802109].

[10] E. Witten, *Anti-de Sitter space and holography*, *Adv. Theor. Math. Phys.* **2** (1998) 253 [hep-th/9802150].

[11] H. Liu, J. McGreevy and D. Vegh, *Non-Fermi liquids from holography*, *Phys. Rev. D* **83** (2011) 065029 [0903.2477].

[12] S.A. Hartnoll, C.P. Herzog and G.T. Horowitz, *Holographic Superconductors*, *JHEP* **12** (2008) 015 [0810.1563].

[13] T. Faulkner, H. Liu, J. McGreevy and D. Vegh, *Emergent quantum criticality, Fermi surfaces, and AdS(2)*, *Phys. Rev. D* **83** (2011) 125002 [0907.2694].

[14] F. Benini, C.P. Herzog and A. Yarom, *Holographic Fermi arcs and a d-wave gap*, *Phys. Lett. B* **701** (2011) 626 [1006.0731].

[15] M.B. Green, J.H. Schwarz and E. Witten, *Superstring Theory*, Cambridge University Press, Cambridge (1987).

[16] J. Polchinski, *Dirichlet branes and ramond-ramond charges*, *Physical Review Letters* **75** (1995) 4724 [arXiv:hep-th/9510017].

[17] M.B. Green and J.H. Schwarz, *Anomaly cancellation in supersymmetric d=10 gauge theory and superstring theory*, *Physics Letters B* **149** (1984) 117.

[18] G.T. Horowitz and A. Strominger, *Black strings and P-branes*, *Nucl. Phys. B* **360** (1991) 197.

[19] J. Polchinski, *String Theory, Volume 2: Superstring Theory and Beyond*, Cambridge University Press, Cambridge (1998).

[20] M.J. Duff, R.R. Khuri and J.X. Lu, *String solitons*, *Physics Reports* **259** (1995) 213.

[21] G. t Hooft, *A planar diagram theory for strong interactions*, *Nuclear Physics B* **72** (1974) 461.

[22] S.S. Gubser, I.R. Klebanov and A.M. Polyakov, *Gauge theory correlators from non-critical string theory*, *Physics Letters B* **428** (1998) 105 [arXiv:hep-th/9802109].

[23] O. Aharony, S.S. Gubser, J.M. Maldacena, H. Ooguri and Y. Oz, *Large N field theories, string theory and gravity*, *Phys. Rept.* **323** (2000) 183 [hep-th/9905111].

[24] V.E. Hubeny, *The AdS/CFT Correspondence*, *Class. Quant. Grav.* **32** (2015) 124010 [1501.00007].

[25] A. Christodoulou, *AdS/CFT: dictionary and applications*, Ph.D. thesis, U. Southampton (main), 11, 2017.

[26] M. Baggioli, *Applied Holography: A Practical Mini-Course*, other thesis, Madrid, IFT, 2019, 10.1007/978-3-030-35184-7, [1908.02667].

[27] P. Di Francesco, P. Mathieu and D. Senechal, *Conformal Field Theory*, Graduate Texts in Contemporary Physics, Springer-Verlag, New York (1997), 10.1007/978-1-4612-2256-9.

[28] P.H. Ginsparg, *APPLIED CONFORMAL FIELD THEORY*, in *Les Houches Summer School in Theoretical Physics: Fields, Strings, Critical Phenomena*, 9, 1988 [hep-th/9108028].

[29] J.D. Qualls, *Lectures on Conformal Field Theory*, 1511.04074.

[30] D.T. Son and A.O. Starinets, *Minkowski space correlators in AdS / CFT correspondence: Recipe and applications*, *JHEP* **09** (2002) 042 [hep-th/0205051].

[31] P. Minces and V.O. Rivelles, *Scalar field theory in the AdS / CFT correspondence revisited*, *Nucl. Phys. B* **572** (2000) 651 [hep-th/9907079].

[32] G.T. Horowitz and V.E. Hubeny, *Quasinormal modes of AdS black holes and the approach to thermal equilibrium*, *Phys. Rev. D* **62** (2000) 024027 [hep-th/9909056].

[33] R.C. Hilborn, *Chaos and Nonlinear Dynamics: An Introduction for Scientists and Engineers*, Oxford University Press (2000-09), DOI: 10.1093/acprof:oso/9780198507239.001.0001.

[34] E.N. Lorenz, *Deterministic nonperiodic flow*, *Journal of Atmospheric Sciences* **20** (1963) 130 .

[35] J.P. Eckmann and D. Ruelle, *Ergodic theory of chaos and strange attractors*, *Rev. Mod. Phys.* **57** (1985) 617.

[36] B.-W. Shen, R.A. Pielke and X. Zeng, *One saddle point and two types of sensitivities within the lorenz 1963 and 1969 models*, *Atmosphere* **13** (2022) .

[37] A.I. Larkin and Y.N. Ovchinnikov, *Quasiclassical method in the theory of superconductivity*, *Journal of Experimental and Theoretical Physics* (1969) .

[38] S.H. Shenker and D. Stanford, *Black holes and the butterfly effect*, *JHEP* **03** (2014) 067 [1306.0622].

[39] S.H. Shenker and D. Stanford, *Stringy effects in scrambling*, *JHEP* **05** (2015) 132 [1412.6087].

[40] J. Maldacena, S.H. Shenker and D. Stanford, *A bound on chaos*, *JHEP* **08** (2016) 106 [1503.01409].

[41] Y. Sekino and L. Susskind, *Fast Scramblers*, *JHEP* **10** (2008) 065 [0808.2096].

[42] P. Hayden and J. Preskill, *Black holes as mirrors: Quantum information in random subsystems*, *JHEP* **09** (2007) 120 [0708.4025].

[43] S. Xu and B. Swingle, *Accessing scrambling using matrix product operators*, *Nature Phys.* **16** (2019) 199 [1802.00801].

[44] C.M. Langlett, C. Jonay, V. Khemani and J.F. Rodriguez-Nieva, *Quantum chaos at finite temperature in local spin Hamiltonians*, 2501.13164.

[45] D.A. Roberts and B. Swingle, *Lieb-Robinson Bound and the Butterfly Effect in Quantum Field Theories*, *Phys. Rev. Lett.* **117** (2016) 091602 [1603.09298].

[46] B. Kobrin, Z. Yang, G.D. Kahanamoku-Meyer, C.T. Olund, J.E. Moore, D. Stanford et al., *Many-Body Chaos in the Sachdev-Ye-Kitaev Model*, *Phys. Rev. Lett.* **126** (2021) 030602 [2002.05725].

[47] Y. Liao and V. Galitski, *Nonlinear sigma model approach to many-body quantum chaos: Regularized and unregularized out-of-time-ordered correlators*, *Phys. Rev. B* **98** (2018) 205124.

[48] J.M. Maldacena, *Eternal black holes in anti-de Sitter*, *JHEP* **04** (2003) 021 [hep-th/0106112].

[49] W. Israel, *Thermo-field dynamics of black holes*, *Physics Letters A* **57** (1976) 107.

[50] S.H. Shenker and D. Stanford, *Multiple Shocks*, *JHEP* **12** (2014) 046 [1312.3296].

[51] W. Fischler, V. Jahnke and J.F. Pedraza, *Chaos and entanglement spreading in a non-commutative gauge theory*, *JHEP* **11** (2018) 072 [1808.10050].

[52] G.t.H. Tevian Dray, *The gravitational shock wave of a massless particle*, *Nuclear Physics B* **253** (1985) 173.

[53] K. Sfetsos, *On gravitational shock waves in curved space-times*, *Nucl. Phys. B* **436** (1995) 721 [hep-th/9408169].

[54] V. Jahnke, *Recent developments in the holographic description of quantum chaos*, *Adv. High Energy Phys.* **2019** (2019) 9632708 [1811.06949].

[55] A. Kitaev, *simple model of quantum holography*, 2015.

[56] G. Turiaci and H. Verlinde, *On CFT and Quantum Chaos*, *JHEP* **12** (2016) 110 [1603.03020].

[57] S. Pasterski and H. Verlinde, *Chaos in celestial CFT*, *JHEP* **08** (2022) 106 [2201.01630].

[58] J. Sonner and B. Strittmatter, *Quantum Chaos in Liouville CFT*, 2407.11124.

[59] S. Khetrapal, *Chaos and operator growth in 2d CFT*, *JHEP* **03** (2023) 176 [2210.15860].

[60] S. Das, B. Ezhuthachan, A. Kundu, S. Porey, B. Roy and K. Sengupta, *Out-of-Time-Order correlators in driven conformal field theories*, *JHEP* **08** (2022) 221 [2202.12815].

[61] P. Biswas, B. Ezhuthachan, A. Kundu and B. Roy, *Moving mirrors, OTOCs and scrambling*, *JHEP* **10** (2024) 146 [2406.05772].

[62] Y. Gu, X.-L. Qi and D. Stanford, *Local criticality, diffusion and chaos in generalized Sachdev-Ye-Kitaev models*, *JHEP* **05** (2017) 125 [1609.07832].

[63] P. Orman, H. Gharibyan and J. Preskill, *Quantum chaos in the sparse SYK model*, 2403.13884.

[64] T. Scaffidi and E. Altman, *Chaos in a classical limit of the sachdev-ye-kitaev model*, *Phys. Rev. B* **100** (2019) 155128.

[65] N. Sorokhaibam, *Phase transition and chaos in charged SYK model*, *JHEP* **07** (2020) 055 [1912.04326].

[66] D.A. Roberts, D. Stanford and L. Susskind, *Localized shocks*, *JHEP* **03** (2015) 051 [1409.8180].

[67] D.A. Roberts and D. Stanford, *Two-dimensional conformal field theory and the butterfly effect*, *Phys. Rev. Lett.* **115** (2015) 131603 [1412.5123].

[68] C.-J. Lin and O.I. Motrunich, *Out-of-time-ordered correlators in a quantum ising chain*, *Physical Review B* **97** (2018) .

[69] Y. Gu and X.-L. Qi, *Fractional Statistics and the Butterfly Effect*, *JHEP* **08** (2016) 129 [1602.06543].

[70] E. Plamadeala and E. Fradkin, *Scrambling in the quantum lifshitz model*, *Journal of Statistical Mechanics: Theory and Experiment* **2018** (2018) 063102.

[71] M. Blake, H. Lee and H. Liu, *A quantum hydrodynamical description for scrambling and many-body chaos*, *JHEP* **10** (2018) 127 [1801.00010].

[72] M. Blake, R.A. Davison, S. Grozdanov and H. Liu, *Many-body chaos and energy dynamics in holography*, *JHEP* **10** (2018) 035 [1809.01169].

[73] S. Grozdanov, *On the connection between hydrodynamics and quantum chaos in holographic theories with stringy corrections*, *JHEP* **01** (2019) 048 [1811.09641].

[74] Y. Ahn, V. Jahnke, H.-S. Jeong and K.-Y. Kim, *Scrambling in Hyperbolic Black Holes: shock waves and pole-skipping*, *JHEP* **10** (2019) 257 [1907.08030].

[75] T. Matsubara, *A New approach to quantum statistical mechanics*, *Prog. Theor. Phys.* **14** (1955) 351.

[76] M. Blake, R.A. Davison and D. Vegh, *Horizon constraints on holographic Green's functions*, *JHEP* **01** (2020) 077 [1904.12883].

[77] M. Natsuume and T. Okamura, *Nonuniqueness of Green's functions at special points*, *JHEP* **12** (2019) 139 [1905.12015].

[78] N. Ceplak, K. Ramdial and D. Vegh, *Fermionic pole-skipping in holography*, *JHEP* **07** (2020) 203 [1910.02975].

[79] N. Ceplak and D. Vegh, *Pole-skipping and Rarita-Schwinger fields*, *Phys. Rev. D* **103** (2021) 106009 [2101.01490].

[80] S. Ning, D. Wang and Z.-Y. Wang, *Pole skipping in holographic theories with gauge and fermionic fields*, *JHEP* **12** (2023) 084 [2308.08191].

[81] K.-Y. Kim, K.-S. Lee and M. Nishida, *Holographic scalar and vector exchange in OTOCs and pole-skipping phenomena*, *JHEP* **04** (2021) 092 [2011.13716].

[82] Y. Ahn, V. Jahnke, H.-S. Jeong, K.-Y. Kim, K.-S. Lee and M. Nishida, *Pole-skipping of scalar and vector fields in hyperbolic space: conformal blocks and holography*, *JHEP* **09** (2020) 111 [2006.00974].

[83] M. Natsuume and T. Okamura, *Holographic chaos, pole-skipping, and regularity*, *PTEP* **2020** (2020) 013B07 [1905.12014].

[84] S. Grozdanov, K. Schalm and V. Scopelliti, *Black hole scrambling from hydrodynamics*, *Phys. Rev. Lett.* **120** (2018) 231601 [1710.00921].

[85] M. Blake and R.A. Davison, *Chaos and pole-skipping in rotating black holes*, *JHEP* **01** (2022) 013 [2111.11093].

[86] X. Wu, *Higher curvature corrections to pole-skipping*, *JHEP* **12** (2019) 140 [1909.10223].

[87] K. Sil, *Pole skipping and chaos in anisotropic plasma: a holographic study*, *JHEP* **03** (2021) 232 [2012.07710].

[88] W. Li, S. Lin and J. Mei, *Thermal diffusion and quantum chaos in neutral magnetized plasma*, *Phys. Rev. D* **100** (2019) 046012 [1905.07684].

[89] M.A.G. Amano, M. Blake, C. Cartwright, M. Kaminski and A.P. Thompson, *Chaos and pole-skipping in a simply spinning plasma*, *JHEP* **02** (2023) 253 [2211.00016].

[90] D.M. Ramirez, *Chaos and pole skipping in CFT_2*, *JHEP* **12** (2021) 006 [2009.00500].

[91] F.M. Haehl, W. Reeves and M. Rozali, *Reparametrization modes, shadow operators, and quantum chaos in higher-dimensional CFTs*, *JHEP* **11** (2019) 102 [1909.05847].

[92] S. Das, B. Ezhuthachan and A. Kundu, *Real time dynamics from low point correlators in 2d BCFT*, *JHEP* **12** (2019) 141 [1907.08763].

[93] Y. Liu and A. Raju, *Quantum Chaos in Topologically Massive Gravity*, *JHEP* **12** (2020) 027 [2005.08508].

[94] N. Abbasi and J. Tabatabaei, *Quantum chaos, pole-skipping and hydrodynamics in a holographic system with chiral anomaly*, *JHEP* **03** (2020) 050 [1910.13696].

[95] S. Mahish and K. Sil, *Quantum information scrambling and quantum chaos in little string theory*, *JHEP* **08** (2022) 041 [2202.05865].

[96] B. Baishya, S. Chakrabarti, D. Maity and K. Nayek, *Pole-skipping and chaos in D3-D7 brane systems*, *Phys. Rev. D* **110** (2024) 086003 [2312.01829].

[97] M. Natsuume and T. Okamura, *Pole-skipping with finite-coupling corrections*, *Phys. Rev. D* **100** (2019) 126012 [1909.09168].

[98] B. Baishya and K. Nayek, *Probing pole-skipping through scalar gauss-bonnet coupling*, *Nuclear Physics B* **1001** (2024) 116521.

[99] H. Yuan and X.-H. Ge, *Pole-skipping and hydrodynamic analysis in Lifshitz, AdS_2 and Rindler geometries*, *JHEP* **06** (2021) 165 [2012.15396].

[100] S. Grozdanov, *Bounds on transport from univalence and pole-skipping*, *Phys. Rev. Lett.* **126** (2021) 051601 [2008.00888].

[101] H.-S. Jeong, K.-Y. Kim and Y.-W. Sun, *Bound of diffusion constants from pole-skipping points: spontaneous symmetry breaking and magnetic field*, *JHEP* **07** (2021) 105 [2104.13084].

[102] N. Abbasi and M. Kaminski, *Constraints on quasinormal modes and bounds for critical points from pole-skipping*, *JHEP* **03** (2021) 265 [2012.15820].

[103] K.-Y. Kim, K.-S. Lee and M. Nishida, *Construction of bulk solutions for towers of pole-skipping points*, *Phys. Rev. D* **105** (2022) 126011 [2112.11662].

[104] H.-S. Jeong, K.-Y. Kim and Y.-W. Sun, *Quasi-normal modes of dyonic black holes and magneto-hydrodynamics*, *JHEP* **07** (2022) 065 [2203.02642].

[105] D. Wang and Z.-Y. Wang, *Pole Skipping in Holographic Theories with Bosonic Fields*, *Phys. Rev. Lett.* **129** (2022) 231603 [2208.01047].

[106] Y.-T. Wang and W.-B. Pan, *Pole-skipping of holographic correlators: aspects of gauge symmetry and generalizations*, *JHEP* **01** (2023) 174 [2209.04296].

[107] H. Yuan, X.-H. Ge, K.-Y. Kim, C.-W. Ji and Y. Ahn, *Pole-skipping points in 2D gravity and SYK model*, *JHEP* **08** (2023) 157 [2303.04801].

[108] M. Natsuume and T. Okamura, *Pole skipping in a non-black-hole geometry*, *Phys. Rev. D* **108** (2023) 046012 [2306.03930].

[109] B. Baishya, S. Chakrabarti and D. Maity, *Effect of scalar condensation on fermionic pole-skipping*, *Eur. Phys. J. C* **84** (2024) 1247 [2311.05314].

[110] G. Yadav, S.S. Kushwah and A. Misra, *Pole-skipping and chaos in hot$\mathcal{M}$QCD*, *JHEP* **05** (2024) 015 [2311.09306].

[111] S. Grozdanov, P.K. Kovtun, A.O. Starinets and P. Tadić, *The complex life of hydrodynamic modes*, *JHEP* **11** (2019) 097 [1904.12862].

[112] N. Abbasi and S. Tahery, *Complexified quasinormal modes and the pole-skipping in a holographic system at finite chemical potential*, *JHEP* **10** (2020) 076 [2007.10024].

[113] B. Baishya and K. Nayek, *Probing pole-skipping through scalar Gauss-Bonnet coupling*, *Nucl. Phys. B* **1001** (2024) 116521 [2301.03984].

[114] B. Baishya, A. Chakraborty and N. Padhi, *Entanglement wedge method, out-of-time-ordered correlators, and pole skipping*, *Phys. Rev. D* **111** (2025) 106013 [2406.18319].

[115] S. Grozdanov and M. Vrbica, *Pole-skipping of gravitational waves in the backgrounds of four-dimensional massive black holes*, *Eur. Phys. J. C* **83** (2023) 1103 [2303.15921].

[116] H.-S. Jeong, C.-W. Ji and K.-Y. Kim, *Pole-skipping in rotating BTZ black holes*, *JHEP* **08** (2023) 139 [2306.14805].

[117] J.L. Blázquez-Salcedo, C.F.B. Macedo, V. Cardoso, V. Ferrari, L. Gualtieri, F.S. Khoo et al., *Perturbed black holes in Einstein-dilaton-Gauss-Bonnet gravity: Stability, ringdown, and gravitational-wave emission*, *Phys. Rev. D* **94** (2016) 104024 [1609.01286].

[118] P. Breitenlohner and D.Z. Freedman, *Positive Energy in anti-De Sitter Backgrounds and Gauged Extended Supergravity*, *Phys. Lett. B* **115** (1982) 197.

[119] S. Chakrabarti, D. Maity and W. Wahlang, *Probing the Holographic Fermi Arc with scalar field: Numerical and analytical study*, *JHEP* **07** (2019) 037 [1902.08826].

[120] Y. Kim, B.-H. Lee, C. Park and S.-J. Sin, *Gluon Condensation at Finite Temperature via AdS/CFT*, *JHEP* **09** (2007) 105 [hep-th/0702131].

[121] M. Bianchi, D.Z. Freedman and K. Skenderis, *Holographic renormalization*, *Nucl. Phys. B* **631** (2002) 159 [hep-th/0112119].

[122] M. Bianchi, D.Z. Freedman and K. Skenderis, *How to go with an RG flow*, *JHEP* **08** (2001) 041 [hep-th/0105276].

[123] R. Emparan, C.V. Johnson and R.C. Myers, *Surface terms as counterterms in the AdS / CFT correspondence*, *Phys. Rev. D* **60** (1999) 104001 [hep-th/9903238].

[124] F.-L. Julié and E. Berti, $d+1$ *formalism in Einstein-scalar-Gauss-Bonnet gravity*, *Phys. Rev. D* **101** (2020) 124045 [2004.00003].

[125] K.-B. Huh, H.-S. Jeong, K.-Y. Kim and Y.-W. Sun, *Upper bound of the charge diffusion constant in holography*, *JHEP* **07** (2022) 013 [2111.07515].

[126] H.-S. Jeong, K.-Y. Kim and Y.-W. Sun, *The breakdown of magneto-hydrodynamics near AdS_2 fixed point and energy diffusion bound*, *JHEP* **02** (2022) 006 [2105.03882].

[127] D. Arean, R.A. Davison, B. Goutéraux and K. Suzuki, *Hydrodynamic Diffusion and Its Breakdown near AdS2 Quantum Critical Points*, *Phys. Rev. X* **11** (2021) 031024 [2011.12301].

[128] T. Hartman, S.A. Hartnoll and R. Mahajan, *Upper Bound on Diffusivity*, *Phys. Rev. Lett.* **119** (2017) 141601 [1706.00019].

[129] P. Kovtun, D.T. Son and A.O. Starinets, *Holography and hydrodynamics: Diffusion on stretched horizons*, *JHEP* **10** (2003) 064 [hep-th/0309213].

[130] A. Buchel, R.C. Myers and A. Sinha, *Beyond eta/s = 1/4 pi*, *JHEP* **03** (2009) 084 [0812.2521].

[131] S. Sakai, Y. Motome and M. Imada, *Evolution of electronic structure of doped mott insulators: Reconstruction of poles and zeros of green's function*, *Physical Review Letters* **102** (2009) .

[132] J. Alsup, E. Papantonopoulos, G. Siopsis and K. Yeter, *Duality between zeroes and poles in holographic systems with massless fermions and a dipole coupling*, *Phys. Rev. D* **90** (2014) 126013 [1404.4010].

[133] P. Breitenlohner and D.Z. Freedman, *Stability in Gauged Extended Supergravity*, *Annals Phys.* **144** (1982) 249.

[134] I.R. Klebanov and E. Witten, *Ads/CFT correspondence and symmetry breaking*, *Nuclear Physics B* **556** (1999) 89.

[135] T. Akutagawa, K. Hashimoto, K. Murata and T. Ota, *Chaos of qcd string from holography*, *Phys. Rev. D* **100** (2019) 046009.

[136] T. Akutagawa, K. Hashimoto, T. Miyazaki and T. Ota, *Phase diagram of qcd chaos in linear sigma models and holography*, *Progress of Theoretical and Experimental Physics* **2018** (2018) .

[137] B. Shukla, D. Dudal and S. Mahapatra, *Anisotropic and frame dependent chaos of suspended strings from a dynamical holographic QCD model with magnetic field*, *JHEP* **06** (2023) 178 [2303.15716].

[138] H. Markum, R. Pullirsch, K. Rabitsch and T. Wettig, *Quantum chaos in QCD at finite temperature*, *Nucl. Phys. B Proc. Suppl.* **63** (1998) 832 [hep-lat/9709103].

[139] E. Bittner, H. Markum and R. Pullirsch, *Quantum chaos and chiral symmetry at the QCD and QED phase transition*, *Nucl. Phys. B Proc. Suppl.* **96** (2001) 189 [hep-lat/0009002].

[140] A. Karch and E. Katz, *Adding flavor to AdS / CFT*, *JHEP* **06** (2002) 043 [hep-th/0205236].

[141] T. Albash, V.G. Filev, C.V. Johnson and A. Kundu, *Finite temperature large N gauge theory with quarks in an external magnetic field*, *JHEP* **07** (2008) 080 [0709.1547].

[142] T. Albash, V.G. Filev, C.V. Johnson and A. Kundu, *Quarks in an external electric field in finite temperature large N gauge theory*, *JHEP* **08** (2008) 092 [0709.1554].

[143] H. Kodama and A. Ishibashi, *A Master equation for gravitational perturbations of maximally symmetric black holes in higher dimensions*, *Prog. Theor. Phys.* **110** (2003) 701 [hep-th/0305147].

[144] M. Blake, R.A. Davison and S. Sachdev, *Thermal diffusivity and chaos in metals without quasiparticles*, *Phys. Rev. D* **96** (2017) 106008 [1705.07896].

[145] G. Policastro, D.T. Son and A.O. Starinets, *From AdS / CFT correspondence to hydrodynamics*, *JHEP* **09** (2002) 043 [hep-th/0205052].

[146] K. Balasubramanian and J. McGreevy, *Gravity duals for nonrelativistic conformal field theories*, *Phys. Rev. Lett.* **101** (2008) 061601.

[147] W.D. Goldberger, *Ads/cft duality for non-relativistic field theory*, *Journal of High Energy Physics* **2009** (2009) 069.

[148] J. Maldacena, D. Martelli and Y. Tachikawa, *Comments on string theory backgrounds with non-relativistic conformal symmetry*, *Journal of High Energy Physics* **2008** (2008) 072.

[149] A. Adams, K. Balasubramanian and J. McGreevy, *Hot spacetimes for cold atoms*, *Journal of High Energy Physics* **2008** (2008) 059.

[150] S. Kachru, X. Liu and M. Mulligan, *Gravity duals of lifshitz-like fixed points*, *Phys. Rev. D* **78** (2008) 106005.

[151] V. Keränen, W. Sybesma, P. Szepietowski and L. Thorlacius, *Correlation functions in theories with lifshitz scaling*, *Journal of High Energy Physics* **2017** (2017) .

[152] M. Kord Zangeneh, B. Wang, A. Sheykhi and Z. Tang, *Charged scalar quasi-normal modes for linearly charged dilaton-lifshitz solutions*, *Physics Letters B* **771** (2017) 257.

[153] C. Park, *Massive quasinormal mode in the holographic lifshitz theory*, *Phys. Rev. D* **89** (2014) 066003.

[154] J. Cheyne and D. Mattingly, *Constructing entanglement wedges for Lifshitz spacetimes with Lifshitz gravity*, *Phys. Rev. D* **97** (2018) 066024 [1707.05913].

[155] J.K. Basak, A. Chakraborty, C.-S. Chu, D. Giataganas and H. Parihar, *Massless Lifshitz Field Theory for Arbitrary z*, 2312.16284.

[156] D.N. Kabat and M. Ortiz, *Eikonal quantum gravity and Planckian scattering*, *Nucl. Phys. B* **388** (1992) 570 [hep-th/9203082].

[157] G. D'Appollonio, P. Di Vecchia, R. Russo and G. Veneziano, *High-energy string-brane scattering: Leading eikonal and beyond*, *JHEP* **11** (2010) 100 [1008.4773].

[158] N.E.J. Bjerrum-Bohr, J.F. Donoghue, B.R. Holstein, L. Planté and P. Vanhove, *Bending of Light in Quantum Gravity*, *Phys. Rev. Lett.* **114** (2015) 061301 [1410.7590].

[159] L. Cornalba, M.S. Costa, J. Penedones and R. Schiappa, *Eikonal Approximation in AdS/CFT: From Shock Waves to Four-Point Functions*, *JHEP* **08** (2007) 019 [hep-th/0611122].

[160] L. Cornalba, M.S. Costa, J. Penedones and R. Schiappa, *Eikonal Approximation in AdS/CFT: Conformal Partial Waves and Finite N Four-Point Functions*, *Nucl. Phys. B* **767** (2007) 327 [hep-th/0611123].

[161] R.C. Brower, M.J. Strassler and C.-I. Tan, *On the eikonal approximation in AdS space*, *JHEP* **03** (2009) 050 [0707.2408].

[162] M. Kulaxizi, G.S. Ng and A. Parnachev, *Black holes, heavy states, phase shift and anomalous dimensions*, *SciPost Phys.* **6** (2019) 065.

[163] J. Chávez-Carlos, B. López-del Carpio, M.A. Bastarrachea-Magnani, P. Stránský, S. Lerma-Hernández, L.F. Santos et al., *Quantum and classical lyapunov exponents in atom-field interaction systems*, *Physical Review Letters* **122** (2019) .

[164] T. Morita, *Extracting classical lyapunov exponent from one-dimensional quantum mechanics*, *Phys. Rev. D* **106** (2022) 106001.

[165] K. Balasubramanian and J. McGreevy, *An Analytic Lifshitz black hole*, *Phys. Rev. D* **80** (2009) 104039 [0909.0263].

[166] M. Taylor, *Lifshitz holography*, *Classical and Quantum Gravity* **33** (2016) 033001.

[167] U.H. Danielsson and L. Thorlacius, *Black holes in asymptotically Lifshitz spacetime*, *JHEP* **03** (2009) 070 [0812.5088].

[168] X. Dong, D. Harlow and A.C. Wall, *Reconstruction of bulk operators within the entanglement wedge in gauge-gravity duality*, *Phys. Rev. Lett.* **117** (2016) 021601.

[169] A.C. Wall, *Maximin Surfaces, and the Strong Subadditivity of the Covariant Holographic Entanglement Entropy*, *Class. Quant. Grav.* **31** (2014) 225007 [1211.3494].

[170] B. Czech, J.L. Karczmarek, F. Nogueira and M. Van Raamsdonk, *The Gravity Dual of a Density Matrix*, *Class. Quant. Grav.* **29** (2012) 155009 [1204.1330].

[171] S. Ryu and T. Takayanagi, *Holographic derivation of entanglement entropy from the anti–de sitter space/conformal field theory correspondence*, *Phys. Rev. Lett.* **96** (2006) 181602.

[172] M. Mezei and D. Stanford, *On entanglement spreading in chaotic systems*, *JHEP* **05** (2017) 065 [1608.05101].

[173] X. Dong, D. Wang, W.W. Weng and C.-H. Wu, *A tale of two butterflies: an exact equivalence in higher-derivative gravity*, *JHEP* **10** (2022) 009 [2203.06189].

[174] M. Taylor, *Lifshitz holography*, *Class. Quant. Grav.* **33** (2016) 033001 [1512.03554].

[175] D. Giataganas and K. Sfetsos, *Non-integrability in non-relativistic theories*, *JHEP* **06** (2014) 018 [1403.2703].

[176] D. Giataganas, U. Gürsoy and J.F. Pedraza, *Strongly-coupled anisotropic gauge theories and holography*, *Phys. Rev. Lett.* **121** (2018) 121601 [1708.05691].

[177] X. Bai, B.-H. Lee, T. Moon and J. Chen, *Chaos in Lifshitz Spacetimes*, *J. Korean Phys. Soc.* **68** (2016) 639 [1406.5816].

[178] V. Jahnke, K.-Y. Kim and J. Yoon, *On the Chaos Bound in Rotating Black Holes*, *JHEP* **05** (2019) 037 [1903.09086].

[179] M. Mezei and G. Sárosi, *Chaos in the butterfly cone*, *JHEP* **01** (2020) 186 [1908.03574].

[180] A.P. Reynolds and S.F. Ross, *Butterflies with rotation and charge*, *Class. Quant. Grav.* **33** (2016) 215008 [1604.04099].

[181] R.R. Poojary, *BTZ dynamics and chaos*, *JHEP* **03** (2020) 048 [1812.10073].

[182] A. Banerjee, A. Kundu and R.R. Poojary, *Rotating black holes in AdS spacetime, extremality, and chaos*, *Phys. Rev. D* **102** (2020) 106013 [1912.12996].

[183] A. Saha and S. Gangopadhyay, *Quantum chaos in the presence of non-conformality*, 2401.05814.

[184] N. Sircar, J. Sonnenschein and W. Tangarife, *Extending the scope of holographic mutual information and chaotic behavior*, *JHEP* **05** (2016) 091 [1602.07307].

[185] V. Jahnke, *Delocalizing entanglement of anisotropic black branes*, *JHEP* **01** (2018) 102 [1708.07243].

[186] A. Alvarez, E. Ayón-Beato, H.A. González and M. Hassaïne, *Nonlinearly charged Lifshitz black holes for any exponent $z > 1$*, *JHEP* **06** (2014) 041 [1403.5985].

[187] K.-X. Zhu, F.-W. Shu and D.-H. Du, *Holographic complexity for nonlinearly charged lifshitz black holes*, *Classical and Quantum Gravity* **37** (2020) 195023.

[188] K.-Y. Kim, K.-S. Lee and M. Nishida, *Regge conformal blocks from the rindler-ads black hole and the pole-skipping phenomena*, *Journal of High Energy Physics* **2021** (2021) .

[189] A. Parnachev and K. Sen, *Notes on AdS-Schwarzschild eikonal phase*, *JHEP* **03** (2021) 289 [2011.06920].

[190] V. Cardoso, A.S. Miranda, E. Berti, H. Witek and V.T. Zanchin, *Geodesic stability, Lyapunov exponents and quasinormal modes*, *Phys. Rev. D* **79** (2009) 064016 [0812.1806].

[191] A.N. Kumara, S. Punacha and M.S. Ali, *Lyapunov Exponents and Phase Structure of Lifshitz and Hyperscaling Violating Black Holes*, 2401.05181.

[192] A. Banerjee, A. Kundu and R. Poojary, *Maximal Chaos from Strings, Branes and Schwarzian Action*, *JHEP* **06** (2019) 076 [1811.04977].

[193] F. Bigazzi, A.L. Cotrone and J. Tarrio, *Charged D3-D7 plasmas: novel solutions, extremality and stability issues*, *JHEP* **07** (2013) 074 [1304.4802].